

**3D STRUCTURAL ANALYSIS OF THE BENTON UPLIFT,
OUACHITA OROGEN, ARKANSAS**

A Thesis

by

HAROLD EVERETT JOHNSON II

Submitted to the Office of Graduate Studies of
Texas A&M University
in partial fulfillment of the requirements for the degree of

MASTER OF SCIENCE

December 2011

Major Subject: Geology

3D Structural Analysis of the Benton Uplift, Ouachita Orogen, Arkansas

Copyright 2011 Harold Everett Johnson II

**3D STRUCTURAL ANALYSIS OF THE BENTON UPLIFT,
OUACHITA OROGEN, ARKANSAS**

A Thesis

by

HAROLD EVERETT JOHNSON II

Submitted to the Office of Graduate Studies of
Texas A&M University
in partial fulfillment of the requirements for the degree of

MASTER OF SCIENCE

Approved by:

Chair of Committee,	David V. Wiltschko
Committee Members,	John H. Spang
	Brent V. Miller
	Andrew G. Klein
Head of Department,	John R. Giardino

December 2011

Major Subject: Geology

ABSTRACT

3D Structural Analysis of the Benton Uplift, Ouachita Orogen, Arkansas.

(December 2011)

Harold Everett Johnson II, B.S., The Ohio State University

Chair of Advisory Committee: Dr. David V. Wiltschko

The date for the formation of the Benton Uplift, Ouachita orogeny, is bracketed by Carboniferous synorogenic sediments deposited to the north and Late Pennsylvanian to Early Permian isotopic dates from the weakly metamorphosed rocks within the uplift. We address the largely unknown structural history between these two constraints by presenting an improved 3-dimensional kinematic model using better constrained retrodeformable sections. These new sections are based on all surface and subsurface data, new zircon fission track dates and thermal maturation data including new ‘crystallinity’ data to constrain the maximum burial depth. Concordant zircon fission track ages range from 307 ± 18.8 Ma to 333.4 ± 38.9 Ma or from the Late Devonian to Early Permian. Maximum ‘crystallinity’ of both illite and chlorite indicate these exposed rocks experienced a temperature of $\sim 300^{\circ}\text{C}$ across the eastern Benton Uplift. This temperature is consistent with reconstructed burial depths using cumulative stratigraphic thickness without having to call on structural thickening. Comparing coarse and fine clay fractions, computed temperature for the fine clay fraction is less by $\sim 100^{\circ}\text{C}$ than that of the coarse clay fraction. This difference is the same for all formations studied. This

uniform difference in temperature may indicate cooling of the orogen as it deformed or more than one thermal event.

DEDICATION

I dedicate this thesis to my parents, Diana and Harold Sr., who have always supported me in my endeavors. Also, I would like to acknowledge the invaluable encouragement from my friends, family, and the community that I worked for during my time in water well drilling in Ohio.

ACKNOWLEDGEMENTS

I would like to express my gratitude to my committee chair, Dr. David V. Wiltschko, for his excellent support as my advisor during my project. A thank you to my committee members, Dr. John H. Spang, Dr. Brent V. Miller, and Andrew G. Klein, for their valuable guidance throughout the course of my project. Interactions with friends, faculty, and staff in our department have been a major part of my experience and I am very grateful to them for all their help.

Thanks to Dr. B.V. Miller for help with the heavy mineral separates. Dr. J.P. Harris generously allowed me use of his clay mineral lab in the Texas Transportation Institute. In addition, Dr. J.P. Harris provided his time at the microscopy center for several SEM images and EDS of ART-6. Dr. H. J. Kisch (Ben-Gurion University of the Negev, Israel) kindly provided illite ‘crystallinity’ calibration standards. Drs. R. N. Guillemette and R.K. Popp helped with the XRD analyses. Dr. S. N. Thomson (University of Arizona) provided zircon fission track dates. Jennifer Piper allowed me to collect samples on her sample collection trip. We appreciate the use of 2D/3D/4DMove[®] structural analysis software provided to TAMU by Midland Valley. Discussions with Drs. R. Groshong and W.A. Thomas materially helped improve structural interpretations. AAPG James E. Hooks Memorial Research Grant and M.T. Halbouty Chair in geology to DVW funded this project.

TABLE OF CONTENTS

	Page
ABSTRACT	iii
DEDICATION	v
ACKNOWLEDGEMENTS	vi
TABLE OF CONTENTS	vii
1. INTRODUCTION.....	1
2. GEOLOGIC OVERVIEW	3
2.1 Regional Geology.....	3
2.2 Structural Provinces	3
3. RETRODEFORMABLE CROSS SECTIONS.....	6
3.1 Previous Regional Cross Sections.....	6
3.1.1 Frontal Thrust Zone.....	6
3.1.2 Maumelle Chaotic Zone	6
3.1.3 Benton Uplift and Southern Ouachitas.....	7
3.2 Data Sources.....	7
3.3 New ‘Crystallinity’ Data	10
3.4 Illite (IC) and Chlorite (ChC) Crystallinity Results	13
3.5 Zircon Fission Track Results.....	14
4. EXPLANATION OF STRUCTURES AND BALANCED CROSS SECTIONS.....	19
4.1 Frontal Thrust Zone.....	19
4.2 Maumelle Chaotic Zone	20
4.3 Benton Uplift.....	20
4.4 Southern Ouachitas	21
5. DISCUSSION	24
5.1 Timing	24

	Page
5.2 Geothermometry.....	24
5.3 Structural Evolution	28
6. CONCLUSIONS.....	30
REFERENCES.....	32
APPENDIX A	42
APPENDIX B	85
APPENDIX C	88
APPENDIX D	102
APPENDIX E.....	171
APPENDIX F	175
APPENDIX G	187
VITA	229

1. INTRODUCTION

The kinematic evolution for the Ouachita orogeny is largely unknown. Synorogenic sediments in the foreland indicate deformation started in the early Carboniferous [*Viele and Thomas, 1989*]. Isotopic dates from the weakly metamorphosed rocks in the core suggest exhumation ended during the Late Pennsylvanian to early Permian [*Bass and Ferrara, 1969; Denison et al., 1977; Shelton et al., 1986; Arbenz, 1989*]. Little is known about the evolution of the Ouachita orogeny between these two groups of ages. Previous thermochronologic work using apatite fission tracking dating in the Ouachita orogen shows that apatite grains were completely reset in the Cretaceous [*Arne, 1992*]. As a result, apatite fission track dating is not useful because the reset episode postdates tectonism. Direct dating of intervening events is challenging at present. However, the chronologic constraints on the thermal evolution might be more feasible.

Lock and Willett [2008] show that thermochronometric ages will have a predictable pattern across a fault-bend fold with a known ramp dip and amount of displacement. Specifically, the ages computed from apatite fission tracks and U-Th/He dating will display a minimum over a thrust ramp (Figure 1). The boundaries of the minimum define the start and end of thrusting. These points are labeled as 1 and 3, respectively, on Figure 1. With thrust motion, the zone of reset ages widens toward the foreland as reset material is carried horizontally above the top flat. The width of reset age zone (i.e., base of U-

This thesis follows the style of *Tectonics*.

shaped pattern) indicates duration of thrust motion whereas the breadth of the minimum yields the duration of motion. The slope of the zone of reset ages, labeled 2 in Figure 1 may be used to compute the rate of thrust motion.

We aim to take advantage of published and new thermal maturation data and thermochronologic data to construct new crustal-scale retrodeformable cross sections through the Benton Uplift, the metamorphic core of the Ouachita orogen. Thermal maturation may be used to constrain the maximum depth of burial providing there have not been anomalous heat sources (e.g., magma intrusions, regional fluid flow events). Thermochronology provides the age when rocks were exhumed through the closure or annealing temperature of the particular mineral.

Our goal is to explore whether the modeled age patterns described by *Lock and Willett* [2008] may exist in the Ouachita orogen in the form of a crustal-scale thrust ramp. If true, the pattern of ages and thermal maturation may provide constraints on the thermal and structured evolution of this orogen [*Pevear*, 1999]. We combine published thermal maturation, new illite and chlorite crystallinity and new zircon fission track ages to better constrain retrodeformable cross sections through the Ouachita orogen.

2. GEOLOGIC OVERVIEW

2.1 Regional Geology

The Ouachita orogen is the largest exposed section of a Late Paleozoic orogeny on the southern margin of North America [*Viele and Thomas*, 1989; see Figure 2]. The orogen is not as well exposed as the Appalachian Mountains to the east. Also unlike the Appalachian Mountains, the origin and nature of the colliding plate is not well known. It is generally assumed by most authors that the Ouachita orogen is the result of a collision with a large microcontinent during the Late Paleozoic [e.g., *Lillie et al.*, 1983; *Arbenz*, 2008]. Whatever the nature of the collider, the deformation resulting from the collision is not as much as in the Appalachian Mountains. Nowhere in the Ouachita orogen are rocks older than Early Ordovician exposed.

2.2 Structural Provinces

The Ouachita orogen may be divided into five provinces based on stratigraphic and structural character [e.g., *Nelson et al.*, 1982; *Lillie et al.*, 1983; *Viele and Thomas*, 1989]. From the north to the south, they are the Arkoma Basin, Frontal Thrust Zone, Maumelle Chaotic Zone, Benton Uplift, and Southern Ouachitas (Figure 3). The Consortium for Continental Reflection Profiling (COCORP) deep-crustal seismic reflection survey published by *Nelson et al.* [1982] provides an important constraint on the geometry of the crustal structures.

The *Arkoma Basin* is a foreland basin filled with synorogenic sediments from the south with some sediment input from the stable North American craton to the north. Formation tops from boreholes indicate that the Pennsylvanian units overlie gently

south-dipping Cambrian platform carbonates [Kruger, 1983]. The Ross Creek thrust fault (Figure 3) is the traditionally used boundary between the *Frontal Thrust Zone* and the Arkoma Basin in Arkansas [Lillie et al., 1983].

The *Frontal Thrust Zone* encompasses a region of broad north-verging folds of syntectonic sediments with up to 5 km of structural relief. Broad synclines are well imaged in this province [Nelson et al., 1982]. Thrust faults are present within the fold limbs and beneath the structures as décollements. Numerous north-verging imbricate thrust faults thicken the section in the southern portion [Lillie et al., 1983].

Maumelle Chaotic Zone (Figure 3) is an intensely deformed region of lower Pennsylvanian Johns Valley Formation and Jackfork Formation rocks (Figure 4) that lies south of the Y city thrust fault [Viele, 1974]. The southern portion is complex and poorly exposed such that determining formation contacts is difficult. Viele [1979] and Nielsen et al. [1989] propose that the *Maumelle Chaotic Zone* represents a tectonic mélange. Other researchers interpret the chaotic units as olistrome deposits [Morris, 1989]. The complexity of the geology increases southward to the northern margin of the Benton Uplift [Blythe et al., 1988]. Exposures of the Mississippian-Devonian Arkansas Novaculite Formation (Figure 3) define the southern boundary of this zone [Nielsen et al., 1989].

The interior of the fold and thrust belt (FTB), part of which is the *Benton Uplift* (Figure 3), is the orogenic core. This area contains rocks that are both the older and more thermally mature than any other portion of the orogen. The central Ouachita orogen consists of upper folded and thrust faulted sedimentary rocks [Viele and Thomas, 1989]

overlying and folded by a crustal-scale antiform, the Benton Uplift [*Nelson et al.*, 1982; *Lillie et al.*, 1983]. Seismic reflection data show a crustal-scale ramp below the Benton Uplift and broad synclines above a detachment in the Frontal Thrust Zone [e.g., *Nelson et al.*, 1982; *Lillie et al.*, 1983; *Kruger and Keller*, 1986; *Arbenz*, 1989; *Viele and Thomas*, 1989]. The Late Ordovician Collier Formation (Figure 3) is the oldest formation exposed in this core. North-verging thrust faults are folded across this uplift. To clarify, thrust faults dip to the north in the northern portion and these same faults dip toward the south in the southern portion [*Haley and Stone*, 2006].

The northern boundary of the *Southern Ouachitas* is defined by the southernmost exposures of the Mississippian-Devonian Arkansas Novaculite (Figure 3). Surface geology of the Southern Ouachitas includes Mississippian Stanley Formation through Early Pennsylvanian Atoka Formation (Figure 4) cut by south-dipping thrust faults [*Haley and Stone*, 2006]. The southern portion of the COCORP profile, including the Southern Ouachitas and the portion below the Gulf Coastal Plain sediments, shows discontinuous planar reflections that dip to the south.

Nelson et al. [1982] interpret these south-dipping reflections to represent thrust imbricated sheets of Paleozoic formations. Under the Cretaceous and younger rocks of the Gulf Coastal Plain (Figure 3) sediment onlap, a continuation of Mississippian-Pennsylvanian rocks is present beneath the onlap for at least 10-20 kilometers further south based on formation tops from wells [*Woods and Addington*, 1973; *Viele*, 1979]. Ouachita aged sediments cannot be traced further south beneath the Gulf Coastal Plain because there are few wells, and the available reflection seismic data is poor.

3. RETRODEFORMABLE CROSS SECTIONS

3.1 Previous Regional Cross Sections

There are a number of published, regional cross sections through the Arkansas segment of the Ouachita orogen. These cross sections are similar since they have a broad anticlinal structure cored by basement below the present-day Benton Uplift and Mississippian-Pennsylvanian formations continuing further south under the cover of the Gulf Coastal Plain sediments [Figure 5A, *Nelson et al.*, 1982; Figure 5B, *Blythe et al.* 1988; Figure 5C, *Viele and Thomas* 1989; Figure 5D, *Arbenz* 2008]. However, there are some important differences with each interpretation that will be discussed below.

3.1.1 Frontal Thrust Zone

Two regional cross sections by *Blythe et al.* [1988] have multiple décollements in the syntectonic units and fault propagation folds in the Frontal Thrust Zone. In this same province, *Arbenz* [2008] does not show fault propagation folds. His interpretation includes a back thrust and triangle zone in the southern portion [*Arbenz*, 2008].

3.1.2 Maumelle Chaotic Zone

In the interpretation of *Nelson et al.* [1982] folded thrust faults are both near vertical and perpendicular to bedding (Figure 5A). *Viele and Thomas* [1989] choose a more deformed interpretation with folded thrust faults having units overturned near the surface [Figure 5C]. By contrast, *Blythe et al.* [1988] and *Arbenz* [2008] simply interpret the Maumelle Chaotic Zone as minor folding of imbricate thrust slices of Johns Valley and Jackfork [Figures 5B and 5D].

Beneath the syntectonic sediments, *Viele and Thomas* [1989] show high-angle normal faults that offset the Precambrian basement at about 10 km based mainly on offsets in wells [*Buchanan and Johnson*, 1968; *Bush et al.*, 1977]. The dip direction is different between the cross sections for faults in this province because they dip north in Figures 5C and 5D [*Viele and Thomas*, 1989; *Arbenz*, 2008]. Whereas, the faults dip south in Figure 5B dip to the north [*Blythe et al.*, 1988]. The interpretation of faults dipping to the south is not in agreement with *Haley and Stone* [2006].

3.1.3. Benton Uplift and Southern Ouachitas

Blythe et al. [1988] have more thrust faults in the Benton Uplift and Southern Ouachitas compared to the other published sections. Still, all of the other regional cross sections do not include all of the faults on *Haley and Stone* [2006].

3.2 Data Sources

Three new regional dip lines and one strike line were constructed from the Arkoma basin to the Southern Ouachitas. These sections were constructed using the following:

- a) Surface geology from the Arkansas Geologic Survey including the Geologic Map of Arkansas [*Haley et al.*, 1976; <http://geostor.arkansas.gov>] and the Geologic Map of the Ouachita Mountain Region [*Haley and Stone*, 2006]. Only the dip direction and not dip angle of faults are given in both literature and geologic maps of the area. However, published sources do not agree on dip direction even for major faults (e.g., Y City Fault) [*Arbenz*, 1989, Figure 9; *Arbenz*, 2008, plate 2]. We have drawn faults to generally parallel to lithologic contacts because of the

observations of faults and dip of formations based on the geologic maps. In addition, lacking any other information, we have drawn the faults parallel to the bedding in the hanging wall. If the COCORP seismic profile or other subsurface data shows faults that cut across bedding, then those observations are honored. Thousands of faults are mapped on the Geologic Map of the Ouachita Mountain Region and a portion of the Arkansas Valley Region in Arkansas [*Haley and Stone, 2006*]. At the regional scale of our cross sections, we were only able to include faults with apparent or true offsets greater than 1 km.

- b) A published ~15 km north-south industry seismic line in the Southern Ouachitas. See Figure 3 for location. This line is depth migrated and extends to ~5 km depth. *Godo et al. [2008]* interpret the line to show south dipping units and broadly folded thrust sheets.
- c) Formation tops from eight industry wells. These wells are labeled W1 – W8 on Figure 3. Wells W1 to W6, located in the Arkoma Basin, provide formation tops for the Lower Atoka, Johns Valley, and Jackfork Formations. Well W7 from the northern portion of the Gulf Coastal Plain provides the location of Stanley Formation top. Formation tops from well W8 prove the existence of syntectonic formations under the Gulf Coastal Plain.
- d) The COCORP deep crustal seismic reflection profile [*Nelson et al., 1982*].
- e) The approximate Moho depth from geophysical data. A depth of 42 km across the Arkoma Basin is based on a northern portion of a geophysical model of *Lillie et al. [1983]*. This model is constructed from gravity data that indicate a gravity high

over the Benton uplift, decreasing both north and south [see also *Woollard and Joesting*, 1964]. The average Moho depth of about 38 km varies from ~32 km in the south to ~ 42 km in the north. [*McCamey and Meyer*, 1966; *Stewart*, 1968; *Mitchell and Landisman*, 1970]. *Zietz* [1981] suggests from magnetic data that continental basement is present to the north of the Benton Uplift but a different basement composition exists in the south.

- f) Mean apparent diameter of recrystallized quartz grains in the central and eastern portion of the Benton Uplift [*Keller et al.*, 1985],
- g) Vitrinite reflectance data from *Houseknecht and Matthews* [1985].
- h) Illite ‘crystallinity’ data from an industry well reaching a depth of 5 km in the Arkoma Basin [*Spötl et al.*, 1993]. Additional illite ‘crystallinity’ data from *Guthrie et al.* [1986] presents maturation trends for the syntectonic formations only.
- i) We have determined the illite ‘crystallinity’ (IC) and chlorite ‘crystallinity’ (ChC) from 15 new samples within the Benton Uplift.
- j) Twelve new zircon fission track dates for the Benton Uplift.
- k) Scanning electron microscope (SEM) and energy dispersive X-ray spectroscopy (EDS) of sample ART-6 show the presence of Fe-rich chlorite and illite, but not kaolinite or smectite (Figure 6). Illite is likely detrital because the clay flakes have sub-rounded edges [*Meunier and Velde* , 2004]. The most abundant of the clay minerals in this sample is Fe-rich chlorite. The Fe-rich chlorite grains have angular edges suggesting that they are authigenic.

3.3 New ‘Crystallinity’ Data

Before discussing the construction of the cross sections, we present our new thermal maturation data. Our new zircon fission track dates follow directly after this section. To augment other published sources of thermal maturation data, we have determined ‘crystallinity’ of both illite (IC) and chlorite (ChC) from 16 samples across the Benton Uplift. Our purpose is to better reconstruct the maximum depth of burial on the cross sections and therefore constrain the original stratigraphic depth of key units.

‘Crystallinity’ data describe the degree of ordering in a crystal lattice of a given clay mineral, commonly illite [Frey, 1987]. ‘Crystallinity’ is commonly measured on an x-ray diffractogram as the full-width half maximum (FWHM) of the characteristic peak and is expressed in $^{\circ}\Delta 2\Theta$ (i.e., Kübler index). For illite, this peak is at 8.85° or approximately 10 \AA lattice spacing. For chlorite, the center of the peak is typically at 12.65° or approximately 7 \AA lattice spacing. Samples are typically oriented mineral aggregate preparations of the $<2\text{-}\mu\text{m}$ size fractions (Kübler, 1967, 1968). Several studies show that increased ‘crystallinity’ is largely controlled by temperature [e.g., Kübler, 1967; Smykatz-Kloss and Althaus, 1974; Schaer and Persoz, 1976; Krumm, 1984]. Frey [1987] states that fluid pressure, stress, lithology, crystal chemistry, mineralogy, and time may also play lesser roles.

We now choose to remove the quotes from crystallinity. When the term crystallinity was introduced in literature, there was not a clear understanding for the physical attributes affecting the change in the 10 \AA peak of illite [Merriman and Pecor, 1999]. More recently, TEM studies have shown that narrower $d(001)$ widths occur

principally with thicker crystallites (i.e., small crystals) of the clay mineral [*Merriman and Peacor, 1999*].

Sample preparation for removing cements, separating out the size fractions, and mounting oriented clay on a glass slide is described in Appendix B. We use two techniques to determine burial depth. First, clay samples are treated with glycol vapor, causing a shift in the smectite peaks. The location of the smectite peaks identify samples that contain between 10-90% smectite [*Środoń, 1980; Hower, 1981*]. The samples that contain more than 10% smectite indicate the lower diagenetic zone [*Merriman and Peacor, 1999*]. For samples with little smectite, the second technique of illite crystallinity is used [*Merriman and Peacor, 1999; Kübler and Jaboyedoff, 2000; Meunier and Velde, 2004*]. The index is the measurement of the full-width half maximum for the 001 illite peak on an x-ray diffractogram. Values of this measurement, called the Kübler index of crystallinity, decrease with increasing thermal maturation as more smectite is converted to illite [*Kübler and Jaboyedoff, 2000*].

Kübler [1967] separated his index into three different metapelitic zones; Epizone ($> \sim 300^{\circ}\text{C}$), Anchizone ($\sim 200^{\circ} - \sim 300^{\circ}\text{C}$), and Diagenetic Zone ($< \sim 200^{\circ}\text{C}$). A thermal correlation diagram, Figure 7, compares TEM crystallite thickness, clay crystallinity, illite percentage, typical XRD pattern, occurrence of select clay minerals, vitrinite reflectance, and metamorphic facies with the metapelitic zones (i.e., increasing temperature assumed to be from burial). The temperature is based on independently computing temperature from metamorphic mineral assemblages in rock for which crystallinity has also been determined [e.g., see *Kisch* [1987] for summary; *Árkai, 1991*].

The estimated range of temperature for the anchizone is $\sim 200^{\circ}\text{C}$ to $\sim 300^{\circ}\text{C}$ according to *Frey* [1987]. The lower boundary of the anchizone is within the prehnite-pumpellyite facies. The upper boundary of the anchizone lies within the pumpellite-actinolite facies [*Frey*, 1987; *Árkai*, 1991]. It is necessary to have the Kübler metapelitic zones because thermal maturation is a relative tool that demonstrates trends in thermal maturation rather than specific temperatures for a given thermal technique value. Only the boundaries of the anchizone are calibrated and provide a means to determine temperature.

For our samples, the crystallinity of both illite and chlorite were determined by measuring the full-width half maximum above background. The peak width is measured in degrees 2Θ which represents the position of the goniometer during the data recording. We calibrated the anchizone boundaries, Figure 8, using polished slate standards kindly supplied by Dr. Hanan J. Kisch. A calibration curve found by plotting a linear regression through the plot of crystallinity on same samples using values established by Kisch and the values found using our XRD machine. The correlation coefficient is 0.9575 for the linear regression, but the curve does not pass through the origin and has a y-intercept of $0.0723^{\circ}2\Theta$ ($\text{CuK}\alpha$). It is not fully clear for the reason our calibration curve to deviate from the origin, but it may be because due to slightly different instrument settings (e.g., time constant, *Kisch* [1990]). The calibration of the IC values allows us to use the Kübler metapelitic zones [*Kisch*, 1991]. The calibrated lower and upper anchizone boundaries for IC are $0.278^{\circ}2\Theta$ ($\text{CuK}\alpha$) and $0.446^{\circ}2\Theta$ ($\text{CuK}\alpha$), respectively.

The ChC values are another thermal indicator on the same specimen [Árkai, 1991; Árkai *et al.*, 1995]. Árkai [1991] finds a positive linear correlation ($r = 0.75$ to 0.85) between these two crystallinity techniques using the same samples. However, other workers show higher thermal maturation using chlorite crystallinity (ChC) that may be related to the chemical composition [Frey, 1987]. Yet, this technique is still useful in determining thermal maturation of a sample lacking illite or when characteristic peaks are obscured by overlapping peaks of other minerals. Using the plot of air-dried illite $d(002)$ against air-dried chlorite $d(002)$ on the same sample, Árkai [1991] calibrates anchizone boundaries for chlorite to $0.260^\circ 2\theta$ (CuK α) and $0.336^\circ 2\theta$ (CuK α).

3.4 Illite (IC) and Chlorite (ChC) Crystallinity Results

A total of 22 specimens from 15 aliquots were analyzed by x-ray diffraction on oriented glass slide mounts to determine the clay mineralogy and the crystallinity of both illite and chlorite (Table 1). In addition, powder x-ray diffraction patterns for the bulk, sand, and silt fractions were obtained in order to identify unknown minerals in the smaller clay-sized samples. The four size fractions are: sand (2 mm to $45\ \mu\text{m}$), silt (45 to $2\ \mu\text{m}$), coarse clay (2 to $.2\ \mu\text{m}$), and fine clay ($<.2\ \mu\text{m}$). All specimens contained less than 10% smectite in the illite/smectite ratio using the technique of Środoń [1980] and Hower [1981]. All of these rocks therefore must have experienced temperatures higher than $\sim 100^\circ\text{C}$ according to Merriman and Peacor [1999].

The IC $d(001)$ fine clay values (Figures 9A and 10, Tables C4-C7, and Appendix D) are between 0.417° to $0.875^\circ \Delta 2\theta$ for air-dried specimens. A few values are in the lower anchizone and the majority of the values span the diagenetic zone.

Illite crystallinity $d(001)$ coarse clay values (Figures 9A and 10, Tables C4-C7, and Appendix D) are between 0.273° to $0.688^\circ \Delta^2\Theta$ (CuK α) for air-dried specimens. The estimated maximum temperature using IC coarse clay values is $\sim 300^\circ\text{C}$. The estimated maximum temperature based on IC fine clay values is $\sim 200^\circ\text{C}$.

Chlorite crystallinity $d(002)$ coarse clay values (Figures 9B and 10, Tables C8-C10, and Appendix D) are between $0.202 \Delta^2\Theta$ (CuK α) to $1.788 \Delta^2\Theta$ (CuK α) for air-dried specimens. Chlorite crystallinity coarse clay values span the diagenetic zone, anchizone, and epizone. The maximum metamorphism temperature based on chlorite crystallinity coarse clay values indicate a slightly higher than $\sim 300^\circ\text{C}$ with one chlorite crystallinity value located in the lower epizone. Chlorite crystallinity $d(002)$ fine clay values (Figures 9B and 10, Tables C8-C10, and Appendix D) are between $0.259 \Delta^2\Theta$ (CuK α) to $1.570 \Delta^2\Theta$ (CuK α) for air-dried specimens. Chlorite crystallinity values span the diagenetic zone, anchizone, and barely the epizone. The maximum metamorphism temperature established by the chlorite crystallinity fine clay values indicate as slightly higher than $\sim 300^\circ\text{C}$ with one value located on the upper boundary of the anchizone.

3.5 Zircon Fission Track Results

Ten thermochronometric ages across the Benton Uplift are from Mt. Ida to Hot Springs Village along the cross section traverses (Figure 11 and Tables 1 and 2). Two additional ages are located in the Mazarn Synclinorium because vitrinite reflectance values suggest temperatures were sufficient to reset zircon fission track ages. Several samples have a low number of zircons analyzed (i.e., 6-11 zircons) because the zircons

are small ($< 60 \mu\text{m}$), metamict, or sparse in the heavy mineral sample separate.

Separation procedure is given by *Donelick et al.* [2005]. Photomicrographs and detailed descriptions of the zircons are found in Appendix E. Full analyses including individual grain ages are given in Appendix F, Tables F1-F12 and Appendix G.

Estimated fission track ages plotted as a histogram show the frequency of grains for a defined time interval. A relative probability density curve is plotted above each histogram to indicate the most representative fission track ages when taking into account the error on the fission track grain ages. *Galbraith* [2005] recommends the use of a plot composed of both a scatter plot of precision (defined below) and deviation for the population central age as well as a radial scale for age. The scatterplot portion of the diagram is defined using the equations,

$$x_i = 1/\sigma_i, \quad (1)$$

$$y_i = (z_i - z_o)/\sigma_i, \quad \text{for } 1 \leq i \leq n_i, \quad (2)$$

x_i is precision, σ_i is the standard error for each grain's age determination, y_i is a measure of age deviation from the mean, z_i is a grain age estimate, and z_o is the central age of the population of grains. *Galbraith* [2005] shows that grains with the largest numbers of tracks have the highest precision. Grains with the smallest standard error, or high precision from Eq. (1), plot farthest to the right.

A radial scale has been inserted on the right side of the x-y described by equations (1) and (2). The equation that describes this scale is,

$$z = \arctan \sqrt{\frac{e^{\lambda t} - 1}{\frac{1}{2} \lambda \hat{\zeta} \hat{\rho}_d}}, \quad (3)$$

z is age estimate, $\lambda = 1.55125 \times 10^{-4} \text{ Ma}^{-1}$ is the total decay rate of ^{238}U , t = geologic age in Ma, $\hat{\zeta} = 121.1$ for laboratory calibration of analyst, and $\hat{\rho}_d = 5.60 \times 10^5$ tracks per square centimeter in the dosimeter is a second laboratory calibration. A Z_o of the central age pins the reference age, t_o , in radial coordinates to the x-y scatterplot. Ages are found by extrapolating a line from the origin, $x_i = 0$ and $y_i = 0$, through a data point (x_i, y_i) and read from the age scale on right side of plot. Standardized error is on y-axis from ± 2 S.E., where S.E. is the standard deviation of all the possible estimates in theory (i.e., a sampling distribution) from a given experiment [Galbraith, 2005]. If a population of grains lies along a line, then the most likely interpretation is that they formed during a single cooling event. Unlike a histogram, a radial plot is a graphical presentation of individual grain ages with their precision.

The mixed-age samples are Mt. Blakely, ART-4, ART-9, and ART-16. The grain ages of these samples have high variance and failed the chi-square test (Tables 3 and 4) meaning that the sample population for each sample is not drawn from a normal distribution of fission track grain ages. Radial plots of these samples show one or more older grain ages with high precision. For example, there are two grain ages between 1300 Ma to 1400 Ma in sample ART-9 (Figure 11E). The ± 2 standard errors of this age (i.e., the short y-axis from 2 to -2 is placed in the same vertical position and centered on the plotted point) with its plot position determines the age interval on the radial age scale. The interval is found by projecting two lines from the origin that are tangent to the S.E. error bars. These lines intersect the radial age scale and provide the 2 S.E. in terms

of age. All of the mixed age samples have old grains that do not share the age of the majority of grains or lie with 2 S.E. of the radial age line. We term a sample to have a “mixed age” when there are both unreset grains and reset grains. The central age given for samples with mixed fission track grain age distributions is not useful as it provides an average calculation for the sample age. More meaningful ages were found using the BINOMFIT that aids in the decomposition of the mixed grain age distributions [Brandon, 2002]. The results from the decomposition, Figure 11, provide two best-fit peak (population) ages using the binomial peak-fitting method of Galbriath and Green [1990]. One population represents the uplift during the formation of the anticlinal structure. We interpret the second population as either not reset or only partially so.

Samples Lake Ouachita 41 and Lake Pineda, Figure 11 K. and L., had fission track ages determined using the LA-ICP-MS method to determine the amount of ^{238}U . BINOFIT must only be used with samples that use the external detector method as the program assumes the ^{238}U has a Poisson distribution. We used IsoPlot and the “Unmix” tool to separate the different fission track grain age populations into Gaussian peak ages [Ludwig, 2003].

The samples that passed the chi-squared test have zircon fission track ages ranging from 307 ± 18.8 Ma to 333.4 ± 38.9 Ma with the youngest ages to the south in the Mazarn Synclinorium. Mixed age samples, excluding Lake Ouachita 41 and Lake Pineda, have been decomposed into distinct population ages with a population that ranges from $340.8 (-25.0, +26.9)$ Ma to $378.5 (-29.4, +31.9)$ Ma for the last cooling event. We chose to separate the fission track analyses of Lake Ouachita 41 and Lake

Pineda from the external detector analyses because of the different statistics used to determine discrete age populations. The last cooling event recorded by these two samples range between 410 ± 14 Ma and 634 ± 21 Ma. Along regional strike, fission track ages are similar within error except for Lake Ouachita 41 and Lake Pineda (Figure 12).

4. EXPLANATION OF STRUCTURES AND BALANCED CROSS SECTIONS

4.1 Frontal Thrust Zone

The top of basement and overlying Early Paleozoic pre-tectonic units dip shallowly to the south based on COCORP deep-crustal seismic reflection survey [Nelson *et al.*, 1982]. The Atoka series, Johns Valley formation, Jackfork formation, and Stanley formation lie above the Early Paleozoic units because of the exposures of these units at the surface along with formation tops from wells [Kruger, 1983]. Above that interval, a thin sequence consisting of Hartshorne formation, McAlester formation, and Savanna formation form broad shallow synclines that overlie the Upper Atoka formation as indicated by the surface geology [Haley and Stone, 2006]. A major south-dipping thrust fault cuts through the Atoka series and serves as a basal detachment for formations above the Johns Valley formation (Figure 13, location 1; Figure 14, location 1; Figure 15, location 1) [Nelson *et al.*, 1982]. The Ross Creek Fault (Figure 3) has a minimum hanging wall displacement of ~9 km on B-B' (Figure 13, location 1), ~23.5 km on C-C' (Figure 14, location 1), and ~15.5 km on D-D' (Figure 15, location 1).

We have included a triangle zone and synclines (Figure 13, location 2; Figure 14, location 2; Figure 16, location 2) above the second décollement in our interpretation of all cross sections for two reasons. First, seismic reflectors in Nelson *et al.* [1982] are sub-horizontal at depth. Dipping reflectors above these sub-horizontal reflectors indicate that folds lie above [Nelson *et al.*, 1982]. Second, the surface geology permits north- and south-dipping panels of rock in the northern and southern Frontal Thrust Zone, respectively [Haley and Stone, 2006]. The southernmost syncline, located in the

southern Frontal Thrust Zone, contains mostly Lower Atoka formation. This syncline contains either a stratigraphic thickness of ~6 km or a stacked thrust sheet to duplicate the published thickness of 3 km.

4.2 Maumelle Chaotic Zone

The repeated sections of Stanley and Jackfork Formations in the Maumelle Chaotic Zone present a problem. We have chosen to minimize structural complexity by duplicating these units with a fore thrust (Figure 13, location 3; Figure 14, location 3; Figure 15, location 3) and adding an addition of a back thrust in D-D' (Figure 15, location 4).

4.3 Benton Uplift

We interpret the Benton Uplift as a simple antiformal stack because discontinuous reflectors in the COCORP deep-crustal seismic reflection survey show a broad arch at depth [Nelson *et al.*, 1982]. To reconstruct the structure of the Benton Uplift we used forward modeling in Midland Valley 2DMove software to test several hypotheses. In doing so, we have ignored smaller amplitude folds. We arbitrarily chose the middle of the Womble formation in the upper thrust sheet as the antiformal stack top in order to represent the present erosional surface.

The simple antiformal stack model was constructed starting with a sequence of pre-tectonic formations from the Arkansas Novaculite formation through basement using the thicknesses given in Figure 4. Most of these formations are exposed at the present surface. The lower detachment is in basement below the Southern Ouachitas (Figure 13,

location 4; Figure 14, location 4) and cuts up section with a 15° cutoff angle (Figure 13, location 5; Figure 14, location 5).

The hanging wall is displaced 20 km along this fault as a fault bend fold. A fault splay with a 15° cutoff angle is initiated 20 km to the north and joins to upper décollement (Figure 13, location 7; Figure 14, location 7; Figure 15, location 6). The basement décollement increases in depth of position from west to east: 17.3 km for B-B' (Figure 13, location 4), 19 km for C-C' (Figure 14, location 4), and ~24.7 km for D-D' (Figure 15, location 7). The surface exposure of the pre-tectonic formations dictates the fault position (i.e., deeper faults exhume more material and creates a wider exposure). The cutoff angle of the décollement is the same for all three sections as it determines the reference position (i.e. elevation) for the top of the model at the surface.

4.4 Southern Ouachitas

The Stanley through Lower Atoka formations are present across the Southern Ouachitas with much of the exposure being of the Stanley formation [*Haley and Stone, 2006*]. The COCORP profile shows predominantly south-dipping reflectors starting at a depth of 1 km [*Nelson et al., 1982*]. There are few near-surface seismic reflectors. Therefore, extending surface contacts into the subsurface with confidence is not possible. In addition, the seismic reflectors are so sufficiently discontinuous that connecting them with any confidence to create continuous horizons is also not feasible. A more recent seismic reflection profile by Shell Western Exploration and Production (SWEPI) and the interpretation of SWEPI Rex Timber #1-9 by *Godo et al. [2008]* suggest broad folds may be present below the Gulf Coastal Plain (see Figure 3 for

location). The Chevron No. 1 well in the northern Gulf Coastal Plain encounters syntectonic formations at depth and prove their existence under the Cretaceous cover (see Figure 3 for location) [Viele and Thomas, 1989].

The Southern Ouachitas represents an imbricate stack of thrust sheets of mainly Stanley through Lower Atoka formations [Haley and Stone, 2006]. Near the southern flank of the Benton Uplift, the décollement on top of basement cuts up-section to the top of the Arkansas Novaculite formation to form an imbricate triple stack of pre-tectonic units (Figure 13, location 8; Figure 14, location 8). Toward the east the décollement moves to top of the Jackfork formation and preserves a package of Jackfork and Stanley formations. The lower thrust sheet continues to the north to form the top of the Benton Uplift (Figure 13, location 9; Figure 14, location 9; Figure 15, location 7). The overlying folded thrust sheet is exposed along the Cossatot Mountains Fold Belt (i.e., Figure 13, location 10, southwestern most ridge of pre-tectonic formations). A second ramp starts at ~4km depth that preserves a complete section of Stanley in the footwall. The upper thrust sheet is not exposed, but its presence is based on the apparent width of exposure of the Stanley formation thickness (see Figure 4).

Another décollement is present on the surface of the Arkansas Novaculite formation that cuts up-section through the Stanley formation and Jackfork formation. A double stack of Stanley formation and Jackfork formation in the east (Figure 15, location 10), whereas a triple stack of this sequence exists further west (Figure 13, location 11). A final décollement is placed at or slightly above the contact between the Stanley formation and Jackfork formation. A minimum stack of 4 imbricate thrust sheets of

Jackfork formation, Johns Valley formation, and Lower Atoka formation are at the southern margin of the Southern Ouachita and beneath the Gulf Coastal Plain (Figure 13, location 12).

5. DISCUSSION

5.1 Timing

The distribution of ages (Figures 16A, 17A, 18A, and 19A) are similar within error and younger than the depositional age. Excluding the mixed age samples that include several unreset grains (i.e., detrital component), zircon fission track ages range from 307 ± 18.8 Ma to 333.4 ± 38.9 Ma or from the Late Devonian to Early Permian. Peak decomposition, does provide a population peak ages for the mixed age samples range from 340.8 (-25.0, +26.9) Ma to 378.5 (-29.4, +31.9) Ma. Fission track ages for Lake Ouachita 41 and Lake Pineda are between 410 ± 14 Ma and 634 ± 21 Ma, which are older cooling ages when compared to the other samples. We interpret these ages to represent a single cooling event during the Carboniferous that records the timing for the uplift related to formation of the crustal-scale anticlinal structure.

5.2 Geothermometry

The crystallinity of illite and chlorite decreases away from the Benton Uplift (Figure 9A-B). Depth plots of the crystallinity values (Figure 10) show a trend of increasing maturation with increasing cumulative stratigraphic thickness. Figure 10 also shows the difference in thermal maturation between the coarse and fine clay fractions. Illite crystallinity $d(001)$ fine and coarse clay fractions increase as cumulative stratigraphic thickness with the exception of a few values (Figure 10). These outliers may be recording an older thermal signature from detrital illite. The fine illite fraction records a lower thermal maturation. This difference in crystallinity may be a record of two thermal

events. If it is found that the coarse clay is partially detrital, then the fine clay may be closer to the true maturation for the area.

The reason for using two size fractions is 1) to separate neo-cryst clay minerals such as smectite from older clay minerals such as detrital illite, 2) to aid in clay mineral identification by segregation of clays to minimize peak overlap and have the fewest peaks, and 3) minimize the effect of grain sorting while pipetting the clay on a glass slide (e.g., coarse grains on bottom and fining upward caused by rapid settling of larger clays) [Moore and Reynolds, 1997].

In comparison, the variance of chlorite crystallinity $d(002)$ values for both size fractions is larger than that for illite. The fine chlorite clay fraction indicates a lower maturation. A $\sim 300^{\circ}\text{C}$ is the maximum temperature reached by these rocks. In addition, unlike illite, there is no correlation with stratigraphic depth. In some cases, the fine clay value is more thermally mature than the coarse clay counterpart for a given sample. Many of the chlorite peaks were only a few hundred counts above the background spectrum and short peaks. This short peak height contributes to a broad peak and thus greater full-width half maximum variability (Tables E8-E10, Appendix F).

The maximum temperature reached as indicated by both illite crystallinity and chlorite crystallinity is $\sim 300^{\circ}\text{C}$ corresponding to a maximum vitrinite reflectance R_o of 4.0-4.1%. Houseknecht and Mathews [1985] found R_o above 4.0 % in the vicinity of Hot Springs Village, Arkansas (see Figures 9A-B). The R_o values decrease to the southwest and away from the culmination of the Benton Uplift. Houseknecht and Mathews [1985]

attribute the pattern of R_o values to the maximum depth of burial that each sample experienced.

Guthrie et al. [1986] demonstrate the same thermal event/burial is responsible for the IC and VR values in the Ouachita syntectonic units (e.g., Maumelle Chaotic Zone, Frontal Thrust Zone, and Arkoma Basin). *Spötl et al.* [1993] measured VR in six industry wells, most of them drilled in Oklahoma. The only Arkansas well, Oxy Danville USA A-1, is located near the Ross Creek Fault (see Figure 3) in north-central Frontal Thrust Zone. *Spötl et al.* [1993] found a transition from digenesis to anchizone (0.8-4.7 % R_o) in the Danville USA A-1 well. The IC did not change with depth and most values lie within the anchizone. *Spötl et al.* [1993] propose that a high sedimentation rate may preserve clay minerals from the source area and is reflected on x-ray diffractograms as the detrital illite signature which is present along with authigenic illite. Detrital input is a problem when authigenic illite is used to determine thermal maturation. To minimize error from detrital illite, illite crystallinity and chlorite crystallinity should be restricted to formations older than the Johns Valley formation. Most of the samples of this study were taken from the pre-tectonic core and adjacent formations (Table 1) and crystallinity should represent the thermal maturation recorded in mainly authigenic illite. Therefore, crystallinity does provide us with a useful thermal constraint.

The mean apparent diameter of recrystallized quartz taken from chert and novaculite show an increasing crystal size toward the eastern portion of the exposed Ouachita Mountains [*Keller et al.*, 1985]. Similar to the contoured vitrinite reflectance values, the mean apparent diameter of recrystallized quartz contours show a trend that follows

regional strike and closely follow the shape of the exposed pre-tectonic formations. The mostly linear vitrinite reflectance contours in the central and western Ouachitas parallel the thrust faults and culmination of the Benton Uplift which suggests the higher temperatures were caused by burial. The burial hypothesis assumes no tectonic burial (i.e. structural thickening from thrust sheets), a uniform regional geothermal gradient, and no stratigraphic variation in cumulative stratigraphic thickness [Houseknecht and Matthews, 1985]. The highest gradient for mean apparent diameter of quartz is east of Hot Springs Village which suggests thermal maturation increases toward the east (see Figure 7).

A simple thermal maturation diagram (Figure 20) presents the range in values for crystallinity and vitrinite reflectance. This diagram compares them with burial by the overlying cumulative thickness. Assuming the Savanna formation and underlying formations were present above the present-day Benton Uplift and then eroded to their present form, temperatures between 200°C - 350°C and would exist below the lower two-thirds of the Jackfork formation. This diagram implies that a stack of thrust sheets did not exist at the regional scale because higher maturation would be expected than observed. An estimated 8-14 km of material has been eroded above the anticlinal structure based on temperature range of 200°C to 350°C. This amount of material removed is in agreement with *Byrnes and Lawyer* [1999] who estimate ~12 km of removed material based on unspecified burial models. Therefore, both illite crystallinity and vitrinite reflectance observed across the Benton Uplift are valid measures of maximum burial depth assuming the cumulative stratigraphic thickness.

5.3 Structural Evolution

Three retrodeformable cross sections perpendicular and one parallel to the antiformal structure (i.e., Benton Uplift) permit the analysis of the regional structures and the progress of deformation (Figures 13-15, 19, 21-24). The model for the structural evolution of the Ouachita orogeny is described as events occurred using the undeformed sections (Figures 21C, 22D, 23D, and 24D). Plots of thermal maturation data (Figures 21A-B, 22B-C, 23B-C, and 24B-C) show the approximate distribution of thermal maturation trends based on the specified values and position on the deformed section. Although shown on the restored sections, Jackfork formation and younger are not present until after the deformation is in progress.

The Ouachita fold and thrust belt started out as a thin-skinned imbricate thrust system of fault-bend folds. Several thrust sheets of Cambrian carbonates through Jackfork formation are stacked as a result of movement on a lower décollement on top of basement. Upper thrust sheets of only Stanley formation through Johns Valley formation form above the upper décollement that lies on the top of the Arkansas Novaculite formation.

This fold and thrust belt is complicated by an out-of-sequence crustal scale basement thrust fault that uplifts basement and deforms the overlying pre-existing imbricate thrust stack. This basement fault dips gradually to the east meaning more is being uplifted from a greater depth as the fault block advances up the ramp. This interpretation explains the increasing thermal maturation toward the east in the metamorphic core. With the part of the Atoka sequence present, a triangle zone forms as

the formations are deformed and translated on a décollement at the top of the Johns Valley formation.

A second crustal scale fault initiated in basement forms an antiformal stack. Displacement on this lower décollement has folded the overlying formations including a wedge of basement into the present-day anticlinal structure. Formation of the crustal-scale antiformal structure was during the Late Devonian (Frasnian) through early Permian (Sakmarian) based on the zircon fission track ages. The displaced hanging wall rotated the Ouachita structures and tilted the stratigraphy so that it dipped to the north.

Table 5 shows the amount of regional shortening for each retrodeformable cross section perpendicular to the anticlinal structure as well as estimate for shortening on several published sections. In comparison to the published sections, our new retrodeformable sections show more shortening in basement, Arkansas Novaculite – Cambrian undivided, and Stanley Formation. There is more shortening in the syntectonic units, Jackfork Formation – Atoka Formation undivided than any of the other units.

We interpret the variation in shortening to be a result the syntectonic units in the Southern Ouachita being deposited on highly distended continental crust because we do not have evidence of turbiditic offshore slope rise sediments [Lowe, 1989]. The origin for the distended continental crust may be explained by an early Paleozoic failed rift system [Lowe, 1985, Figure 8b]. Evidence for a distended continental crust is the periodic input from the south of quartzose, lithic-rich debris to the Ouachita trough during the reactivation and uplift of the Ouachita trough [Lowe, 1989].

6. CONCLUSIONS

We have addressed the largely unknown tectonic history of the Ouachita orogen by presenting an improved 3-dimensional kinematic model using our better constrained retrodeformable sections. The five main conclusions as a result of this project are listed in this section.

1. New crustal-scale retrodeformable cross sections show that a thrust motion on a moderate number of faults can explain all surface and subsurface constraints. While important in places, detachment folds or highly-folded to overturned thrusts are not necessary.
2. A crustal-scale antiform formed below the present-day Benton Uplift from 307 ± 19 Ma to 333 ± 39 Ma based on the zircon fission track ages. The youngest ages are located in the south-southwest whereas the oldest are in the northeast near Hot Springs Village, Arkansas.
3. The maximum temperature calculated from both illite and chlorite crystallinity is $\sim 300^\circ\text{C}$ in the Ouachita orogen, Arkansas.
4. Illite crystallinity is less on the fine clay fraction compared to the coarse clay fraction. While the reason is not known, the coarse clay fraction may have a greater detrital component than the fine clay fraction. If true, the fine clay fraction is more nearly recording the thermal maturation of the Benton Uplift.
5. Regionally, the illite and chlorite crystallinity increases toward the central axis of the Benton Uplift. This increase in crystallinity may be explained by the exhumation of

the rocks from greater depth. There are no data that require either a regional thermal fluid flow event or significant stacking of thrust sheets.

REFERENCES

- Arbenz, J. K. (1989), The Ouachita System, in *The Geology of North America - An Overview, The Geology of North America*, vol. A, edited by A. W. Bally and A. R. Palmer, pp. 371-396, Geol. Soc. Am., Boulder, Colo.
- Arbenz, J. K. (2008), Structural framework of the Ouachita Mountains, in *Stratigraphic and Structural Evolution of the Ouachita Mountains and Arkoma Basin, Southeastern Oklahoma and West-Central Arkansas: Applications to Petroleum Exploration: 2004 Field Symposium*, Circular 112A, edited by N. H. Suneson, pp. 4-40, Okla. Geol. Surv., Norman, Okla.
- Árkai, P. (1991), Chlorite crystallinity: an empirical approach and correlation with illite crystallinity, coal rank, and mineral facies as exemplified by Paleozoic and Mesozoic rocks of northeast Hungary, *J. Metamorph. Geol.*, 9, 723-734.
- Árkai, P., F. P. Sassi, and R. Sassi (1995), Simultaneous measurements of chlorite and illite crystallinity: a more reliable tool for monitoring low- to very low metamorphisms in metapelites. A case study from the Southern Alps (NE Italy), *Eur. J. Mineral.*, 7, 1115-1128.
- Arne, D. C. (1992), Evidence from apatite fission-track analysis for regional Cretaceous cooling in the Ouachita Mountain fold belt and Arkoma Basin of Arkansas, *AAPG Bull.*, 76, 392-402.
- Bass, M. N., and G. Ferrara (1969), Age of the adularia and metamorphism, Ouachita mountains, Arkansas, *Am. J. Sci.*, 267, 491-498.

- Blythe, A. E., A. Sugar, and S. P. Phipps (1988), Structural profiles of Ouachita Mountains, western Arkansas, *AAPG Bull.*, 72, 810-819.
- Brandon, M. T. (2002), Decomposition of mixed grain age distributions using BINOFIT, *On Track*, 24, 13-18.
- Briggs, G., and D. H. Roeder (1975), Sedimentation and plate tectonics, Ouachita Mountains and Arkoma basin, in *Sedimentology of Paleozoic Flysch and Associated Deposits, Ouachita Mountains - Arkoma basin, Oklahoma*, edited by G. Briggs, E. F. McBride, and R. J. Moiola, pp. 1-22, Dallas Geol. Soc., Dallas, Tex.
- Buchanan, R. S., and F. K. Johnson (1968), Bonanza gas field - A model for Arkoma Basin growth faulting, in *A Guidebook to the Geology of the Western Arkoma Basin and Ouachita Mountains, Oklahoma*, edited by L. M. Kline, pp. 75-85, Okla. City Geol. Soc., Okla. City, Okla.
- Bush, W. V., B. R. Haley, C. G. Stone, and J. D. McFarland, III (1977), *Guidebook to the Geology of the Arkansas Paleozoic Area*, Guidebook 77-1, Ark. Geol. Comm., Little Rock, Ark.
- Byrnes, A. P., and G. Lawyer (1999) Burial, maturation, and petroleum generation history of the Arkoma Basin and Ouachita Foldbelt, Oklahoma and Arkansas, *Nat. Resources Research*, 8, 3-26.
- Denison, R. E., W. H. Burke, J. B. Otto, and E. A. Hetherington (1977), Age of igneous and metamorphic activity affecting the Ouachita foldbelt, in *Symposium on the Geology of the Ouachita Mountains; Stratigraphy, Sedimentology, Tectonics, and*

Paleontology, vol. 1, edited by C. G. Stone et al., pp. 25-40, Ark. Geol. Comm., Little Rock, Ark.

Dixon, J. B., and S. B. Weed (Eds.) (1989), *Minerals in Soil Environments, Second Edition*, Soil Soc. of Am., Madison, Wis.

Donelick, R. A., P. B. O'Sullivan, and R. A. Ketcham (2005), Apatite fission-track analysis, in *Low-Temperature Thermochronology: Techniques, Interpretations, and Applications*, *Rev. Mineral. & Geochem.*, vol. 58, edited by P.W. Reiner, and T.A., Ehlers, pp. 49-94, Mineral Soc. of Am., Chantilly, Va.

Flawn, P. T., A., Goldstein, Jr., P. B., King, and C. E., Weaver (1961), *The Ouachita System, Publication 6120*, Univ. of Texas, Austin, Tex.

Frey, M. (1987), Very low-grade metamorphism of clastic sedimentary rocks, in *Low Temperature Metamorphism*, edited by M. Frey, pp. 9-58, Blackie & Son, Glasgow and London, United Kingdom.

Galbraith, R. F. (2005), *Statistics for Fission Track Analysis*, Chapman & Hall/CRC, University College, London, United Kingdom.

Galbraith, R. F., and Green, P. F. (1990) Estimating the component ages in a finite mixture, *Nuc. Tracks and Rad. Meas.*, 17, 197-206.

Galbraith, R.F., and Laslett, G.M. (1993), Statistical models for mixed fission track ages, *Nucl. Tracks*, 21, 459-470.

Godo, T., P. Li, and M. E. Ratchford (2008), Structural and Stratigraphic Analysis of the Shell Rex Timber No. 1-9 Well, Southern Ouachita Fold and Thrust Belt, Clark County, Circular 39A (CD-ROM), Ark. Geol. Surv., Little Rock, Ark.

- Guthrie, J. M., D. W. Houseknecht, and W. D. Johns (1986) Relationships among vitrinite reflectance, illite crystallinity, and organic geochemistry in Carboniferous strata, Ouachita Mountains, Oklahoma and Arkansas, *AAPG Bull.*, 70, 26-33.
- Haley, B. R., E. E. Glick, W. V. Bush, B. F. Clardy, C. G. Stone, M. B. Woodward, and D. L. Zachary (1976), Geologic Map of Arkansas, sheet 1, scale 1:500,000, Ark. Geol. Comm. and U.S. Geol. Surv., Little Rock, Ark.
- Haley, B. R., and C. G. Stone (2006), Geologic Map of the Ouachita Mountain Region and a portion of the Arkansas Valley Region in Arkansas, *DGM-OMR-001*, 1 sheet, scale 1:125,000, Ark. Geol. Surv., Little Rock, Ark.
- Hanawalt, J. D., H. W., Rinn, and L. K. Frevel (1938), Chemical analysis by x-ray diffraction, *Industr. Eng. Chem.*, 10, 457-512.
- Houseknecht, D. W., and S. M. Matthews (1985), Thermal maturity of the Carboniferous strata, Ouachita mountains, *AAPG Bull.*, 69, 335-345.
- Hower, J. (1981), X-ray diffraction identification of mixed-layer clay minerals, in *Short Course in Clay and the Resource Geologist*, edited by F. J. Longstaffe, pp. 39-80, Mineral. Assoc. of Can., Calgary, Alberta, Canada.
- Jackson, M. L. (1956), Soil Chemical Analysis--Advanced Course: Published by the author, Dept. of Soils, Univ. of Wisconsin, Madison, Wis.
- Keller, W. D., C. G. Stone, and A. L. Hoersch (1985), Textures of Paleozoic chert and novaculite in the Ouachita Mountains of Arkansas and Oklahoma and their geological significance, *Geol. Soc. Am. Bull.*, 96, 1353-1363.

- Kisch, H. J. (1987), Correlation between indicators of very low-grade metamorphism, in *Low Temperature Metamorphism*, edited by M. Frey, pp. 227-304, Blackie & Son, Glasgow and London, United Kingdom.
- Kisch, H. J. (1990), Calibration of the anchizone: a critical comparison of illite 'crystallinity' scales used for definition, *J. Metamorph. Geol.*, 8, 31-46.
- Kisch, H. J. (1991), Illite crystallinity: recommendations of sample preparation, x-ray diffraction settings, and interlaboratory samples, *J. Metamorph. Geol.*, 9, 665-670.
- Kruger, J. M. (1983), Regional anomalies in the Ouachita system and adjacent areas, M.S thesis, Dept. of Geophysics, Univ. of Texas, El Paso, Tex.
- Kruger, J. M., and G. R. Keller (1986), Interpretation of regional gravity anomalies in the Ouachita Mountains area and adjacent Gulf coastal plain: *AAPG Bull.*, 70, 667-689.
- Krumm, H. (1984), Anchimetamorphose im Anis und Ladin (Trias) der Nordlichen Kalkalpen zwischen Arlberg und Kaisergebirge-ihre Verbreitung und ihre baugeschichtliche Bedeutung, *Geol. Rundsch*, 73, 223-257.
- Kübler, B. (1967), La cristallinité de l'illite et les zones tout a fait supérieures du métamorphisme, in *Colloque sur les étages tectoniques*, edited by J. P. Schaer, pp. 105-122, Á la Baconnière, Neuchâtel, Switzerland.
- Kübler, B. (1968), Évaluation quantitative du métamorphisme par la cristallinité de l'illite: *Bull. Centre Rech. Pau-SPNA*, 2, 385-397.

- Kübler, B., and M. Jaboyedoff (2000), Crystallinity of illite. Le POINT SUR... (Illite crystallinity concise review paper), *Comptes Rendus de l'Académie des Sciences-Series IIA-Earth and Planetary Science*, 331, 75-89.
- Lillie, R. J., K. D. Nelson, B. de Voogd, J. A. Brewer, J. E. Oliver, L. D. Brown, S. Kaufman, and G. W. Viele (1983), Crustal structure of Ouachita Mountains, Arkansas: A model based on integration of COCORP reflection profiles and regional geophysical data, *AAPG Bull.*, 67, 907-931.
- Lock, J. and S. Willett (2008), Low-temperature thermochronometric ages in fold-and-thrust belts, *Tectonophysics*, 456, 147-162.
- Lowe, D. R. (1985), Ouachita trough: Part of a Cambrian failed rift system, *Geology*, 13, 790-793.
- Lowe, D. R. (1989), Stratigraphy, sedimentology, and depositional setting of pre-orogenic rocks of the Ouachita Mountains, Arkansas and Oklahoma, in *The Appalachian-Ouachita Orogen in the United States: Boulder, Colorado, Geological Society of America, The Geology of North America*, v. F-2, edited by R. D. Hatcher, Jr., W. A. Thomas, and G. W. Viele, pp. 695-728, Geol. Soc. Am., Boulder, Colo.
- Ludwig, K.R. (2003), *Isoplot 3.0: A Geochronological Toolkit for Microsoft Excel*, Berkeley Geochron. Cent. Special Publication No. 4, Berkeley, Calif.
- McCamey, K., and R. P. Meyer (1966), Crustal results of fixed multiple shots in the Mississippi embayment, in *The Earth Beneath the Continents: Am. Geophys. Monogr. Ser.*, no. 10, edited by J. S. Steinhardt, and T. J. Smith, pp. 370-381, AGU, Washington D.C.

- McMurdie, H. F., M. C. Morris, E. H. Evans, B. Paretzkin, W. Wong-Ng, and C. R. Hubbard (1986), Methods of producing standard x-ray patterns, *Powder Diffraction*, v.1, 40-43.
- Meunier, A., and B. Velde (2004), *Illite: Origins, Evolution, and Metamorphism*, Springer-Verlag, Berlin, Germany.
- Merriman, R. J., and D. R. Peacor (1999), Very low-grade metapelites: mineralogy, microfabrics and measuring reaction progress in *Low-Grade Metamorphism*, edited by M. Frey and D. Robinson, pp. 61-107, Blackwell Science, Cambridge, Great Britain.
- Merriman, R. J., and M. Frey (1999), Patterns of very low-grade metamorphism in metapelitic rocks in *Low-Grade Metamorphism*, edited by M. Frey and D. Robinson, pp. 61-107, Blackwell Science, Cambridge, Great Britain.
- Mitchell, B. J., and M. Landisman (1970), Interpretation of a crustal section across Oklahoma, *Geol. Soc. Am. Bull.*, 81, 2647-2656.
- Moore, D. M., and R. C. Reynolds, Jr. (1997), *X-ray Diffraction and the Identification and Analysis of Clay Minerals*, Oxford University Press, New York, N. Y.
- Morris, R. C. (1989), Stratigraphy and sedimentary history of post-Arkansas Novaculite Carboniferous rocks of the Ouachita Mountains, in *The Appalachian-Ouachita Orogen in the United States: Boulder, Colorado*, Geological Society of America, *The Geology of North America*, v. F-2, edited by R. D. Hatcher, Jr., W. A. Thomas, and G. W. Viele, pp. 591-602, Geol. Soc. Am., Boulder, Colo.

- Nelson, K. D., R. J. Lillie, B. Voogd, J. A. Brewer, J. E. Oliver, S. Kaufman, and L. Brown (1982), COCORP seismic reflection profiling in the Ouachita mountains of western Arkansas: Geometry and geologic interpretations, *Tectonics*, *1*, 413-430.
- Nielson, K. C., G. W. Viele, and J. Zimmerman (1989), Structural setting of the Benton-Broken Bow uplifts, in *The Appalachian-Ouachita Orogen in the United States: Boulder, Colorado, Geological Society of America, The Geology of North America*, v. F-2, edited by R. D. Hatcher, Jr., W. A. Thomas, and G. W. Viele, pp. 591-602, Geol. Soc. Am., Boulder, Colo.
- Pevear, D. R. (1999) Illite and hydrocarbon exploration, *Pro. Natl. Acad. Sci.*, *96*, 3440-3446.
- Schaer, J. P., and F. Persoz (1976), Aspects structuraux et petrographiques du Haut-Atlas calcaire de Midelt (Maroc): *Bull. Soc. Geol. France*, *18*, 1239-1250.
- Shelton, K. L., J. M. Reader, L. M. Ross, G. W. Viele, and D. E. Seidemann (1986), Barich adularia from the Ouachita Mountains, Arkansas: Implications for a postcollisional hydrothermal system: *Am. Mineral.*, *71*, 916-923.
- Smykatz-Kloss, W., and E. Althaus (1974), Experimental investigation of the temperature dependence of the "crystallinity" of illites and glauconites, *Bull. Groupe Francais des Argiles*, *26*, 319-325.
- Spötl, C., D. W. Houseknecht, R. Jaques (1993) Clay mineralogy and illite crystallinity of the Atoka formation, Arkoma Basin, and Frontal Ouachita Mountains, *Clay and Clay Minerals*, *41*, 745-754.

- Środoń, J. (1980), Precise identification of illite/smectite interstratifications by x-ray powder diffraction, *Clays and Clay Minerals*, 28, 401-411.
- Stewart, S. W. (1968), Crustal structure in Missouri by seismic refraction methods, *Bull. Seis. Soc. Am.*, 58, 291-323.
- Thomas, W. A. (1977), Structural and stratigraphic continuity of the Ouachita and Appalachian mountains, in *Symposium on the Geology of the Ouachita Mountains; Stratigraphy, Sedimentology, Tectonics, and Paleontology*, vol. 1, edited by C. G. Stone et al., pp. 9-24, Ark. Geol. Comm., Little Rock, Ark.
- Viele, G. W. (1974), Structure and tectonic history of the Ouachita Mountains, Arkansas, in *Gravity and Tectonics*, edited by K. De Jong, and R. Scholten, John Wiley, New York, N. Y.
- Viele, G. W. (1979), Geologic map and cross section, eastern Ouachita Mountains, Arkansas: map summary, *Geol. Soc. Am. Bull.*, 90, 1096-1099.
- Viele, G. W., and W. A. Thomas (1989), Tectonic synthesis of the Ouachita orogenic belt, in *The Appalachian-Ouachita Orogen in the United States: Boulder, Colorado*, Geological Society of America, *The Geology of North America*, v. F-2, edited by R. D. Hatcher, Jr., W. A. Thomas, and G. W. Viele, pp. 695-728, Geol. Soc. Am., Boulder, Colo.
- Woods, R. D., and J. W. Addington (1973), Pre-Jurassic geologic framework northern Gulf basin, *Gulf Coast Assoc. Geol. Soc. Trans.*, 23, 92-108.
- Woollard, G., and H. Joesting (1964), Bouguer gravity anomaly map of the United States, scale 1:2,500,000, U.S. Geol. Surv., Washington D. C.

Zietz, I. (1981), Preliminary composite magnetic anomaly map of the conterminous United States, Open-File Report 81-1132, U.S. Geol.Surv., Washington D. C.

APPENDIX A
FIGURES/TABLES

Table 1. Sample attributes

Sample	Latitude (°N)	Longitude (°W)	Elevation ^a (m)	Formation(s) ^b	Rock type Collected ^c	Analysis ^d
ARM-1	34.478615	-93.116110	147.00	Stanley	Sh	Cr
ARM-5	34.511394	-93.206393	141.00	Stanley	Sh	Cr
ARM-6	34.514999	-93.383061	199.00	Blakely	Sh	Cr
ARM-7	34.563613	-93.668333	200.00	Womble	Sh	Cr
ARM-8	34.389444	-93.608616	203.00	Missouri Mtn, Polk Creek, & Blaylock	Sh	Cr
ART-2	34.485835	-93.087226	170.00	Stanley	Sst	Cr, ZFT
ART-3	34.633614	-93.058337	223.00	Womble	Sst	Cr, ZFT
ART-4	34.678056	-93.072505	229.00	Collier	Sst	ZFT
ART-5	34.777774	-93.098888	339.00	Stanley	Sst	Cr
ART-6	34.849999	-93.096666	189.00	Jackfork	Sst	Cr
ART-8	34.514999	-93.383061	199.00	Missouri Mtn, Polk Creek, & Blaylock	Sst	ZFT
ART-9	34.524444	-93.401671	235.00	Crystal Mountain	Sst	Cr, ZFT
ART-12	34.650554	-93.532779	182.00	Bigfork	Sst	Cr, ZFT
ART-15	34.757782	-93.492504	309.00	Jackfork	Sst	Cr
ART-16	34.499168	-93.688329	298.00	Crystal Mountain	Sst	ZFT
ART-18	34.343611	-93.560001	195.00	Stanley	Sst	Cr, ZFT
ART-19	34.364447	-93.863334	367.00	Missouri Mtn, Polk Creek, & Blaylock	Sst	Cr
Chung	34.563324	-93.674969	211.00	Womble	Sis/Sst	Cr, ZFT
Mt. Blakely	34.572165	-93.196600	182.00	Blakely	Sst	Cr, ZFT

^aElevation determined from USGS 30 m digital elevation model.

^bFormation from 'Geologic Map of the Ouachita Mountain Region and a portion of the Arkansas Valley Region in Arkansas' [Haley and Stone, 2006]

^cSh = Shale; Sst = Sandstone; Sis = Siltstone.

^dCr = 'Crystallinity' analysis of illite and/or chlorite; ZFT = Zircon fission track analysis.

Table 2. Zircon Fission Track Ages External Detector Method

Sample	No. of grains	Track Density (x 10 ⁶ tr cm ⁻²)			Age Dispersion	Central Age (Ma)
		ρ_s (N _S)	ρ_i (N _i)	ρ_d (N _d)	(P χ^2)	($\pm 1\sigma$)
Chung (b)	6	21.81 (684)	2.296 (72)	0.5649 (3615)	<0.01% (95.0%)	317.0 \pm 40.7
Mt. Blakely	17	20.95 (3191)	1.825 (278)	0.5664 (3625)	25.9% (0.01%)	342.3 \pm 33.0 (mixed age)
ART-2	20	21.16 (3548)	2.254 (378)	0.5634 (3605)	<0.01% (99.9%)	312.5 \pm 19.9
ART-3	8	15.71 (885)	1.563 (88)	0.5619 (3596)	<0.01% (99.8%)	333.4 \pm 38.9
ART-4	11	19.61 (2749)	1.755 (246)	0.5604 (3586)	14.8% (14.5%)	361.9 \pm 31.8 (mixed age)
ART-8 (b)	7	31.53 (1998)	3.188 (202)	0.5589 (3577)	<0.01% (99.3%)	326.3 \pm 26.4
ART-9	17	17.77 (2855)	1.386 (213)	0.5573 (3567)	29.8% (0.13%)	412.8 \pm 44.4 (mixed age)
ART-12	6	30.02 (903)	2.959 (89)	0.5558 (3557)	<0.01% (87.8%)	332.7 \pm 38.6
ART-16	18	21.59 (3882)	1.779 (320)	0.5543 (3548)	6.6% (43.1%)	393.9 \pm 27.2 (mixed age)
ART-18	20	16.19 (3927)	1.723 (418)	0.5528 (3538)	<0.01% (99.9%)	307.0 \pm 18.8

Explanation: a, density of spontaneous tracks and number counted; b, density of induced tracks and number counted; c, density of tracks and number counted on dosimeter glass (IRMM 541); d, Age dispersion is the measure of the variability of ages based on the population standard deviation of values of $\log(\rho_s/\rho_i)$. $P\chi^2$ is the probability of obtaining a χ^2 value for ν degrees of freedom where $\nu = \text{no. of crystals} - 1$. The higher the probability the more likely the values represent a common value; e, Central age is an estimated age of the random effects model where the different grain ages represent a population [Galbraith and Laslett, 1993; Galbraith, 2005].

Table 3. Statistics for Zircon Fission Track Analyses External Detector Method.

	a	b	c	d	e	f	g	h	i	j		k	l	m	n	o	p
Sample	Pooled Ratio	± 1 S.E.	Mean Ratio	± 1 S.E.	Pooled Age (Ma)	± 1 S.E. (Ma)	Mean Crystal Age (Ma)	± 1 S.E. (Ma)	Binomial Age (Ma)	" +95% "	" -95% "	Central Age ^a (Ma)	± 1 S.E. (Ma)	Age Dispersion	Chi-squared	Degrees of freedom	P (Chi-Sq)
ART-2	9.3862	0.5966	9.2429	0.2534	312.50	19.86	307.84	8.64	312.83	34.60	31.17	312.50	19.86	0.00	4.262	19	99.98
ART-3	10.0568	1.1731	10.2508	0.3828	333.39	38.89	339.66	13.01	334.87	82.31	65.95	333.39	38.89	0.00	0.699	7	99.83
ART-4	11.1748	0.8320	11.3610	1.3086	368.45	27.43	374.42	44.25	369.03	50.79	44.62	361.86	31.76	14.84	14.660	10	14.50
ART-8	9.8911	0.8015	9.8365	0.2411	326.33	26.44	324.57	8.15	326.96	50.55	43.77	326.33	26.44	0.00	0.766	6	99.30
ART-9	13.4038	1.0521	15.5106	2.7989	437.14	34.31	503.23	93.76	437.90	64.35	56.04	412.78	44.41	29.76	38.462	16	0.13
ART-12	10.1461	1.1771	10.6508	0.7498	332.72	38.60	348.83	25.18	334.18	81.58	65.45	332.72	38.60	0.00	1.784	5	87.81
ART-16	12.1313	0.8138	12.5364	0.9379	394.82	26.48	407.59	31.40	395.28	46.95	41.94	393.86	27.20	6.62	17.351	17	43.08
ART-18	9.3947	0.5765	9.2894	0.2367	307.03	18.84	303.67	7.92	307.32	32.23	29.19	307.03	18.84	0.00	4.140	19	99.99
Chung	9.5000	1.2189	9.3619	0.5468	317.02	40.68	312.52	18.68	318.76	88.37	69.05	317.02	40.68	0.00	1.145	5	95.01
Mt. Blakely	11.4784	0.8134	11.3437	1.8670	382.11	27.08	377.75	63.72	382.63	49.18	43.56	342.33	32.98	25.92	45.107	16	0.01

Explanation: a, estimated age using N_s/N_i ; b, standard error (see text); c, Average N_s / average N_i ; d, standard error (see text); e, average age from all individual grain ages; f, standard error (see text); g, estimated age from arithmetic mean of individual ratios of spontaneous to induced tracks; h, standard error (see text); i, estimated age using a binomial peak-fitting equation; j, estimated interval in which the true age lies 95% of the time; k, estimated age assuming the random effects model that has a symmetrical distribution; k, standard error (see text); m, population standard deviation; n, probability that the data are related to a similar data set; o, number of values the chi-squared is allowed to statistically vary; p, probability of obtaining a sample as extreme as the one observed.

Table 4. Zircon Fission Track Ages LA-ICP-MS

	a	b	c	d	e	f	g	h	i	j	
Sample	A2Z Sample Number	Grains (dmnls)	N _s (tracks)	Area Analyzed (cm ² x 10 ⁻⁵)	Σ(PΩ) (cm ² x10 ⁻⁵)	1σ Σ(PΩ) (cm ² x 10 ⁻⁵)	ζ _{MS} ±1σ	²⁹ Si (zircon) bkg:sig (x 10 ⁻²) (dmnls)	²³⁸ U bkg:sig (x 10 ⁻²) (dmnls)	Pooled Fission-Track Age ± 1 σ (Ma)	Chi-squared
Lake Ouachita 41	9161a	20	1466	8.83	0.847	0.00339	7.2123±0.23	9.69	4.17	596+/- 24	73.1
Lake Pineda	963-1	20	1060	9.66	1.00	0.00382	8.4817±0.27	7.87	4.01	433+/- 19	-

Abbreviations: dmnls, dimensionless; bkg:sig, background:signal. Explanation: a, Apatite to Zircon, Inc.; b, number of spontaneous tracks; c, area studied; d, area weighted ²³⁸U/⁴³CaF, e, standard deviation of area weighted ²³⁸U/⁴³Ca; f, ζ_{MS} = calibration factor based on LA-ICP-MS of fission-track age standards; g, background of ²⁹Si; h, background of ²³⁸U; i, pooled fission track age with one standard deviation; j, probability that the data are related to a similar data set.

Table 5. Estimated Regional Shortening in the Ouachita orogen^a

Formation	Retrodeformable Sections			<i>Nelson et al.</i> [1982]	<i>Blythe et al.</i> [1988]	<i>Viele and Thomas</i> [1989]	<i>Arbenz</i> [2008]
	B-B'	C-C'	D-D'				
Jackfork-Atoka, undivided	58 (35.3)	26.5 (19.1)	-	45 (34.4)	35 (27.3)	<5 (<2.3)	35 26.5
Stanley	59 (35.9)	18 (13.1)	{ 10 (8.2)	<5 (<3.8)	<5 (<3.9)	15 (6.8)	<5 (<3.8)
Arkansas Novaculite – Cambrian, undivided	38 (23.0)	31.5 (22.7)		5 (3.8)	47 (36.6)	<5 (<2.3)	<5 (<3.8)
Basement	38 (23.2)	37 (26.8)	37 (30.1)	10 (7.6)	12 (9.3)	<5 (<2.3)	<5 (<3.8)

^aShortening values are given in km. Percent shortening is provided in parenthesis for each. See text for further explanation.

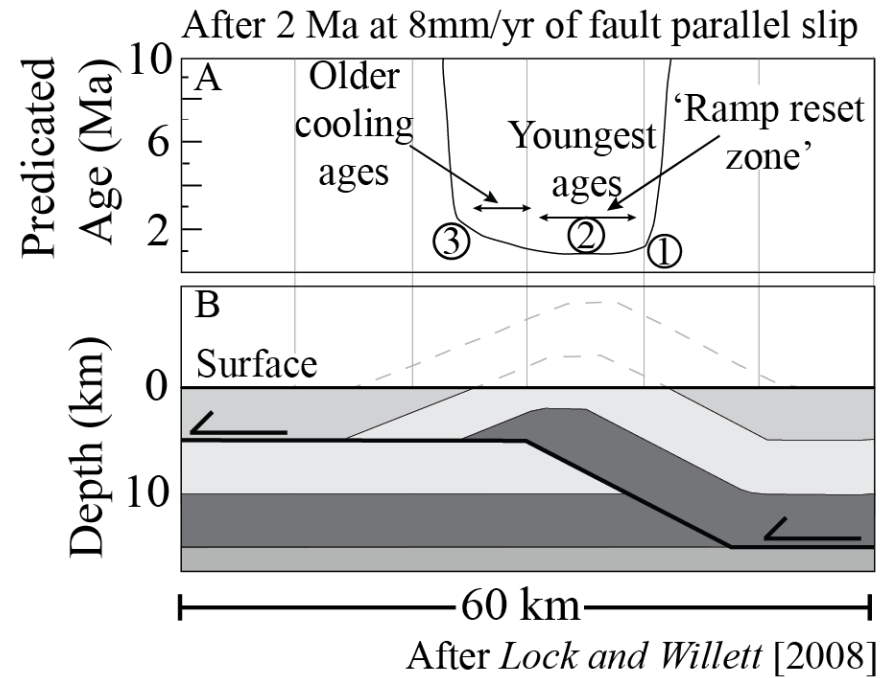


Figure 1. Lock and Willett [2008] model for expected thermochronologic ages for apatite fission track ages above an eroding fault-bend fold using the dimensions and properties of the Taiwan foreland fold and thrust belt. A: Apatite fission track cooling ages measured from surface rocks. B. Simple fault bend fold model. See text for discussion.

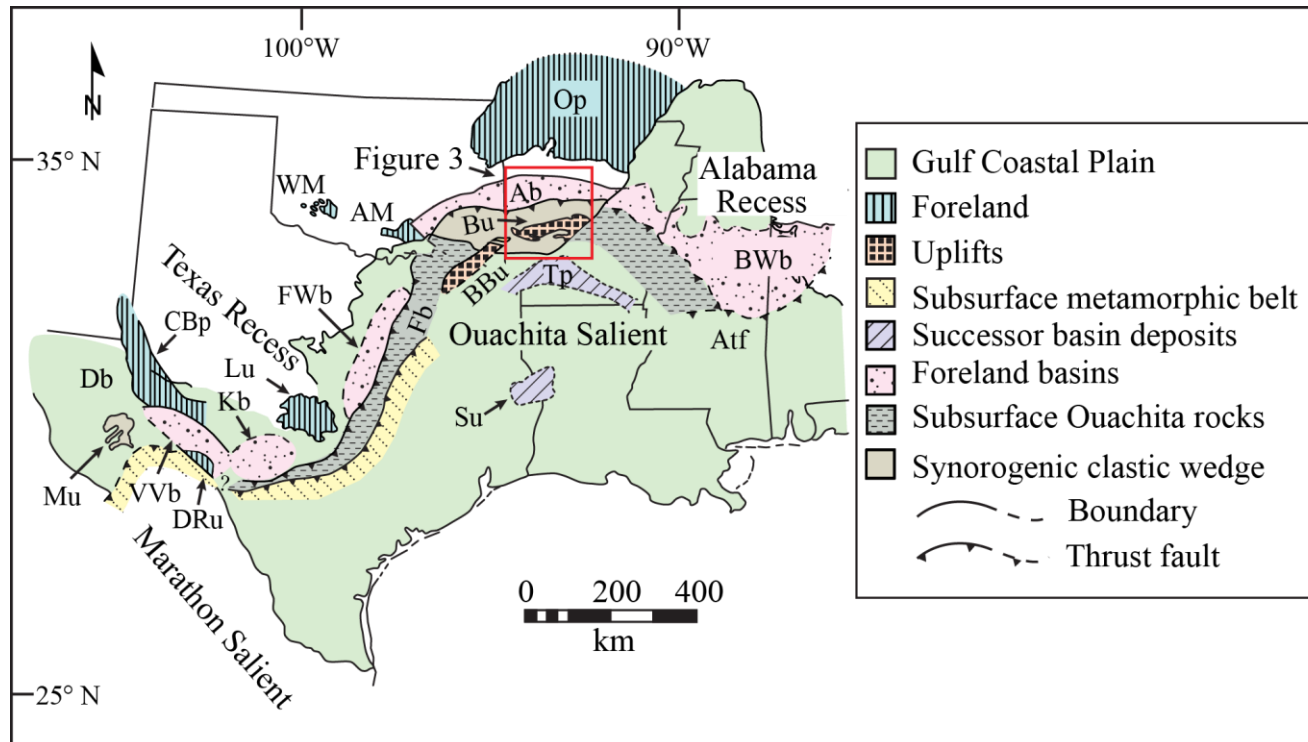


Figure 2. Tectonic overview map for the southern margin of North America (modified from *Viele and Thomas* [1989]).

Abbreviations -- AtF- Appalachian tectonic front; Fb - Frontal belt; Basins: Ab - Arkoma, BWb - Black Warrior, Db -

Delaware, FWb - Fort Worth, Kb - Kerr, VVb - Val Verde; Platforms: CBp - Central Basin, Op - Ozark, Tp - Texarkana;

Mountains: AM - Arbuckle, WM - Wichita; Uplifts: BBU - Broken Bow, Bu - Benton, DRu - Devil's River, Lu - Llano, Mu -

Marathon, Su - Sabine.

Figure 3. A. Geologic setting of western Arkansas with sample and section locations.

Well identifications: W1, Arkla #1 Ford Estate; W2, Arkansas - Louisiana Gas #1 John Weeks; W3, Malka Prod. #1 - 31 Hefley; W4, Mobil Oil #1 C. E. Isom; W5, Pacific Oil and Gas #1 Plez Garner; W6, El Paso Natural Gas #1 Chessman; W7, W8, Shell E&P Rex Timber #1-9; Chevron #1 Cabe [*Viele*, 1979; Kruger, 1983; *Godo et al.*, 2008].

Industry seismic is from Shell's Moccasin prospect [*Godo et al.*, 2008]. Sections AA', BB', CC' and DD' are shown in Figures 13 through 23.

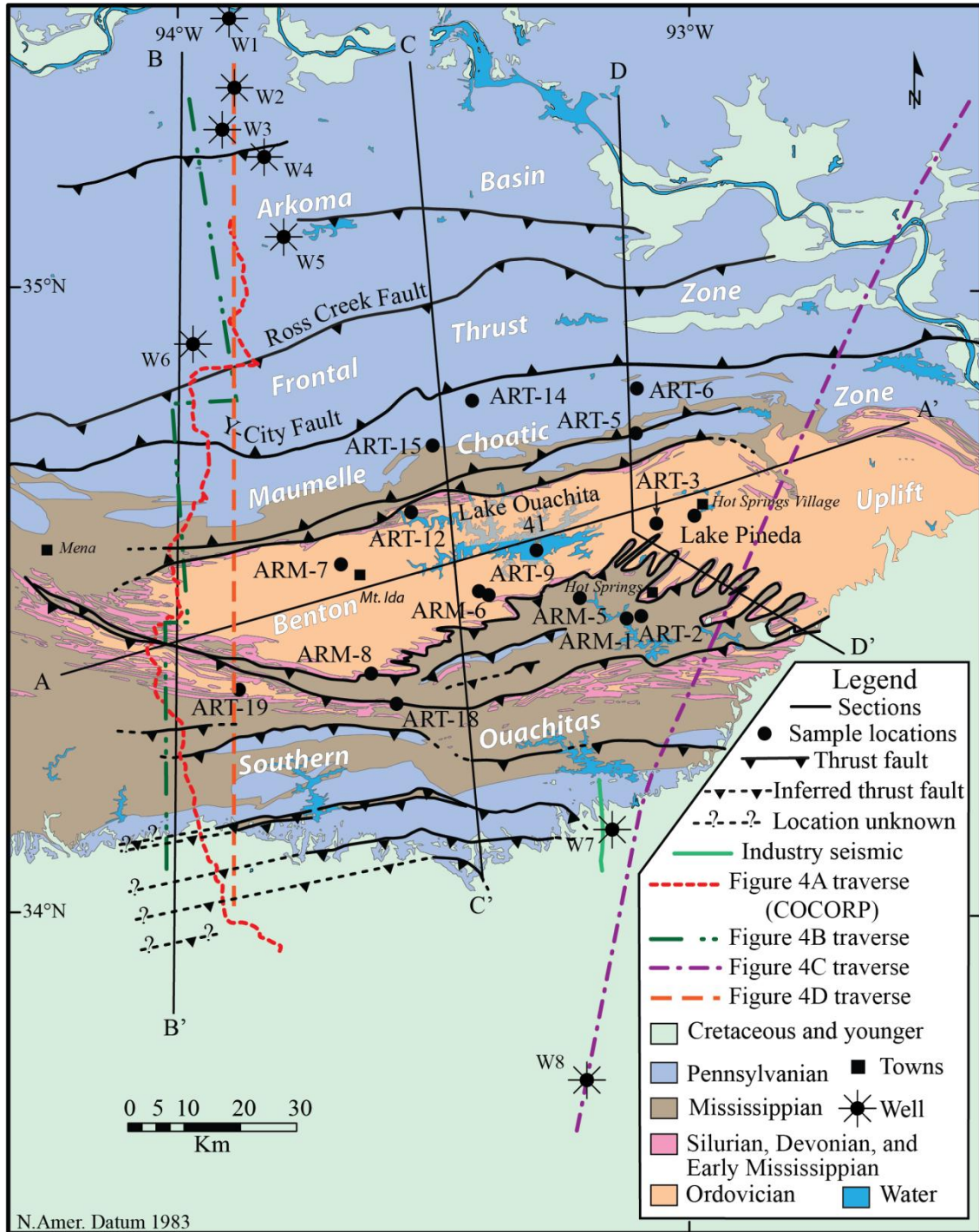


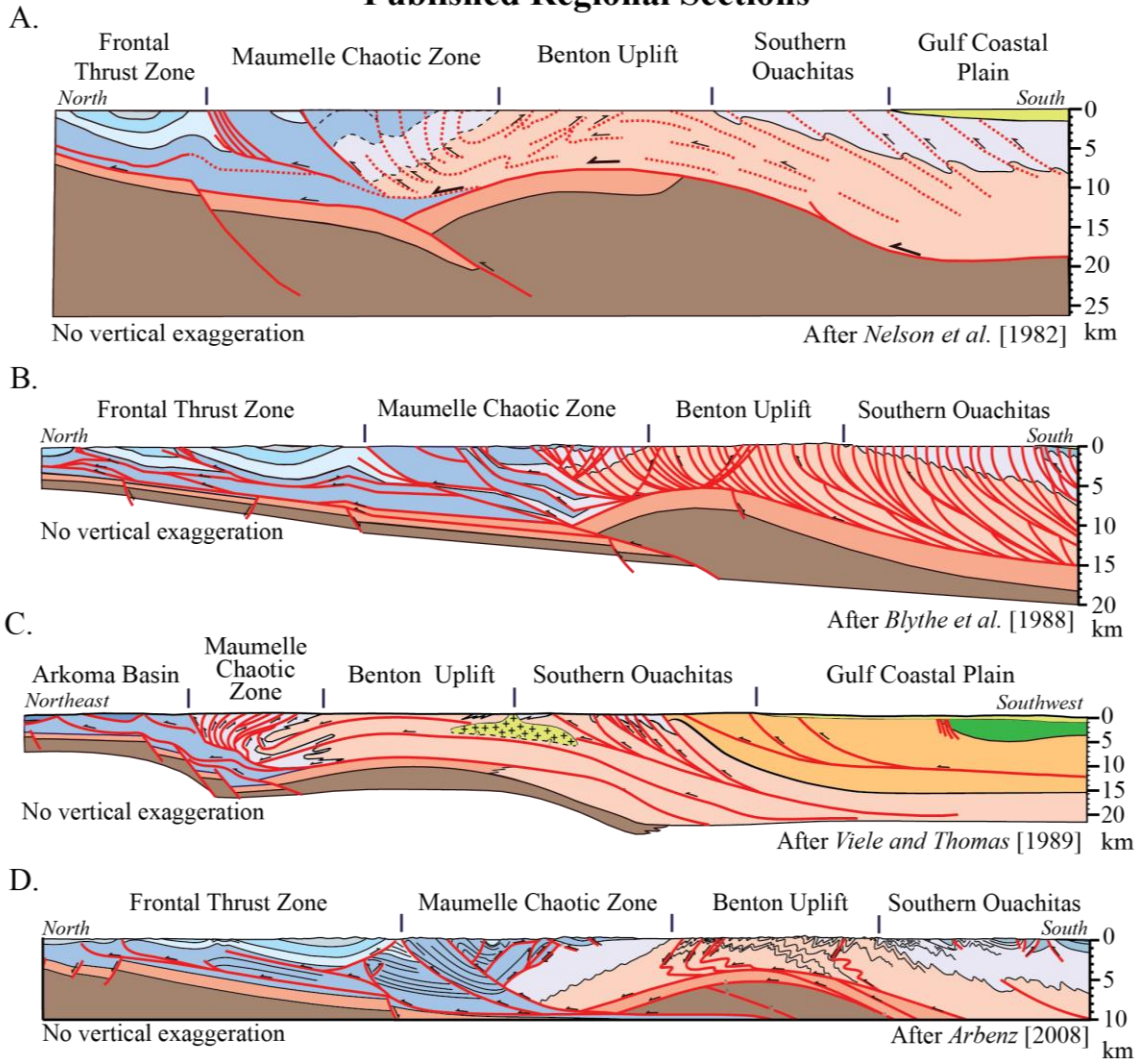
Figure 4. Simplified central Ouachita stratigraphy. Cumulative stratigraphic thickness is computed assuming the Savanna Formation is top of stratigraphic section. Section thickness is the average thickness used to construct the cross sections. The thickness range is compiled from *Flawn et al.* [1961]; *Briggs et al.* [1975]; *Thomas* [1977]; *Lowe* [1989]; *Viele and Thomas* [1989]; *Haley and Stone* [2006]; *Arbenz* [2008]. The lithology of the Cambrian is based on the formation top from industry wells [*Kruger*, 1983]. Bottom legend provides description of thin units.

Age	Formation	Thickness (m)		Description	
		Sections	Range		
Pennsylvanian	Savanna	480	194-480	Shale, sandstone, and coal.	
	McAlester	690	210-690	Shale, sandstone, and coal.	
	(A) unconformity				
	Atoka	Upper	1500	1140-3729	Shale and sandstone.
	Atoka	Middle	1200	858-1860	Shale and minor sandstone.
	Atoka	Lower	1500	1650-4800	Shale.
	Johns Valley	450	60-484	Shale with exotic boulders.	
Mississippian	Jackfork	2000	350-2250	Sandstone and shale.	
	Stanley	2100	300-3600	Shale to slate with interlayered sandstone, siltstone, and minor tuff.	
Ordovician	(B)				
	Bigfork	200	135-285	Chert and shale.	
	Womble	500	73-1050	Shale to phyllite.	
	(D)				
	Mazarn	500	300-1050	Shale.	
Cambrian, undivided	(E)				
	Collier	280	22-475	Shale.	
	500	Unknown	Carbonates (not exposed in Ouachitas).		
Pre-Cambrian	Varies	Unknown	Not exposed.		

Legend for Thin Units				
Symbol	Formation	Thickness (m)		Description
		This study	Range	
(A)	Hartshorne	150	15-165	Sandstone.
(B)	Arkansas Novaculite	100	18-297	Novaculite and shale.
(C)	Missouri Mtn., Polk Creek, and Blaylock, undivided (Silurian)	65 - 135	0-627	Shale and sandstone.
(D)	Blakely	140	0-180	Shale, sandstone, and minor limestone.
(E)	Crystal Mtn.	190	15-300	Sandstone with minor shale.

Figure 5. Previous regional cross section, located on Figure 2. A. *Nelson et al.* [1982]. Dashed red lines show geometry of structures and possible thrust faults inferred from seismic reflections. Formation abbreviations: K, Cretaceous undivided; IPhs - IPm, Hartshorne and McAlester undivided; IPau, Upper Atoka; IPam, Middle Atoka; IPj - IPal, Jackfork, Johns Valley, and Lower Atoka undivided; Ms - Stanley, MDSO - Arkansas Novaculite, Missouri Mtn., Polk Creek, Blaylock, Bigfork, Womble, Blakely, Mazarn, Crystal Mtn., and Collier; C, Cambrian; PC, Pre-cambrian. B. *Blythe et al.* [1988]. Smaller faults in the Benton Uplift and Southern Ouachitas have not been represented at this scale. Red lines with arrows are thrust faults and motion direction, respectively. C. *Viele and Thomas* [1989]. Formation abbreviations: Ki, Cretaceous intrusive; P, Permian undivided; IPam-IPau, Middle Atoka and Upper Atoka undivided. D. *Arbenz* [2008]. Gray contacts outline the geometry of structures.

Published Regional Sections



Key for sections:
A, B, and D

Cretaceous	K
Pennsylvanian	IPhs-IPm
	IPau
	IPam
Mississippian	IPj-IPal
Mississippian	Ms
Mississippian, Devonian, Silurian, and Ordovician	MDSO
Cambrian	€
Pre-cambrian	PC

Key for section:
C

Cretaceous	K
	✱Ki✱
Permian	P
Pennsylvanian	IPam-IPau
	IPj-IPal
Pennsylvanian-Mississippian	Ms-IPal
Mississippian	Ms
Mississippian, Devonian, Silurian, and Ordovician	MDSO
Cambrian	€
Pre-cambrian	PC

Figure 6. A. - C., scanning electron microphotographs (SEM) of sample ART-6, Pennsylvanian Jackfork Formation. See Figure 2 for location. The sub-rounded edges on several illite flakes in C indicate these grains are detrital. D. X-Ray diffraction pattern for the coarse clay fraction of ART-6. Identification of minerals based on peak positions. Peak abbreviations: S001, $d(001)$ smectite; C001, $d(001)$ chlorite; I/S, illite and smectite interlayered; C002, $d(002)$ chlorite; I002, $d(002)$ illite; C003, $d(003)$ chlorite; Q100, $d(100)$ quartz; C004, $d(004)$ chlorite; I003 + Q101, $d(003)$ illite and $d(101)$ quartz overlapping peaks; S005, $d(005)$ smectite; C005, $d(005)$ chlorite; E. - G., Energy-dispersive X-ray spectrograms (EDS) for sample ART-6. The main clay minerals are Fe-rich chlorite and illite. Locations of analyses are given in A. - C as lowercase letters. Location a on A., ART_1_02a. Location a on A., ART_1_02b. Location b on B., ART6_2_01a. Location c on C, ART6_2-03a. See text for further explanation.

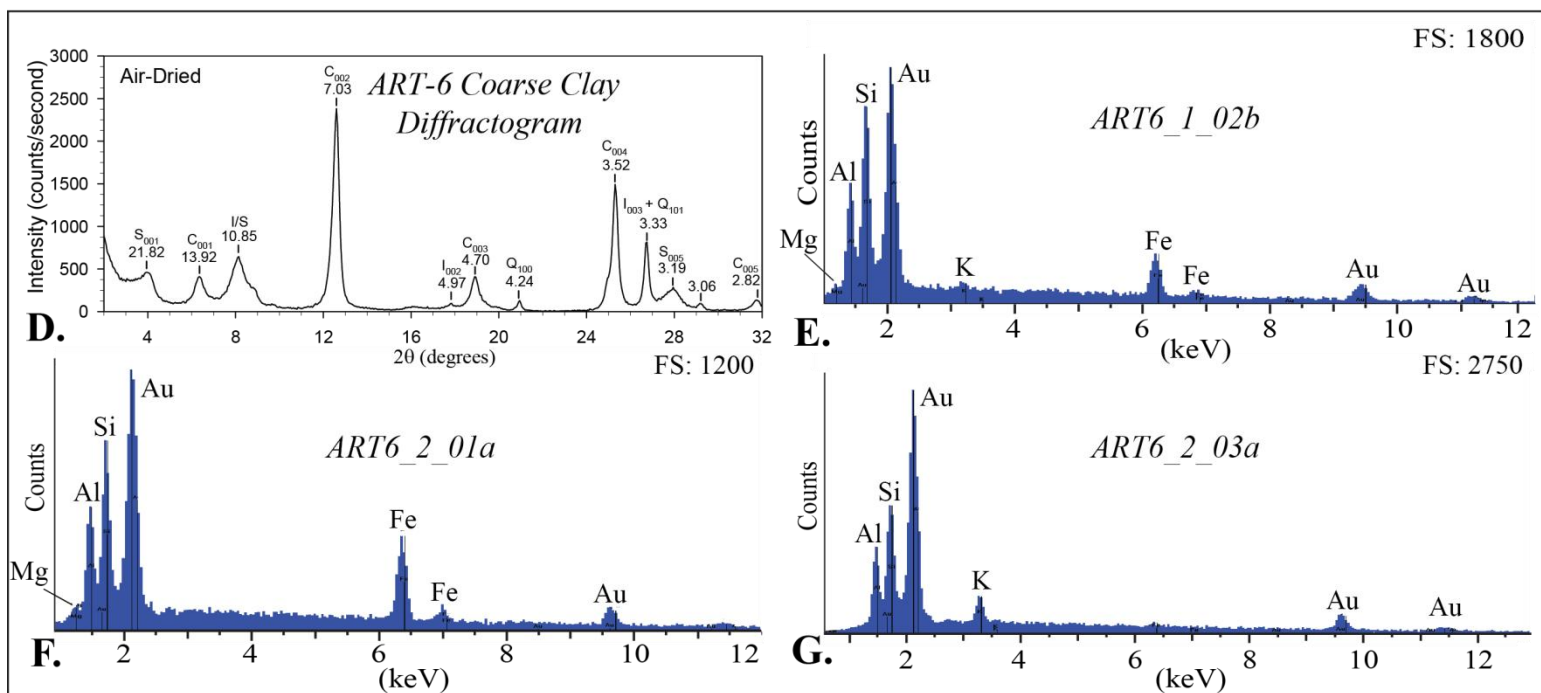
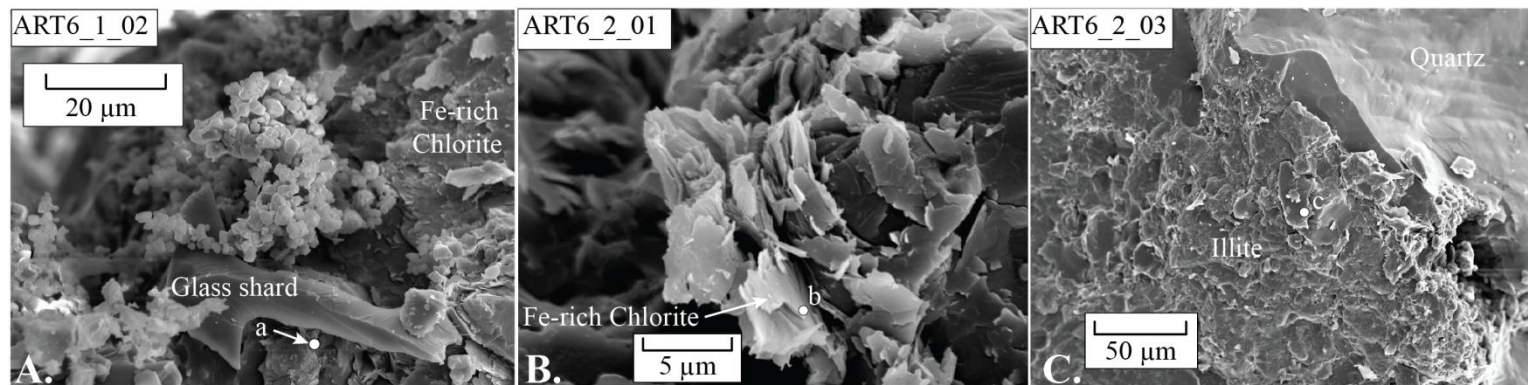
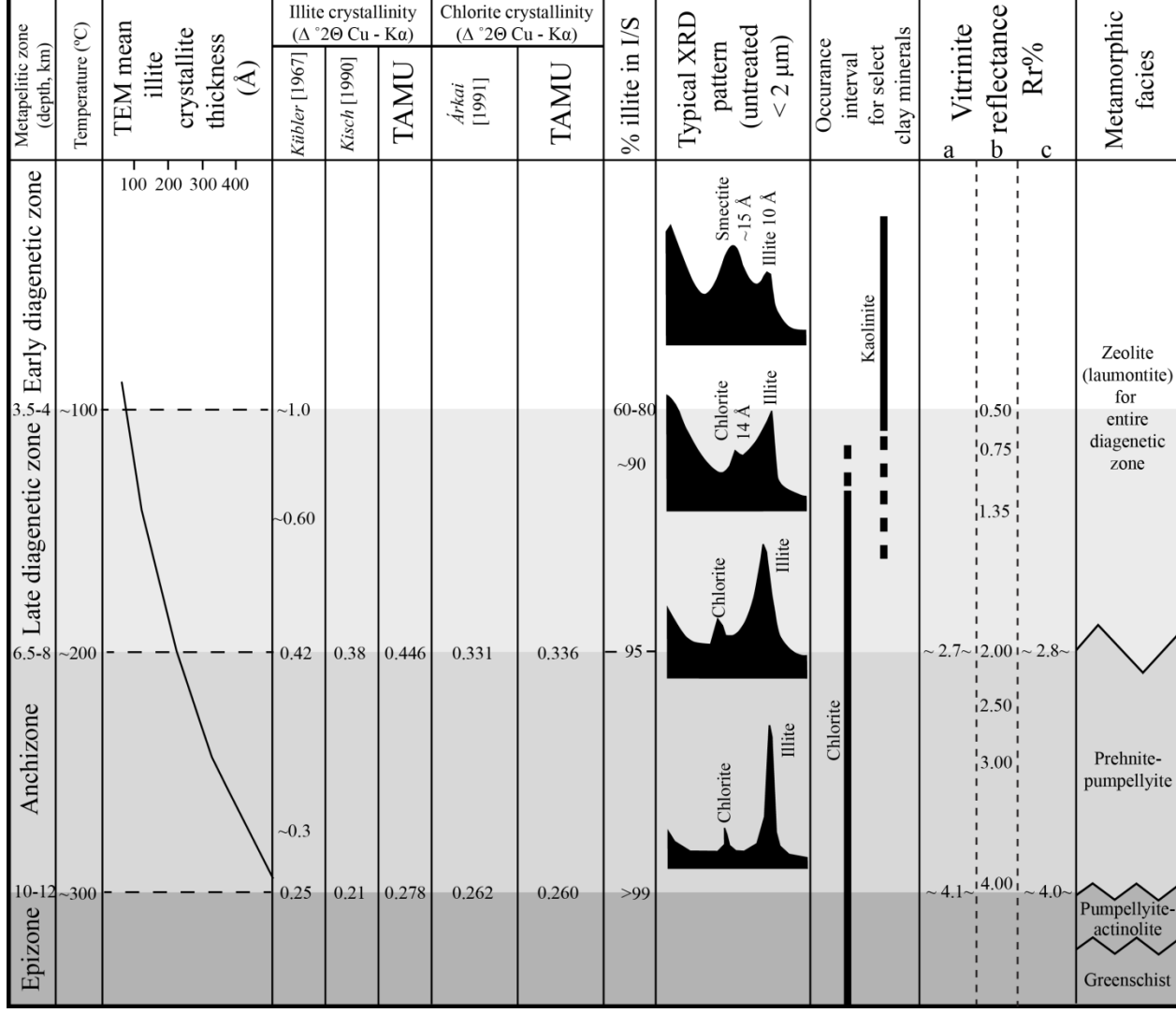
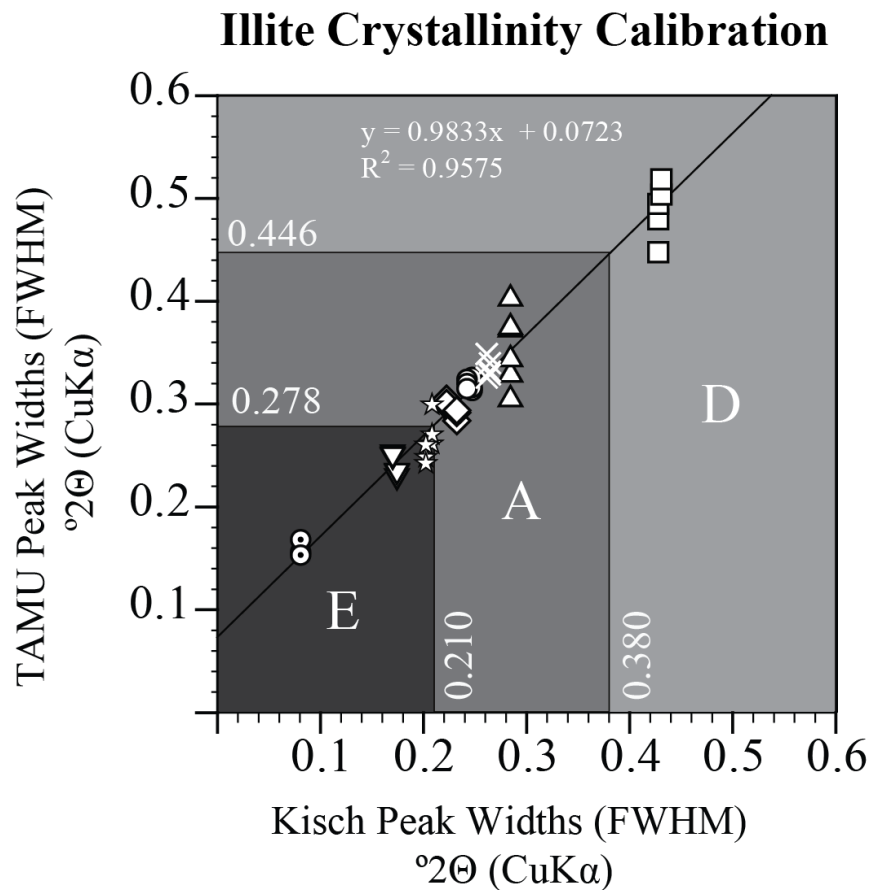


Figure 7. Metapelitic zones and thermal correlation diagram. Values for chlorite crystallinity are for the $d(002)$ peak.

Compiled from *Árkai* [1991], *Merriman and Frey* [1999], *Merriman and Peacor* [1999], and *Kübler and Jaboyedoff* [2000].

Vitrinite reflectance values: a, *Árkai* [1991]; b, *Merriman and Frey* [1999]; c, *Kübler and Jaboyedoff* [2000].





○ K-N92-26A-IV	▽ K-N75-13B-VIII
△ K-N75-65-VI	× K-N75-59A-VIII
◇ K-N92-26B-V	□ K-AP80-41-III
☆ K-N92-13A-VII	⊙ Muscovite XV

Figure 8. Calibration for illite ‘crystallinity’ using polished slate standards and pegmatitic muscovite flake [Kisch, 1991]. Standards kindly provided by H. J. Kisch. Abbreviations: E, Epizone; A, Anchizone; D, Diagenetic Zone.

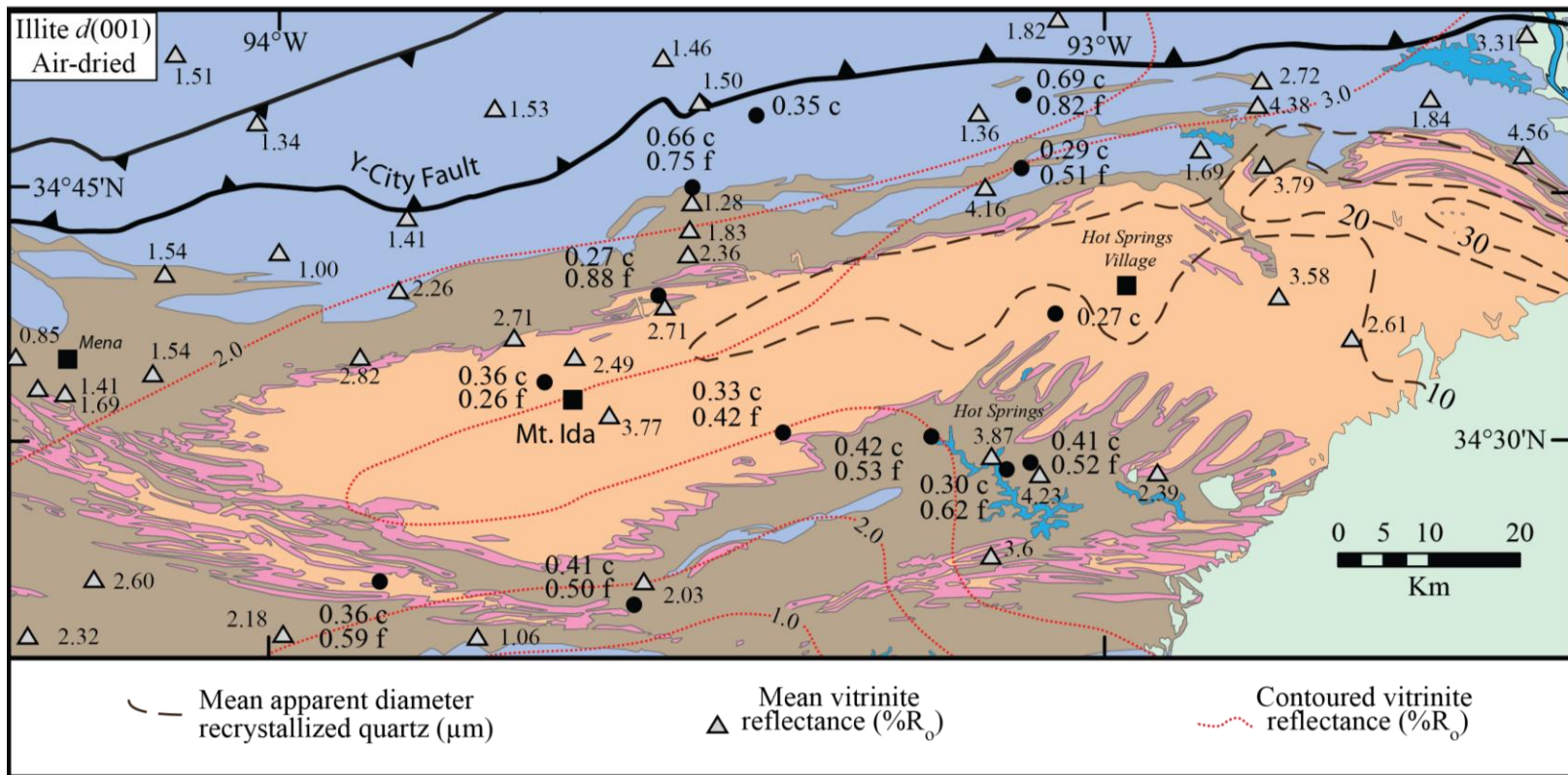


Figure 9A. Crystallinity values for air-dried coarse clay fraction and fine clay fraction of illite $d(001)$. Crystallinity is given in FWHM $^{\circ}2\theta$ $\text{CuK}\alpha$, where c is coarse clay and f is fine clay. The fine clay fraction indicates lower thermal maturation ($\sim 100^{\circ}\text{C}$) in comparison to the coarse clay fraction. Mean apparent diameter of recrystallized quartz are given by Keller *et al.* [1985]. Mean vitrinite reflectance values and contours are given by Houseknecht and Matthews [1985].

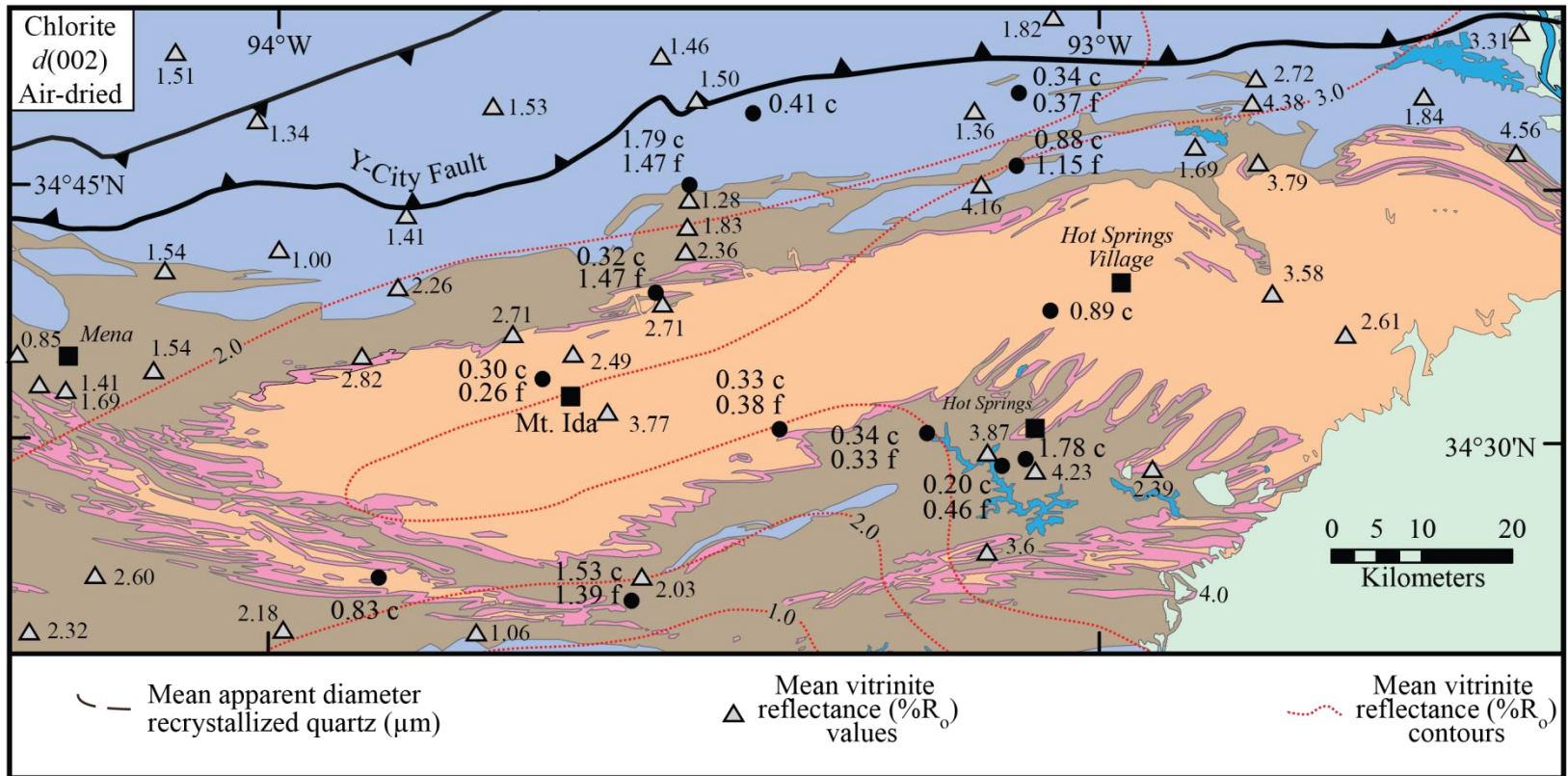
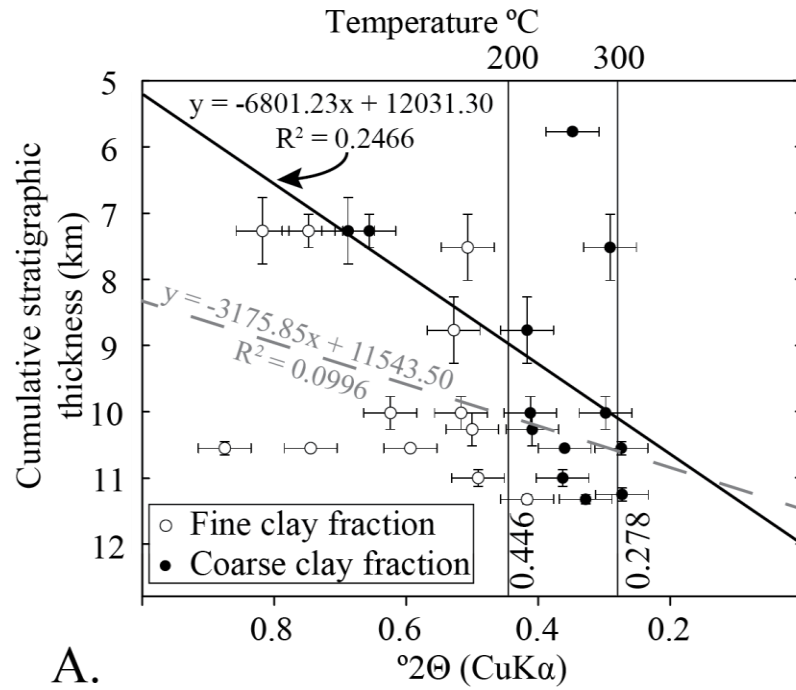


Figure 9B. Crystallinity values for air-dried coarse clay fraction and fine clay fraction of chlorite $d(002)$. See Figure 9A for explanation.

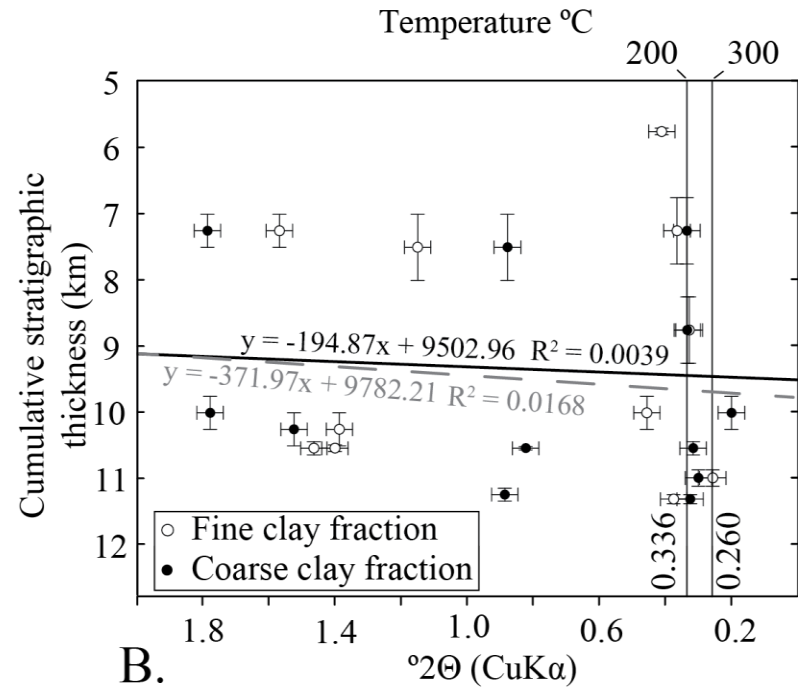
Figure 10. Crystallinity of samples vs. the cumulative stratigraphic thickness (see Figure 4). All samples K-saturated, air-dried and x-rayed at room temperature. Solid and open dots are coarse and fine clay fractions, respectively. Solid black line with equation and R^2 represents a linear regression fit through the coarse clay fraction. Dashed grey line with equation and R^2 represents a linear regression fit through the fine clay fraction. Cumulative stratigraphic thickness is the thickness of sediments above a particular sample that would have existed assuming no erosion. These values were determined from Figure 4. A. Illite. Crystallinity increases with cumulative stratigraphic thickness. B. Chlorite. Chlorite does not increase with stratigraphic thickness.

Illite $d(001)$ Crystallinity



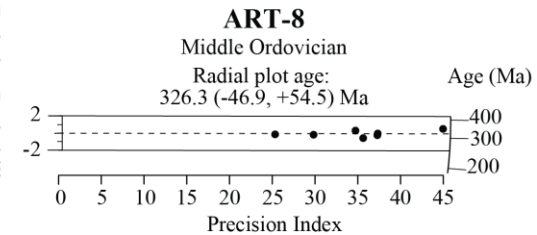
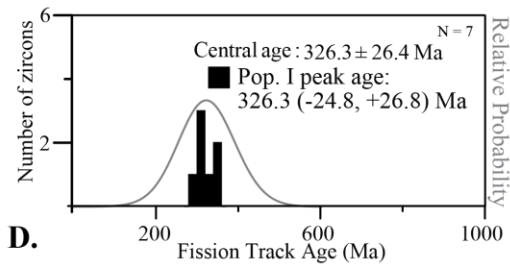
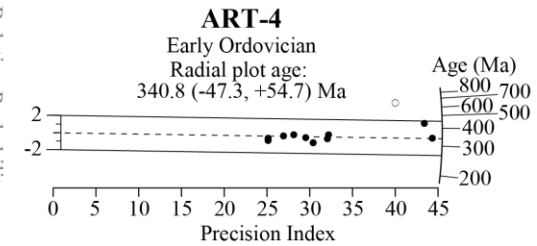
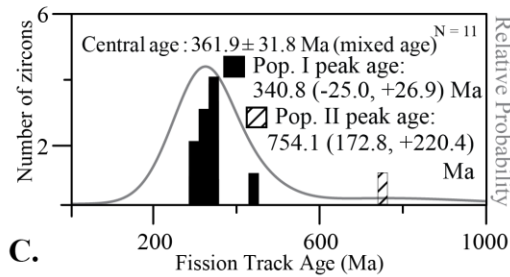
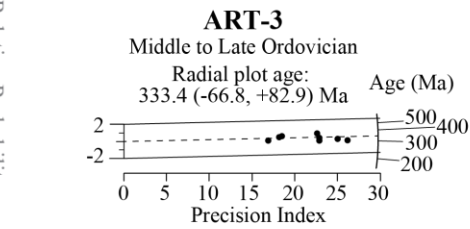
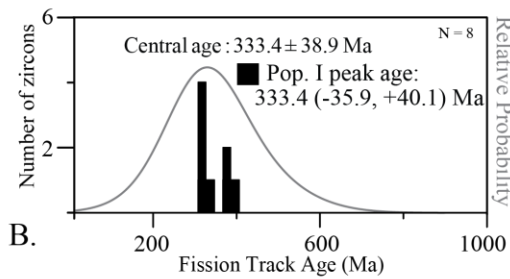
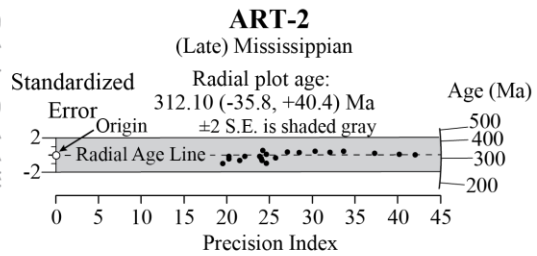
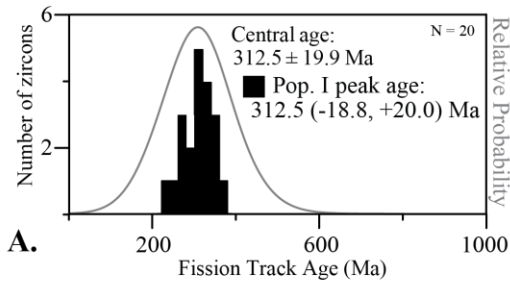
A.

Chlorite $d(002)$ Crystallinity



B.

Figure 11. Histogram and radial plots of fission track age data. Arranged by sample number. Central age is given with 1 standard error. Probability-density plots (grey line) were calculated using IsoPlot [Ludwig, 2003]. Population peak ages with 1 standard error were determined using BINOMFIT [Brandon, 2002] and the binomial model of Galbraith and Green [1990]. Radial plot ages determined using BINOMFIT and are given with 2 standard errors. Open circles are fission track grain ages that lie outside the main age component with 2 S.E. and not been included in determining the radial plot age. ART-2 radial plot only has the parts labeled as all the radial plots have the same labels. See text for further explanation.



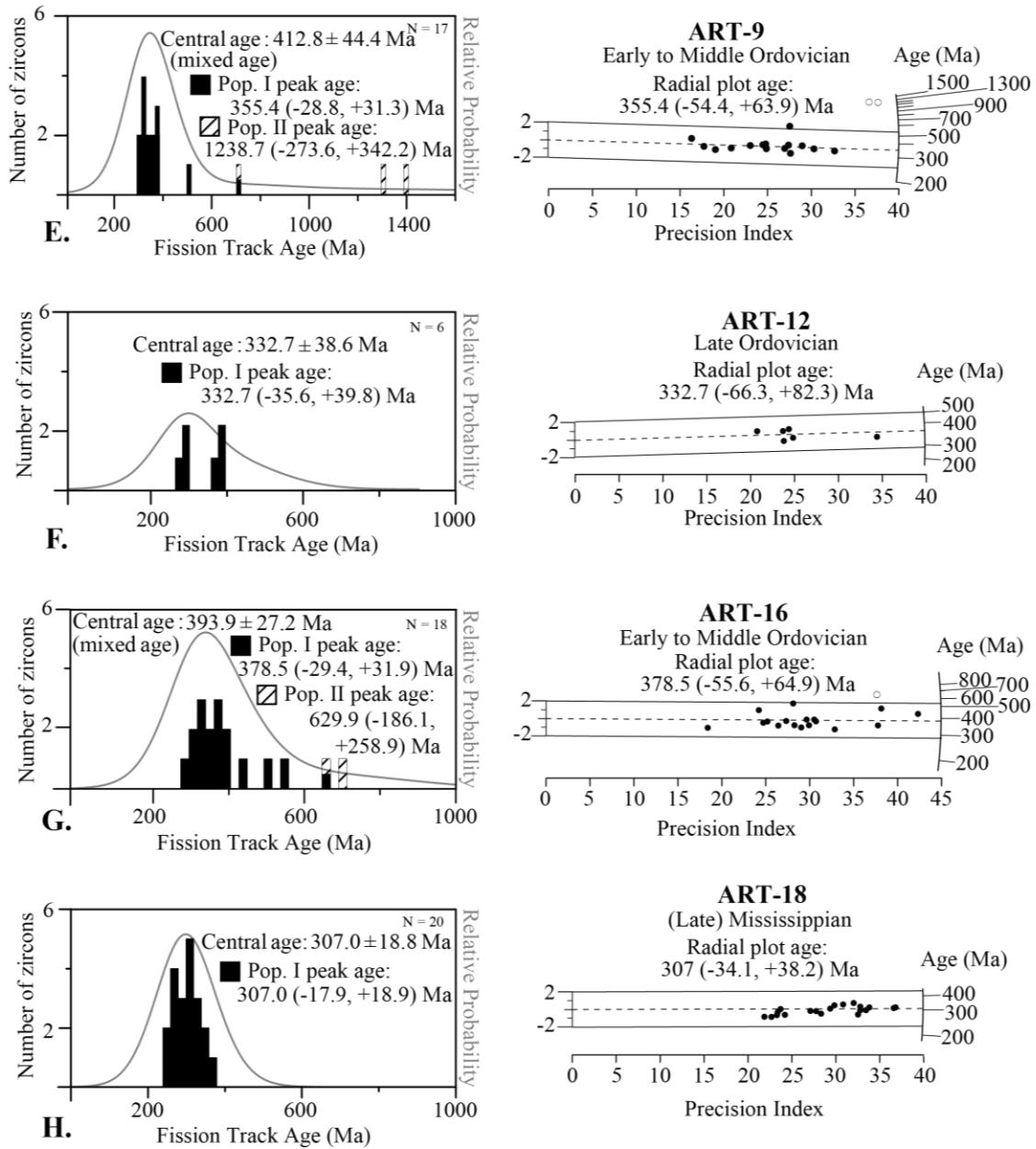


Figure 11 (cont.) E., Note change in scale for age in histogram.

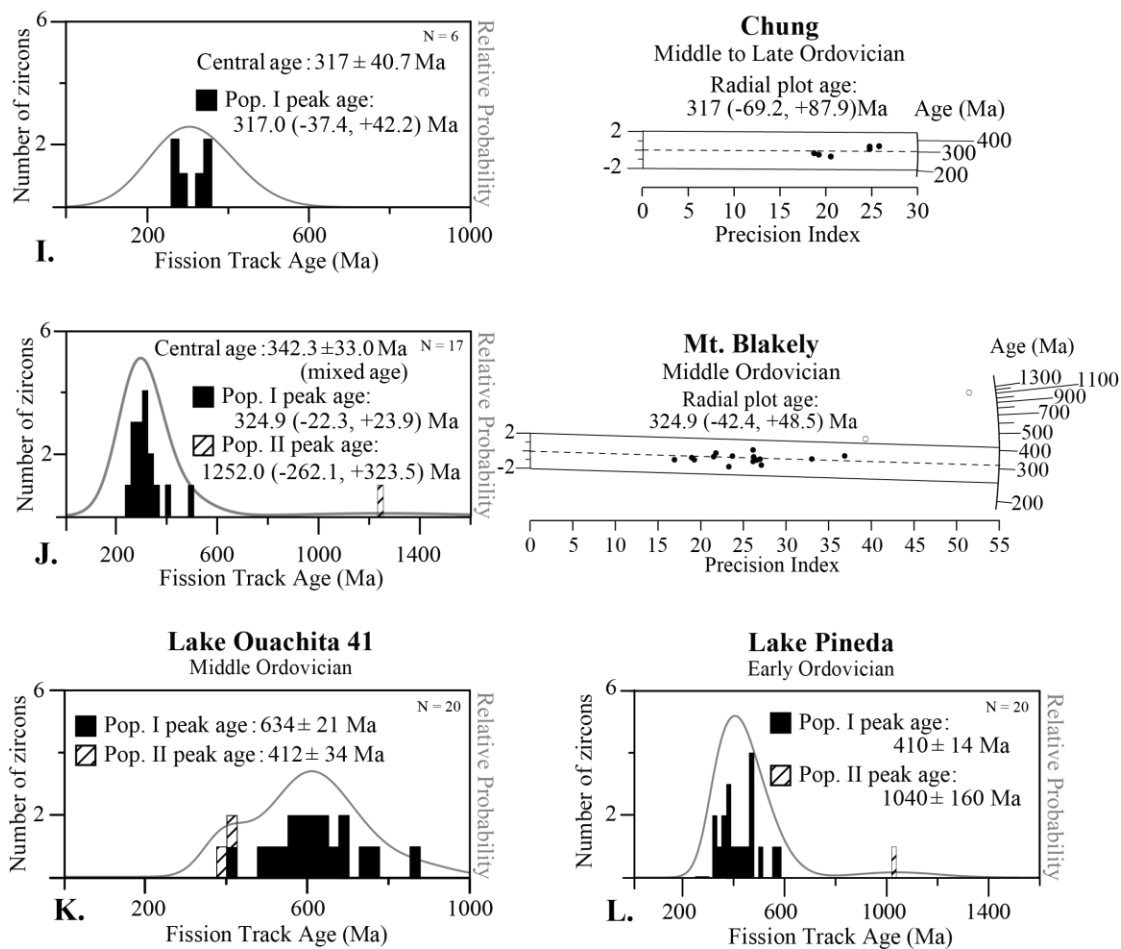


Figure 11 (cont). J., L., Note change in scale for age in histogram. K., L., Gaussian peak ages shown with 1 sigma error were determined using “Unmix” tool in IsoPlot [Ludwig, 2003].

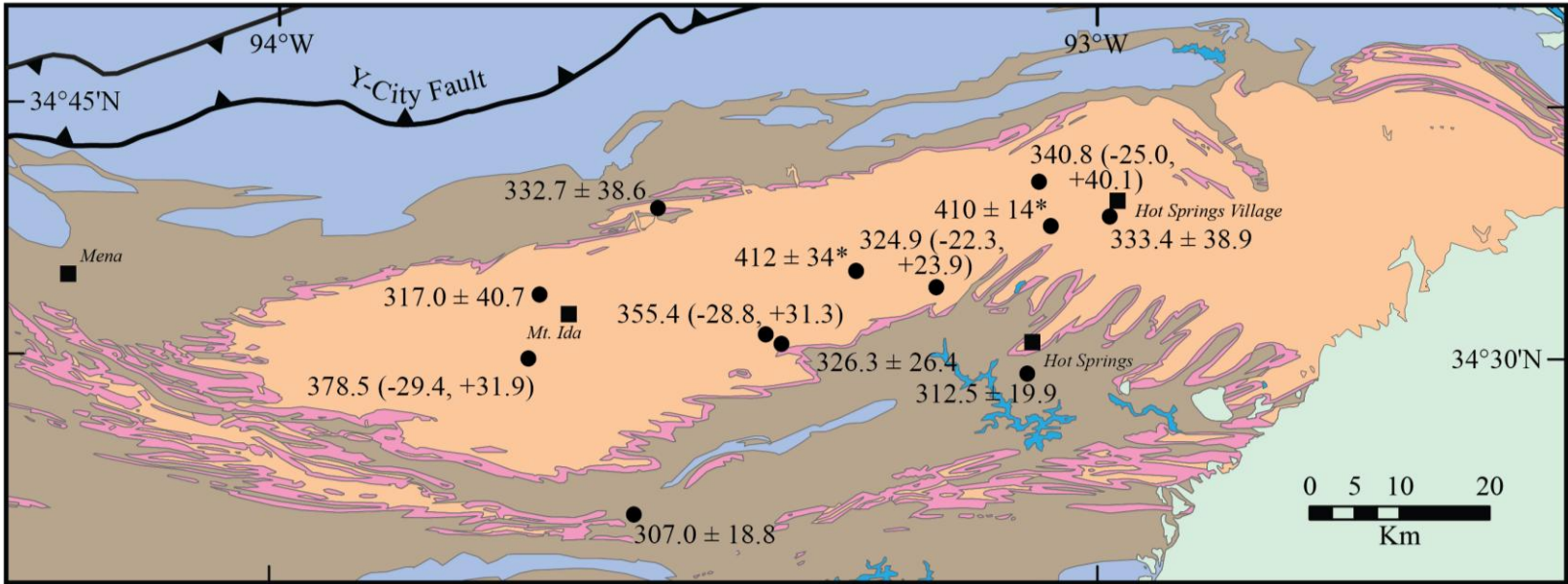


Figure 12. Zircon fission track ages. Age error is expressed in 1 standard error. The two fission track ages with 1 standard deviation determined using LA-ICP-MS fission track analysis have an asterisk beside the age. See Figures 3 and 11 for further explanation

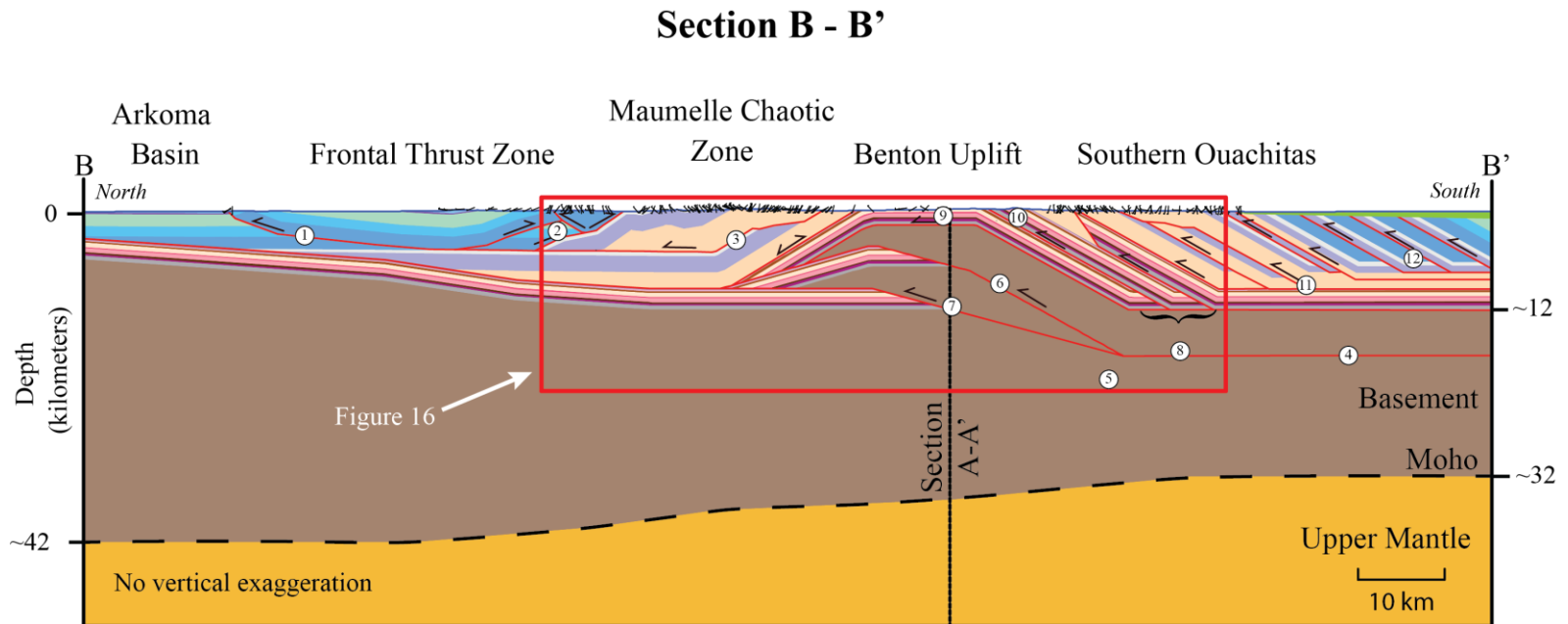


Figure 13. B-B' section. Red lines are thrust faults. Dip data shown at surface. See Figure 3 for location and Figure 4 for formations. See text for further explanation.

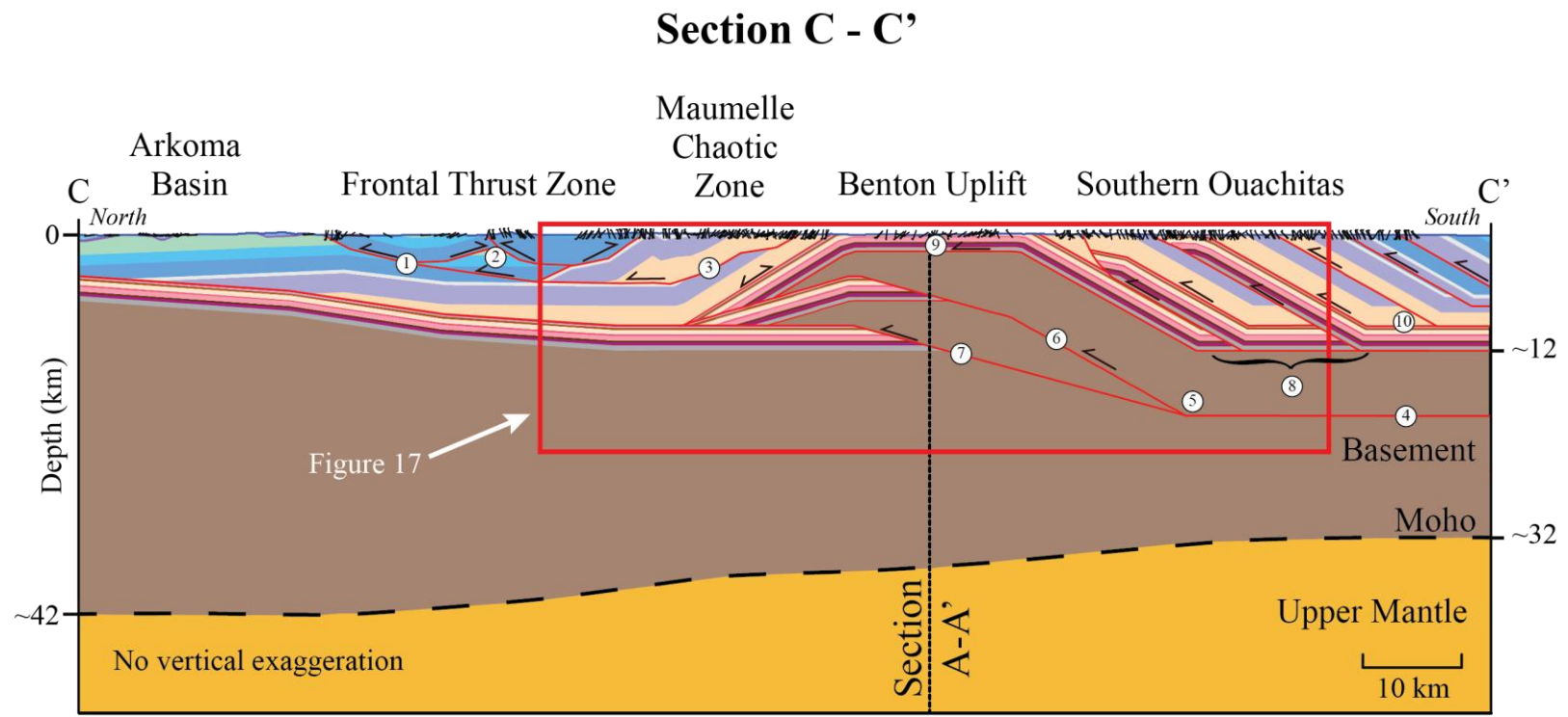


Figure 14. C-C' section. See Figure 13 and text for further explanation.

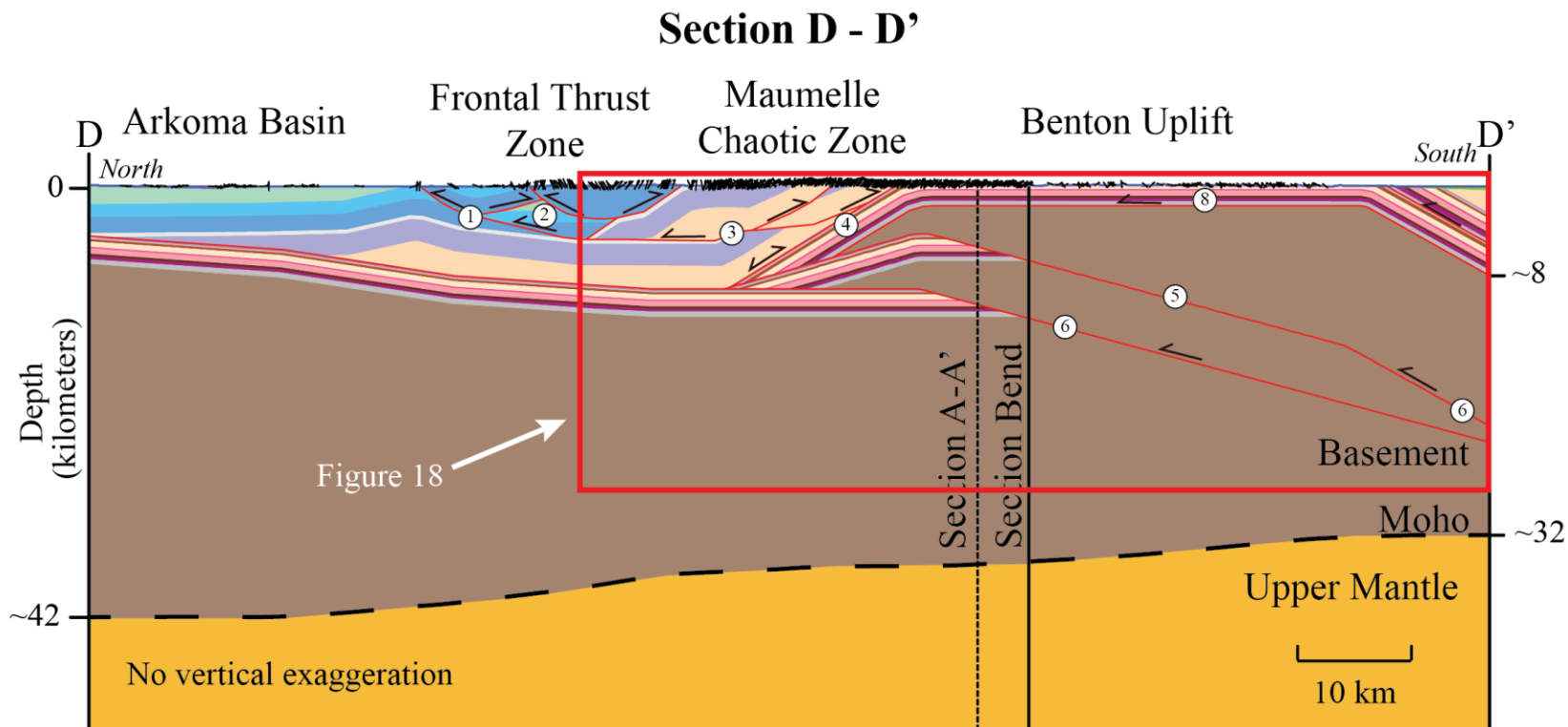


Figure 15. D-D' section. See Figure 13 and text for further explanation.

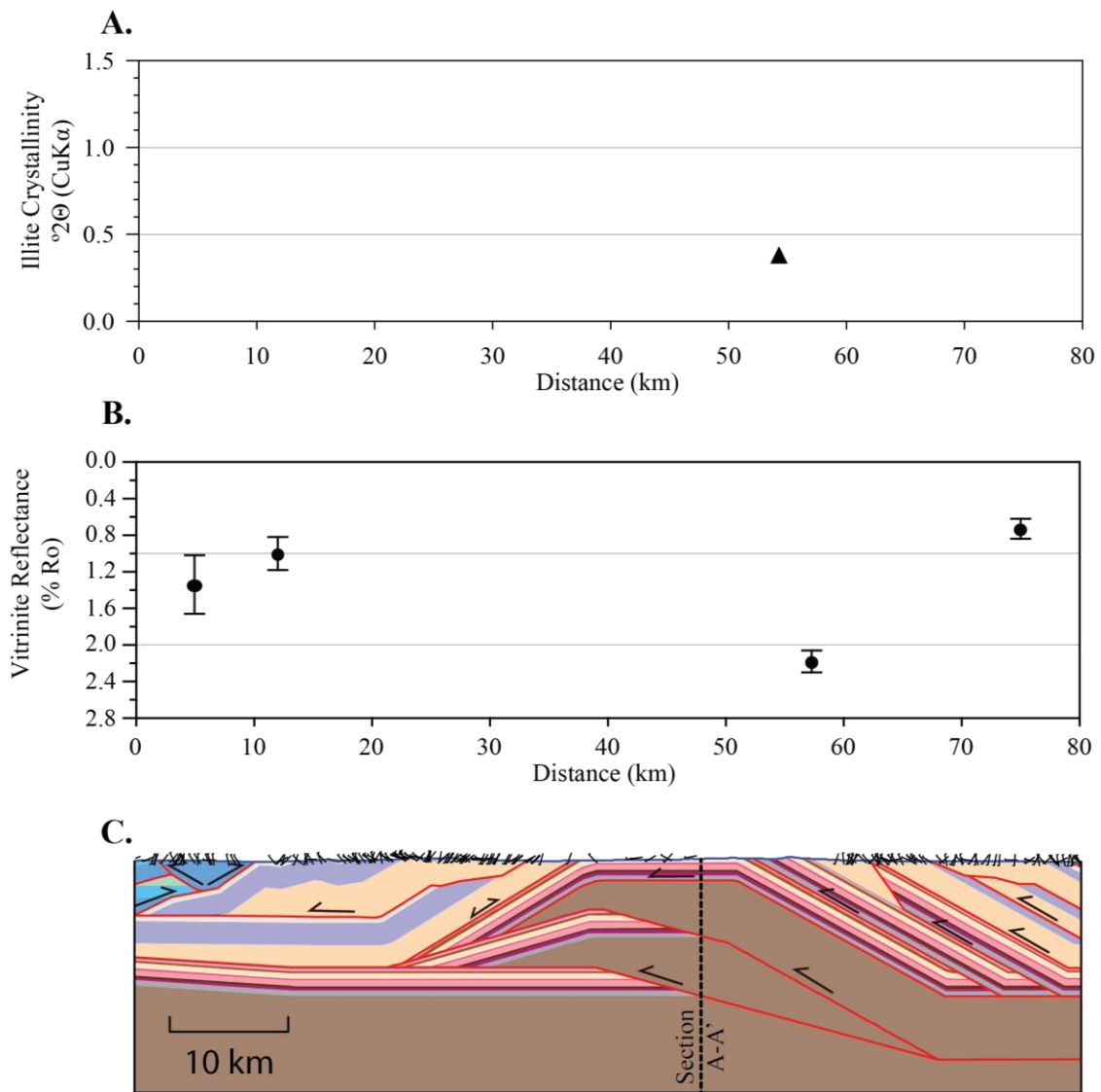


Figure 16. Thermal maturation across a portion of Section B - B'. A. Illite crystallinity plotted is for $d(001)$ air-dried coarse clay with 0.04° error. B. Vitrinite reflectance from *Houseknecht and Matthews* [1985]. C. Portion of Section B - B', no vertical exaggeration. See Figure 13 for location and further explanation.

Figure 17. Thermal maturation and thermochronologic ages across a portion of section C - C'. A. Zircon fission track ages. Ages with an asterisk are mixed ages as defined in the text. B. Illite crystallinity. C. Vitrinite reflectance. D. Portion of section C-C'. See Figure 14 for location and Figure 13 for further explanation.

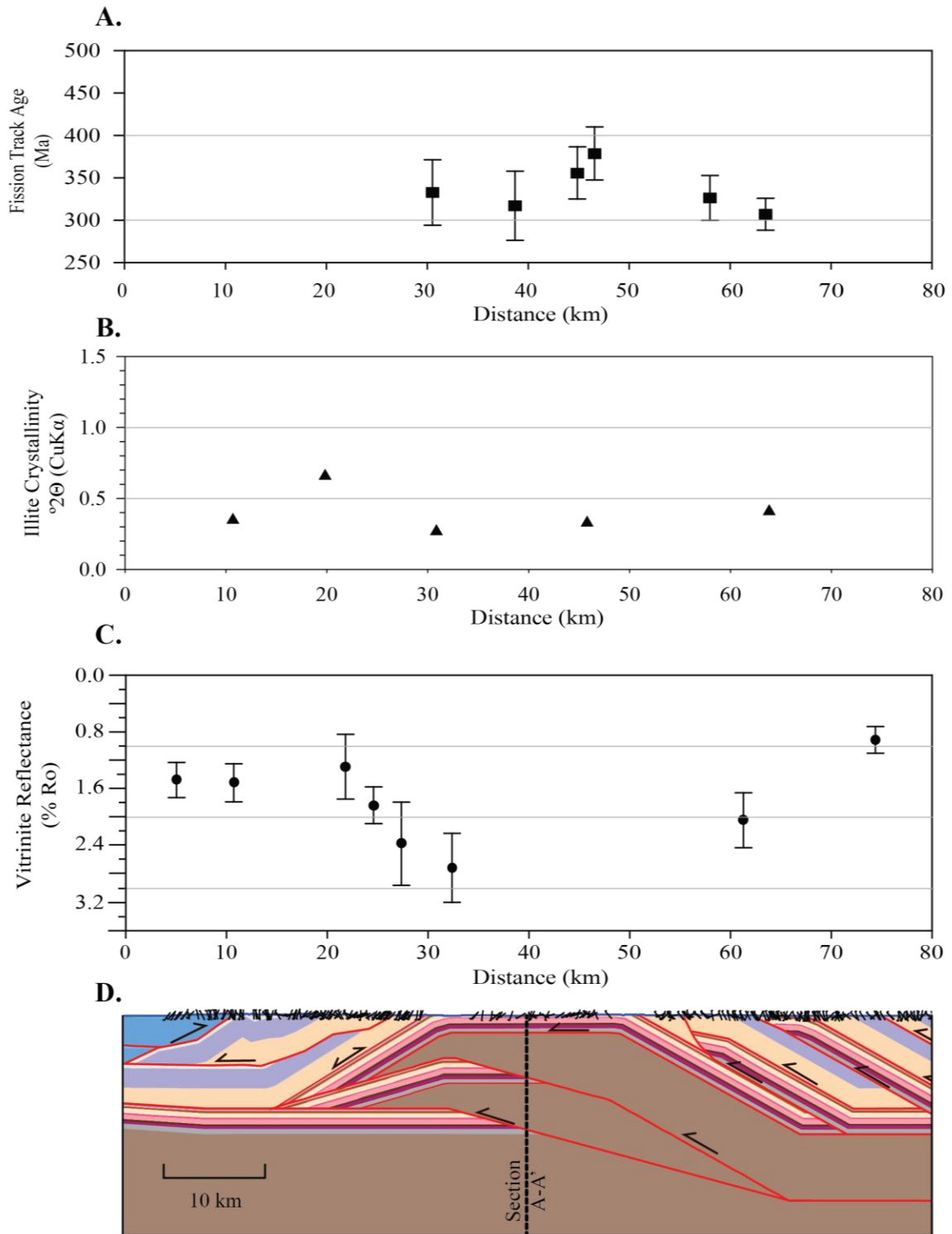


Figure 18. Thermal maturation and thermochronologic ages of a D - D' portion. A. Zircon fission track ages. B. Illite crystallinity C. Vitrinite reflectance. D. Portion of D-D'. See Figure 15 for location and Figure 13 for further explanation.

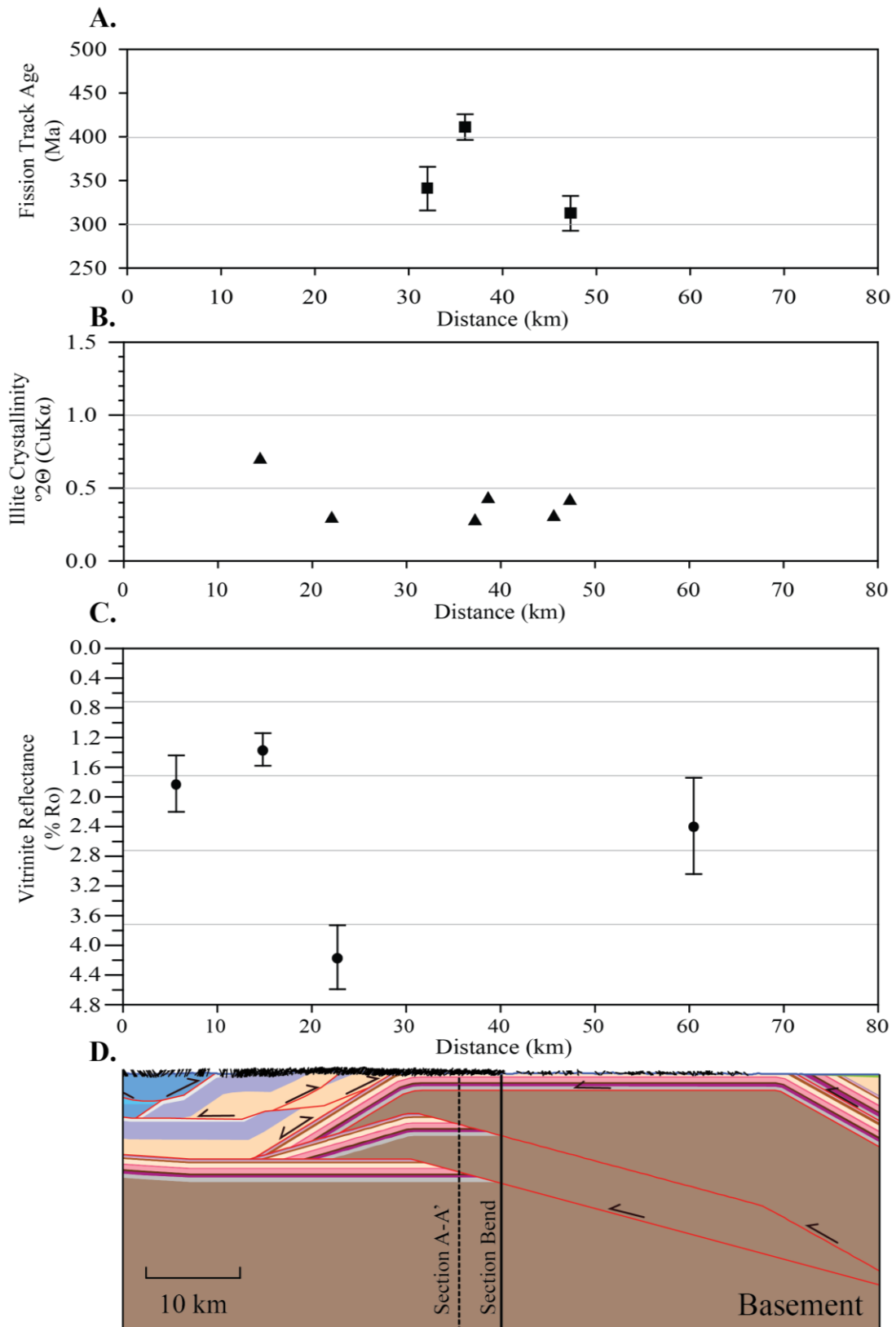


Figure 19. Thermal maturation and thermochronologic ages across A - A'. A. Zircon fission track ages. B. Illite crystallinity C. Vitrinite reflectance. D. Interpretation of section A -A'. See Figures 13 and 14 for further explanation.

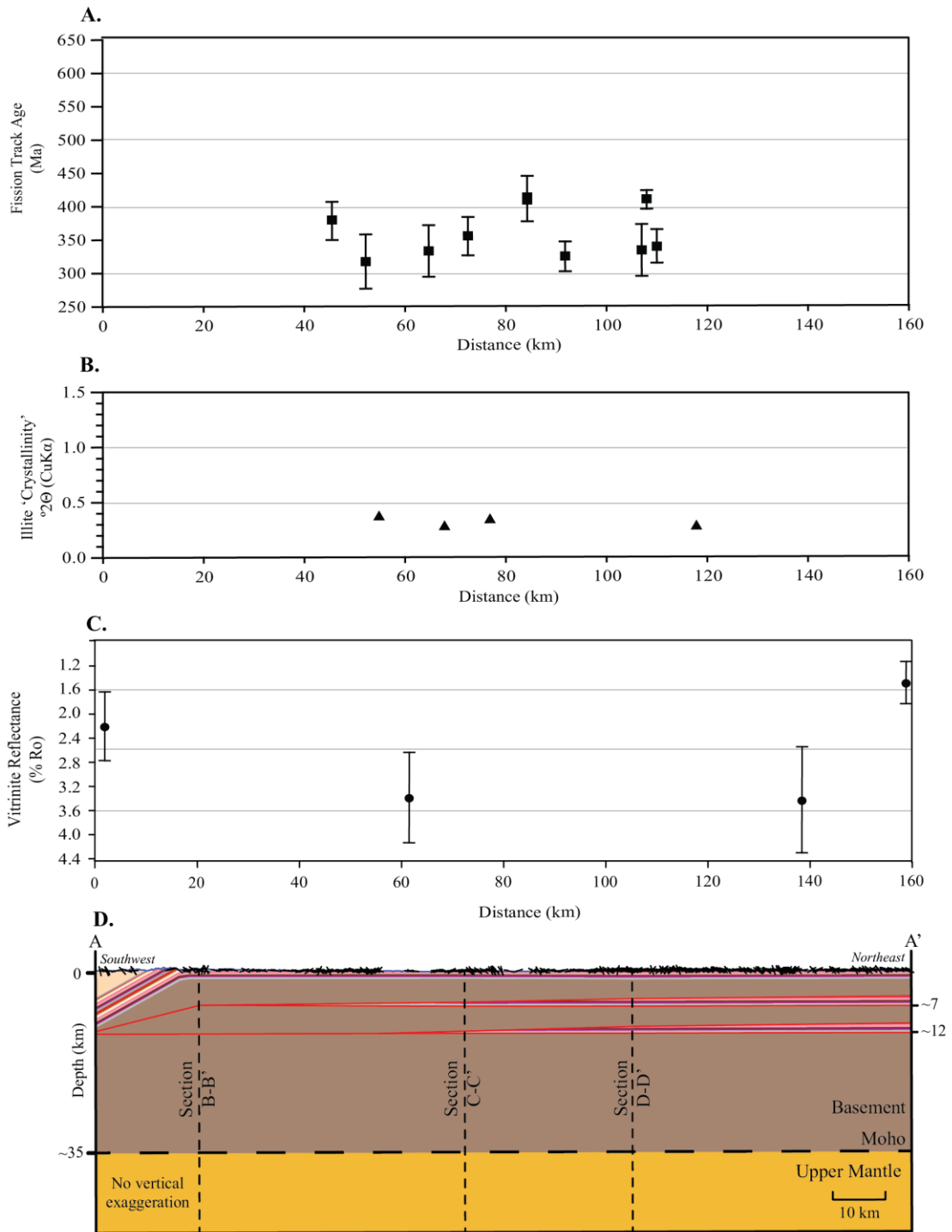
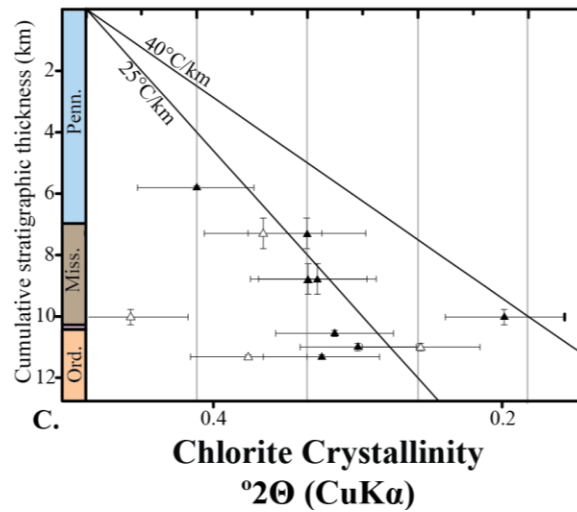
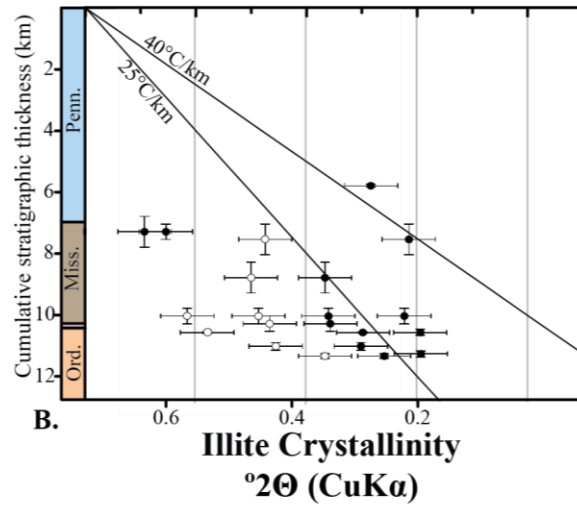
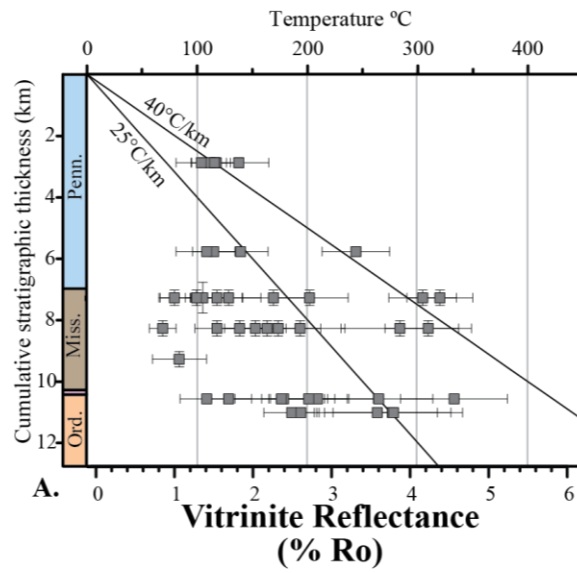
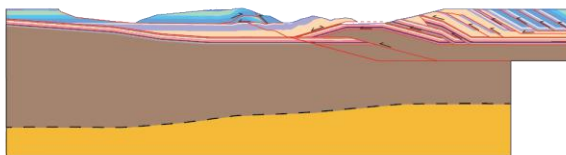


Figure 20. Comparison with different types of thermal maturation. A. Vitrinite reflectance. B. Illite crystallinity. C. Chlorite crystallinity. Filled symbols are coarse clay and open symbols are fine clay. Not all data is plotted at this scale and see Figure 10 for plot of all data. See Figure 4 for further explanation and sources. Both thermal maturation measures increase with increasing cumulative stratigraphic thickness to reach lower greenschist transition.

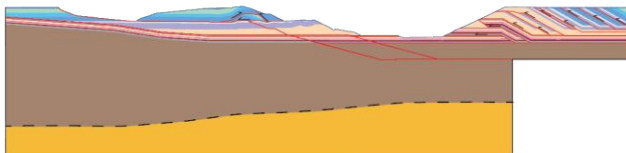


Restoration of Section B - B'

A. Restoration of lowermost basement fault



B. Restoration of uppermost basement fault



C. Restored

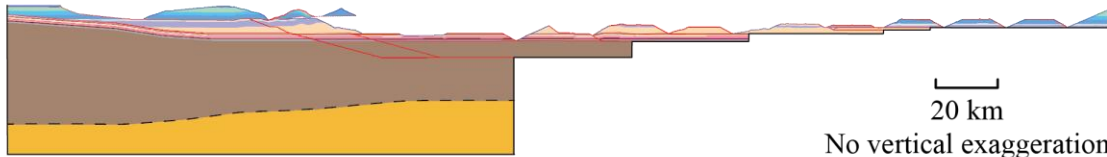


Figure 21. A. - C., Sequential restoration of B-B'. See Figure 13 for further explanation.

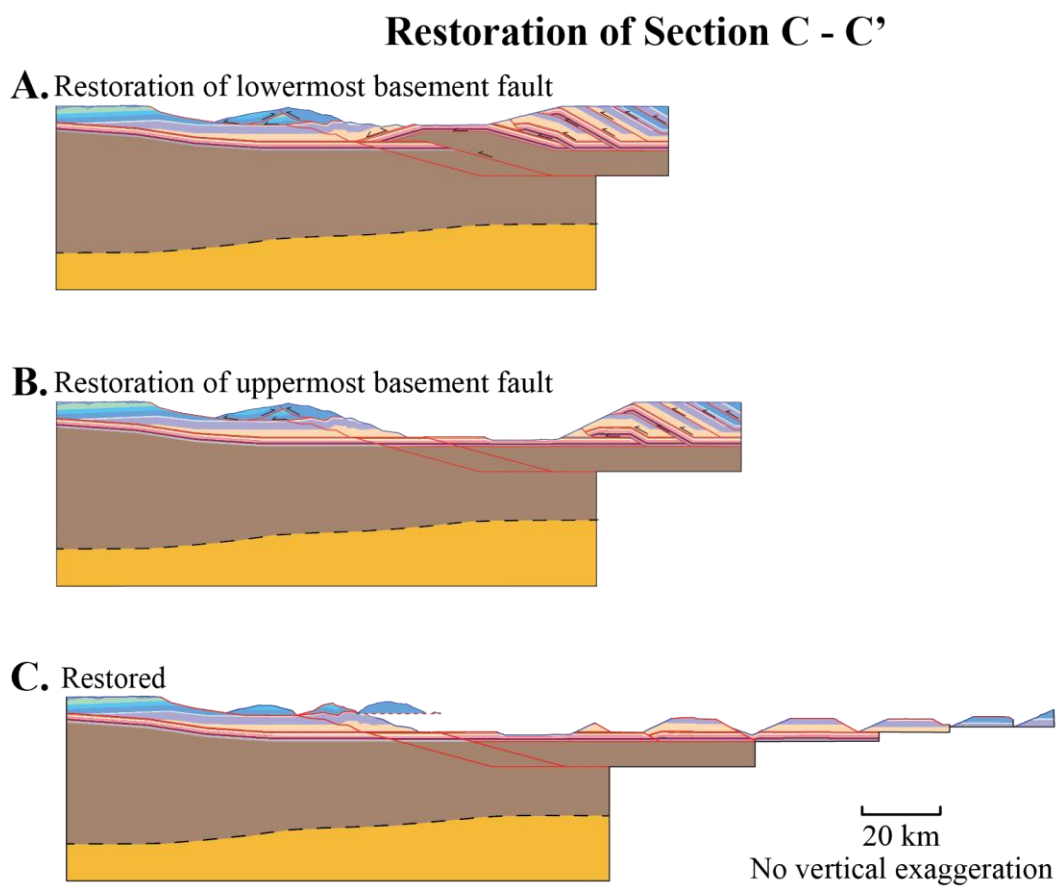


Figure 22. A. - C., Sequential restoration of section C-C'. See Figure 13 for further explanation.

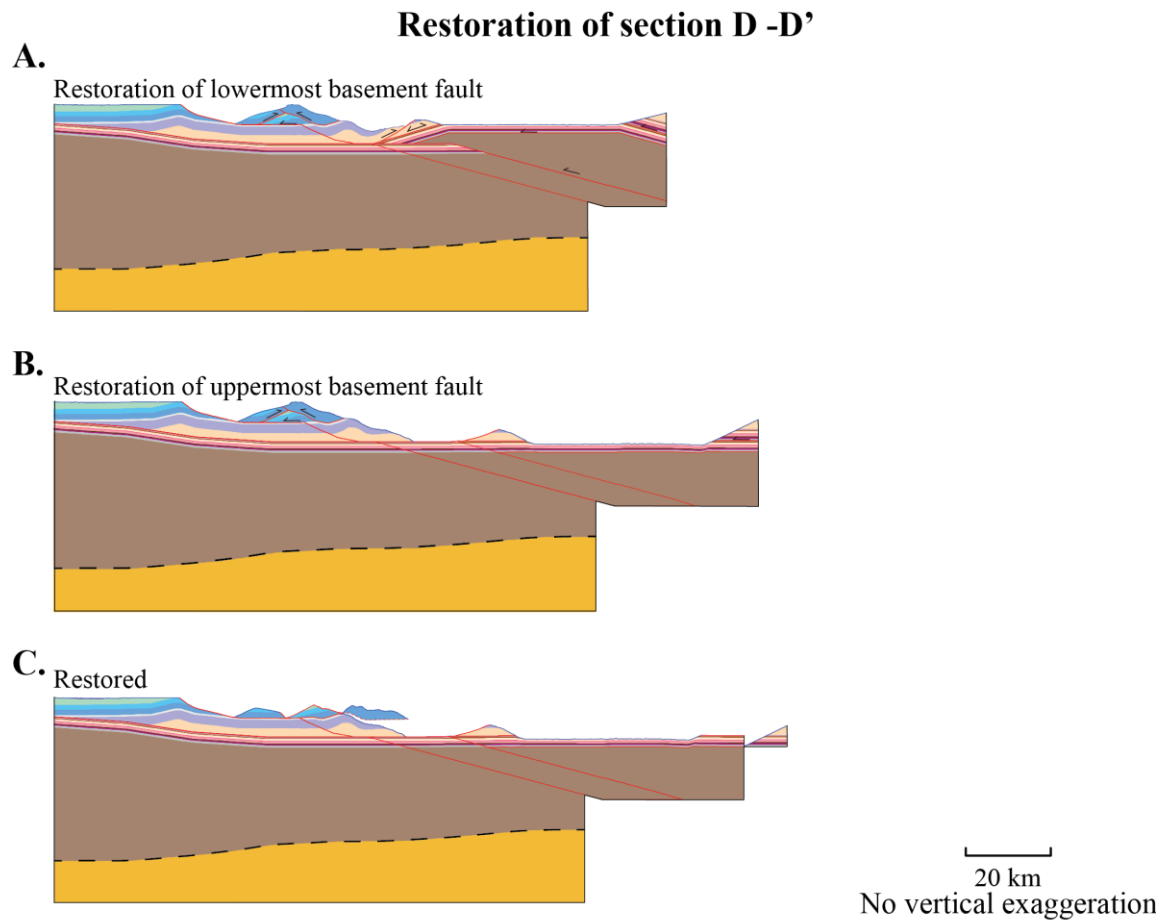
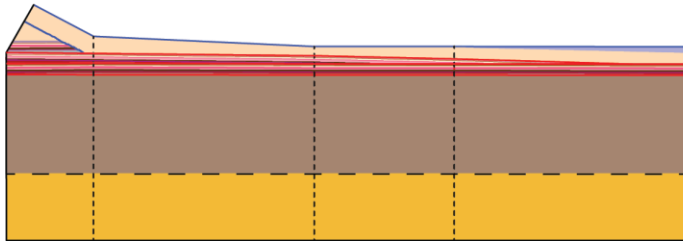


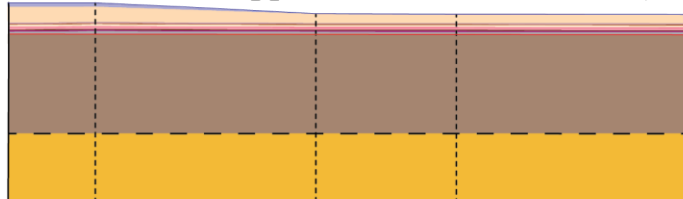
Figure 23. A. - C., Sequential restoration of section D-D'. See Figure 13 for further explanation.

Restoration of section A - A'

A.
Restoration of lowermost basement fault



B.
Restoration of uppermost basement fault (restored)



┌───┐
20 km

No vertical exaggeration

Figure 24. A. - B., Sequential restoration of section A-A'. See Figure 13 for further explanation.

APPENDIX B

METHODS

Illite and Chlorite Crystallinity

For shale and slate samples, approximately a 50 grams aliquot of disaggregated rock yields 1 gram of clay minerals. Sandstones require a larger 100 grams aliquot of disaggregated rock for the same quantity of clay minerals as their abundance will likely be less. A series of chemical pretreatments outlined by *Jackson* [1956] removed carbonate and organic cements from the mineral grains.

With the cementing material removed, the sample is separated into 4 different size fractions: sand (2 mm to 45 μm), silt (45 to 2 μm), coarse clay (2 to .2 μm), and fine clay (<.2 μm). The bulk sample and sand fraction were crushed in a mortar and pestle until the material passes through a 45 μm mesh sieve. The smaller grain size may help get an excellent counting statistic on the minerals present [*J. P. Harris*, personal communication, 2010].

A Rigaku D/Max-III-VBX Power X-Ray Diffractometer (XRD) in the geology and geophysics department at Texas A&M University was used to x-ray the specimens. The instrument details and settings are: $\text{CuK}\alpha$, normal focus tube, 40kV, 20 mA, slit sizes (from shutter to goniometer) are 1° divergence slit, 1° anti-scatter slit, .08mm receiving slit, and .06mm receiving slit on the goniometer, and a graphite-diffracted beam monochromator. The bulk sample, sand fraction, and silt fraction was side-loaded into an aluminum sample holder for a random oriented mount and continuously scanned from 2° to 65° 2θ using a 0.02° step at 2° 2θ /min [*McMurdie et al.*, 1986]. For both coarse and fine clay, the specimen was sedimented onto a Vicor glass slide at $\geq 2 \text{ mg/cm}^2$ to

avoid intersample variation from x-ray absorption of thinly sedimented slides. [Moore and Reynolds, 1997, Table 9.2] Clay sedimented slides are air dried at room conditions overnight. These slides were continuously scanned from 2° to 32° 2Θ using a 0.05° step at 0.75° 2Θ /min. All samples were x-rayed at room temperature and relative humidity.

Each of these fractions along with a whole rock sample is scanned using an x-ray diffractometer to yield diffraction patterns. Sample mineralogy is determined using the Hanawalt method to qualitatively analyze the diffraction patterns [Hanawalt *et al.*, 1938]. Identification of the clay mineral was aided by comparison with published clay mineral patterns and an in-house diffractogram of source clay SAz-1 Ca-rich montmorillonite “Cheto” from the Clay Mineral Society. MacDiff XRD analysis software version 4.2.5 was used to process the digital data for peak positions, peak full-width half maximum (FWHM), and the integrated area of the peak after a baseline of intensity was established.

The identification of clay minerals for both the coarse clay and fine clay specimens is confirmed by a comparison of each characteristic peak spectrum produced by the different treatments. A specimen from each clay fraction was 1) saturated with K^{+} for at least 12 hours, 2) vapor solvated with ethylene glycol for 24 hours in a closed vapor vessel heated to $60^{\circ}\pm 10^{\circ}C$, 4) heat treated to $300^{\circ}C$ for 2 hours, and finally 5) heat treated to $550^{\circ}C$ for 2 hours [Dixon and Weed, 1989; Moore and Reynolds, 1997]. Both glycol vapor solvated and heat treated specimens are scanned immediately after their removal from the vapor chamber or oven, respectively.

A JEOL JSM-6400 equipped with a PGT EDS system at the Texas A&M University Microscopy & Imaging Center was used to investigate ART-6 to confirm the

clay mineral assemblage. Sample preparation, microphotographs and elemental compositions were undertaken with the guidance of Dr. John P. Harris. Sample stubs are made by crosscutting the sample and plucking a small specimen. The stub is mounted rough side up in the holder using graphite paint and followed by $\sim 200\text{\AA}$ coating of gold for the conductive surface. Instrument voltage set at 15 kV.

ART6_1_02 was analyzed at 10,000X magnification, 15 kV acceleration voltage, 13mm working distance, 11 spot size, and 0° tilt. ART_2_01a was analyzed at 4,500X magnification, 15 kV acceleration voltage, 15mm working distance, 12 spot size and 0° tilt.

APPENDIX C
X-RAY DIFFRACTION DATA

TABLE C1. Semi-quantitative mineralogical analysis using X-ray Diffraction^a

Sample	Sand fraction		Silt fraction		Coarse clay fraction		Fine clay fraction		Carbonate, organic material, and procedural loss %
	%	Mineralogy ^b	%	Mineralogy ^b	%	Mineralogy ^b	%	Mineralogy ^b	
<u>Pennsylvanian Johns Valley Formation</u>									
ART-14	68.63	Q	27.13	C?,Q	0.15	C,I,Q	N.D.	N.D. ^c	4.09
<u>Pennsylvanian Jackfork Formation</u>									
ART-6	85.09	Q	12.37	C?,Q	1.02	S,C,I/S,I,Q	0.18	S,C,I/S,I,Q	1.34
ART-15	73.88	F,Q	21.06	F,Q	2.58	C,I,Q	0.12	C,I	2.35
<u>Mississippian Stanley Formation</u>									
ARM-1	46.60	C,I,F	38.69	C,I,F	10.69	C,I	1.20	C,I	2.81
ARM-5	36.66	C,I,F,Q	52.08	C,I,F,Q	9.15	C,I,Q	0.48	C,I,Q?	1.63
ART-2	80.26	C,I?,F,Q	15.64	C,I?,F,Q	1.66	C,I,Q	0.22	C?,I,Q	2.22
ART-5	69.51	I?,F,Q	26.51	C,I,F,Q	2.42	C,I,Q	0.18	C,I	1.38
ART-18	67.68	C,I?,F,Q	26.54	C,I?,F,Q	3.09	C,I,Q	0.38	C,I,Q	2.31
<u>Silurian-Ordovician, Undivided</u>									
ARM-8	29.02	I?,Q	44.14	I?,Q	11.76	I,Q	3.63	I,Q	11.46
ART-19	80.58	I?,Q	12.86	C?,I?,Q	2.78	C?,I,Q	0.24	C,I,Q	3.53
<u>Ordovician Bigfork Formation</u>									
ART-12	83.29	Q	13.25	Q	0.76	C,I,Q	0.13	C,I,Q	2.57
<u>Ordovician Womble Formation</u>									
ARM-7	22.22	C,I,F,Q	59.19	C,I,F,Q	15.35	C,I	1.23	I,C	2.01
ART-3	82.43	Q	15.36	I?,Q	0.28	I,K,Q	N.D. ^c	N.D. ^c	1.93
<u>Ordovician Blakely Formation</u>									
ARM-6	26.37	C,I,Q	56.91	C,I,Q	12.72	C,I	1.01	C,I	3.00
<u>Ordovician Crystal Mountain Formation</u>									
ART-9	91.63	Q	6.97	Q	0.37	Q	N.D. ^c	N.D. ^c	1.03

^a Sand and silt fractions are randomly oriented and side loaded into an aluminum holder. Both clay fractions are oriented and mineralogy determined from inspection of the diffractograms of each treatment type (i.e., ethylene glycol vapor solvation and heat treatments). Carbonate, organic material, and procedural loss determined by subtracting combined weight of the fractions from the initial sample weight prior to pretreatments.

^bMinerals present denoted using the following abbreviations: C--chlorite, F--feldspars, I--illite, I/S--interlayered illite and smectite, K--kaolinite, and Q--quartz.

^cN.D. =no data.

TABLE C2. CHLORITE 001 PEAK VALUES AT AIR DRIED, ETHYLENE GLYCOL VAPOR SOLVATED, HEATED 300°C, AND HEATED 550°C

Sample, clay fraction	2 θ (degrees)	D-spacing (angstroms)	Peak max counts (counts/second)	Peak area (integrated counts)	FWHM (degrees)	Sample, clay fraction	2 θ (degrees)	D-spacing (angstroms)	Peak max counts (counts/second)	Peak area (integrated counts)	FWHM (degrees)
<u>Pennsylvanian Johns Valley Formation</u>						<u>Mississippian Stanley Formation</u>					
ART-14, coarse						ARM-1, fine					
Air-dried	6.30	14.030	113.8	1224.5	0.472	Air-dried	6.40	13.811	62.7	709.3	0.560
Ethylene Glycol Vapor	6.45	13.704	106.1	1107.1	0.485	Ethylene Glycol Vapor	6.35	13.919	45.0	474.9	0.636
Heated 300°C	N.D.*	N.D.*	N.D.*	N.D.*	N.D.*	Heated 300°C	6.45	13.704	31.8	357.5	0.595
Heated 550°C	N.D.*	N.D.*	N.D.*	N.D.*	N.D.*	Heated 550°C	6.60 [†]	13.393 [†]	44.3 [†]	711.4 [†]	0.589 [†]
<u>Pennsylvanian Jackfork Formation</u>						ARM-5, coarse					
ART-6, coarse [§]						Air-dried					
Air-dried	6.35	13.919	259.2	2414.1	0.420	Ethylene Glycol Vapor	6.65	13.292	13.1	59.7	0.222
Ethylene Glycol Vapor	6.35	13.919	343.4	4255.0	0.511	Heated 300°C	6.90 [†]	12.811 [†]	17.2 [†]	212.6 [†]	0.828 [†]
Heated 300°C	6.45	13.704	75.4	725.1	0.433	Heated 550°C	N.D.*	N.D.*	N.D.*	N.D.*	N.D.*
Heated 550°C	6.85 [†]	12.904 [†]	29.4 [†]	472.6 [†]	.788 [†]	ARM-5, fine					
ART-6, fine [§]						Air-dried					
Air-dried	6.40	13.811	71.1	729.0	0.541	Ethylene Glycol Vapor	6.35	13.919	45.9	320.4	0.374
Ethylene Glycol Vapor	N.D.*	N.D.*	N.D.*	N.D.*	N.D.*	Heated 300°C	6.35	13.919	35.8	282.8	0.516
Heated 300°C	N.D.*	N.D.*	N.D.*	N.D.*	N.D.*	Heated 550°C	6.65	13.292	53.8	528.8	0.480
Heated 550°C	N.D.*	N.D.*	N.D.*	N.D.*	N.D.*	ART-2, coarse					
<u>Mississippian Stanley Formation</u>						Air-dried					
ARM-1, coarse						Ethylene Glycol Vapor					
Air-dried	6.30	14.030	12.5	53.1	0.210	Heated 300°C	7.25 [†]	12.193 [†]	22.3 [†]	160.5 [†]	0.168 [†]
Ethylene Glycol Vapor	6.30	14.030	14.7	69.0	0.173	Heated 550°C	7.65 [†]	11.557 [†]	64.1 [†]	1138.7 [†]	0.799 [†]
Heated 300°C	N.D.*	N.D.*	N.D.*	N.D.*	N.D.*						
Heated 550°C	6.50	13.598	36.8	239.9	0.323						

Note: Samples without C₀₀₁ data omitted.

*N.D. =no data.

[†]Broad peak measurement.

[§]Possible smectite interlayering, mainly with illite.

TABLE C3. CHLORITE 001 PEAK VALUES AT AIR DRIED, ETHYLENE GLYCOL VAPOR SOLVATED, HEATED 300°C, AND HEATED 550°C

Sample, clay fraction	2 θ (degrees)	D-spacing (angstroms)	Peak max counts (counts/second)	Peak area (integrated counts)	FWHM (degrees)	Sample, clay fraction	2 θ (degrees)	D-spacing (angstroms)	Peak max counts (counts/second)	Peak area (integrated c- ounts)	FWHM (degrees)
<u>Mississippian Stanley Formation</u>						<u>Ordovician Blakely Formation</u>					
ART-2, fine						ARM-6, fine					
Air-dried	N.D.*	N.D.*	N.D.*	N.D.*	N.D.*	Air-dried	6.95 [†]	12.719 [†]	273.5 [†]	7473.0 [†]	1.286 [†]
Ethylene Glycol Vapor	6.25	14.142	19.3	270.2	0.161	Ethylene Glycol Vapor	N.D.*	N.D.*	N.D.*	N.D.*	N.D.*
Heated 300°C	N.D.*	N.D.*	N.D.*	N.D.*	N.D.*	Heated 300°C	N.D.*	N.D.*	N.D.*	N.D.*	N.D.*
Heated 550°C	7.65 [†]	11.557 [†]	63.6 [†]	1125.5 [†]	.963 [†]	Heated 550°C	6.70	13.193	83.7	626.8	0.471
ART-5, coarse											
Air-dried	6.40 [†]	13.811 [†]	25.3 [†]	519 [†]	1.027 [†]						
Ethylene Glycol Vapor	6.65 [†]	13.292 [†]	25.3 [†]	480.7 [†]	1.101 [†]						
Heated 300°C	N.D.*	N.D.*	N.D.*	N.D.*	N.D.*						
Heated 550°C	7.60 [†]	11.633 [†]	19.9 [†]	124.1 [†]	.241 [†]						
<u>Ordovician Bigfork Formation</u>											
ART-12, course											
Air-dried	6.35	13.919	18.5	72.0	0.220						
Ethylene Glycol Vapor	6.35	13.919	26.9	85.1	0.111						
Heated 300°C	6.40	13.811	15.7	42.3	0.060						
Heated 550°C	6.50	13.598	38.4	217.6	0.289						
<u>Ordovician Blakely Formation</u>											
ARM-6, coarse											
Air-dried	N.D.*	N.D.*	N.D.*	N.D.*	N.D.*						
Ethylene Glycol Vapor	N.D.*	N.D.*	N.D.*	N.D.*	N.D.*						
Heated 300°C	N.D.*	N.D.*	N.D.*	N.D.*	N.D.*						
Heated 550°C	6.45	13.704	53.0	271.4	0.203						

Note: Samples without C₀₀₁ data omitted.

*N.D. =no data.

[†]Broad peak measurement.

[§]Possible smectite interlayering, mainly with illite.

TABLE C4. ILLITE 001 PEAK VALUES AT AIR DRIED, ETHYLENE GLYCOL VAPOR SOLVATED, HEATED 300°C, AND HEATED 550°C

Sample, clay fraction	2 θ (degrees)	D-spacing (angstroms)	Peak max counts (counts/second)	Peak area (integrated counts)	FWHM (degrees)	Sample, clay fraction	2 θ (degrees)	D-spacing (angstroms)	Peak max counts (counts/second)	Peak area (integrated counts)	FWHM (degrees)
<u>Pennsylvanian Johns Valley Formation</u>						<u>Pennsylvanian Jackfork Formation</u>					
ART-14, coarse						ART-15, fine					
Air-dried	8.95	9.8807	18.4	78.3	0.348	Air-dried	8.95*	9.8807*	55.2*	855.3*	0.748*
Ethylene Glycol Vapor	8.95*	9.8807*	14.3*	56.8*	0.317*	Ethylene Glycol Vapor	8.85	9.9922	49.1	849.1	0.562
Heated 300°C	N.D. [†]	N.D. [†]	N.D. [†]	N.D. [†]	N.D. [†]	Heated 300°C	8.85*	9.9922*	67.9*	1105.9*	0.756*
Heated 550°C	N.D. [†]	N.D. [†]	N.D. [†]	N.D. [†]	N.D. [†]	Heated 550°C	8.80*	10.049*	79.0*	2048.7*	1.308*
<u>Pennsylvanian Jackfork Formation</u>						<u>Mississippian Stanley Formation</u>					
ART-6, coarse [§]						ARM-1, coarse					
Air-dried	8.15*	10.8490*	528.8*	8955.8*	0.688*	Air-dried	8.90	9.9361	53.7	379.1	0.298
Ethylene Glycol Vapor	8.85*	9.9922*	145.7*	1425.0*	0.433*	Ethylene Glycol Vapor	8.95	9.8807	49.7	353.6	0.274
Heated 300°C	8.85*	9.9922*	241.6*	5864.8*	1.128*	Heated 300°C	8.96	9.8751	36.6	205.9	0.241
Heated 550°C	9.20*	9.6128*	50.9*	812.9*	0.757*	Heated 550°C	8.85	9.9922	65.6	364.4	0.244
ART-6, fine [§]						ARM-1, fine					
Air-dried	8.05	10.9830	516.7	11196.2	0.818	Air-dried	8.85	9.9922	647.6	9230.5	0.624
Ethylene Glycol Vapor	N.D. [†]	N.D. [†]	N.D. [†]	N.D. [†]	N.D. [†]	Ethylene Glycol Vapor	8.90	9.9361	629.2	8836.2	0.613
Heated 300°C	8.25*	10.717*	195.4*	4264.7*	0.992*	Heated 300°C	8.90	9.9361	705.8	9050.5	0.543
Heated 550°C	9.50*	9.3099*	59.3*	694.1*	0.555*	Heated 550°C	8.90	9.9361	374.6	5054.8	0.549
ART-15, coarse						ARM-5, coarse					
Air-dried	8.90	9.9361	207.3	3769.3	0.656	Air-dried	9.10	9.7182	192.7	1898.5	0.417
Ethylene Glycol Vapor	8.95	9.8807	212.8	3445.8	0.624	Ethylene Glycol Vapor	9.15	9.6652	197.9	2099.1	0.458
Heated 300°C	9.00*	9.8259*	52.4*	1075.1*	0.833*	Heated 300°C	9.25	9.5609	229.5	2109.8	0.389
Heated 550°C	8.30*	10.6530*	76.6*	2410.9*	1.571*	Heated 550°C	9.23	9.5868	61.4	719.7	0.522

Note: Samples without I₀₀₁ data omitted.

*Broad peak measurement.

[†]N.D. = no data.

[§]Possible smectite interlayering, mainly with illite.

TABLE C5. ILLITE 001 PEAK VALUES AT AIR DRIED, ETHYLENE GLYCOL VAPOR SOLVATED, HEATED 300°C, AND HEATED 550°C

Sample, clay fraction	2 θ (degrees)	D-spacing (angstroms)	Peak max counts (counts/second)	Peak area (integrated counts)	FWHM (degrees)	Sample, clay fraction	2 θ (degrees)	D-spacing (angstroms)	Peak max counts (counts/second)	Peak area (integrated counts)	FWHM (degrees)
<u>Mississippian Stanley Formation</u>						<u>Mississippian Stanley Formation</u>					
ARM-5, fine						ART-5, fine					
Air-dried	8.90	9.9361	628.9	7681.5	0.528	Air-dried	9.00	9.8259	54.3	475.2	0.507
Ethylene Glycol Vapor	8.95	9.8807	586.6	7546.2	0.543	Ethylene Glycol Vapor	9.00	9.8259	55.0	489.9	0.385
Heated 300°C	8.95	9.8807	667.2	7437.1	0.468	Heated 300°C	9.00	9.8259	33.3	253.4	0.394
Heated 550°C	8.90	9.9361	348.2	3466.9	0.425	Heated 550°C	8.85	9.9922	26.3	173.4	0.143
ART-2, coarse						ART-18, coarse					
Air-dried	8.85	9.9922	319.2	3047.3	0.412	Air-dried	8.95	9.8807	162.5	2050.1	0.409
Ethylene Glycol Vapor	8.90	9.9361	311.7	3032.2	0.414	Ethylene Glycol Vapor	8.95	9.8807	162.3	2056.4	0.404
Heated 300°C	8.90	9.9361	212.9	1647.9	0.306	Heated 300°C	N.D. [†]	N.D. [†]	N.D. [†]	N.D. [†]	N.D. [†]
Heated 550°C	8.90	9.9361	99.3	948.9	0.361	Heated 550°C	N.D. [†]	N.D. [†]	N.D. [†]	N.D. [†]	N.D. [†]
ART-2, fine						ART-18, fine					
Air-dried	8.75	10.1060	35.6	395.9	0.517	Air-dried	9.05	9.7718	36.9	412.0	0.500
Ethylene Glycol Vapor	8.80	10.0490	39.8	395.2	0.377	Ethylene Glycol Vapor	9.05*	9.7718*	37.1*	530.8*	0.677*
Heated 300°C	8.85	9.9922	35.2	391.8	0.551	Heated 300°C	9.05*	9.7718*	17.9*	145.7*	0.173*
Heated 550°C	8.85	9.9922	121.8	1475.0	0.532	Heated 550°C	N.D. [†]	N.D. [†]	N.D. [†]	N.D. [†]	N.D. [†]
ART-5, coarse						<u>Silurian-Ordovician, Undivided</u>					
Air-dried	8.95	9.8807	454.3	3207.0	0.291	ARM-8, coarse					
Ethylene Glycol Vapor	8.95	9.8807	441.2	3236.3	0.301	Air-dried	N.D. [†]	N.D. [†]	N.D. [†]	N.D. [†]	N.D. [†]
Heated 300°C	8.90	9.9361	97.4	763.4	0.338	Ethylene Glycol Vapor	8.95	N.D. [†]	20.5	153.8	0.387
Heated 550°C	8.80	10.0490	60.7	423.6	0.310	Heated 300°C	8.90	9.9361	24.6	318.6	0.656
						Heated 550°C	N.D. [†]	N.D. [†]	N.D. [†]	N.D. [†]	N.D. [†]

Note: Samples without I₀₀₁ data omitted.

*Broad peak measurement.

[†]N.D. = no data.

[§]Possible smectite interlayering, mainly with illite.

TABLE C6. ILLITE 001 PEAK VALUES AT AIR DRIED, ETHYLENE GLYCOL VAPOR SOLVATED, HEATED 300°C, AND HEATED 550°C

Sample, clay fraction	2 θ (degrees)	D-spacing (angstroms)	Peak max counts (counts/second)	Peak area (integrated counts)	FWHM (degrees)	Sample, clay fraction	2 θ (degrees)	D-spacing (angstroms)	Peak max counts (counts/second)	Peak area (integrated counts)	FWHM (degrees)
<u>Silurian-Ordovician, Undivided</u>						<u>Ordovician Bigfork Formation</u>					
ARM-8, fine						ART-12, fine					
Air-dried	8.90	9.9361	1245.2	21144.1	0.745	Air-dried	8.90*	9.9361*	56.9*	1151.5*	0.875*
Ethylene Glycol Vapor	8.90	9.9361	1119.4	19089.4	0.727	Ethylene Glycol Vapor	8.95*	9.8807*	49.9*	848.6*	0.780*
Heated 300°C	8.95	9.8807	1218.2	18401.0	0.650	Heated 300°C	9.00*	9.8259*	27.8*	500.2*	0.706*
Heated 550°C	8.90	9.9361	1229.7	17802.7	0.625	Heated 550°C	8.85*	9.9922*	22.7*	402.3*	1.130*
ART-19, coarse						<u>Ordovician Womble Formation</u>					
Air-dried						ARM-7, coarse					
Air-dried	8.90	9.9361	775.4	6977.6	0.360	Air-dried	8.85	9.9922	4344.6	39109.5	0.363
Ethylene Glycol Vapor	8.90	9.9361	784.8	7167.5	0.363	Ethylene Glycol Vapor	8.90	9.9361	3978.2	38284.2	0.388
Heated 300°C	9.00	9.8259	47.5	390.1	0.311	Heated 300°C	8.95	9.8807	1723.4	13309.1	0.297
Heated 550°C	8.95	9.8807	39.4	230.5	0.089	Heated 550°C	9.40	9.4087	336.2	3167.6	0.371
ART-19, fine						ARM-7, fine					
Air-dried	8.85	9.9922	219.4	2892.5	0.594	Air-dried	8.85	9.9922	629.9	7379.7	0.491
Ethylene Glycol Vapor	8.90	9.9361	219.0	3050.3	0.615	Ethylene Glycol Vapor	8.90	9.9361	628.9	7660.3	0.498
Heated 300°C	8.80	10.0490	437.0	5184.2	0.506	Heated 300°C	8.85	9.9922	600.2	6811.3	0.486
Heated 550°C	8.85	9.9922	195.2	2407.9	0.527	Heated 550°C	8.90	9.9361	161.9	1860.0	0.528
<u>Ordovician Bigfork Formation</u>						ART-3, coarse					
ART-12, coarse						Air-dried					
Air-dried	8.85	9.9922	61.1	415.1	0.274	Air-dried	8.95	9.8807	288.5	2026.2	0.273
Ethylene Glycol Vapor	8.90	9.9361	68.8	487.3	0.311	Ethylene Glycol Vapor	8.95	9.8807	284.1	2171.5	0.303
Heated 300°C	8.90*	9.9361*	35.0*	244.5*	0.330*	Heated 300°C	8.95	9.8807	86.6	580.7	0.234
Heated 550°C	8.85	9.9922	14.8	71.2	0.241	Heated 550°C	9.05	9.7718	34.3	317.2	0.515

Note: Samples without I₀₀₁ data omitted.

*Broad peak measurement.

†N.D. = no data.

§Possible smectite interlayering, mainly with illite.

TABLE C7. ILLITE 001 PEAK VALUES AT AIR DRIED, ETHYLENE GLYCOL VAPOR SOLVATED, HEATED 300°C, AND HEATED 550°C

Sample, clay fraction	2 θ (degrees)	D-spacing (angstroms)	Peak max counts (counts/second)	Peak area (integrated counts)	FWHM (degrees)
<u>Ordovician Blakely Formation</u>					
ARM-6, coarse					
Air-dried	8.95	9.8807	478.2	3769.5	0.328
Ethylene Glycol Vapor	8.90	9.9361	459.1	3805.2	0.340
Heated 300°C	8.95	9.8807	459.8	3833.7	0.332
Heated 550°C	8.90	9.9361	252.8	2164.7	0.333
ARM-6, fine					
Air-dried	9.00	9.8259	1274.2	13740.7	0.417
Ethylene Glycol Vapor	9.05	9.7718	806.5	7860.0	0.398
Heated 300°C	9.05	9.7718	1230.5	14869.9	0.432
Heated 550°C	9.00	9.8259	1140.7	13494.3	0.443
<i>Note:</i> Samples without I ₀₀₁ data omitted.					
*Broad peak measurement.					
†N.D. = no data.					
§Possible smectite interlayering, mainly with illite.					

TABLE C8. CHLORITE 002 PEAK VALUES AT AIR DRIED, ETHYLENE GLYCOL VAPOR SOLVATED, HEATED 300°C, AND HEATED 550°C

Sample, clay fraction	2 θ (degrees)	D-spacing (angstroms)	Peak max counts (counts/second)	Peak area (integrated counts)	FWHM (degrees)	Sample, clay fraction	2 θ (degrees)	D-spacing (angstroms)	Peak max counts (counts/second)	Peak area (integrated counts)	FWHM (degrees)
<u>Pennsylvanian Johns Valley Formation</u>						<u>Pennsylvanian Jackfork Formation</u>					
ART-14, coarse						ART-15, fine					
Air-dried	12.65	6.9978	773.7	8828.4	0.413	Air-dried	11.90*	7.4371*	95.8*	3565.8*	1.570*
Ethylene Glycol Vapor	12.60	7.0255	793.9	8855.8	0.404	Ethylene Glycol Vapor	12.05*	7.3449*	91.7*	3042.0*	1.693*
Heated 300°C	12.55	7.0533	62.6	1005.4	0.598	Heated 300°C	11.95*	7.4061*	115.2*	3656.1*	1.369*
Heated 550°C	N.D.†	N.D.†	N.D.†	N.D.†	N.D.†	Heated 550°C	N.D.†	N.D.†	N.D.†	N.D.†	N.D.†
<u>Pennsylvanian Jackfork Formation</u>						<u>Mississippian Stanley Formation</u>					
ART-6, coarse [§]						ARM-1, coarse					
Air-dried	12.60	7.0255	2332.6	19790.4	0.337	Air-dried	12.60	7.0255	40	174.7	0.202
Ethylene Glycol Vapor	12.60	7.0255	2418.7	20459.0	0.336	Ethylene Glycol Vapor	12.60	7.0255	34.6	185.4	0.192
Heated 300°C	12.60	7.0255	1031.6	10743.0	0.420	Heated 300°C	12.65	6.9978	13.4?	83.9	0.226
Heated 550°C	N.D.†	N.D.†	N.D.†	N.D.†	N.D.†	Heated 550°C	N.D.†	N.D.†	N.D.†	N.D.†	N.D.†
ART-6, fine [§]						ARM-1, fine					
Air-dried	12.55	7.0533	405.7	3809.4	0.367	Air-dried	12.65	6.9978	307	3699.6	0.458
Ethylene Glycol Vapor	12.55	7.0533	361.7	3449.2	0.388	Ethylene Glycol Vapor	12.60	7.0255	294.8	3611.7	0.461
Heated 300°C	12.70	6.9704	163.1	1935.0	0.512	Heated 300°C	12.70	6.9704	150.2	2095.6	0.517
Heated 550°C	N.D.†	N.D.†	N.D.†	N.D.†	N.D.†	Heated 550°C	13.95*	6.3485*	50.8*	1160.3*	1.087*
ART-15, coarse						ARM-5, coarse					
Air-dried	11.85*	7.4684*	307.1*	11633.7*	1.788*	Air-dried	12.75	6.9432	125.2	1067.5	0.336
Ethylene Glycol Vapor	12.20*	7.2549*	286.4*	10970.5*	1.843*	Ethylene Glycol Vapor	12.85	6.8893	135.8	1193.0	0.383
Heated 300°C	12.10*	7.3146*	110.0*	3355.6*	1.161*	Heated 300°C	12.90	6.8628	104.1	983.0	0.394
Heated 550°C	N.D.†	N.D.†	N.D.†	N.D.†	N.D.†	Heated 550°C	N.D.†	N.D.†	N.D.†	N.D.†	N.D.†

Note: Samples without C₀₀₂ data omitted.

*Broad peak measurement.

†N.D. = no data.

§Possible smectite interlayering, mainly with illite.

TABLE C9. CHLORITE 002 PEAK VALUES AT AIR DRIED, ETHYLENE GLYCOL VAPOR SOLVATED, HEATED 300°C, AND HEATED 550°C

Sample, clay fraction	2 θ (degrees)	D-spacing (angstroms)	Peak max counts (counts/second)	Peak area (integrated counts)	FWHM (degrees)	Sample, clay fraction	2 θ (degrees)	D-spacing (angstroms)	Peak max counts (counts/second)	Peak area (integrated counts)	FWHM (degrees)
<u>Mississippian Stanley Formation</u>						<u>Mississippian Stanley Formation</u>					
ARM-5, fine						ART-18, coarse					
Air-dried	12.65	6.9978	224.5	2009.6	0.330	Air-dried	12.20*	7.2549*	117.3*	3758.0*	1.526*
Ethylene Glycol Vapor	12.60	7.0255	224.0	1894.9	0.316	Ethylene Glycol Vapor	12.15*	7.2846*	119.4*	4167.8*	1.536*
Heated 300°C	12.65	6.9978	134.6	1355.6	0.375	Heated 300°C	N.D.†	N.D.†	N.D.†	N.D.†	N.D.†
Heated 550°C	13.45*	6.5833*	45.1*	918.6*	1.003*	Heated 550°C	N.D.†	N.D.†	N.D.†	N.D.†	N.D.†
ART-2, coarse						ART-18, fine					
Air-dried	12.10*	7.3146*	80.1*	3267.3*	1.780*	Air-dried	12.05*	7.3449*	52.4*	1551.3*	1.389*
Ethylene Glycol Vapor	12.20*	7.2549*	84.7*	3273.4*	1.866*	Ethylene Glycol Vapor	12.30*	7.1961*	51.5*	1674.4*	1.269*
Heated 300°C	12.05*	7.3449*	59.7*	1913.6*	1.699*	Heated 300°C	12.50*	7.0814*	21.9*	347.5*	0.427*
Heated 550°C	N.D.†	N.D.†	N.D.†	N.D.†	N.D.†	Heated 550°C	N.D.†	N.D.†	N.D.†	N.D.†	N.D.†
ART-5, coarse						<u>Silurian-Ordovician, Undivided</u>					
Air-dried	12.20*	7.2549*	225.3*	5377.6*	0.880*	ARM-8, fine					
Ethylene Glycol Vapor	12.25*	7.2254*	235.4*	5518.1*	0.864*	Air-dried	13.80*	6.4171*	68.1*	1686.8*	1.402*
Heated 300°C	12.25*	7.2254*	79.6*	1828.6*	0.889*	Ethylene Glycol Vapor	13.80*	6.4171*	54.7*	1168.1*	1.043*
Heated 550°C	N.D.†	N.D.†	N.D.†	N.D.†	N.D.†	Heated 300°C	13.90*	6.3712*	71.9*	1512.5*	1.227*
ART-5, fine						Heated 550°C					
Air-dried	12.35*	7.1671*	66.1*	1834.0*	1.152*	Heated 550°C	13.60*	6.5111*	103.3*	2750.5*	1.322*
Ethylene Glycol Vapor	12.40*	7.1383*	76.4*	1933.6*	1.027*	ART-19, coarse					
Heated 300°C	12.35*	7.1671*	47.1*	994.7*	0.778*	Air-dried	12.00*	7.3754*	47.9*	945.2*	0.825*
Heated 550°C	N.D.†	N.D.†	N.D.†	N.D.†	N.D.†	Ethylene Glycol Vapor	12.25*	7.2257*	48.7*	1072.6*	1.128*
						Heated 300°C	N.D.†	N.D.†	N.D.†	N.D.†	N.D.†
						Heated 550°C	N.D.†	N.D.†	N.D.†	N.D.†	N.D.†

Note: Samples without C₀₀₂ data omitted.

*Broad peak measurement.

†N.D. = no data.

§Possible smectite interlayering, mainly with illite.

TABLE C10. CHLORITE 002 PEAK VALUES AT AIR DRIED, ETHYLENE GLYCOL VAPOR SOLVATED, HEATED 300°C, AND HEATED 550°C

Sample, clay fraction	2 θ (degrees)	D-spacing (angstroms)	Peak max counts (counts/second)	Peak area (integrated counts)	FWHM (degrees)	Sample, clay fraction	2 θ (degrees)	D-spacing (angstroms)	Peak max counts (counts/second)	Peak area (integrated counts)	FWHM (degrees)
<u>Silurian-Ordovician, Undivided</u>						<u>Ordovician Womble Formation</u>					
ART-19, fine						ARM-7, fine					
Air-dried	N.D. [†]	N.D. [†]	N.D. [†]	N.D. [†]	N.D. [†]	Air-dried	12.60	7.0255	31.8	227.1	0.259
Ethylene Glycol Vapor	N.D. [†]	N.D. [†]	N.D. [†]	N.D. [†]	N.D. [†]	Ethylene Glycol Vapor	12.55	7.0533	33.3	216.1	0.228
Heated 300°C	12.40*	7.1383*	34.2*	572.6*	0.882*	Heated 300°C	12.60	7.0255	18.5	128.5	0.212
Heated 550°C	N.D. [†]	N.D. [†]	N.D. [†]	N.D. [†]	N.D. [†]	Heated 550°C	N.D. [†]	N.D. [†]	N.D. [†]	N.D. [†]	N.D. [†]
<u>Ordovician Bigfork Formation</u>						ART-3, coarse					
ART-12, coarse						Air-dried					
Air-dried	12.60	7.0255	74.4	623.8	0.318	Ethylene Glycol Vapor	12.3*	7.1961*	137.8*	3334.4*	0.888*
Ethylene Glycol Vapor	12.60	7.0255	77.1	624.9	0.288	Heated 300°C	12.35*	7.1671*	85.3*	1521.7*	0.553*
Heated 300°C	12.5*	7.0814*	46.6*	418.9*	0.451*	Heated 550°C	N.D. [†]	N.D. [†]	N.D. [†]	N.D. [†]	N.D. [†]
Heated 550°C	N.D. [†]	N.D. [†]	N.D. [†]	N.D. [†]	N.D. [†]	<u>Ordovician Blakely Formation</u>					
ART-12, fine						ARM-6, coarse					
Air-dried	12.25*	7.2254*	77.4*	2179.4*	1.466*	Air-dried	12.55	7.0533	66.8	491.1	0.327
Ethylene Glycol Vapor	12.15*	7.2846*	59.4*	1914.4*	1.735*	Ethylene Glycol Vapor	12.55	7.0533	65.4	587.5	0.355
Heated 300°C	12.40*	7.1383*	43.0*	1249.2*	1.377*	Heated 300°C	12.50	7.0814	55.0	549.0	0.504
Heated 550°C	N.D. [†]	N.D. [†]	N.D. [†]	N.D. [†]	N.D. [†]	Heated 550°C	N.D. [†]	N.D. [†]	N.D. [†]	N.D. [†]	N.D. [†]
<u>Ordovician Womble Formation</u>						ARM-6, fine					
ARM-7, coarse						Air-dried					
Air-dried	12.55	7.0533	181.1	1553.0	0.302	Ethylene Glycol Vapor	12.70	6.9704	38.2	290.6	0.421
Ethylene Glycol Vapor	12.60	7.0255	164.0	1517.2	0.318	Heated 300°C	12.65	6.9978	31.5	213.7	0.319
Heated 300°C	12.60	7.0255	92.8	622.5	0.254	Heated 550°C	13.85*	6.3941*	74.5*	1593.9*	1.094*
Heated 550°C	N.D. [†]	N.D. [†]	N.D. [†]	N.D. [†]	N.D. [†]						

Note: Samples without C₀₀₂ data omitted.

*Broad peak measurement.

[†]N.D. = no data.

[§]Possible smectite interlayering, mainly withillite.

TABLE C11. ILLITE 002 PEAK VALUES AT AIR DRIED, ETHYLENE GLYCOL VAPOR SOLVATED, HEATED 300°C, AND HEATED 550°C

Sample, clay fraction	2 θ (degrees)	D-spacing (angstroms)	Peak max counts (counts/second)	Peak area (integrated counts)	FWHM (degrees)	Sample, clay fraction	2 θ (degrees)	D-spacing (angstroms)	Peak max counts (counts/second)	Peak area (integrated counts)	FWHM (degrees)
<u>Pennsylvanian Johns Valley Formation</u>						<u>Pennsylvanian Jackfork Formation</u>					
ART-14, fine						ART-15, fine					
Air-dried	N.D. [†]	N.D. [†]	N.D. [†]	N.D. [†]	N.D. [†]	Air-dried	N.D. [†]	N.D. [†]	N.D. [†]	N.D. [†]	N.D. [†]
Ethylene Glycol Vapor	18.06*	4.9109*	19.6*	153.5*	0.458*	Ethylene Glycol Vapor	17.90	4.9555	62.9	911.3	0.637
Heated 300°C	N.D. [†]	N.D. [†]	N.D. [†]	N.D. [†]	N.D. [†]	Heated 300°C	17.90*	4.9555*	51.5*	912.4*	1.105*
Heated 550°C	N.D. [†]	N.D. [†]	N.D. [†]	N.D. [†]	N.D. [†]	Heated 550°C	17.50*	5.0678*	68.3*	1194.0*	0.904*
<u>Pennsylvanian Jackfork Formation</u>						<u>Mississippian Stanley Formation</u>					
ART-6, coarse [§]						ARM-1, coarse					
Air-dried	17.85	4.9692	72.7	707.2	0.505	Air-dried	18.10*	4.9012*	32.7*	767.0*	1.099*
Ethylene Glycol Vapor	17.95*	4.9431*	89.5*	1154.2*	0.894*	Ethylene Glycol Vapor	18.05*	4.9146*	34.5*	721.2*	1.133*
Heated 300°C	17.85	4.9692	103.5	1513.9	0.727	Heated 300°C	18.08	4.9079	52.4	633.8	0.55
Heated 550°C	18.35*	4.835*	94*	1913.6*	1.094*	Heated 550°C	17.85*	4.9692*	50.0*	1203.9*	1.484*
ART-6, fine [§]						ARM-1, fine					
Air-dried	N.D. [†]	N.D. [†]	N.D. [†]	N.D. [†]	N.D. [†]	Air-dried	17.75	4.9970	366.1	5656.5	0.641
Ethylene Glycol Vapor	18.70*	4.7452*	207.2*	4298.0*	0.780*	Ethylene Glycol Vapor	17.80	4.9831	422.3	5940.3	0.589
Heated 300°C	N.D. [†]	N.D. [†]	N.D. [†]	N.D. [†]	N.D. [†]	Heated 300°C	17.85	4.9692	445.8	6027.6	0.519
Heated 550°C	18.60*	4.7705*	81.0*	3447.6*	0.769*	Heated 550°C	17.80	4.9831	468.1	6207.8	0.528
ART-15, coarse						ARM-5, coarse					
Air-dried	17.90*	4.9555*	45.3*	585.8*	0.632*	Air-dried	17.95	4.9418	174.7	2290.6	0.521
Ethylene Glycol Vapor	17.95*	4.9418*	43.8*	659.4*	0.712*	Ethylene Glycol Vapor	18.00	4.9282	192.5	2390.1	0.494
Heated 300°C	17.97	4.9365	28.4	401.3	0.681	Heated 300°C	18.05	4.9146	176.1	2480.5	0.491
Heated 550°C	17.80*	4.9822*	41.6*	739.0*	0.675*	Heated 550°C	18.05	4.9146	145.2	2098.7	0.53
<i>Note:</i> Samples without I ₀₀₂ data omitted.											
*Broad peak measurement.											
[†] N.D. = no data.											
[§] Possible smectite interlayering, mainly with illite											

TABLE C12. ILLITE 002 PEAK VALUES AT AIR DRIED, ETHYLENE GLYCOL VAPOR SOLVATED, HEATED 300°C, AND HEATED 550°C

Sample, clay fraction	2 θ (degrees)	D-spacing (angstroms)	Peak max counts (counts/second)	Peak area (integrated counts)	FWHM (degrees)	Sample, clay fraction	2 θ (degrees)	D-spacing (angstroms)	Peak max counts (counts/second)	Peak area (integrated counts)	FWHM (degrees)
<u>Mississippian Stanley Formation</u>						<u>Mississippian Stanley Formation</u>					
ARM-5, fine						ART-5, fine					
Air-dried	17.85	4.9692	370.0	4787.7	0.536	Air-dried	17.90	4.9555	39.0	349.4	0.389
Ethylene Glycol Vapor	17.80	4.9831	385.8	4907.8	0.522	Ethylene Glycol Vapor	17.95	4.9418	35.3	356.8	0.402
Heated 300°C	17.85	4.9692	434.3	4949.4	0.470	Heated 300°C	17.85	4.9692	56.8	621.5	0.388
Heated 550°C	17.70	5.0110	472.6	5415.7	0.457	Heated 550°C	17.77*	4.9912*	49.3*	1381.6*	0.869*
ART-2, coarse						ART-18, coarse					
Air-dried	17.80	4.9831	155.5	1271.9	0.391	Air-dried	17.85	4.9692	47.3	399.7	0.414
Ethylene Glycol Vapor	17.85	4.9692	148.2	1299.4	0.344	Ethylene Glycol Vapor	17.90	4.9555	60.3	456.8	0.485
Heated 300°C	17.85	4.9692	110.4	1105.3	0.322	Heated 300°C	N.D.†	N.D.†	N.D.†	N.D.†	N.D.†
Heated 550°C	17.70	5.0110	115.6	1179.2	0.350	Heated 550°C	N.D.†	N.D.†	N.D.†	N.D.†	N.D.†
ART-2, fine						ART-18, fine					
Air-dried	N.D.†	N.D.†	N.D.†	N.D.†	N.D.†	Air-dried	18.00	4.9282	27.0	418.8	0.702
Ethylene Glycol Vapor	17.78*	4.9900*	71.2*	1124.3*	.884*	Ethylene Glycol Vapor	18.10	4.9012	20.1	301.1	0.769
Heated 300°C	17.75	4.9970	73.4	962.9	0.750	Heated 300°C	N.D.†	N.D.†	N.D.†	N.D.†	N.D.†
Heated 550°C	17.75	4.9970	120.6	1271.6	0.443	Heated 550°C	17.75*	4.996*	20.2*	213.6*	0.240*
ART-5, coarse						<u>Silurian-Ordovician, Undivided</u>					
Air-dried	17.85	4.9692	234.5	1734.8	0.303	ARM-8, fine					
Ethylene Glycol Vapor	17.85	4.9692	240.8	1734.2	0.278	Air-dried	17.90	4.9555	687.9	13324.2	0.762
Heated 300°C	N.D.†	N.D.†	N.D.†	N.D.†	N.D.†	Ethylene Glycol Vapor	17.90	4.9555	711.9	12466.7	0.709
Heated 550°C	17.71	5.0092	129.7	1827.8	0.468	Heated 300°C	17.95	4.9418	784.4	13325.8	0.654
						Heated 550°C	17.80	4.9831	1057.8	17501.7	0.636

Note: Samples without I₀₀₂ data omitted.

*Broad peak measurement.

†N.D. = no data.

§Possible smectite interlayering, mainly with illite.

TABLE C13. ILLITE 002 PEAK VALUES AT AIR DRIED, ETHYLENE GLYCOL VAPOR SOLVATED, HEATED 300°C, AND HEATED 550°C

Sample, clay fraction	2 θ (degrees)	D-spacing (angstroms)	Peak max counts (counts/second)	Peak area (integrated counts)	FWHM (degrees)	Sample, clay fraction	2 θ (degrees)	D-spacing (angstroms)	Peak max counts (counts/second)	Peak area (integrated counts)	FWHM (degrees)
<u>Silurian-Ordovician, Undivided</u>						<u>Ordovician Womble Formation</u>					
ART-19, coarse						ARM-7, coarse					
Air-dried	17.80	4.9831	261.5	2265.8	0.383	Air-dried	17.80	4.9831	2626.8	25643.4	0.375
Ethylene Glycol Vapor	17.80	4.9831	285.4	2313.1	0.343	Ethylene Glycol Vapor	17.75	4.9970	2762.6	25505.6	0.347
Heated 300°C	17.90*	4.9555*	60.9*	1875.6*	1.238*	Heated 300°C	17.85	4.9692	1422.6	11894.0	0.313
Heated 550°C	17.79*	4.9856*	61.4*	1459.2*	0.911	Heated 550°C	18.25	4.8612	738.4	6633.7	0.367
ART-19, fine						ARM-7, fine					
Air-dried	17.85	4.9692	115.4	1272.2	0.502	Air-dried	17.80	4.9831	365.8	4664.1	0.527
Ethylene Glycol Vapor	17.80	4.9831	120.1	1353.7	0.530	Ethylene Glycol Vapor	17.80	4.9831	416.4	4817.1	0.454
Heated 300°C	17.80	4.9831	257.5	3617.7	0.575	Heated 300°C	17.75	4.9970	400.2	5325.0	0.472
Heated 550°C	17.80	4.9831	241.6	3494.7	0.554	Heated 550°C	17.75	4.9970	322.4	4395.6	0.501
<u>Ordovician Bigfork Formation</u>						ART-3, coarse					
ART-12, coarse						Air-dried					
Air-dried	17.90	4.9555	38.6	267.8	0.321	Ethylene Glycol Vapor	17.90	4.9555	167.3	1095.4	0.281
Ethylene Glycol Vapor	17.90	4.9555	43.4	308.7	0.296	Heated 300°C	17.90	4.9555	64.7	717.6	0.349
Heated 300°C	17.95	4.9418	32.2	309.6	0.464	Heated 550°C	17.70*	5.0110*	61.3*	861.3*	0.576*
Heated 550°C	17.70	5.0110	40.0	515.9	0.199	<u>Ordovician Blakely Formation</u>					
ART-12, fine						ARM-6, coarse					
Air-dried	17.95*	4.9418*	37.1*	543.1*	0.763*	Air-dried	17.90	4.9555	428.0	4051.1	0.357
Ethylene Glycol Vapor	17.90*	4.9555*	33.9*	716.6*	0.906*	Ethylene Glycol Vapor	17.90	4.9555	442.1	4045.6	0.349
Heated 300°C	N.D.†	N.D.†	N.D.†	N.D.†	N.D.†	Heated 300°C	17.90	4.9555	445.3	3941.0	0.335
Heated 550°C	N.D.†	N.D.†	N.D.†	N.D.†	N.D.†	Heated 550°C	17.75	7.9970	360.0	4042.4	0.378

Note: Samples without I₀₀₂ data omitted.

*Broad peak measurement.

†N.D. = no data.

§Possible smectite interlayering, mainly with illite.

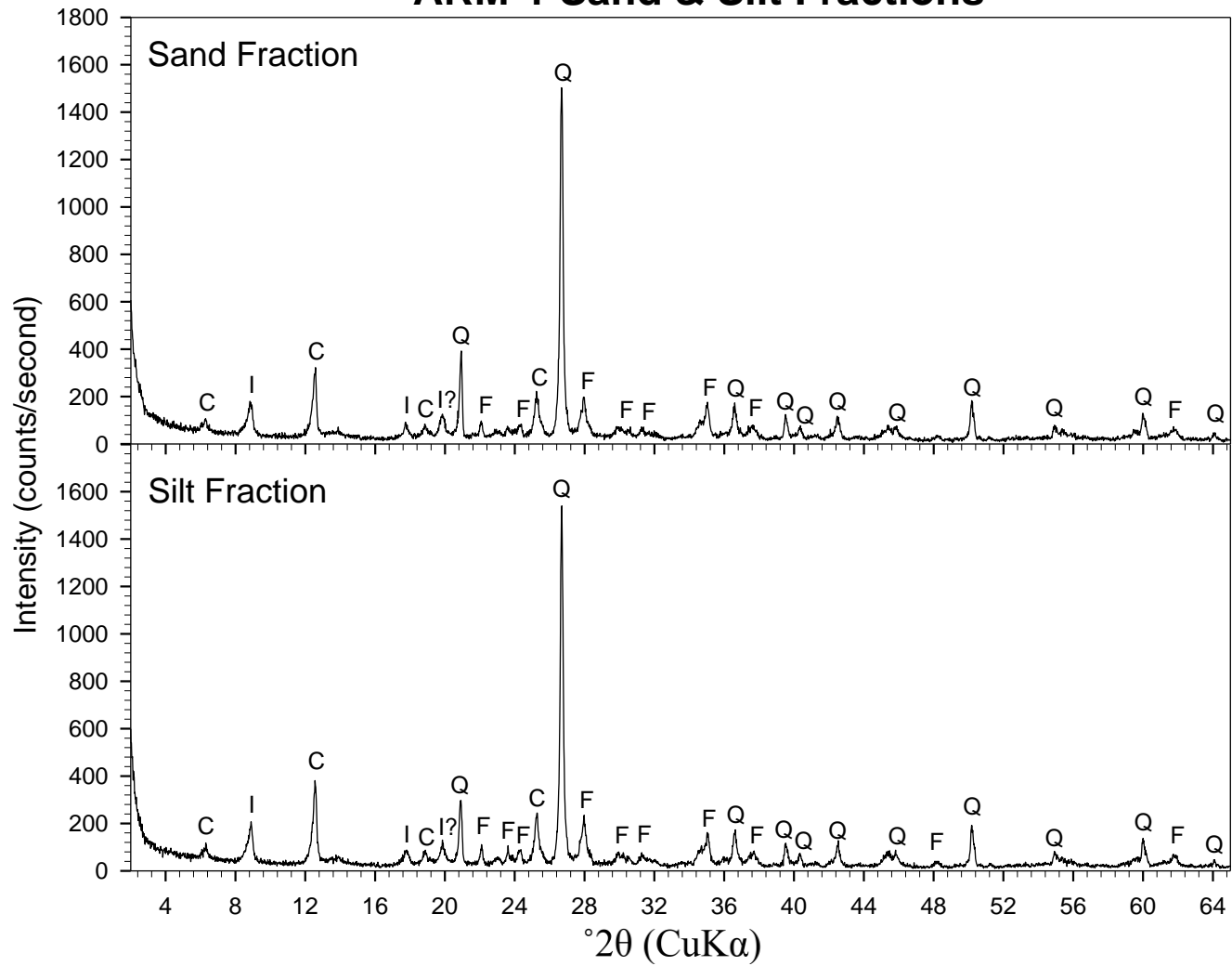
TABLE C14. ILLITE 002 PEAK VALUES AT AIR DRIED, ETHYLENE GLYCOL VAPOR SOLVATED, HEATED 300°C, AND HEATED 550°C

Sample, clay fraction	2 θ (degrees)	D-spacing (angstroms)	Peak max counts (counts/second)	Peak area (integrated counts)	FWHM (degrees)
<u>Ordovician Blakely Formation</u>					
ARM-6, fine					
Air-dried	17.95	4.9418	760.2	8199.5	0.440
Ethylene Glycol Vapor	18.00	4.9282	572.8	6427.3	0.413
Heated 300°C	18.00	4.9282	772.1	8616.5	0.425
Heated 550°C	17.80	4.9831	1038.4	11157.8	0.421
<i>Note:</i> Samples without I ₀₀₂ data omitted.					
*Broad peak measurement.					
†N.D. = no data.					
§Possible smectite interlayering, mainly with illite.					

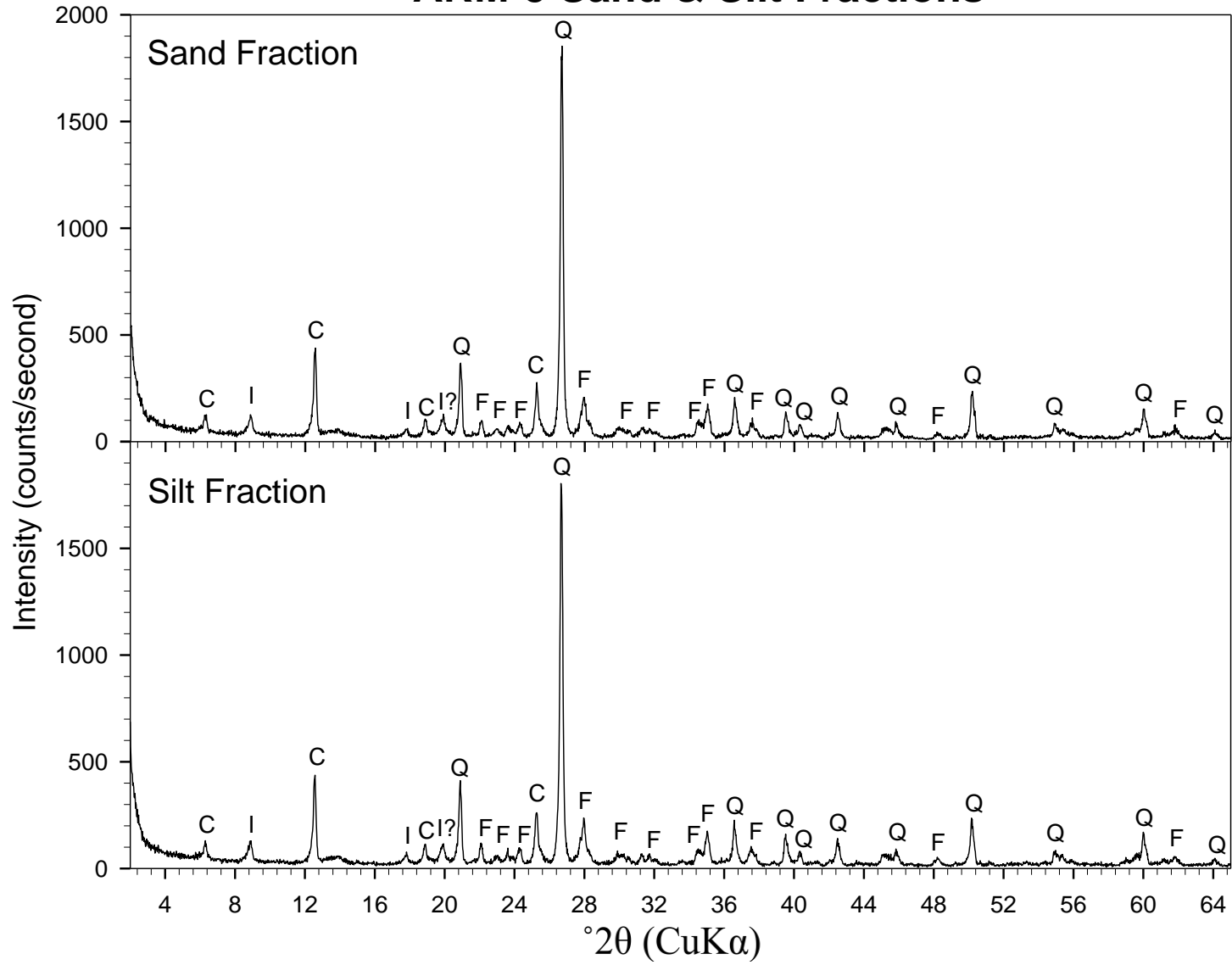
APPENDIX D

X-RAY DIFFRACTOGRAMS

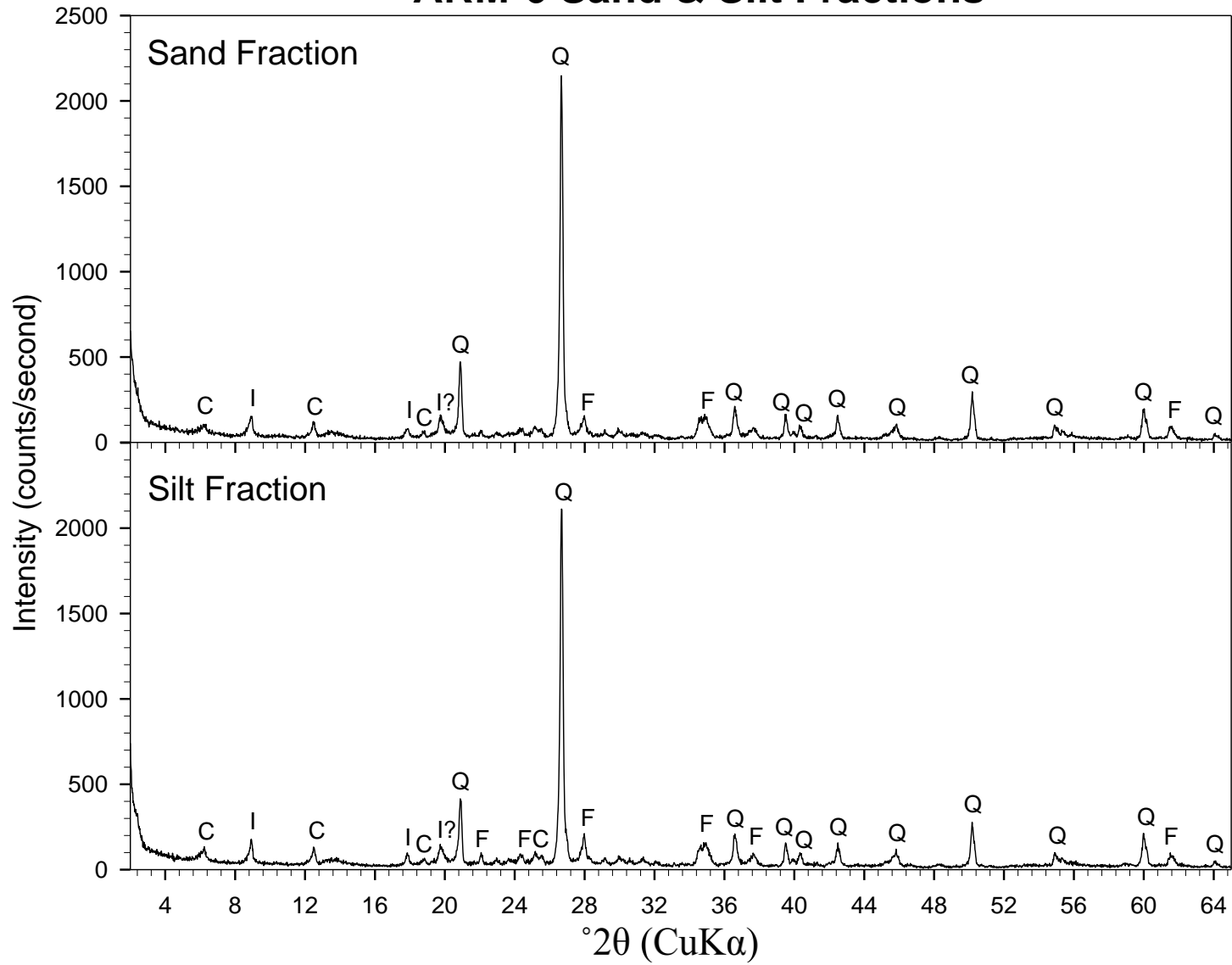
ARM-1 Sand & Silt Fractions



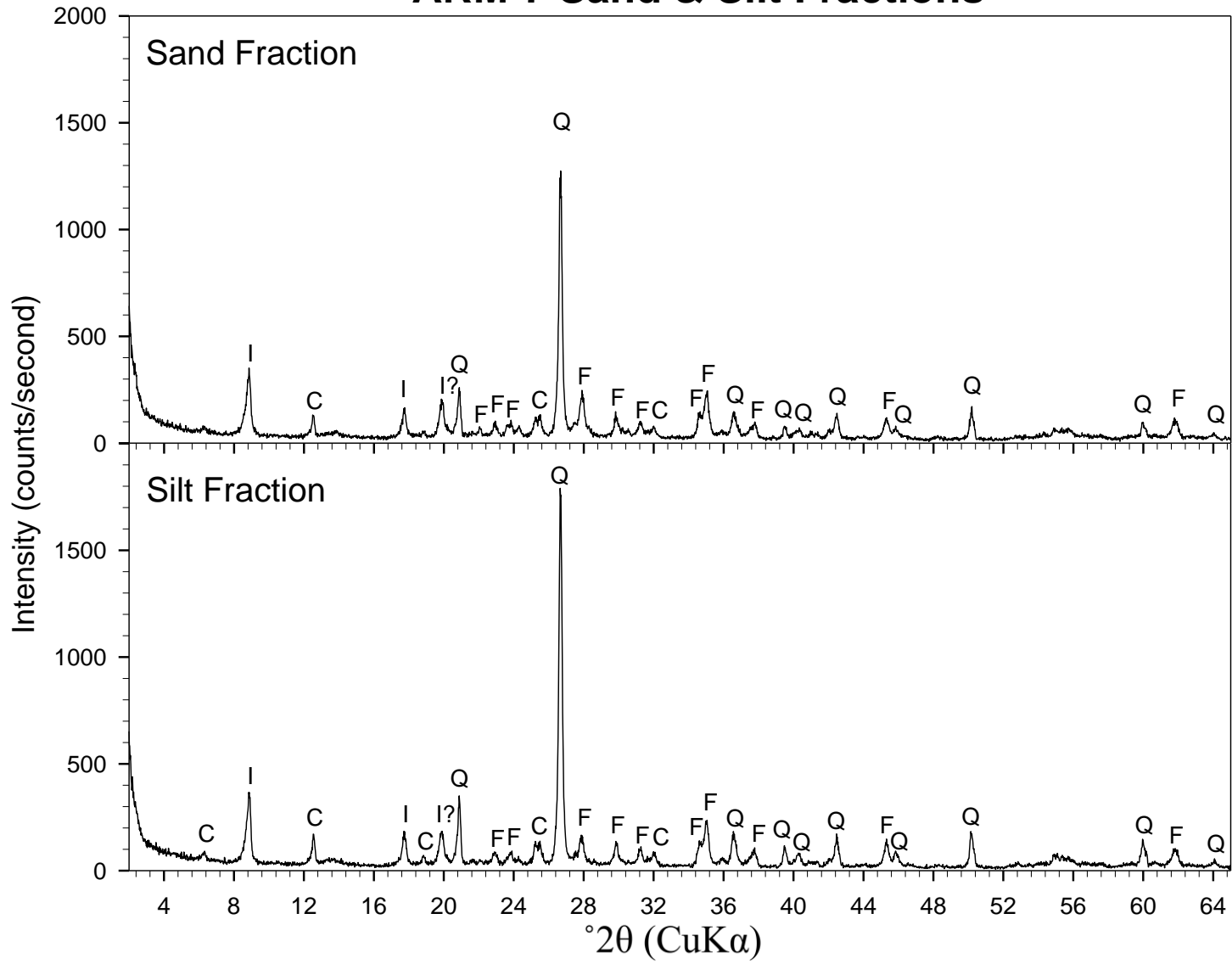
ARM-5 Sand & Silt Fractions



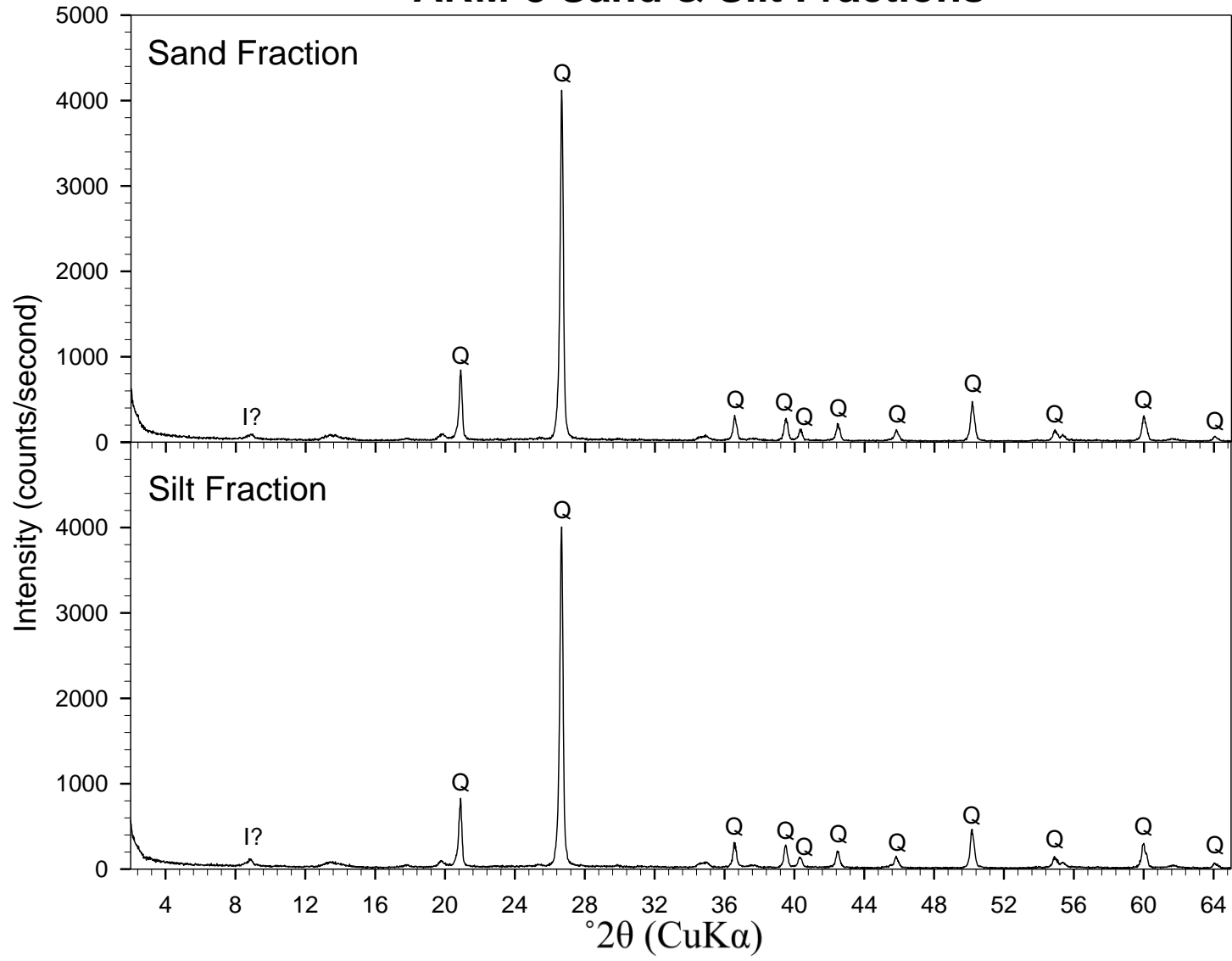
ARM-6 Sand & Silt Fractions



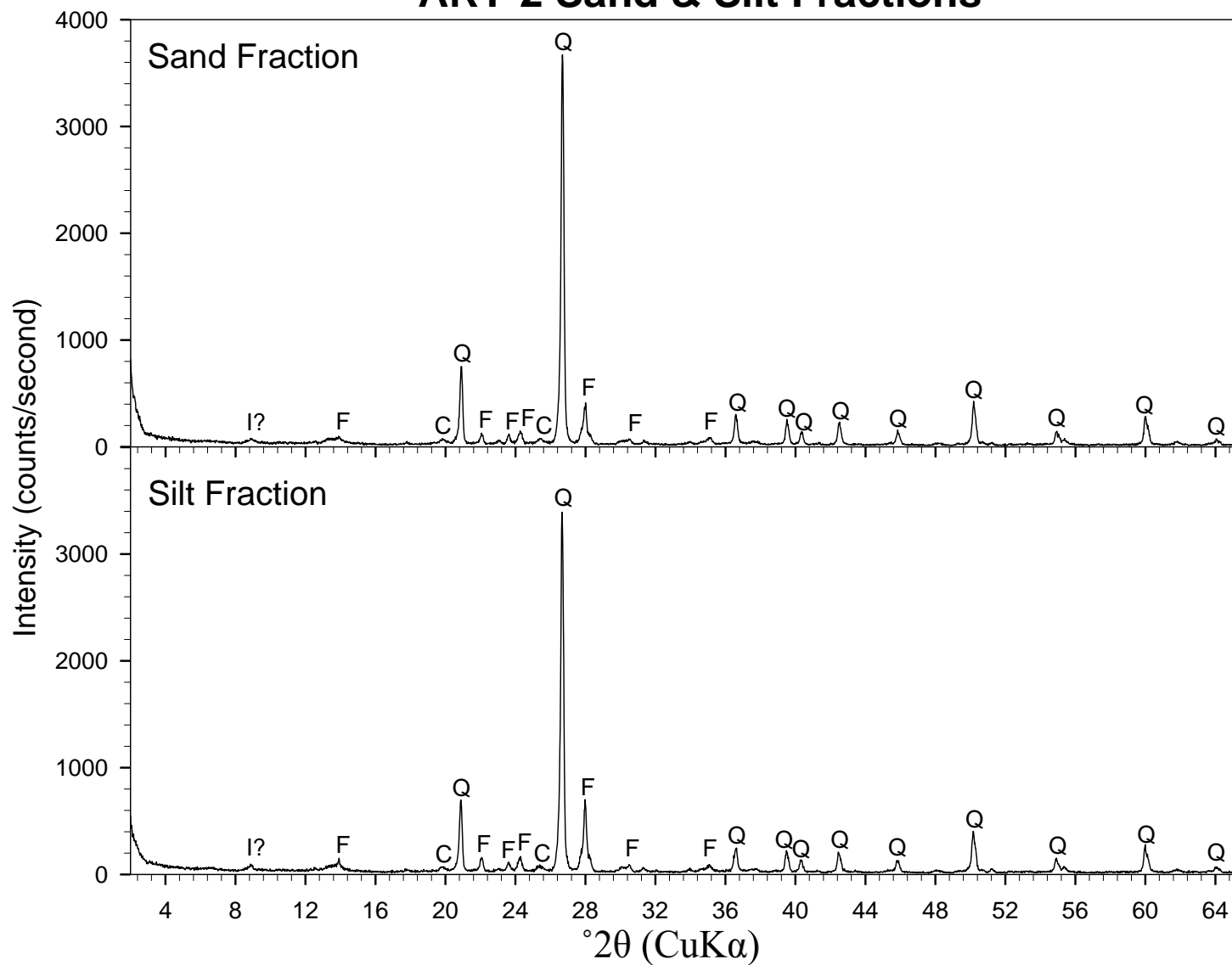
ARM-7 Sand & Silt Fractions



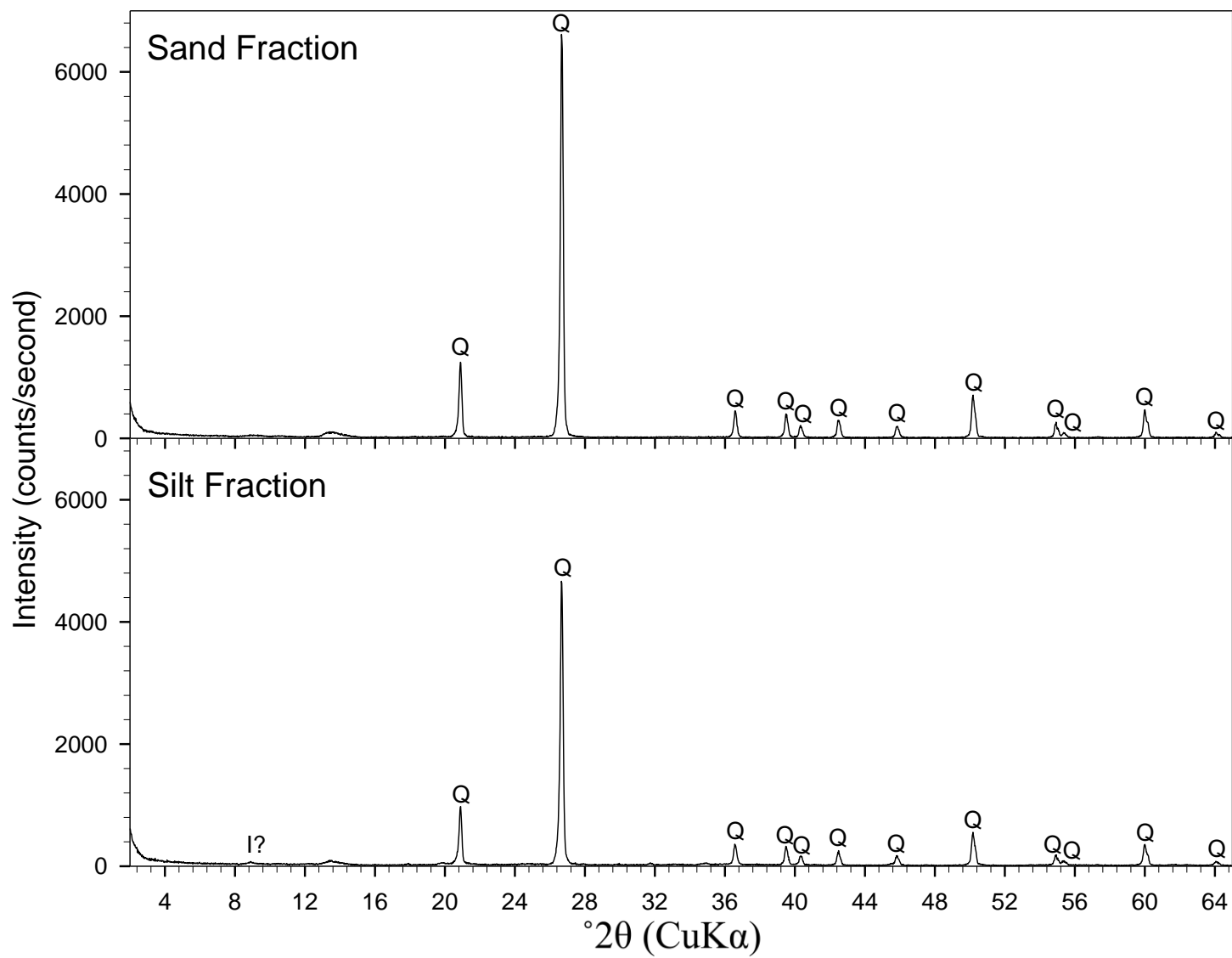
ARM-8 Sand & Silt Fractions



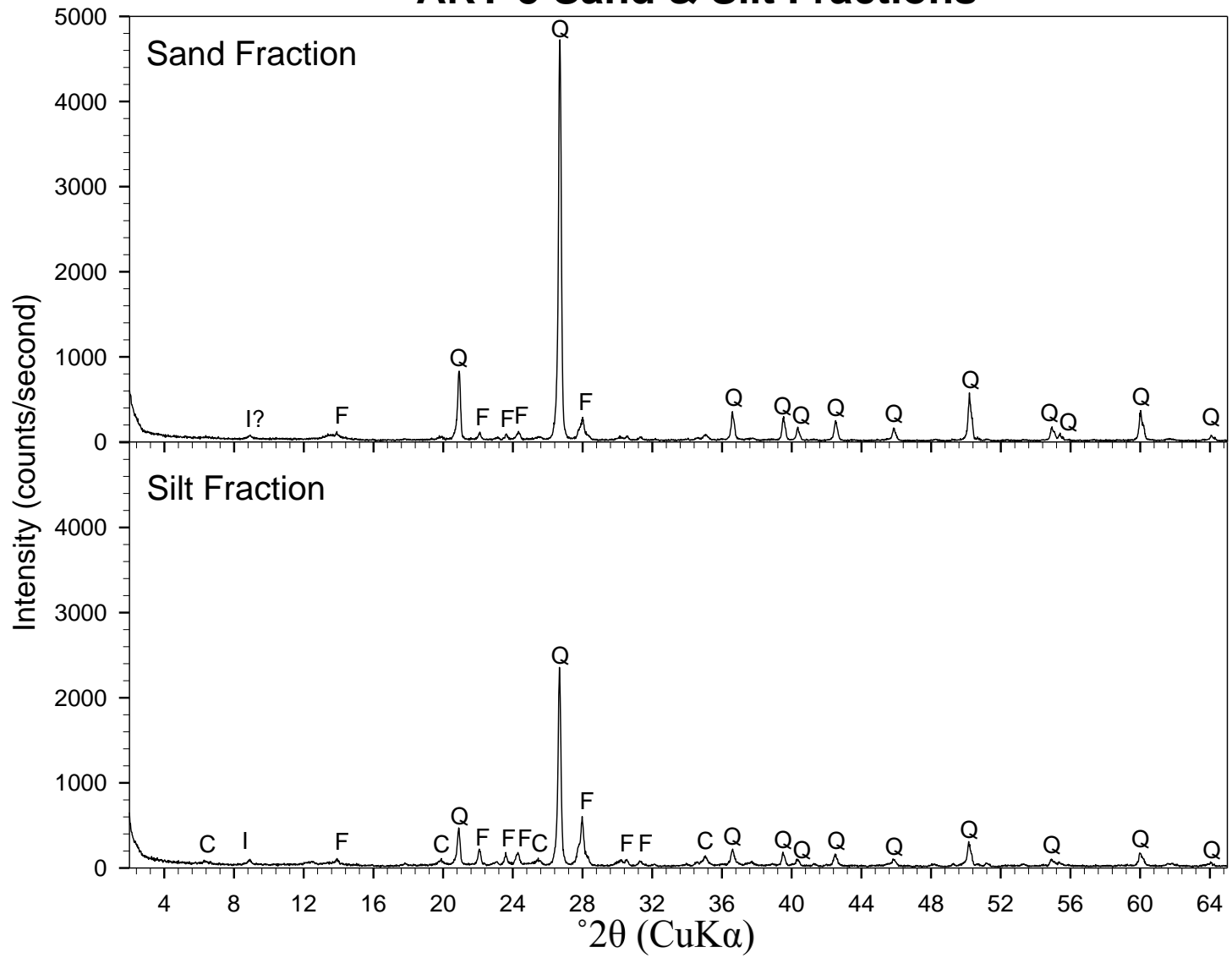
ART-2 Sand & Silt Fractions



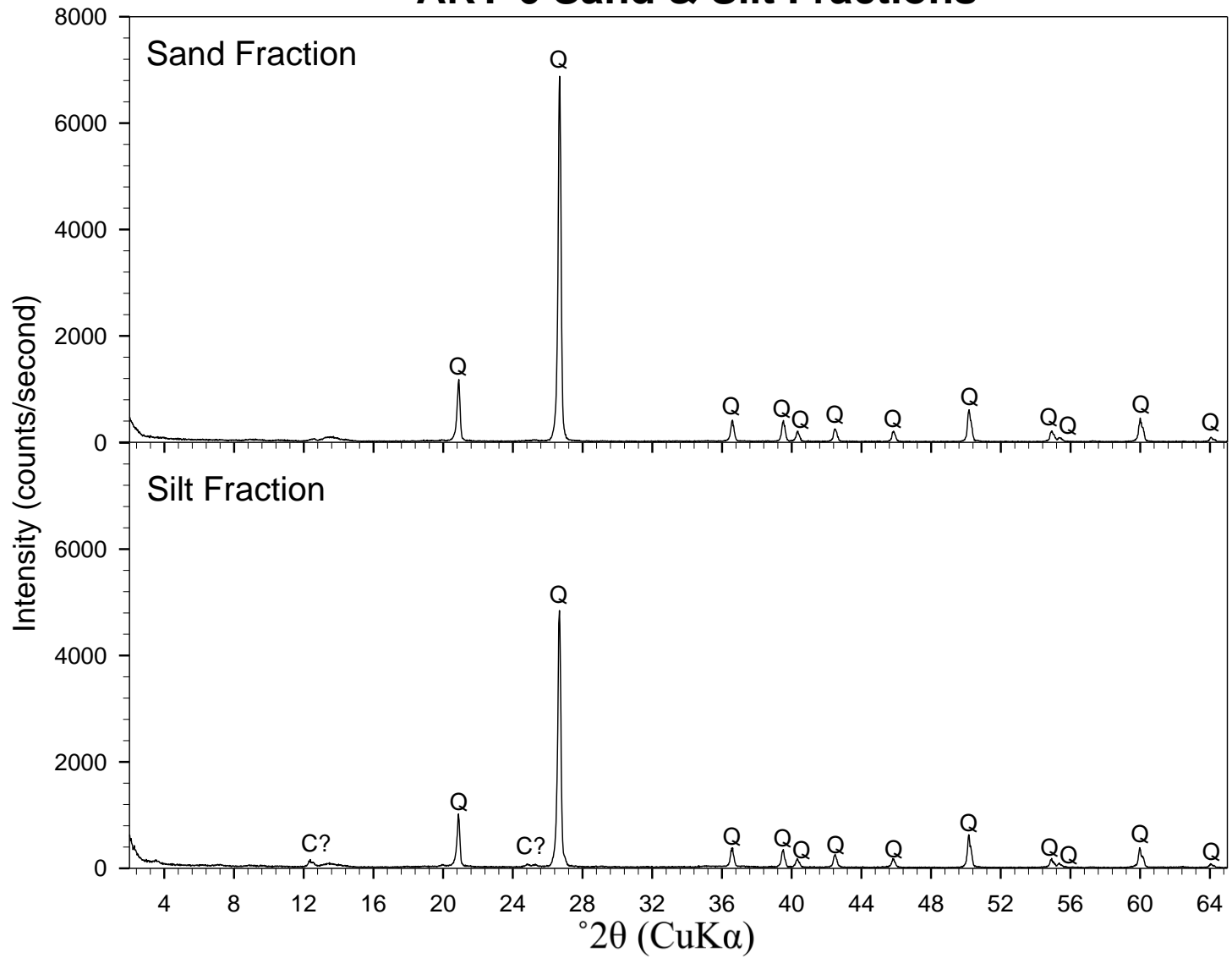
ART-3 Sand & Silt Fractions



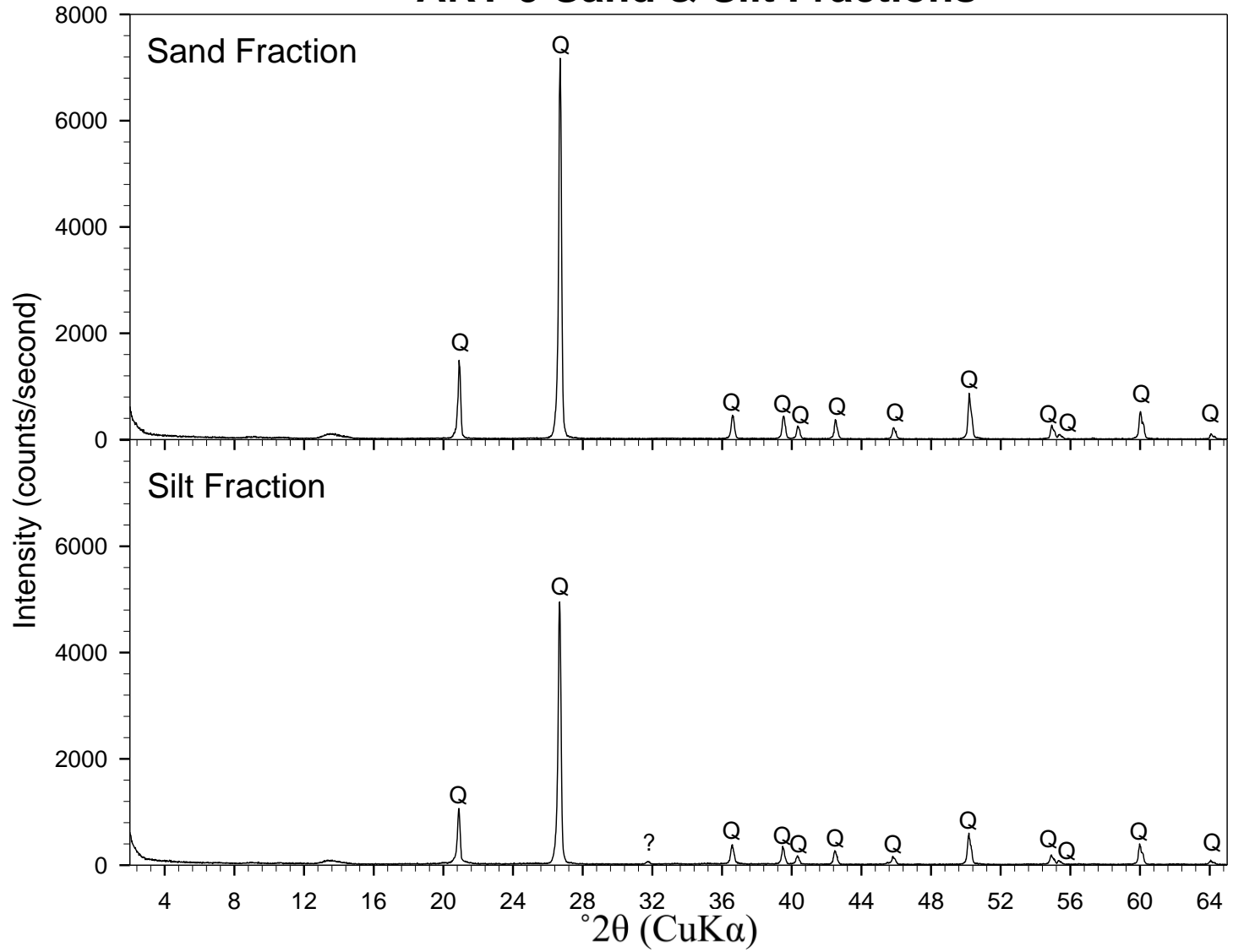
ART-5 Sand & Silt Fractions



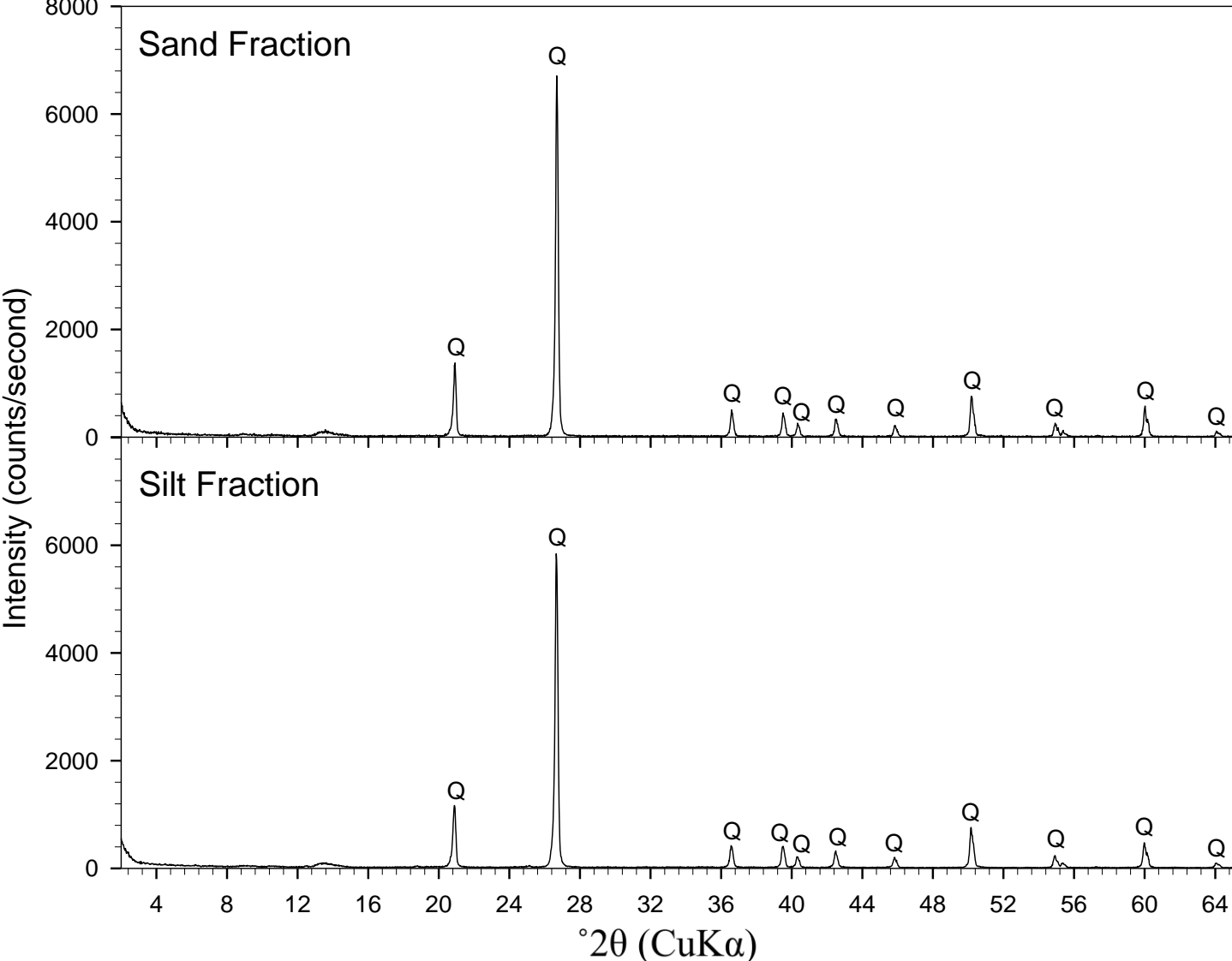
ART-6 Sand & Silt Fractions



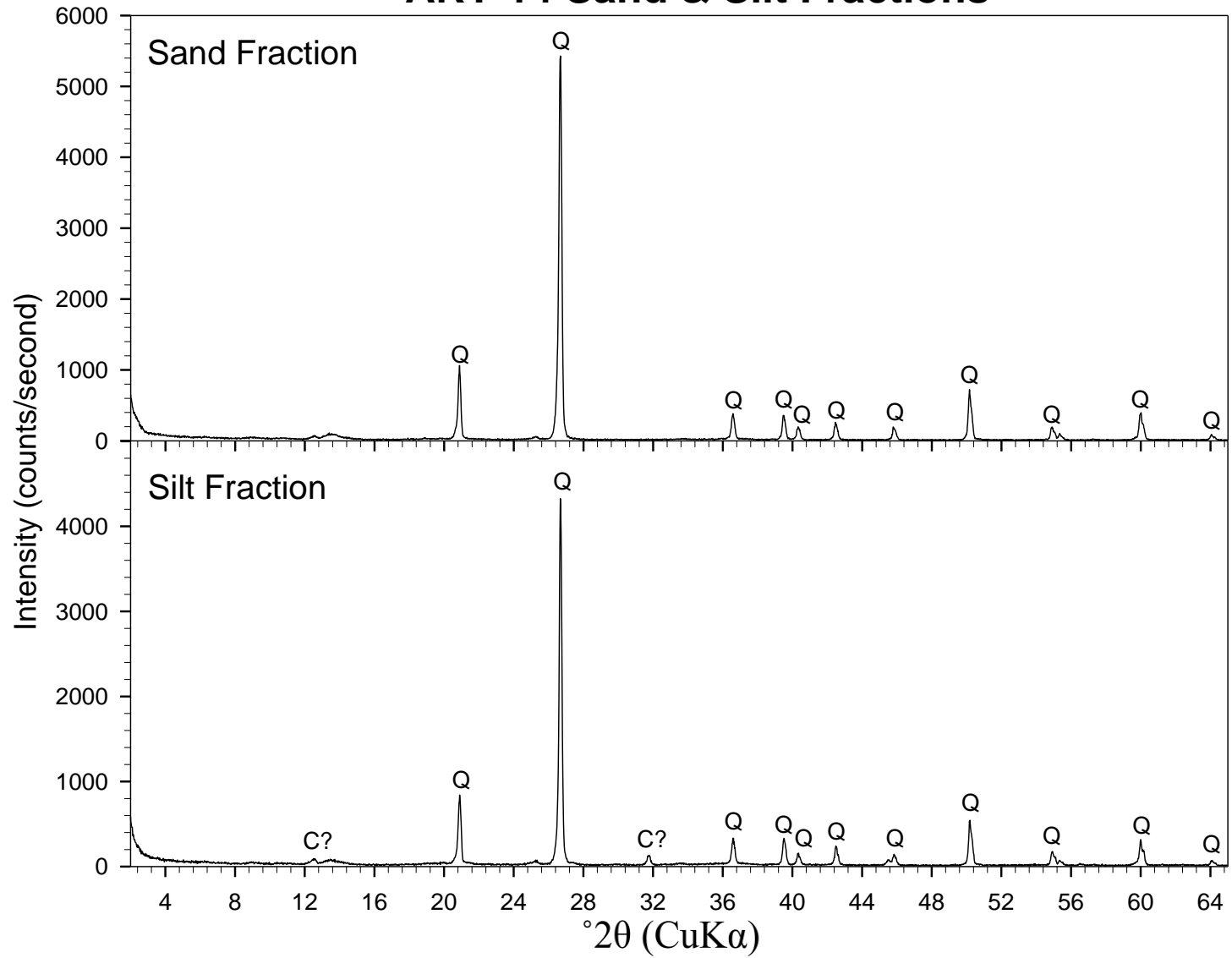
ART-9 Sand & Silt Fractions



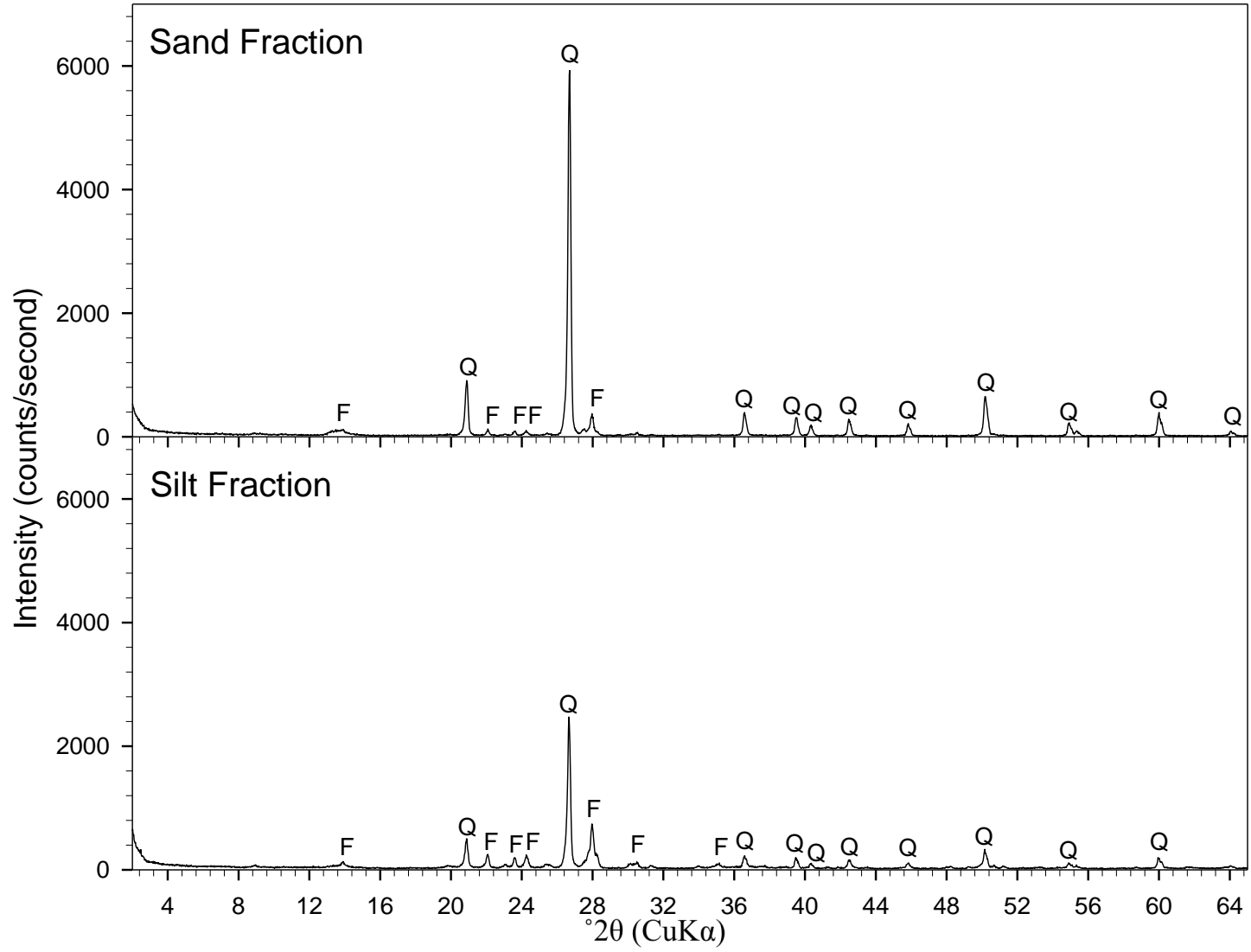
ART-12 Sand & Silt Fractions



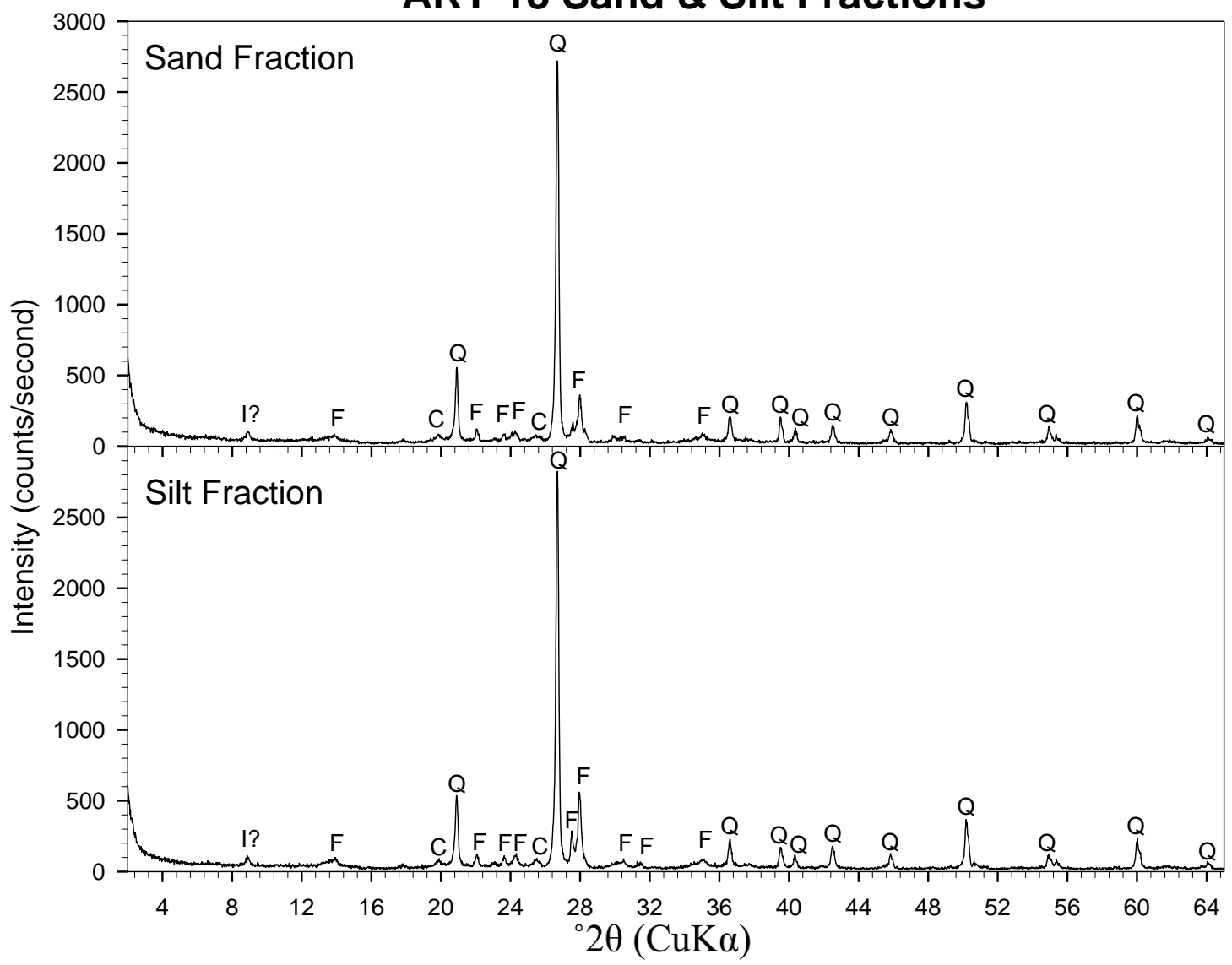
ART-14 Sand & Silt Fractions



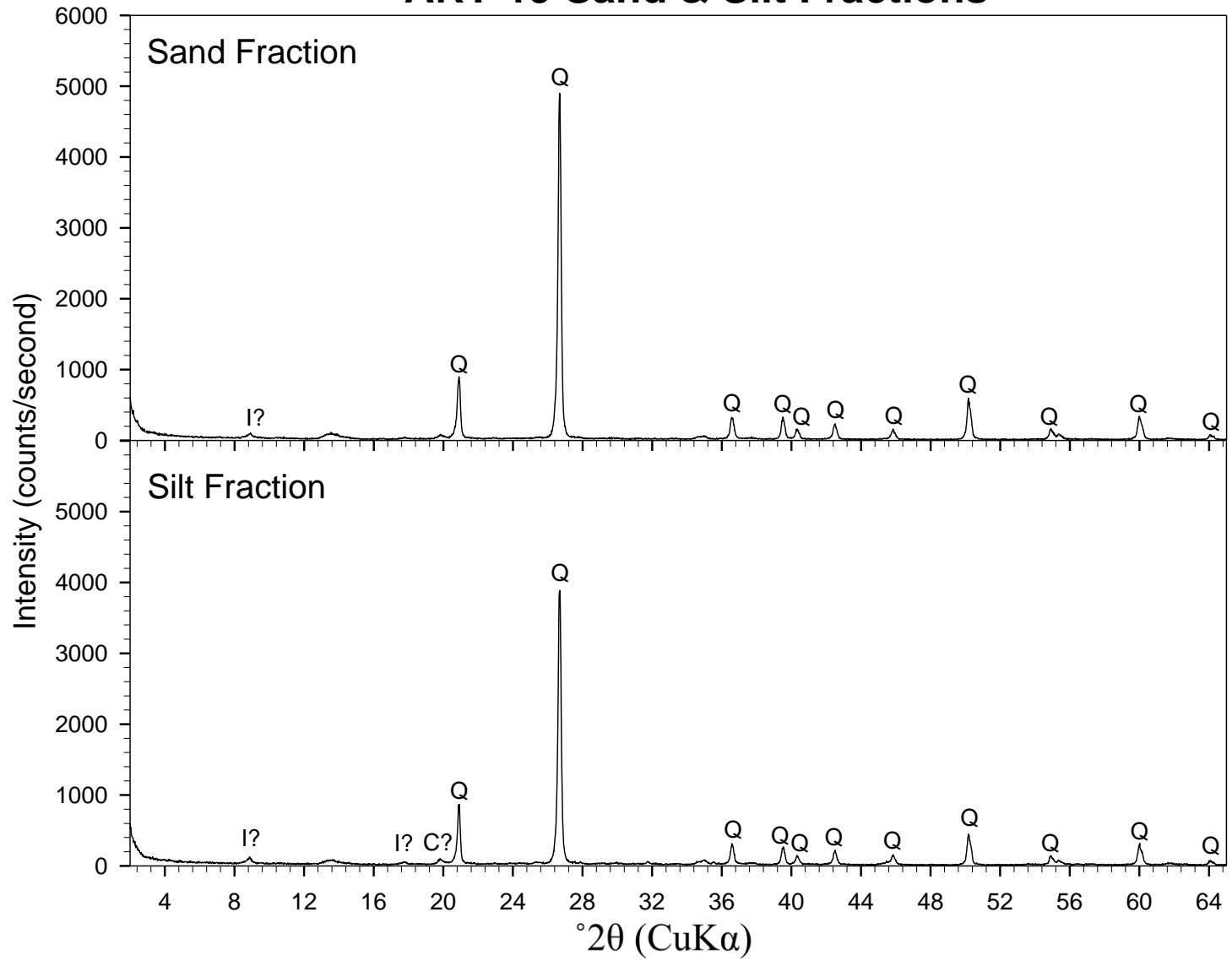
ART-15 Sand & Silt Fractions



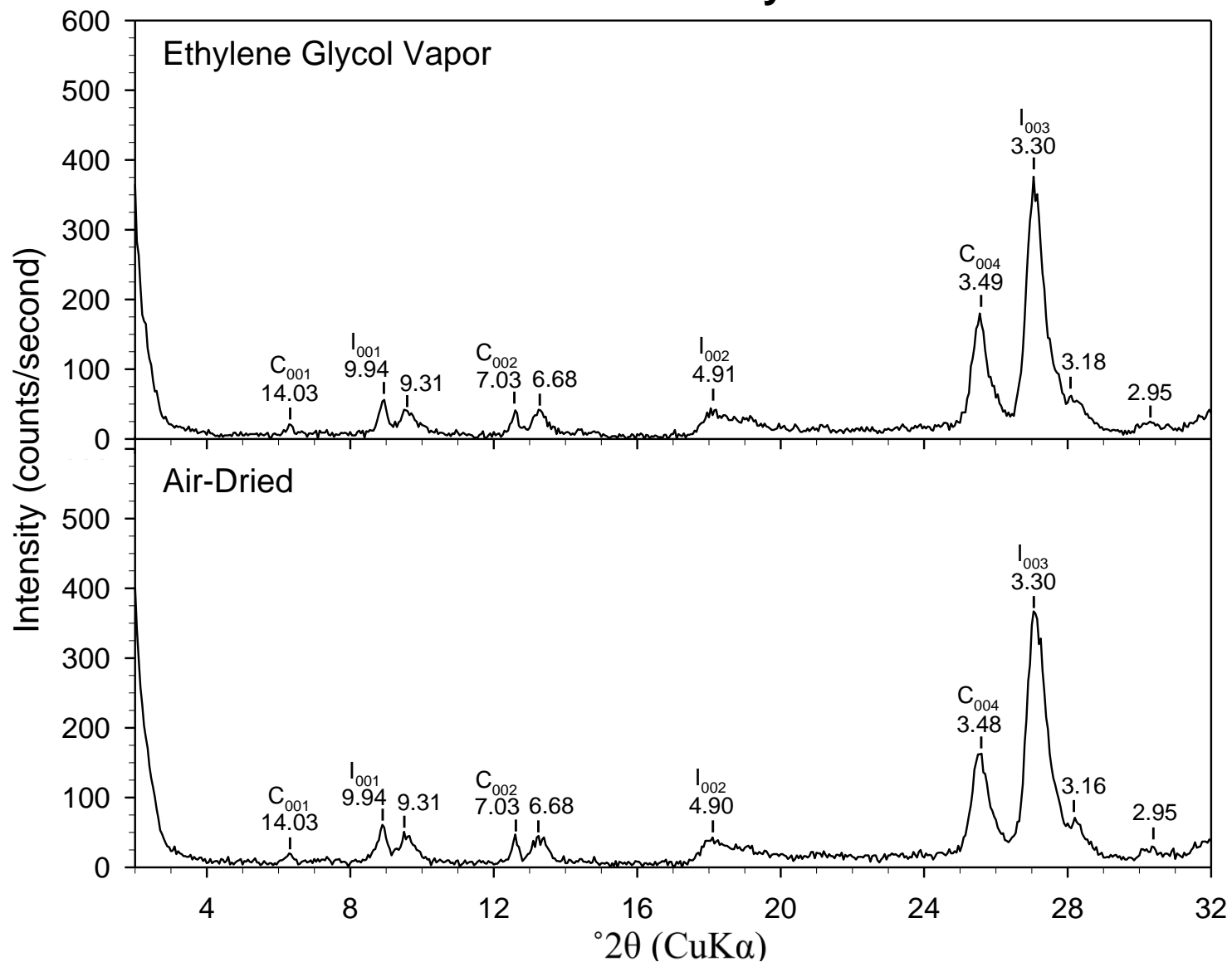
ART-18 Sand & Silt Fractions



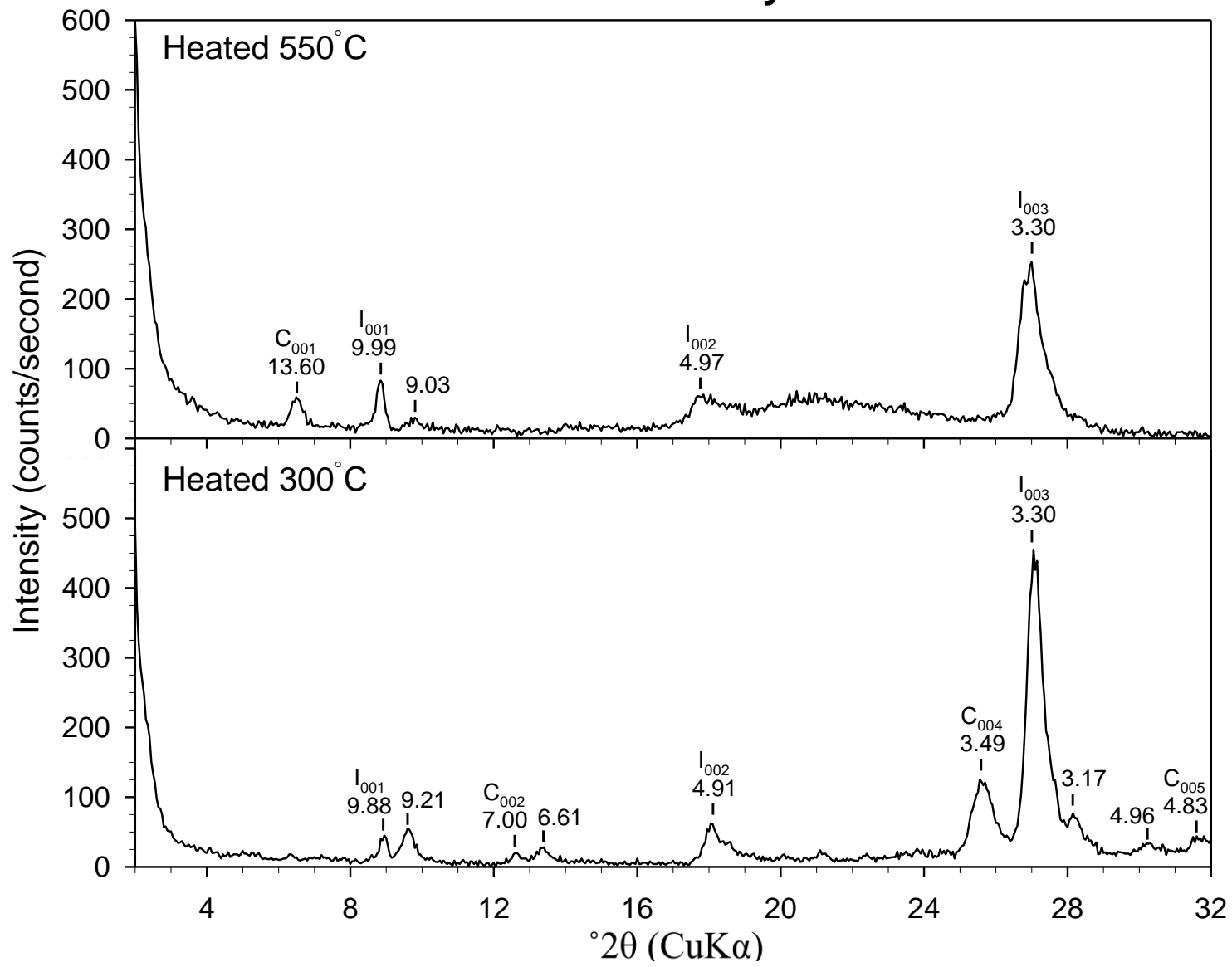
ART-19 Sand & Silt Fractions



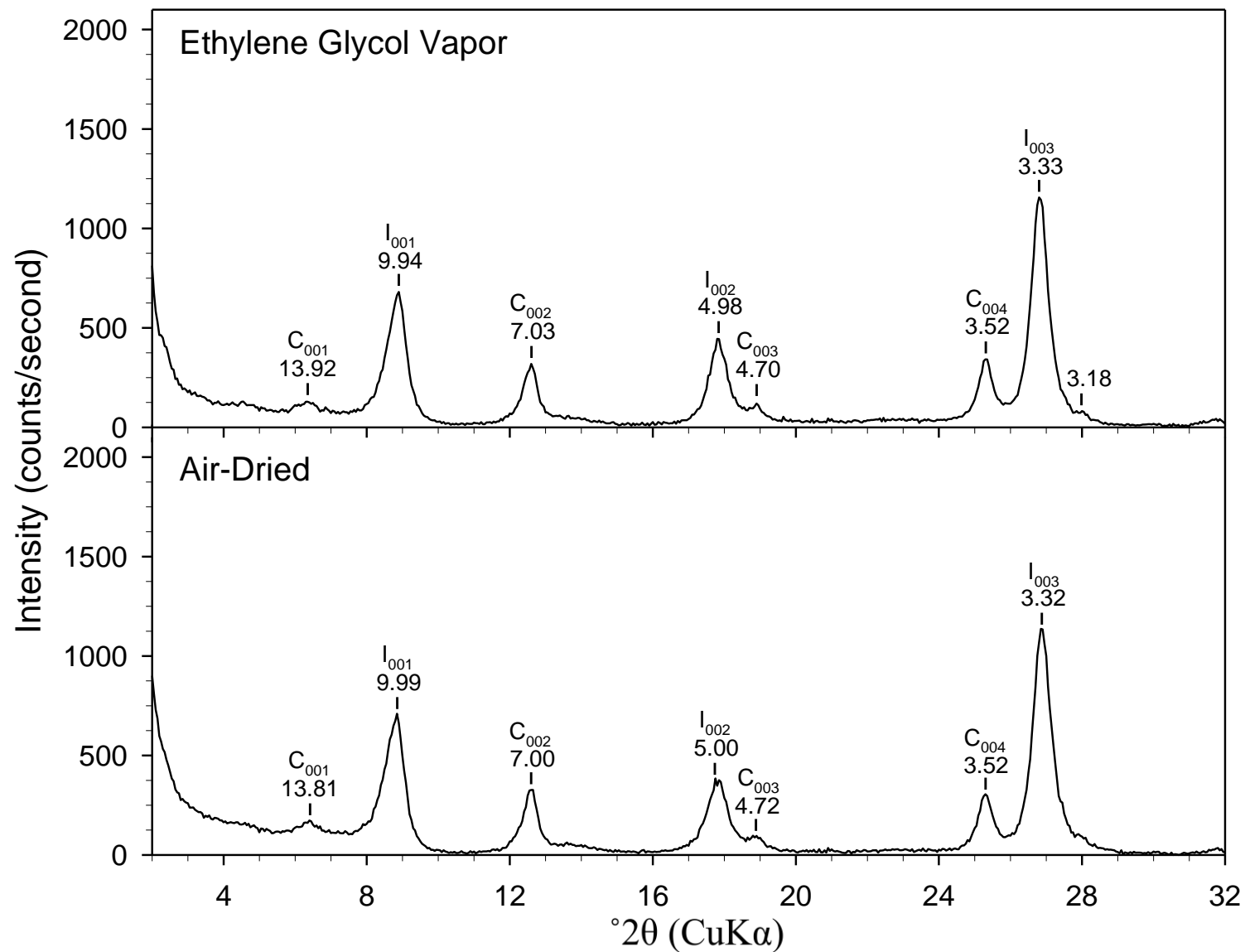
ARM-1 Coarse Clay Fraction



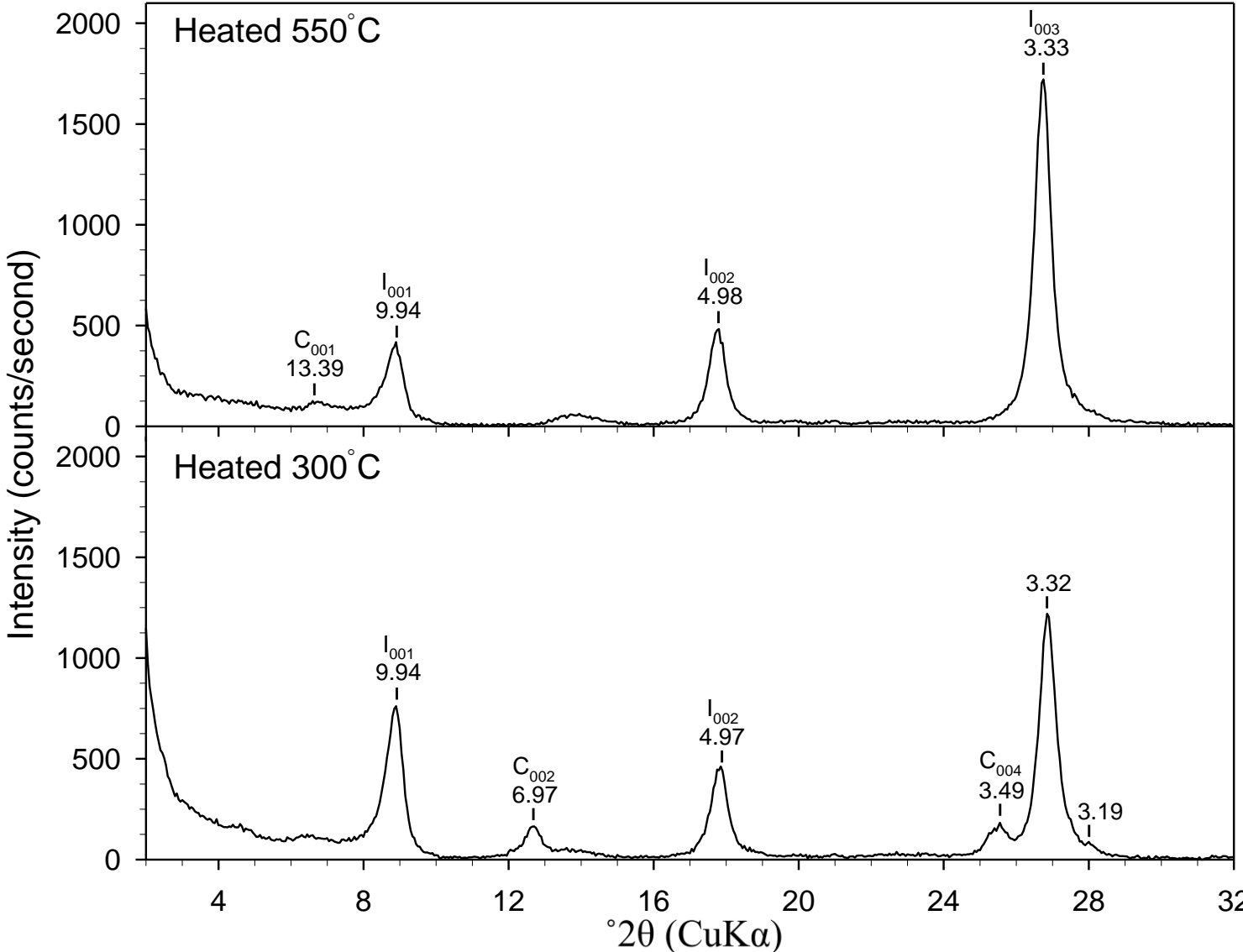
ARM-1 Coarse Clay Fraction



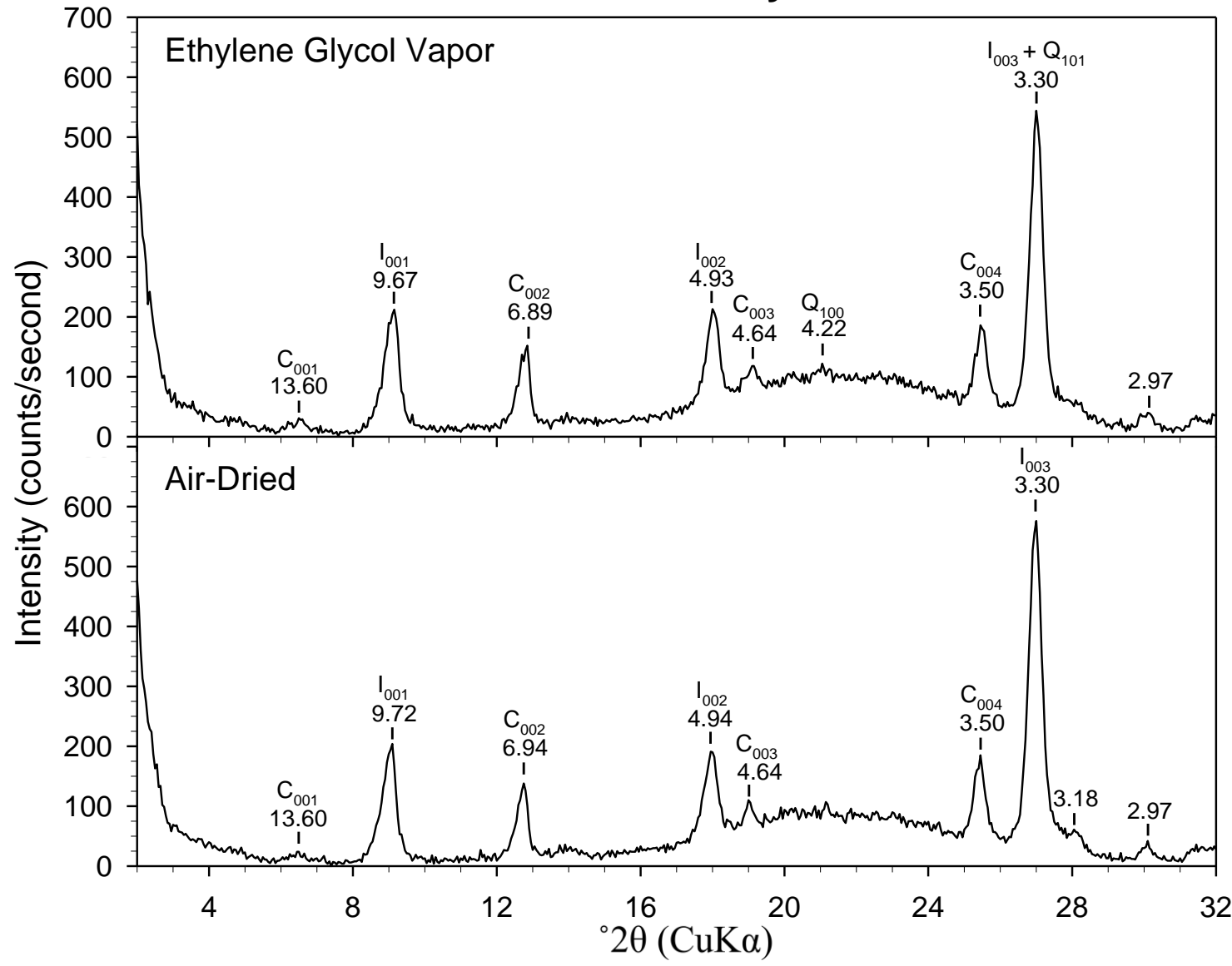
ARM-1 Fine Clay Fraction



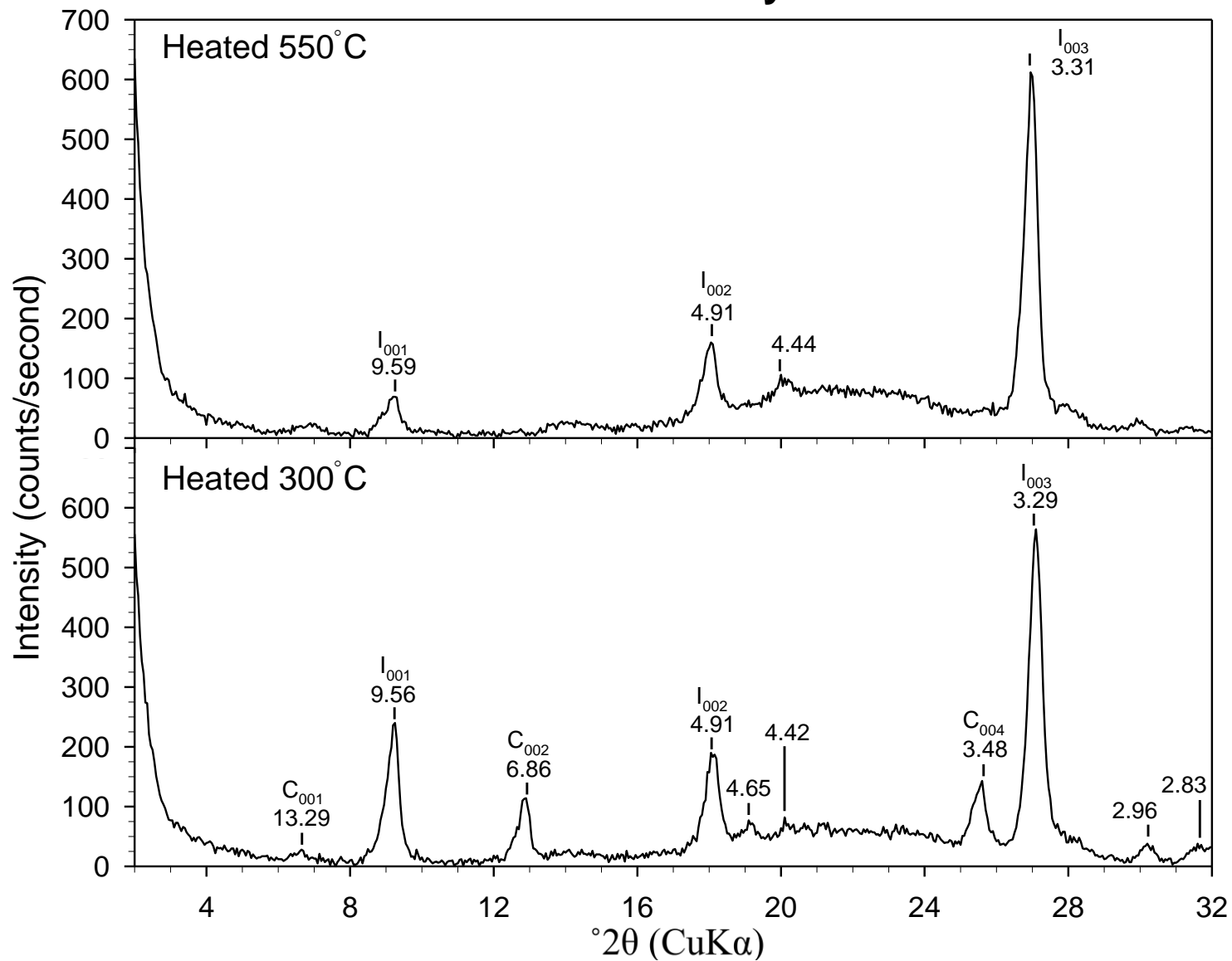
ARM-1 Fine Clay Fraction



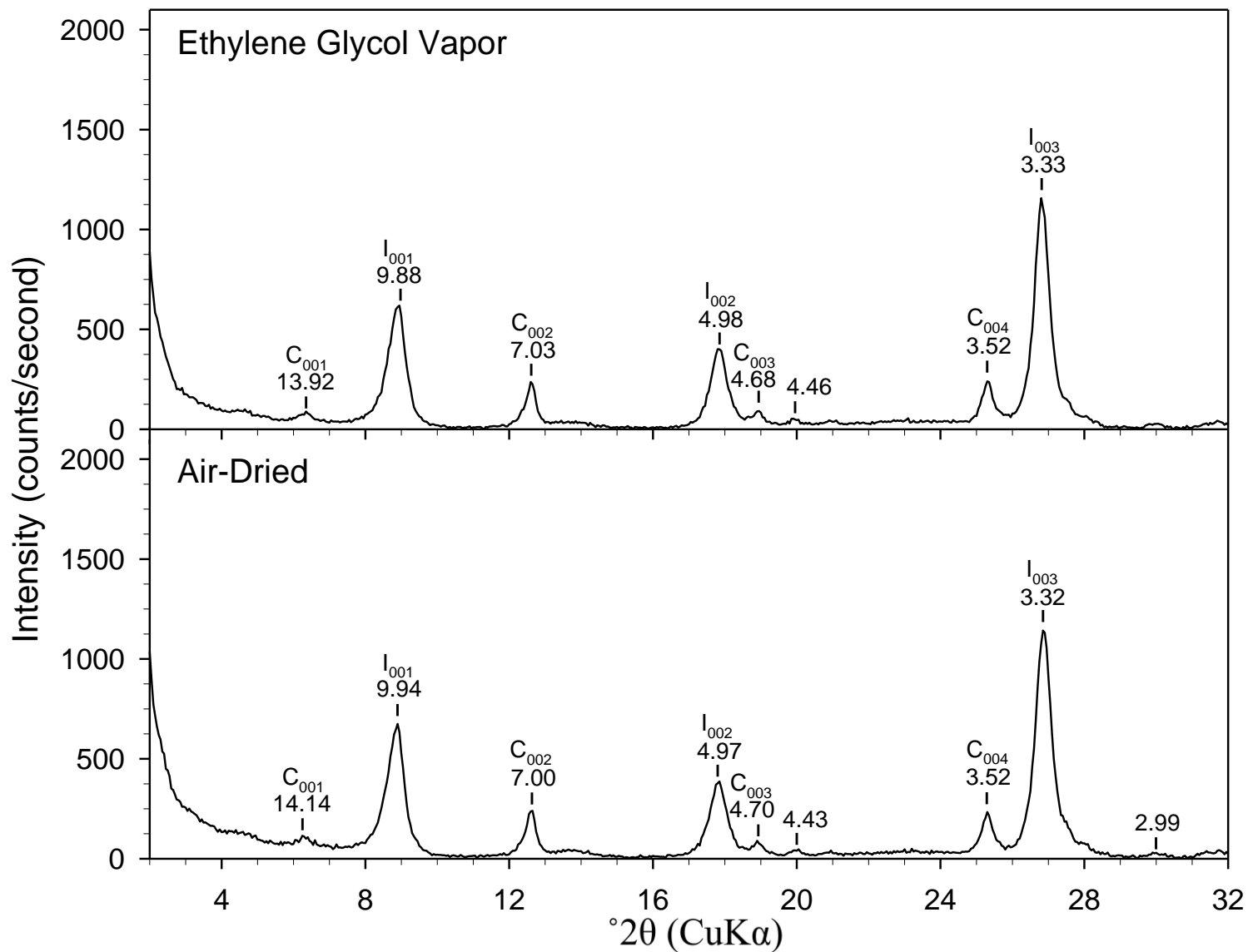
ARM-5 Coarse Clay Fraction



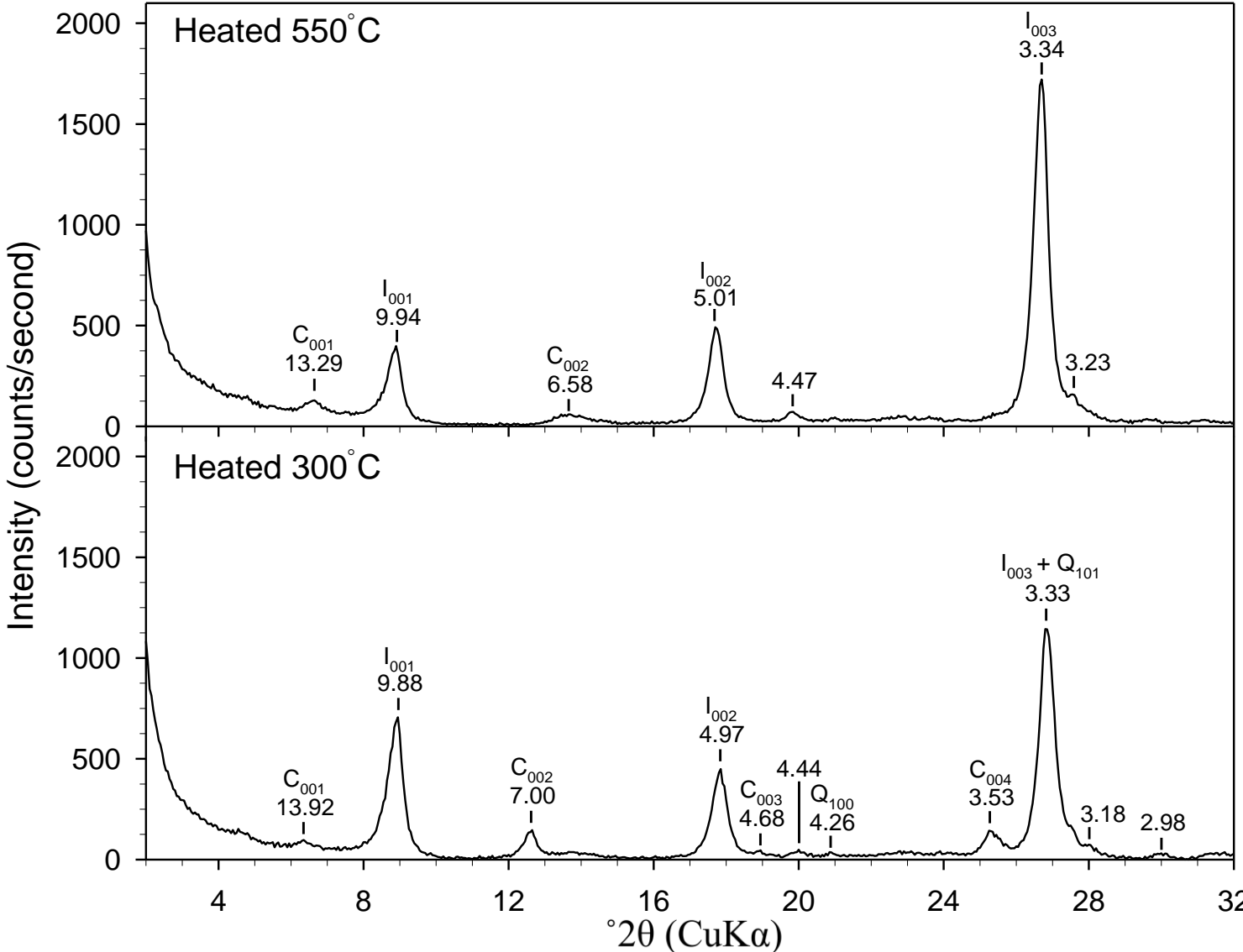
ARM-5 Coarse Clay Fraction



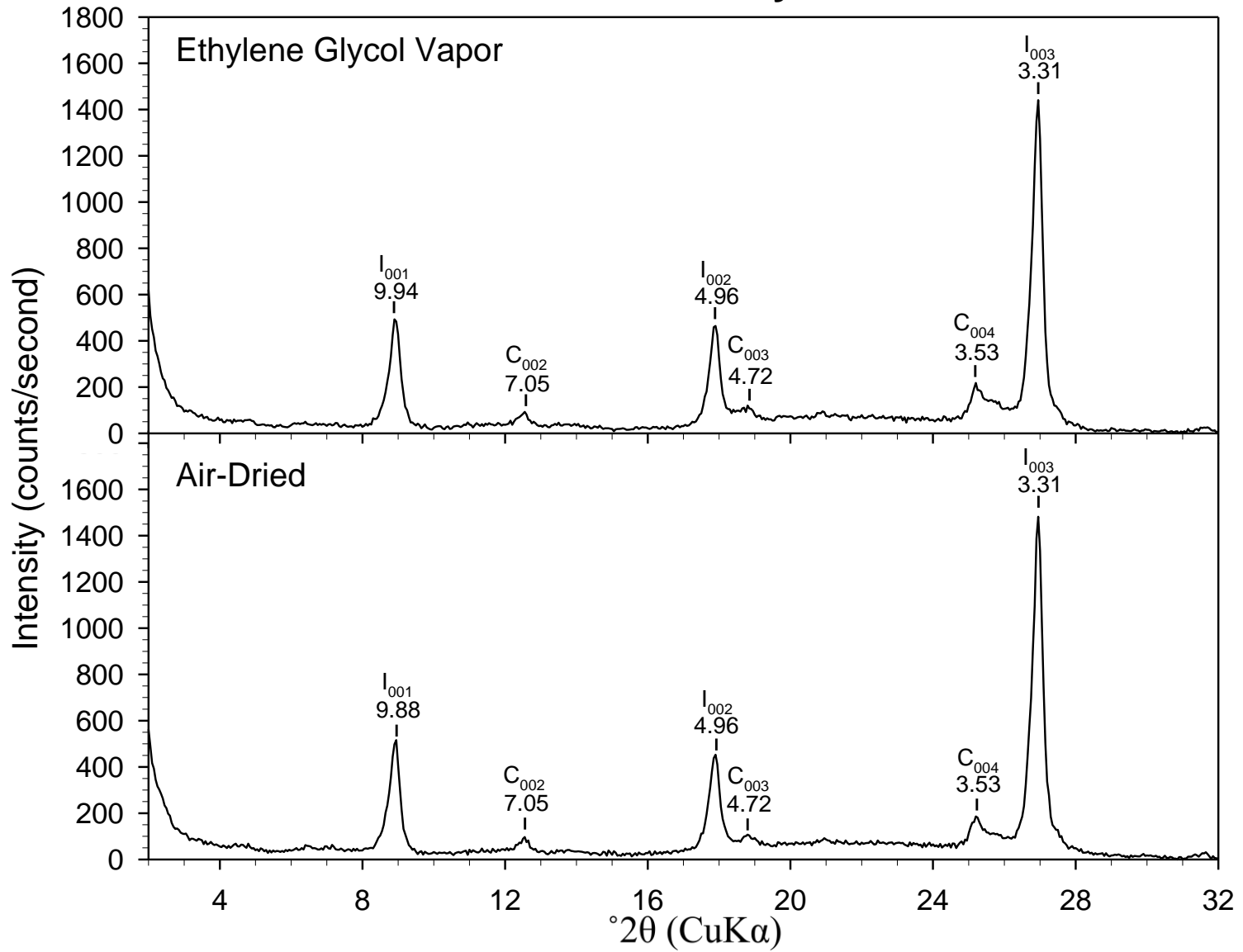
ARM-5 Fine Clay Fraction



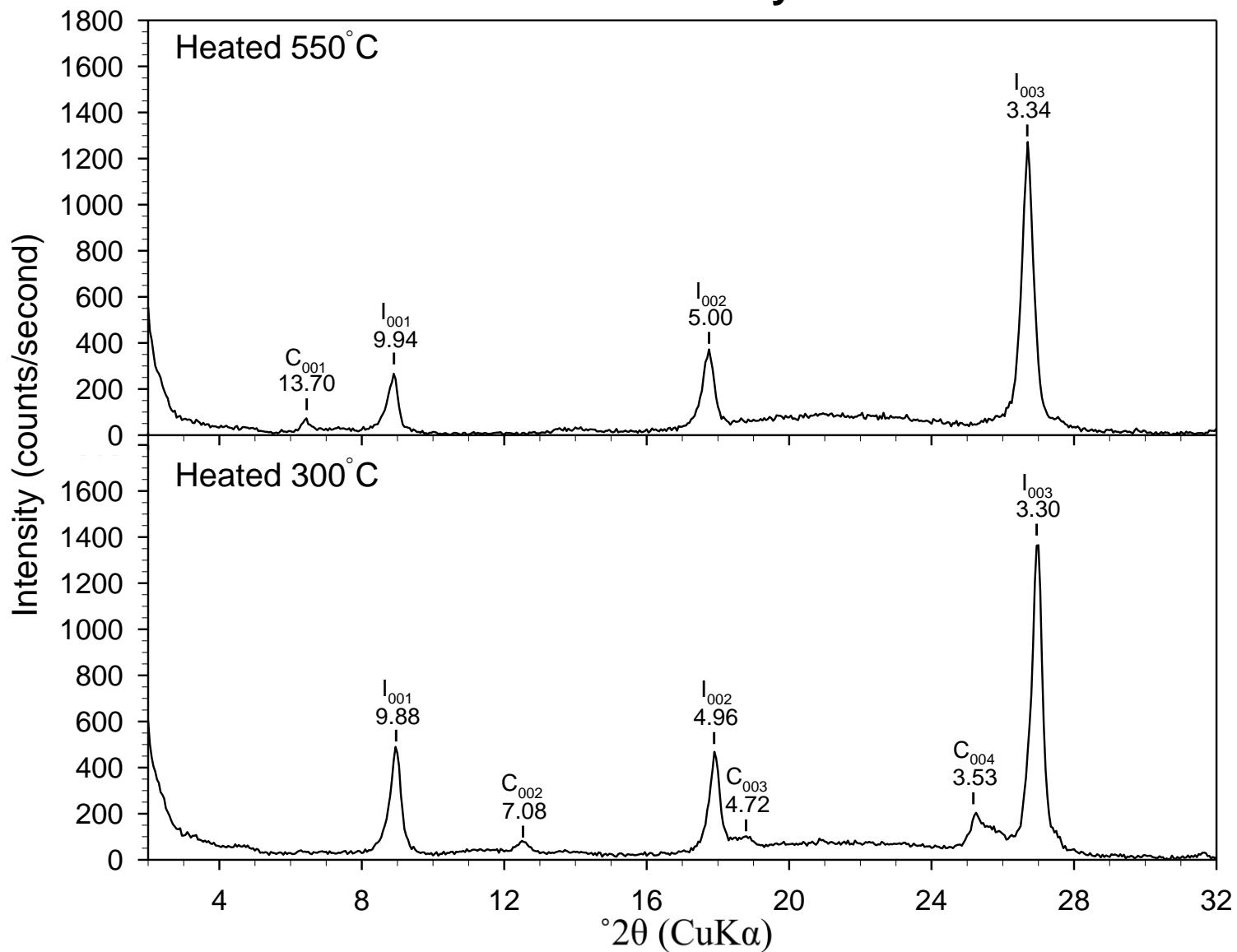
ARM-5 Fine Clay Fraction



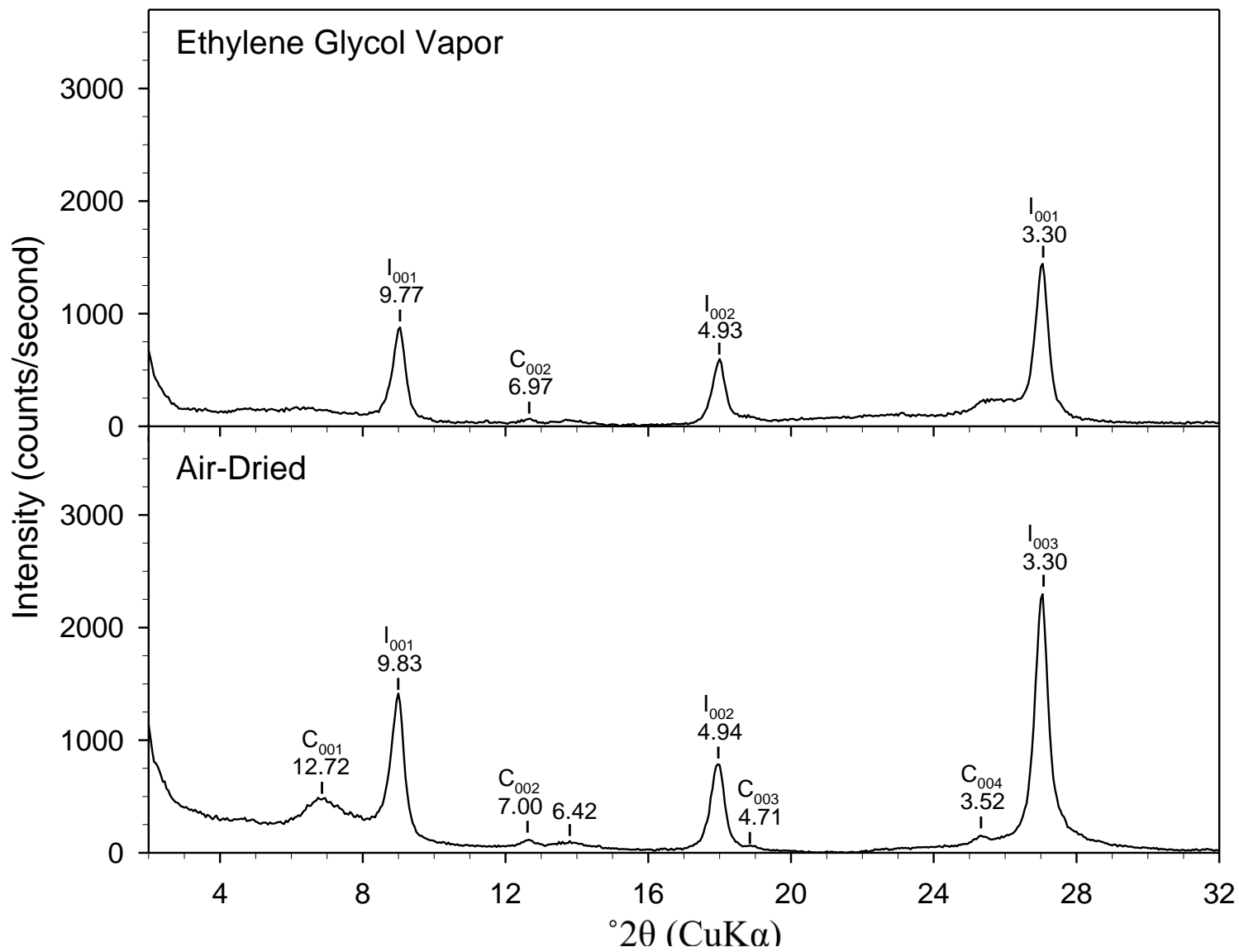
ARM-6 Coarse Clay Fraction



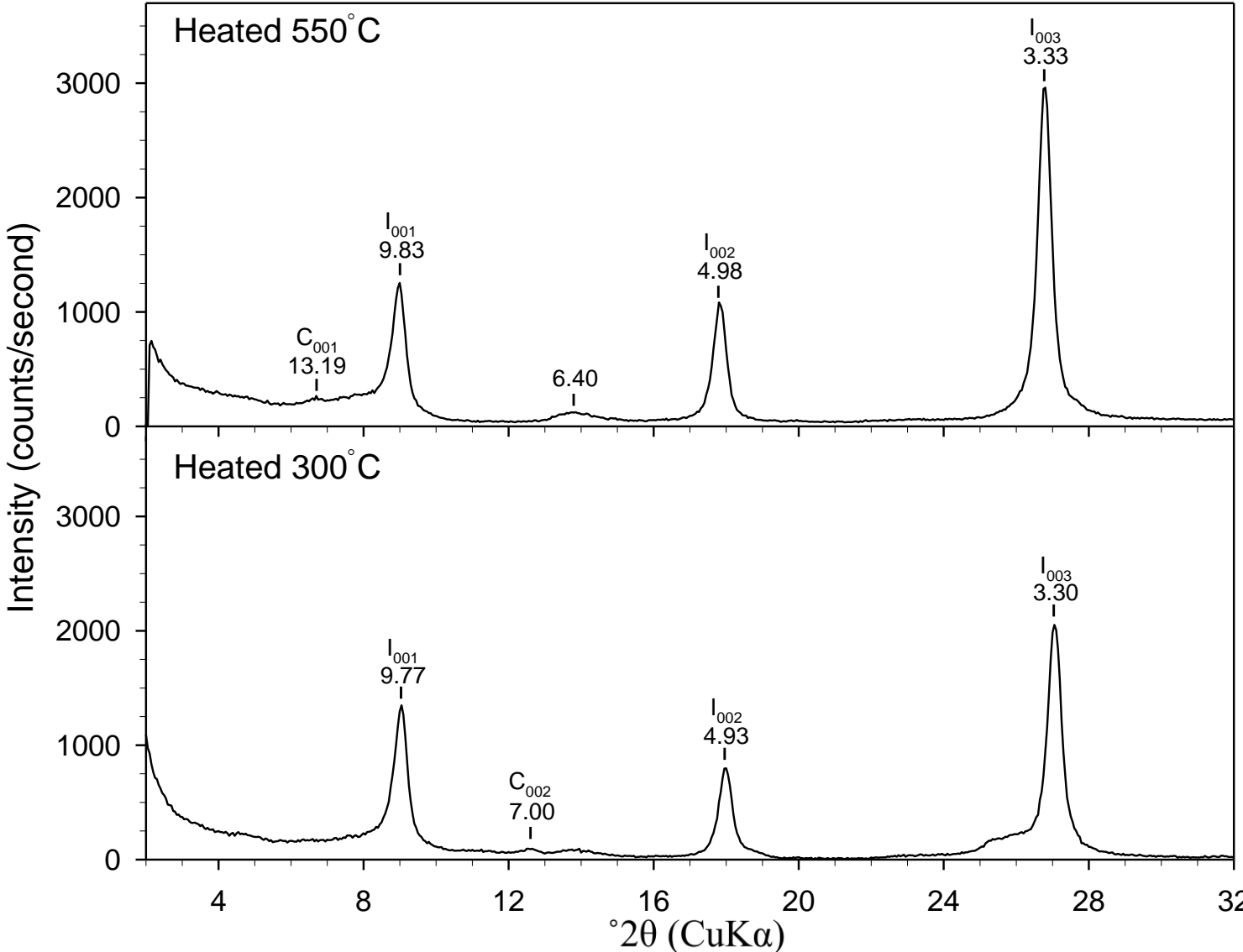
ARM-6 Coarse Clay Fraction



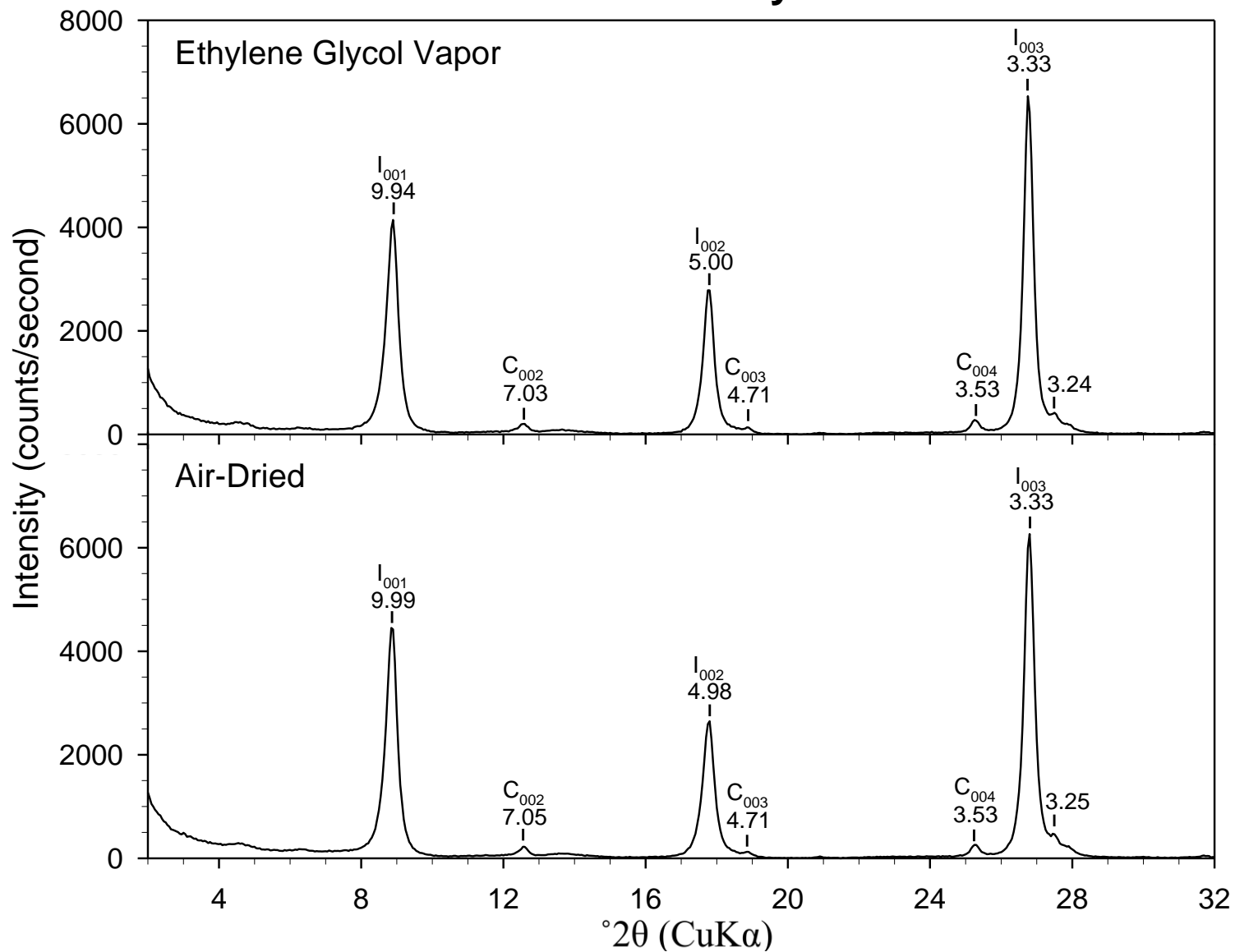
ARM-6 Fine Clay Fraction



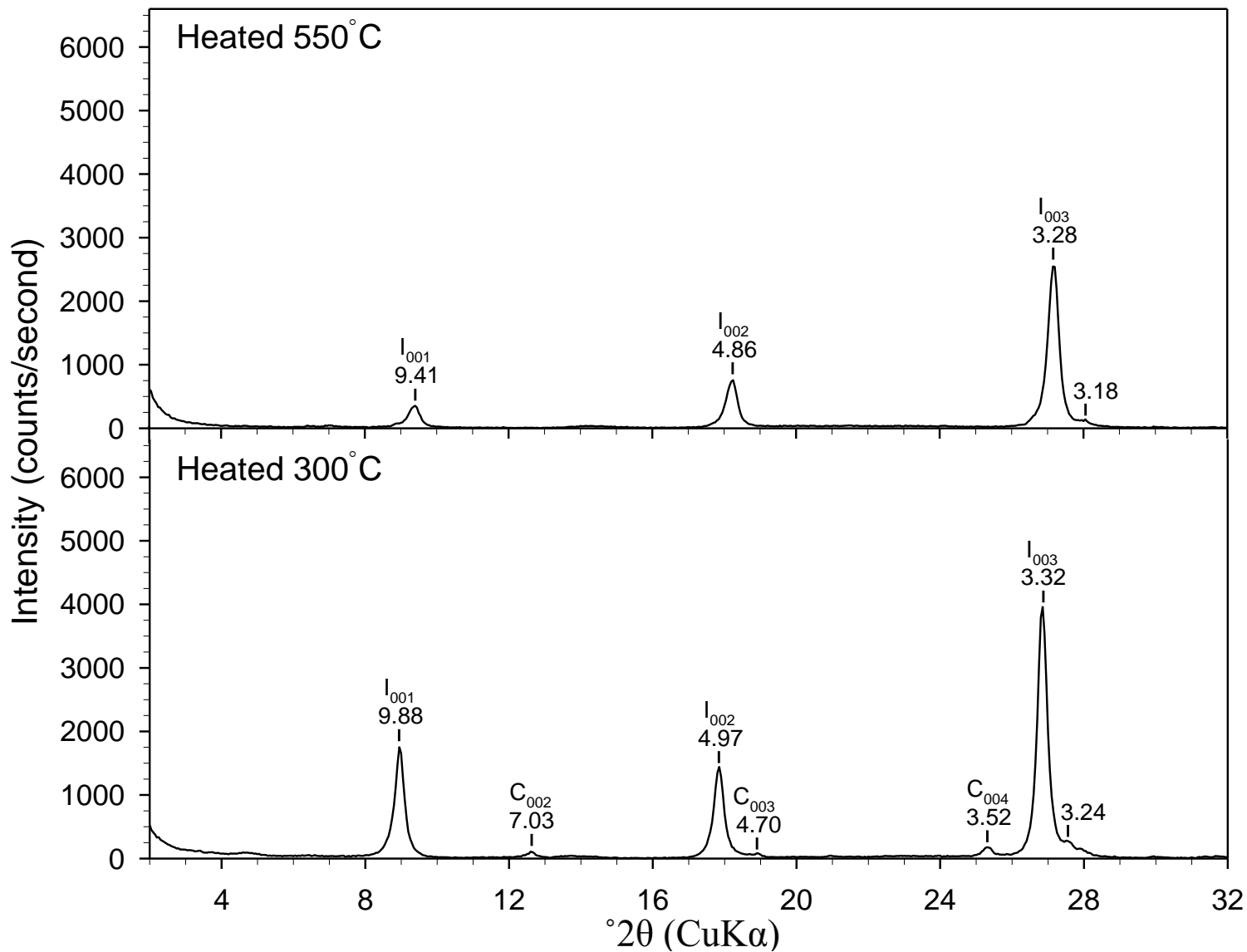
ARM-6 Fine Clay Fraction



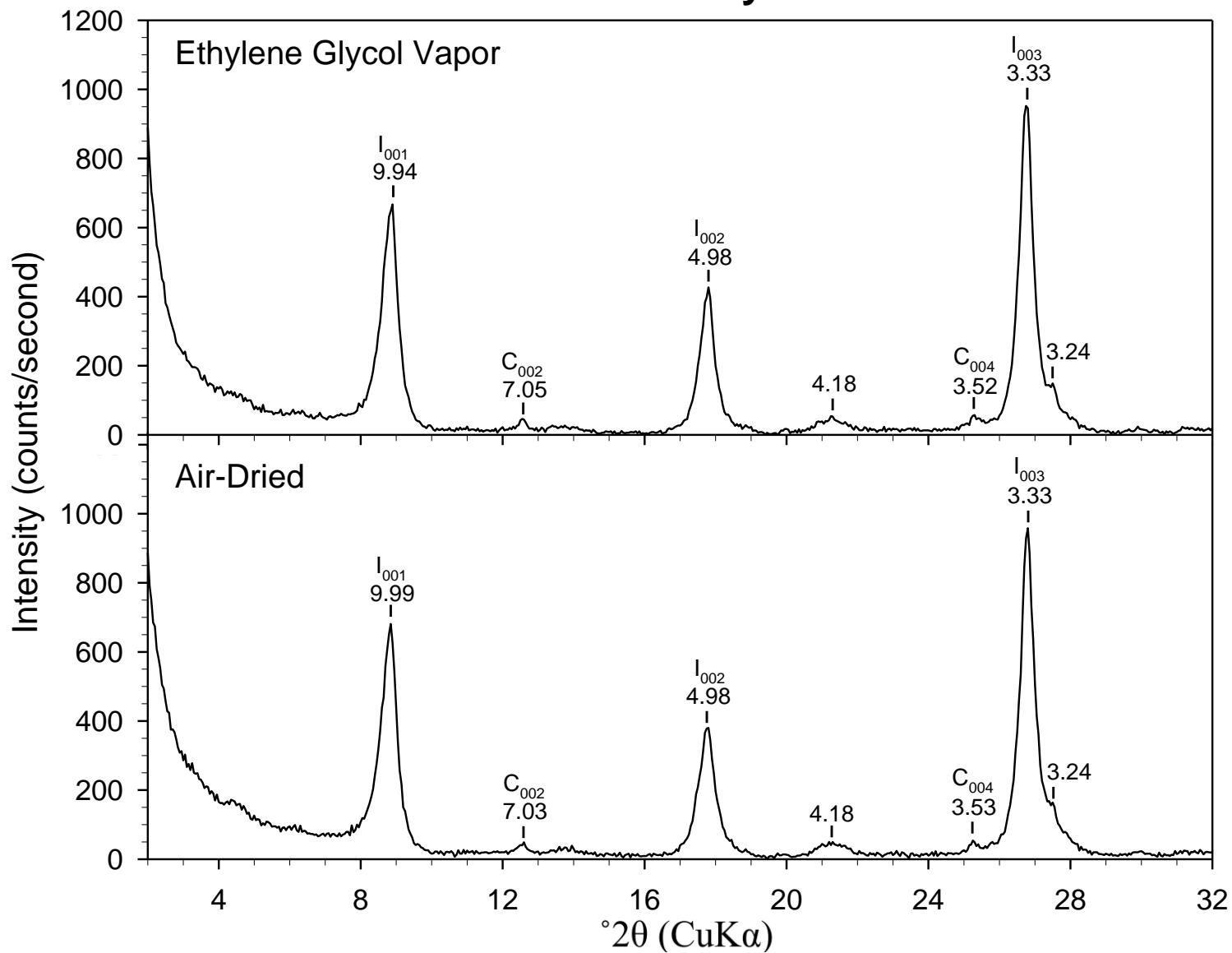
ARM-7 Coarse Clay Fraction



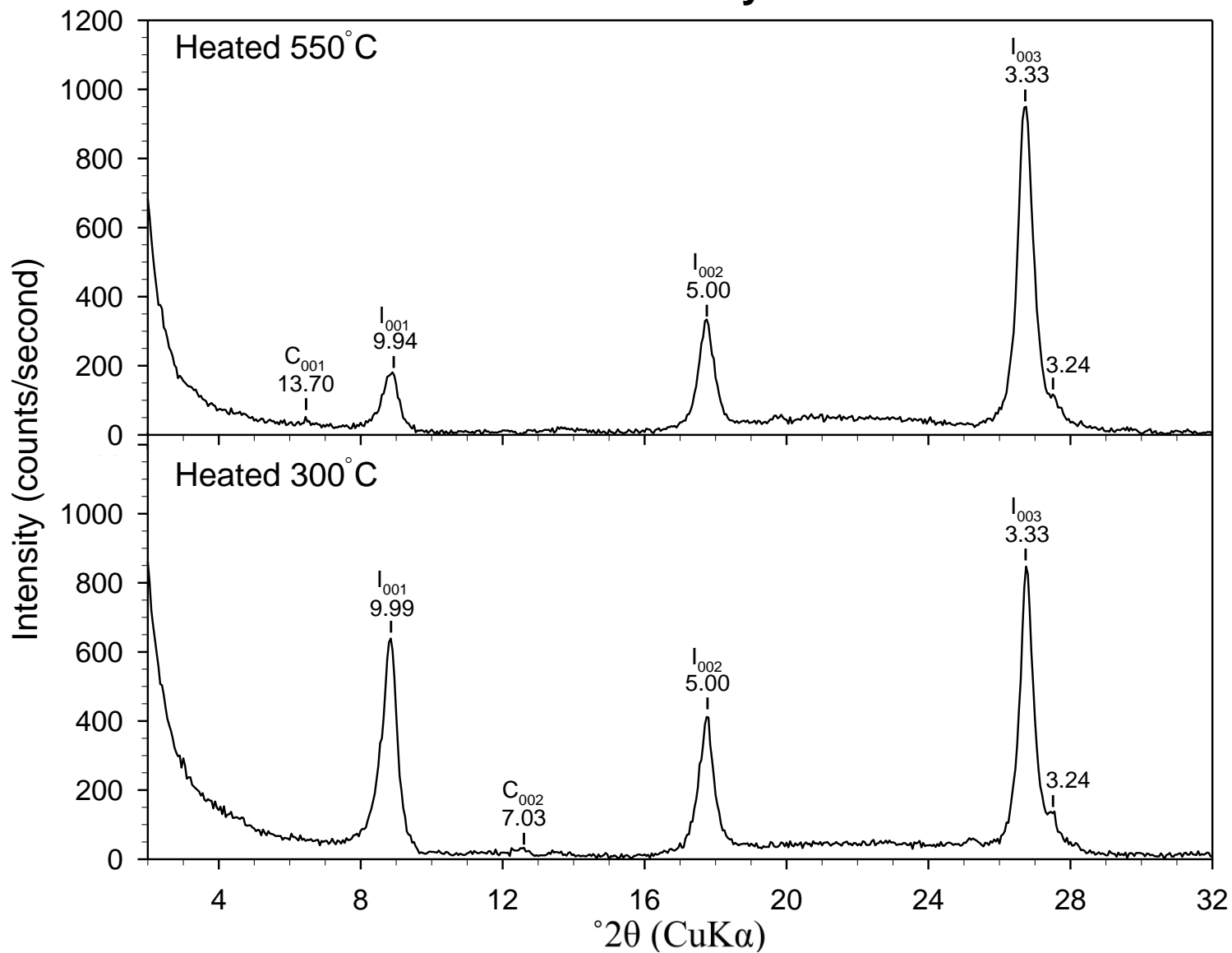
ARM-7 Coarse Clay Fraction



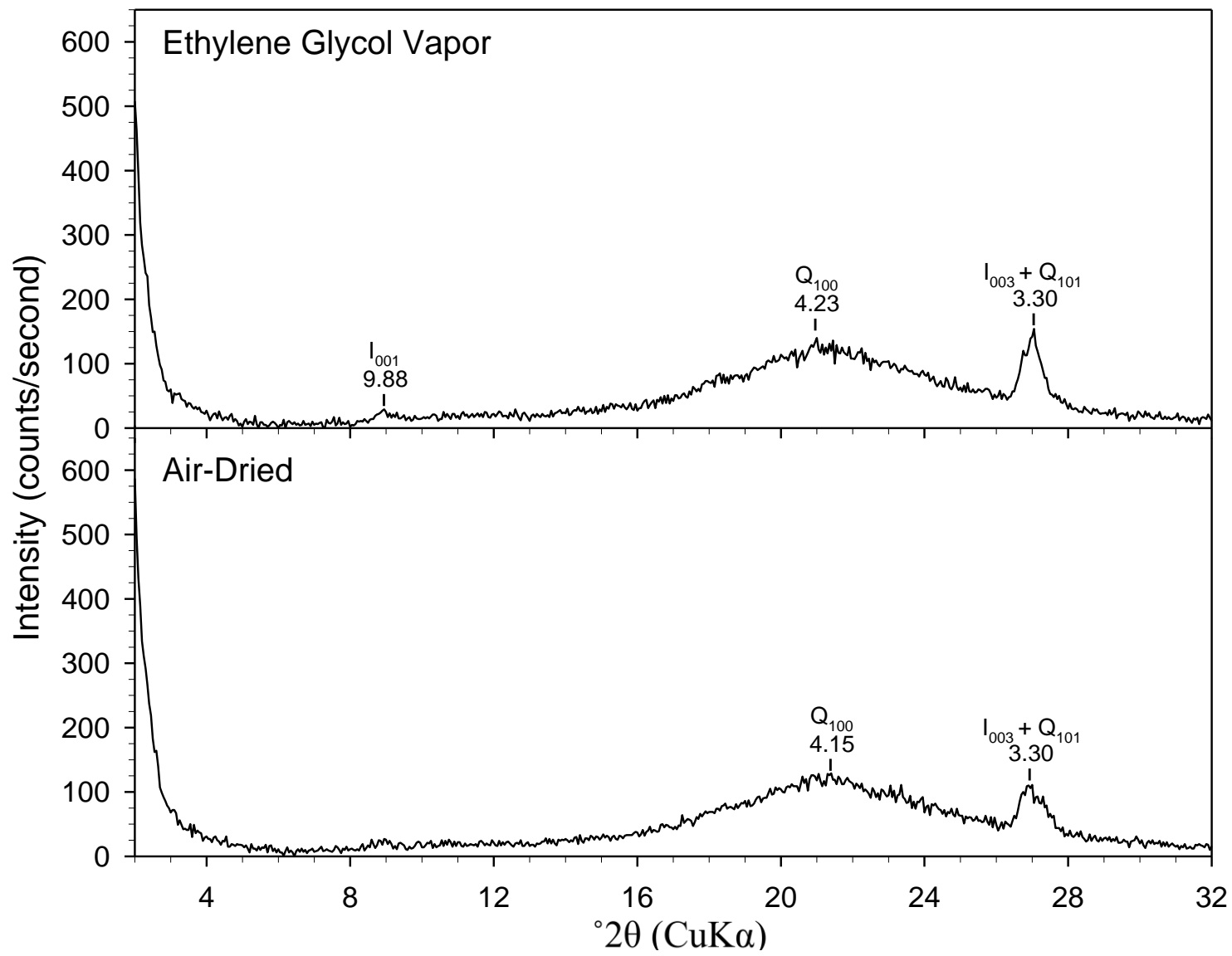
ARM-7 Fine Clay Fraction



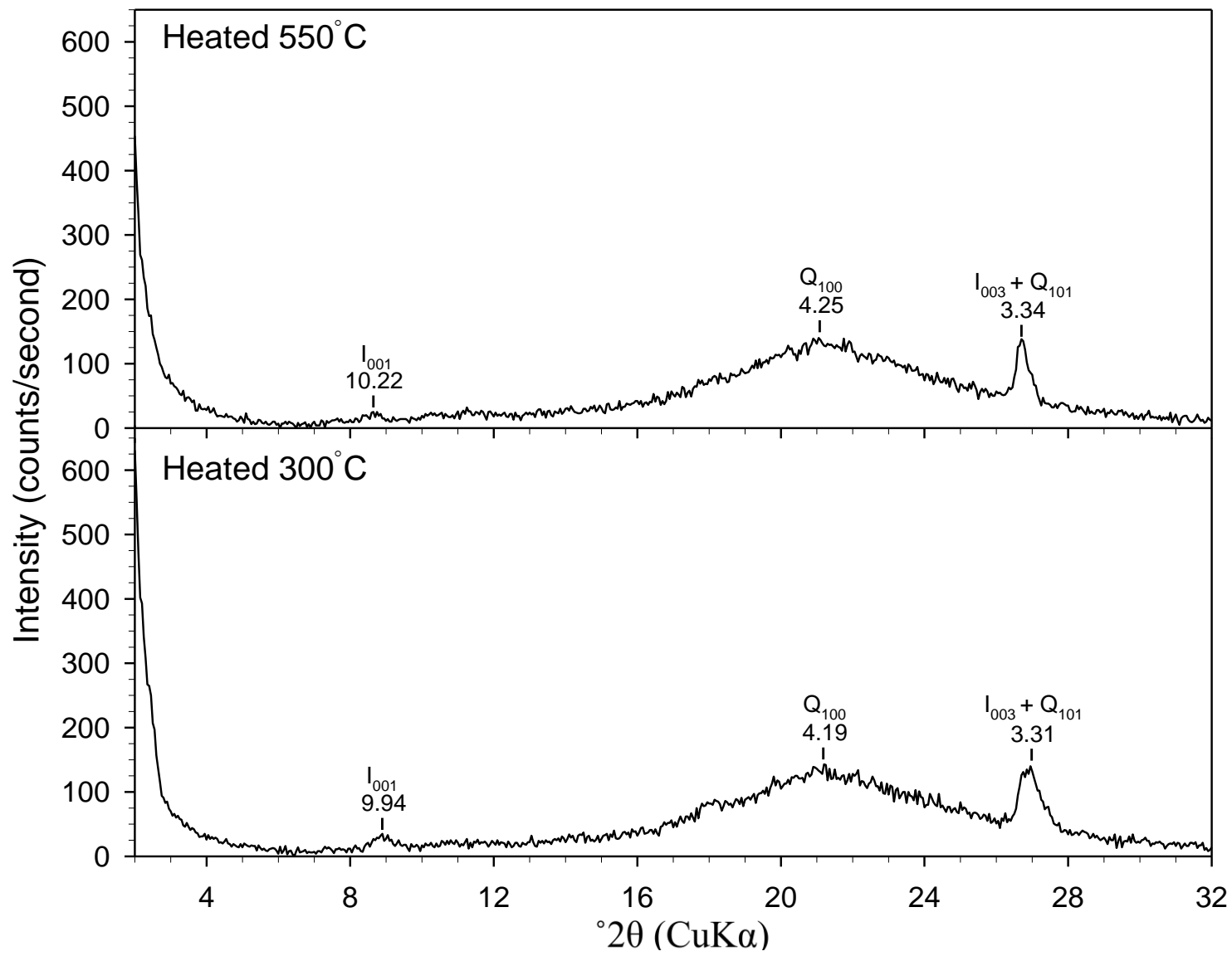
ARM-7 Fine Clay Fraction



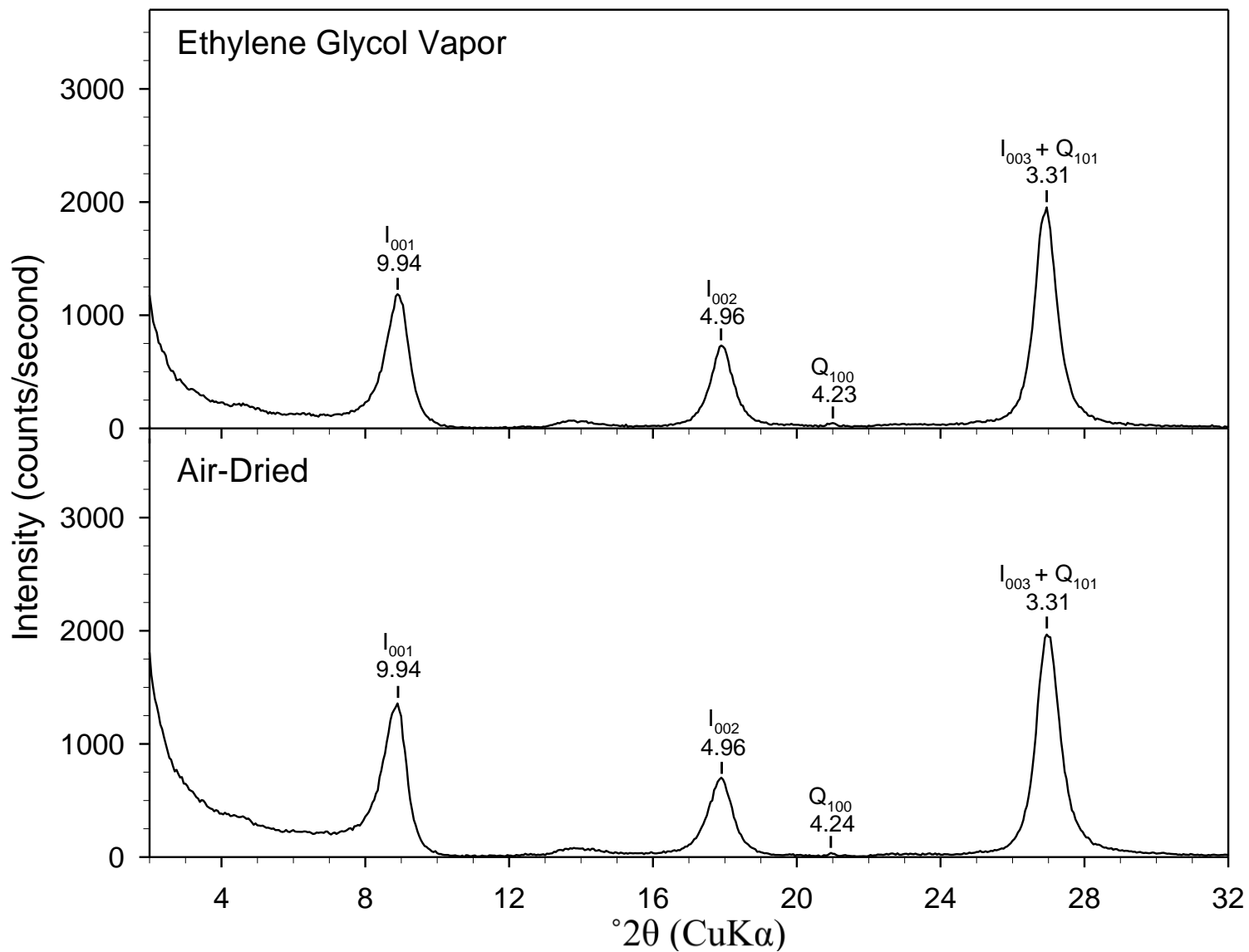
ARM-8 Coarse Clay Fraction



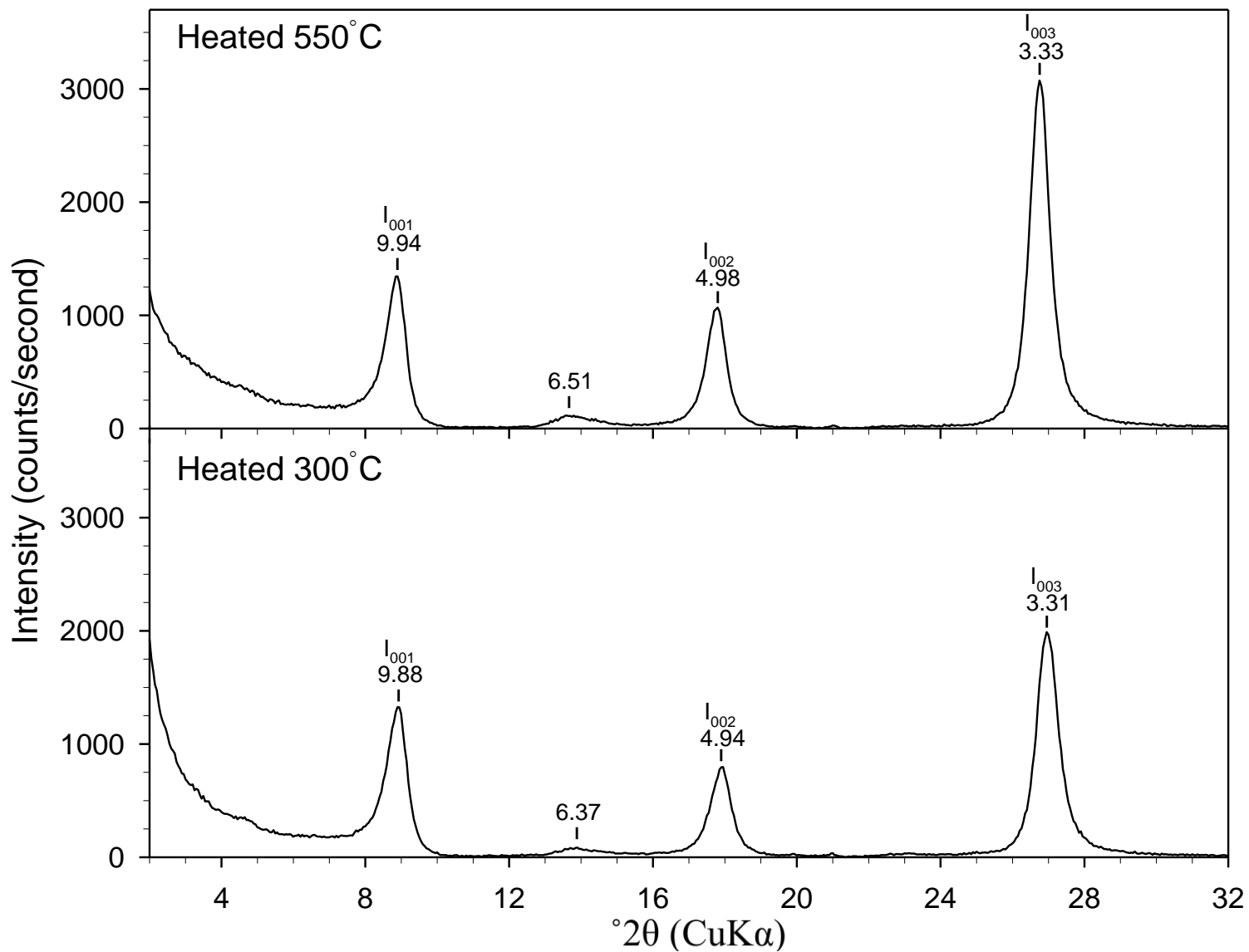
ARM-8 Coarse Clay Fraction



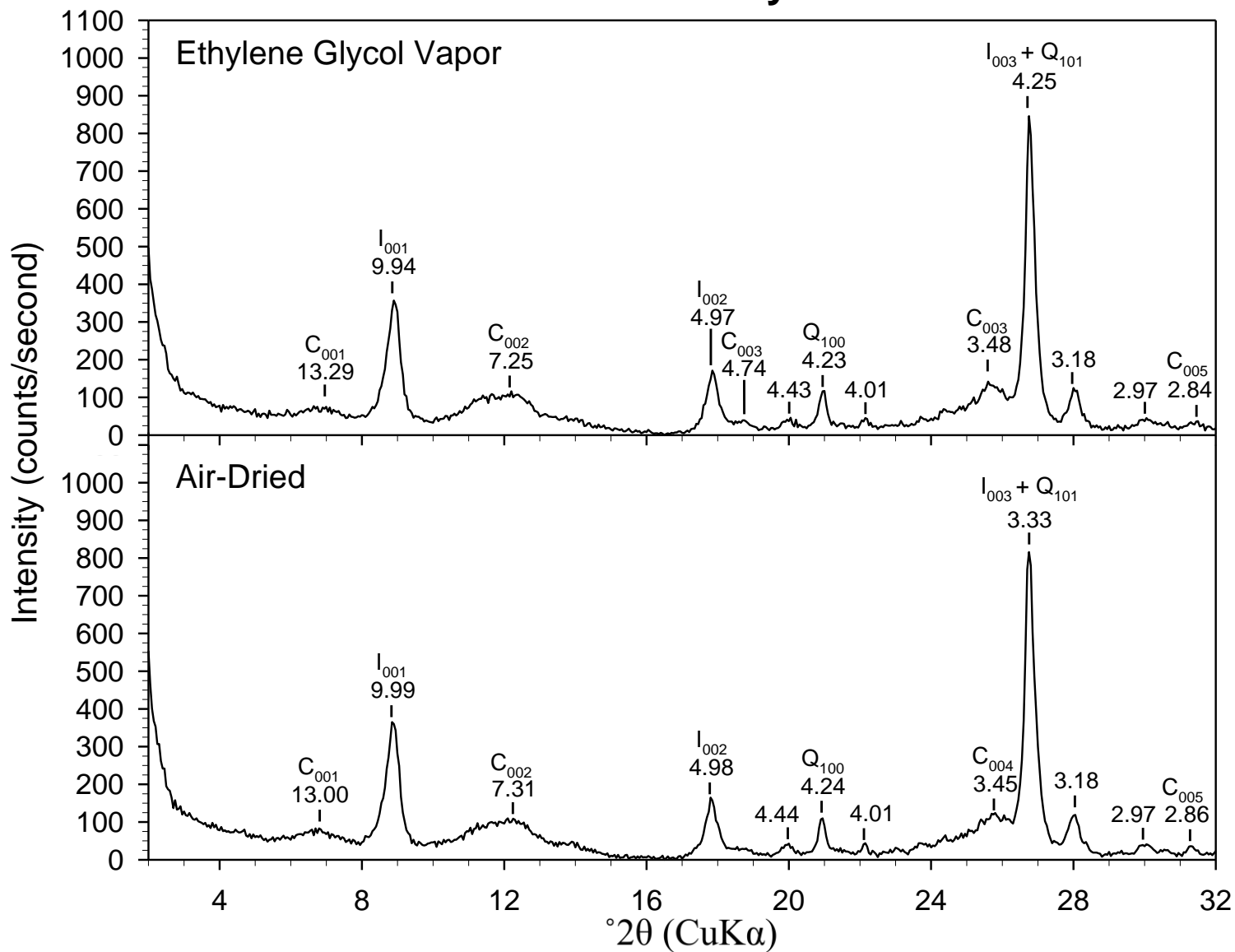
ARM-8 Fine Clay Fraction



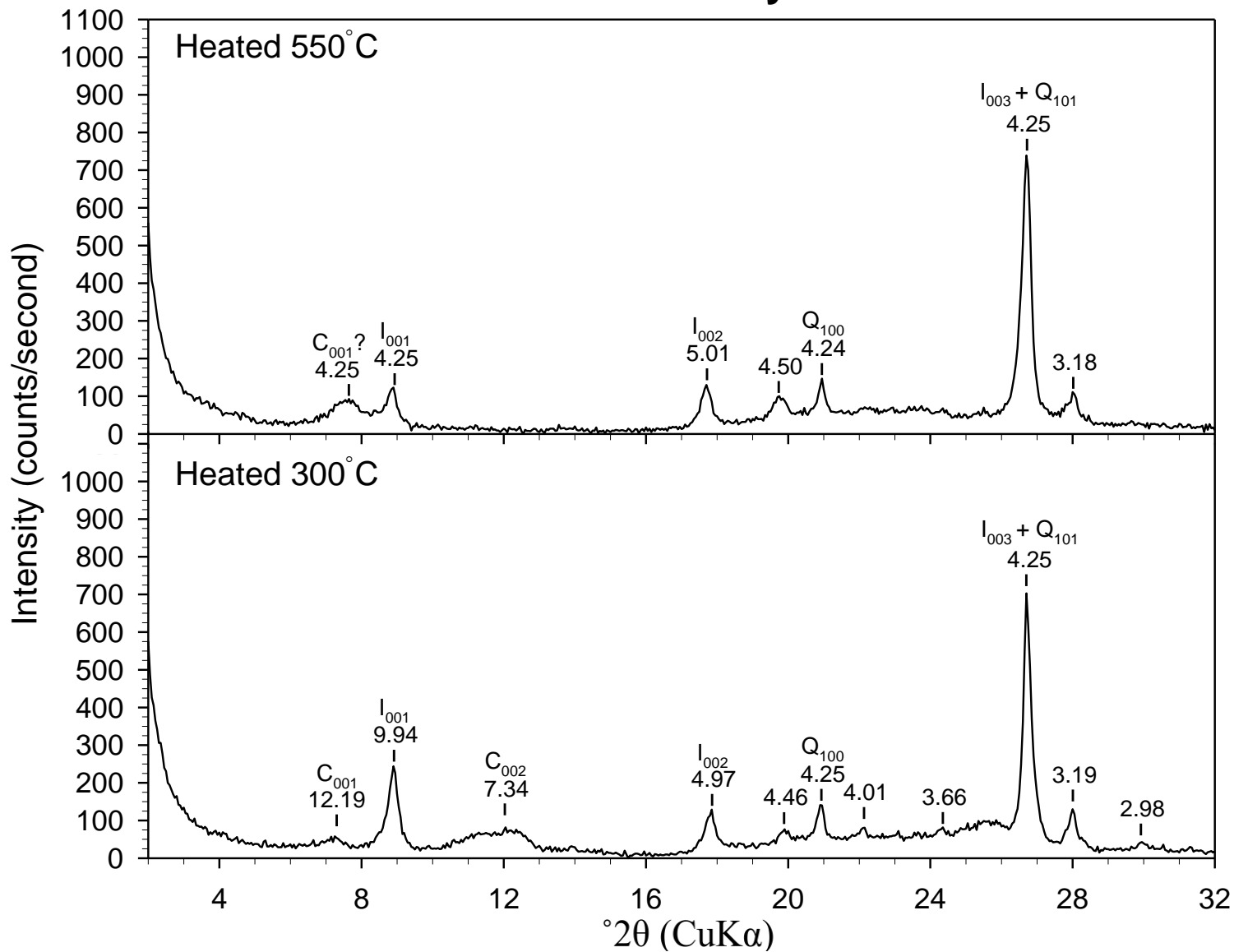
ARM-8 Fine Clay Fraction



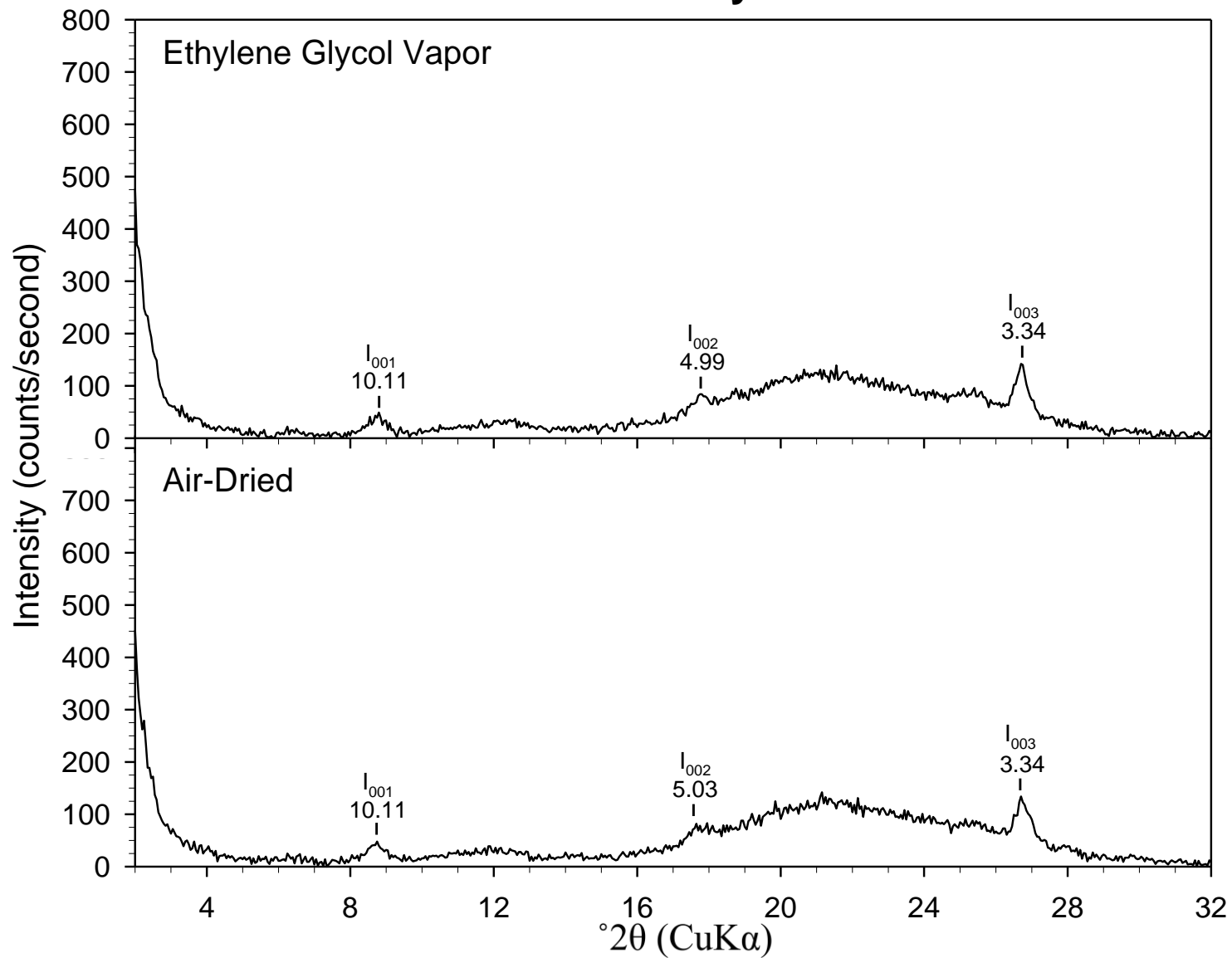
ART-2 Coarse Clay Fraction



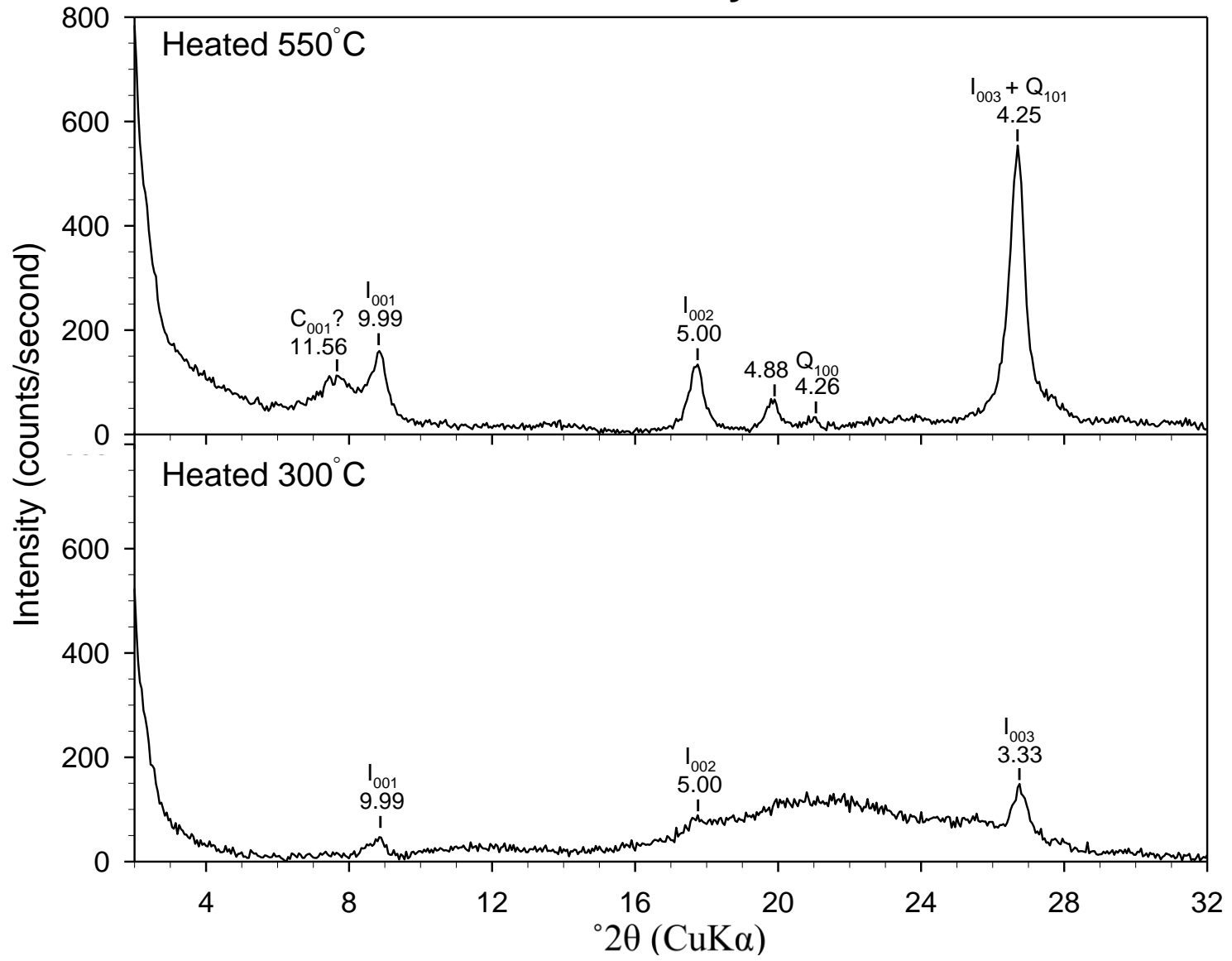
ART-2 Coarse Clay Fraction



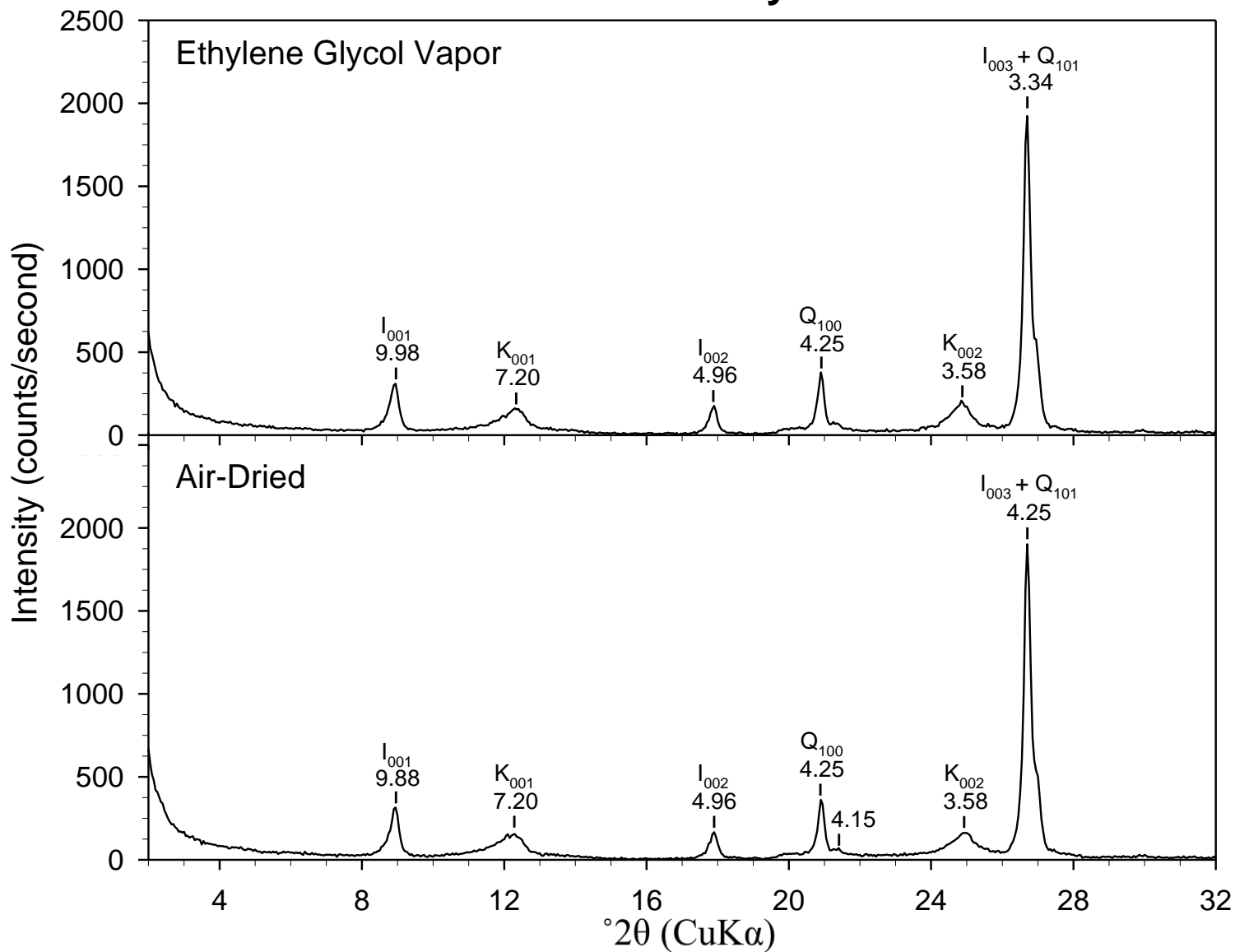
ART-2 Fine Clay Fraction



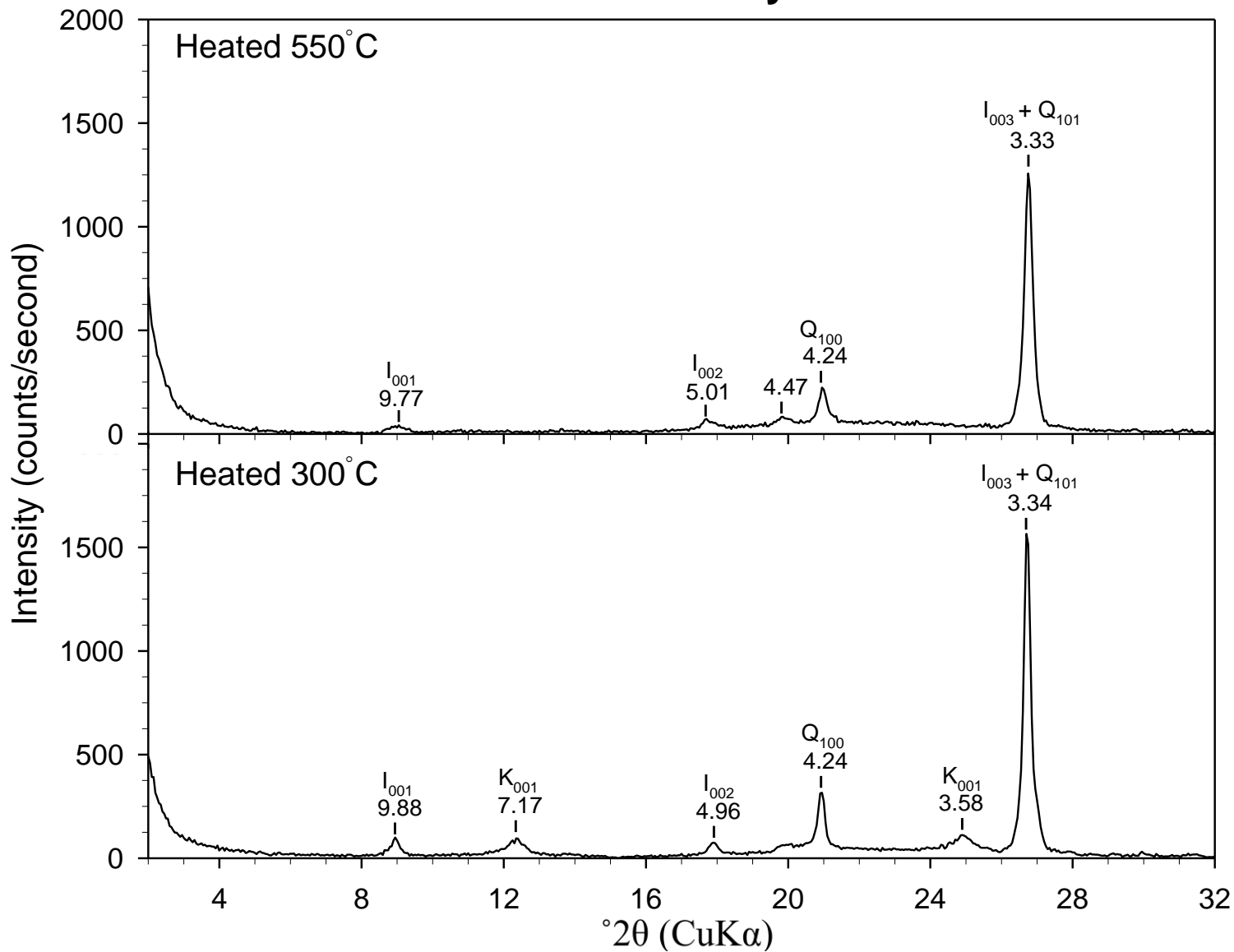
ART-2 Fine Clay Fraction



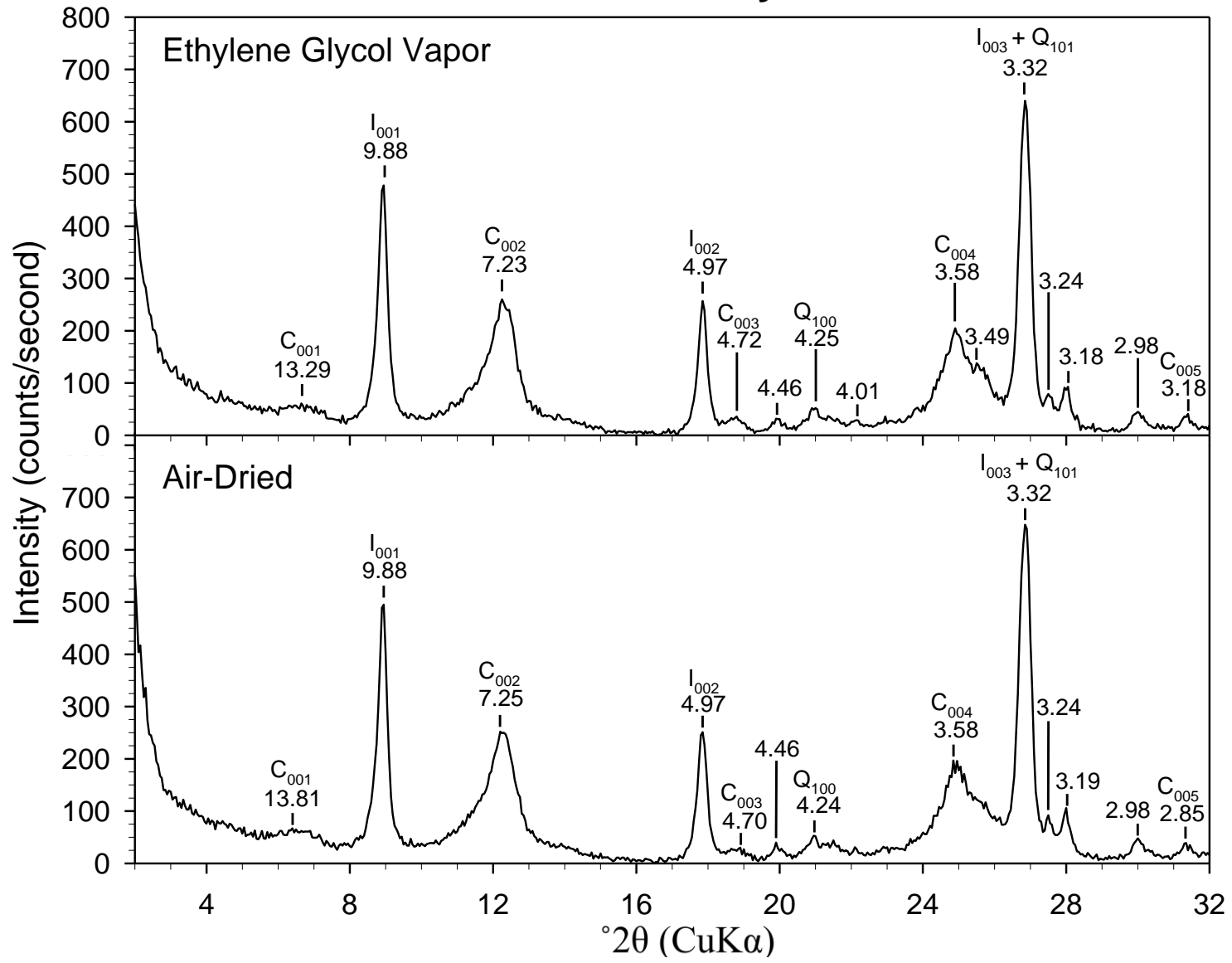
ART-3 Coarse Clay Fraction



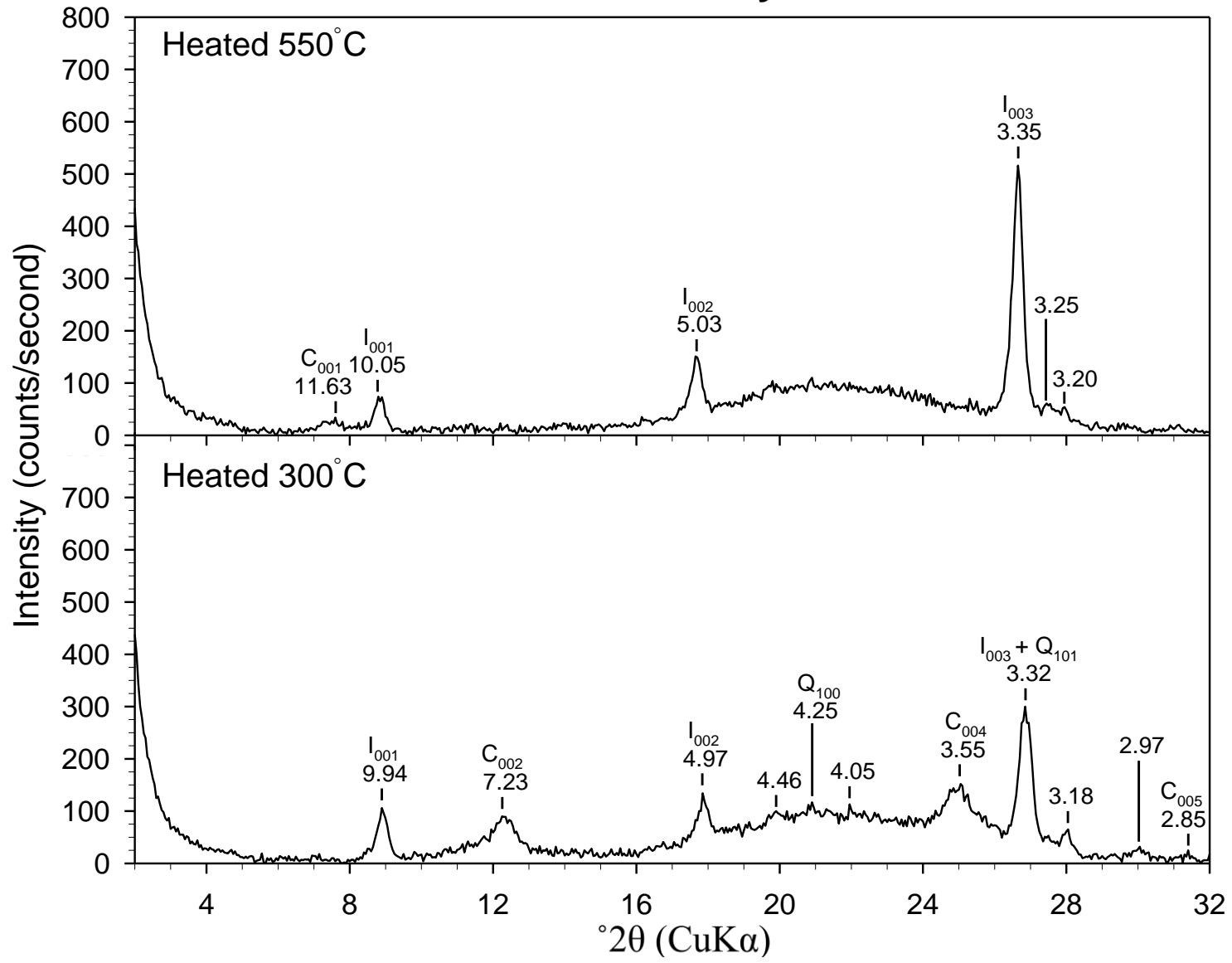
ART-3 Coarse Clay Fraction



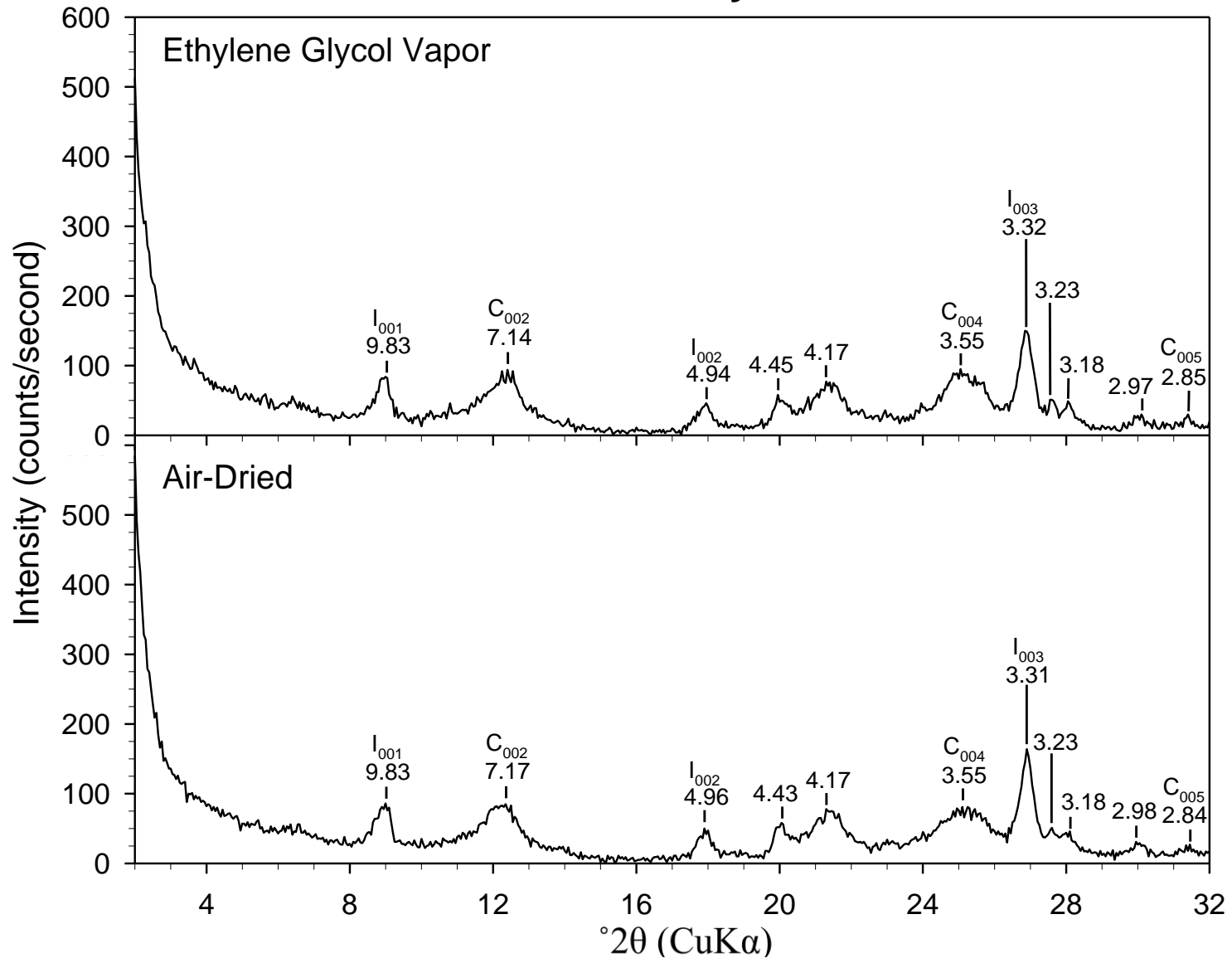
ART-5 Coarse Clay Fraction



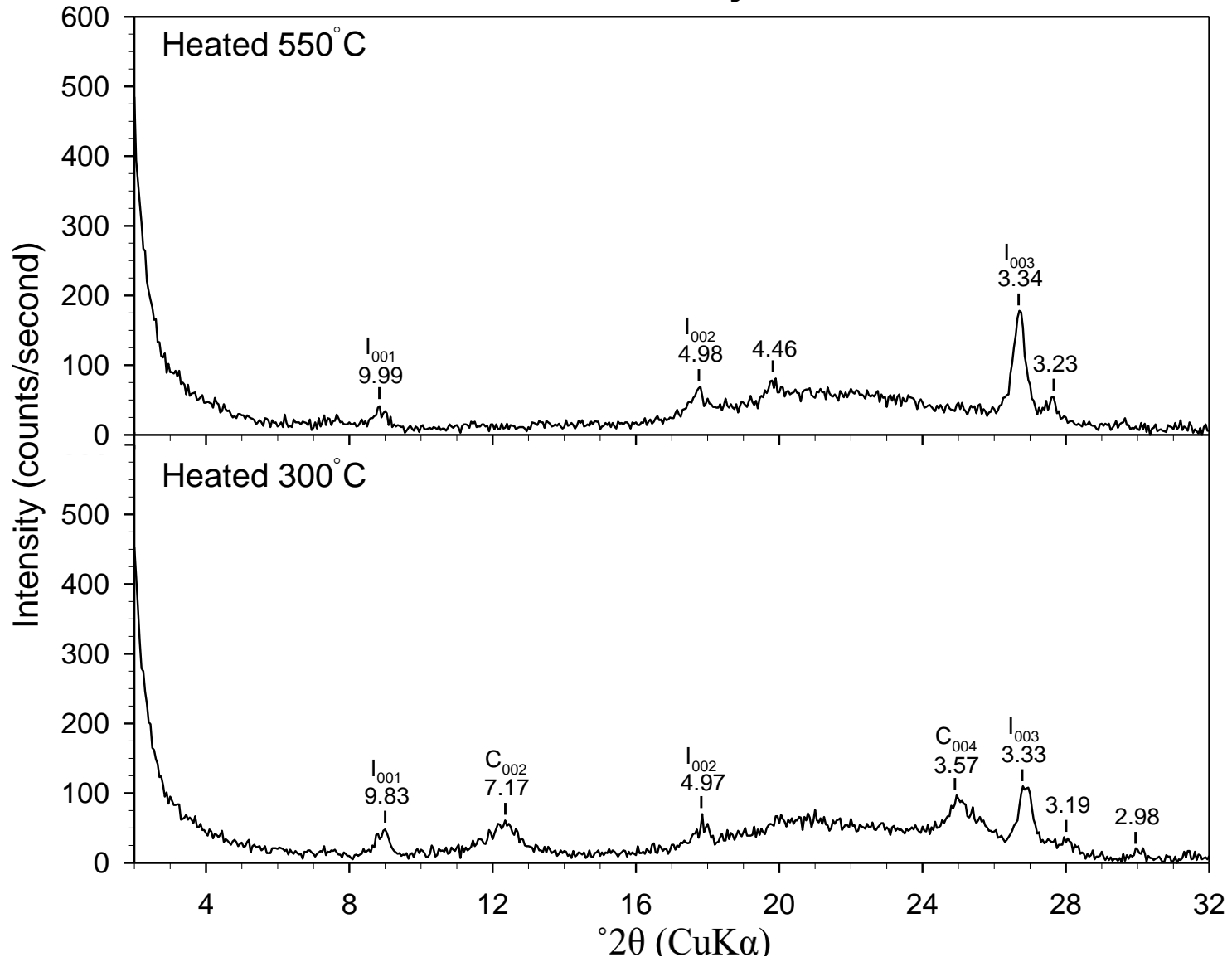
ART-5 Coarse Clay Fraction



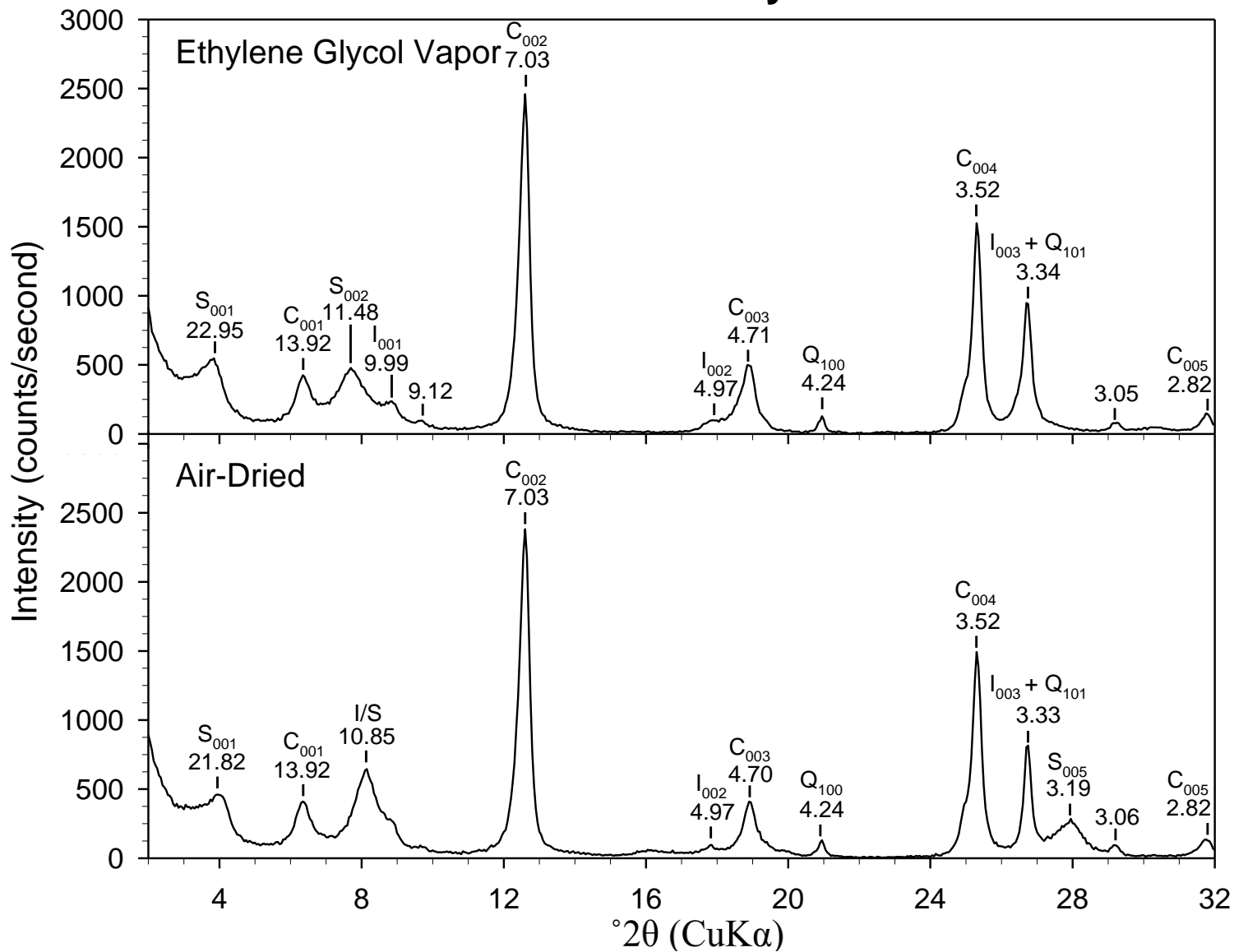
ART-5 Fine Clay Fraction



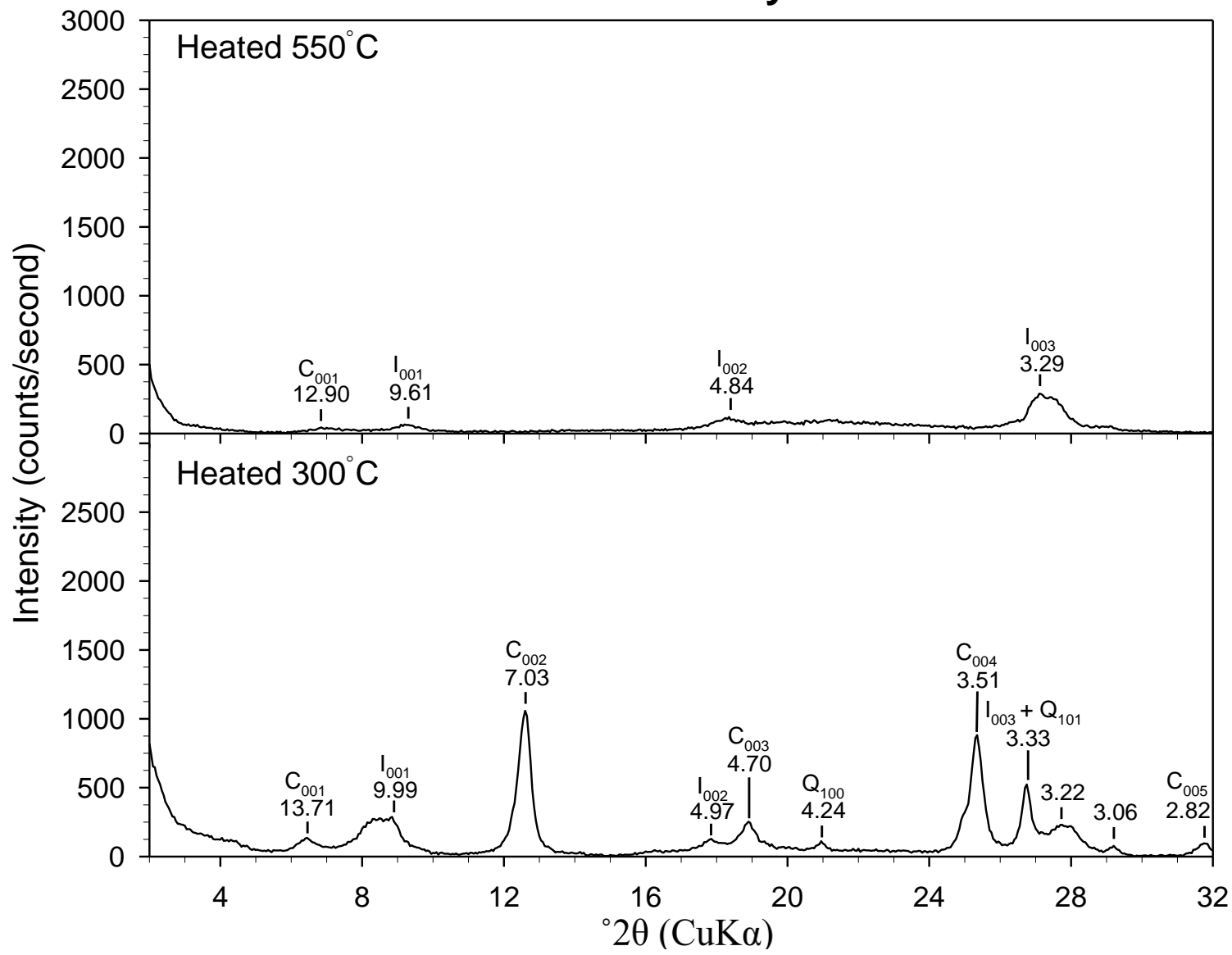
ART-5 Fine Clay Fraction



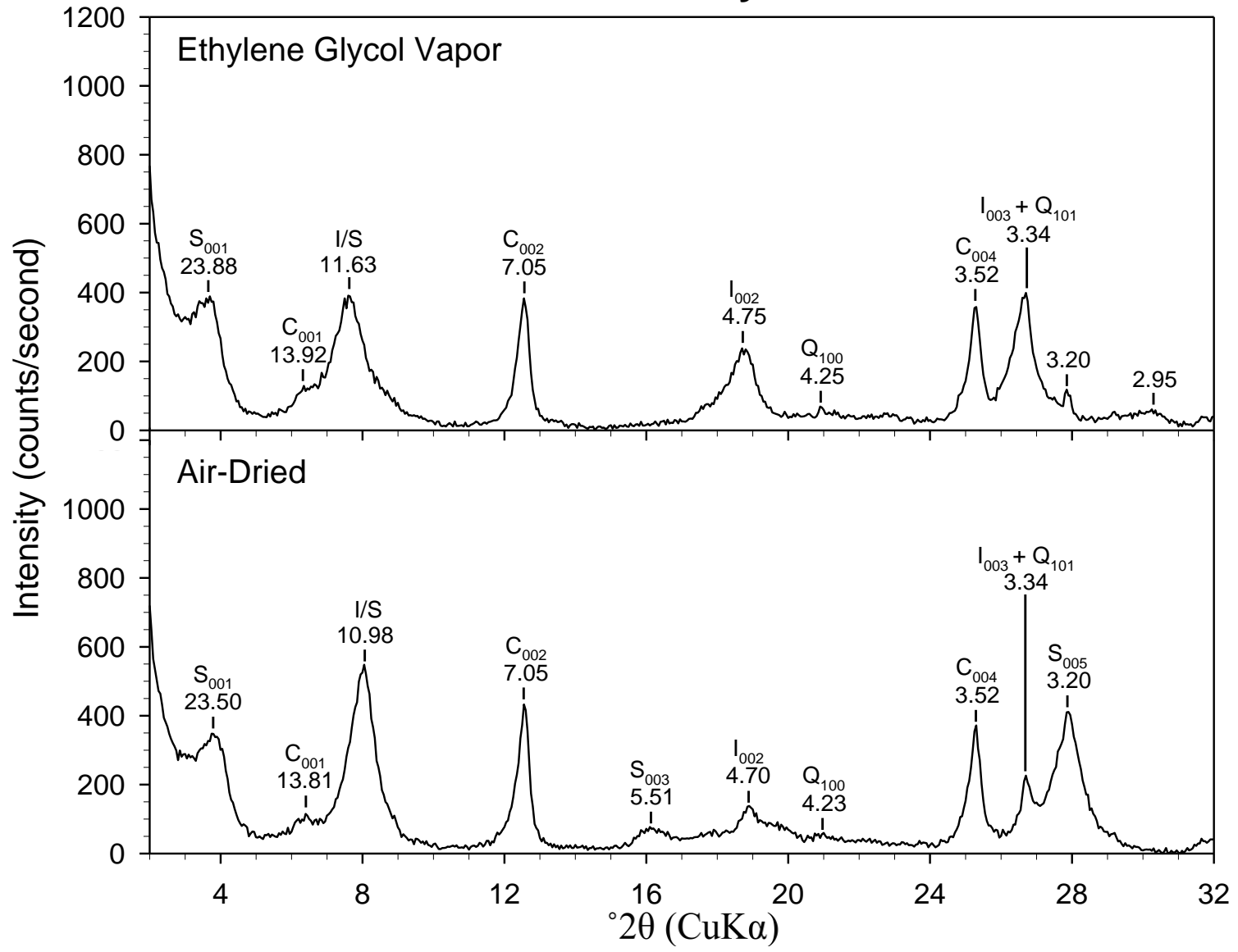
ART-6 Coarse Clay Fraction



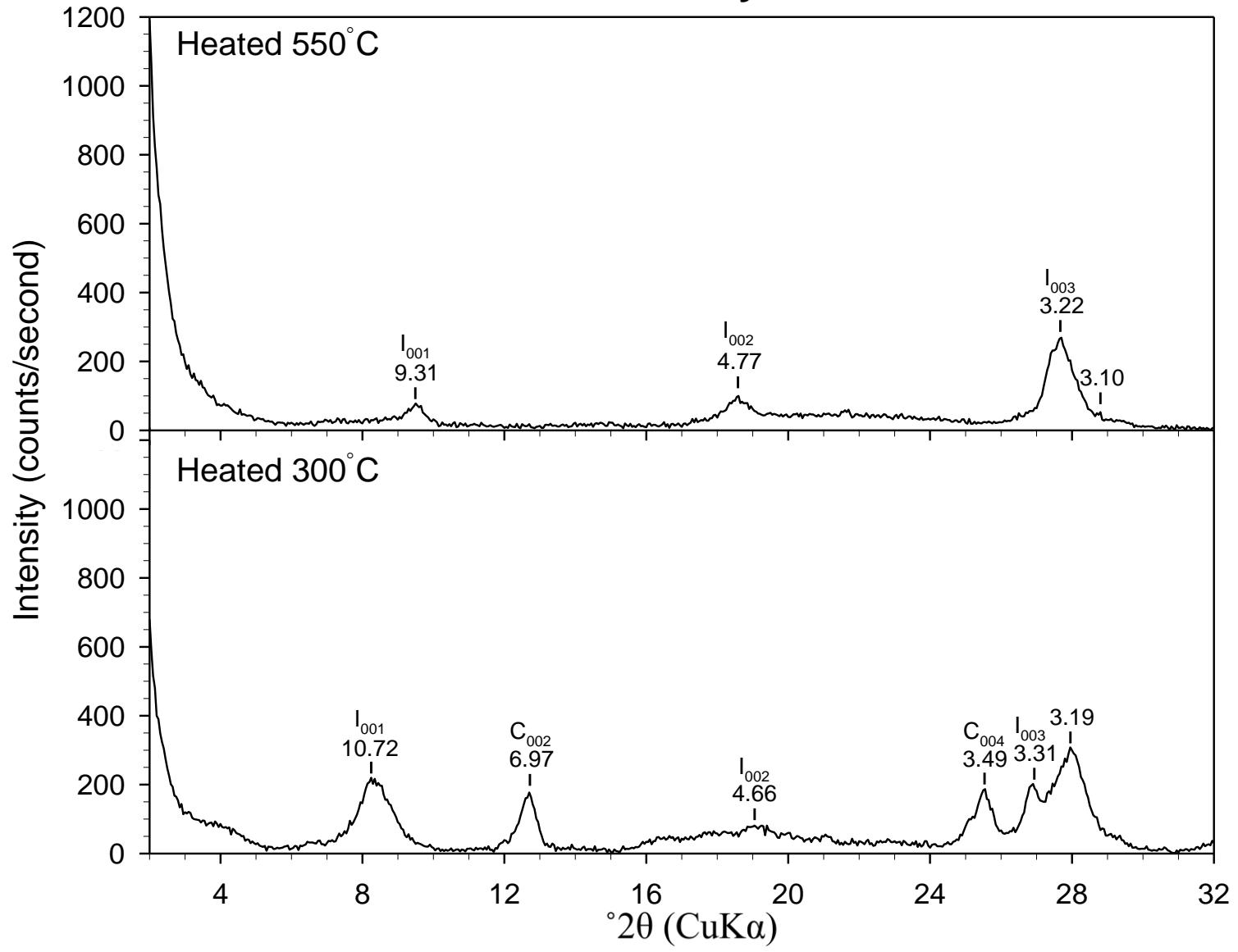
ART-6 Coarse Clay Fraction



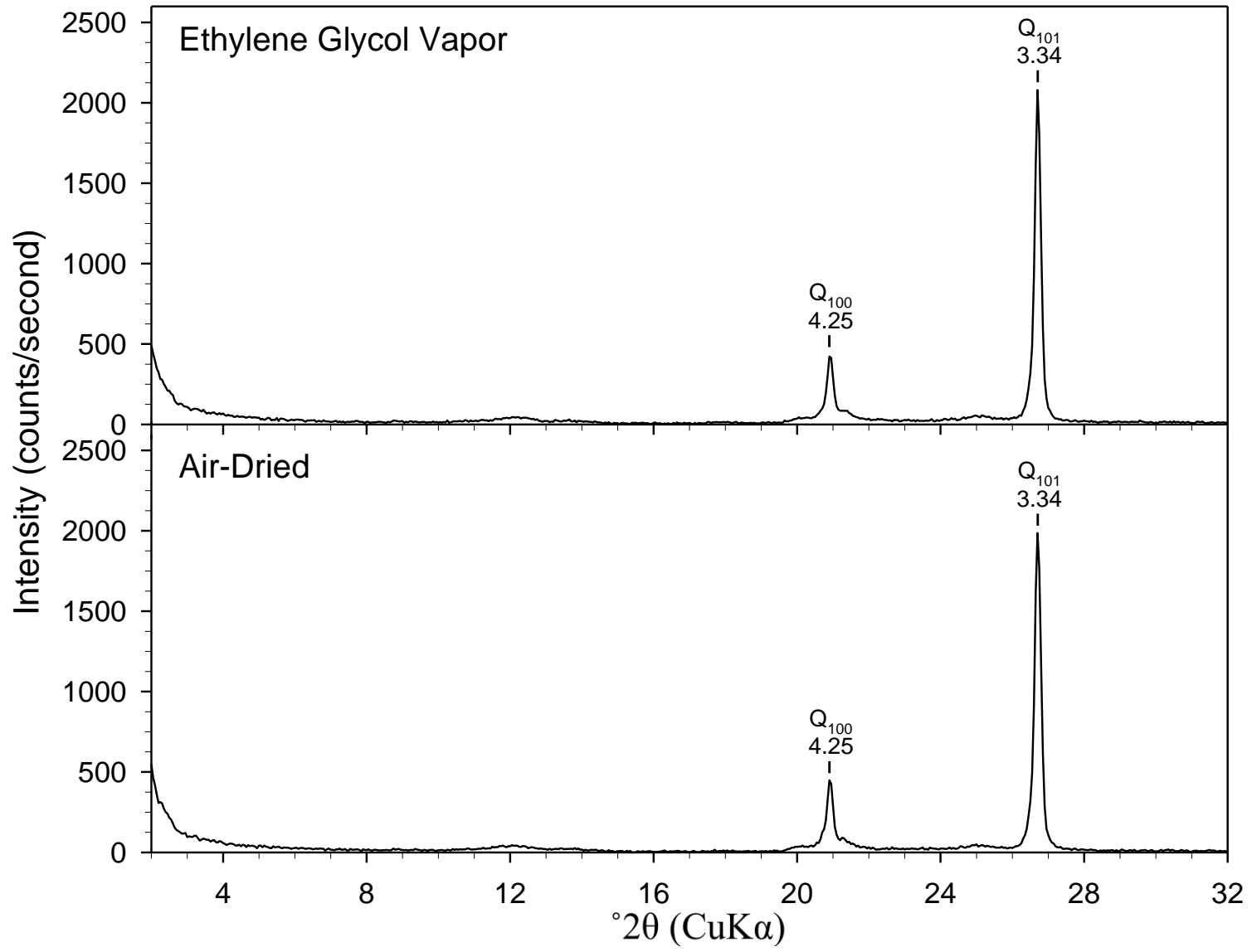
ART-6 Fine Clay Fraction



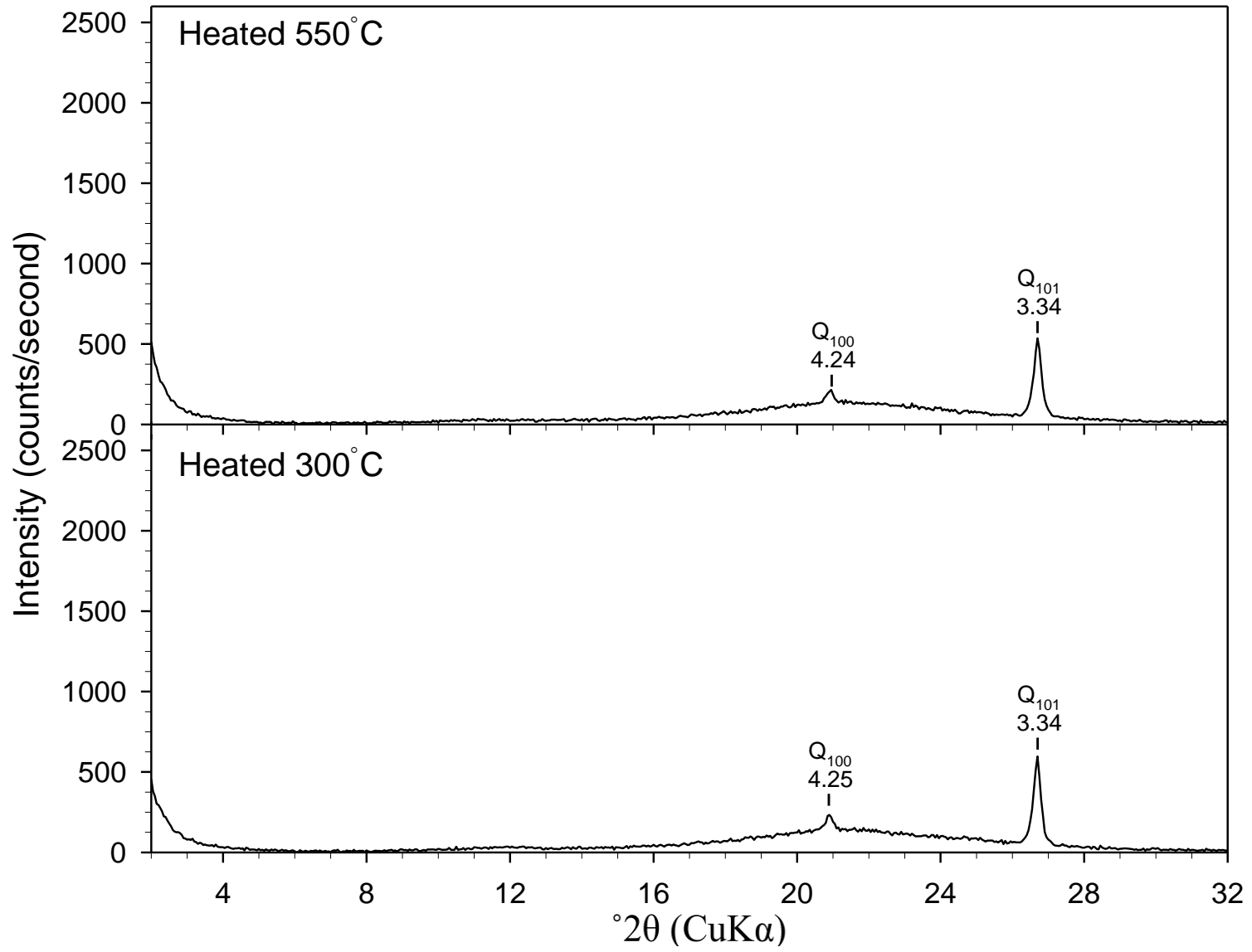
ART-6 Fine Clay Fraction



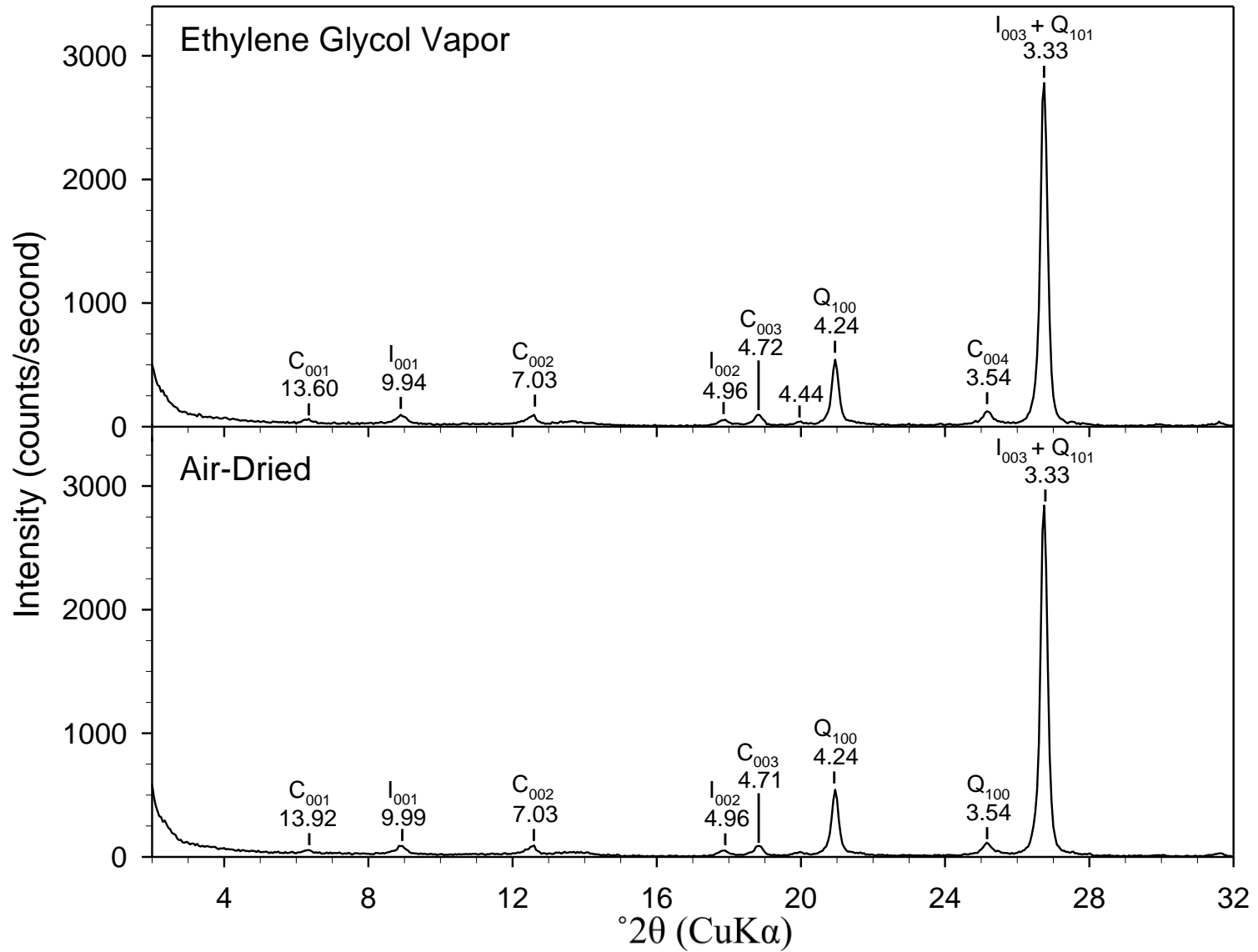
ART-9 Coarse Clay Fraction



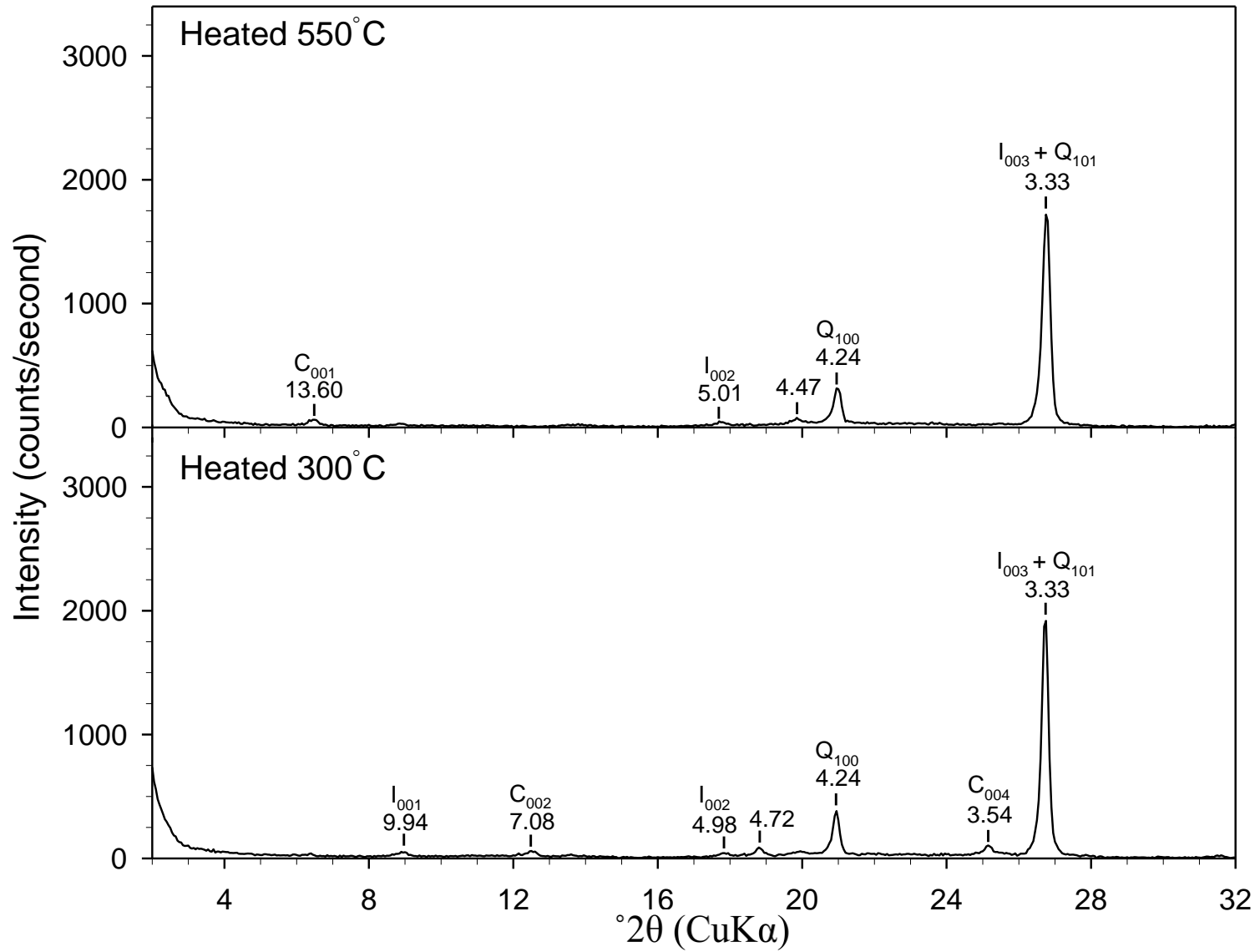
ART-9 Coarse Clay Fraction



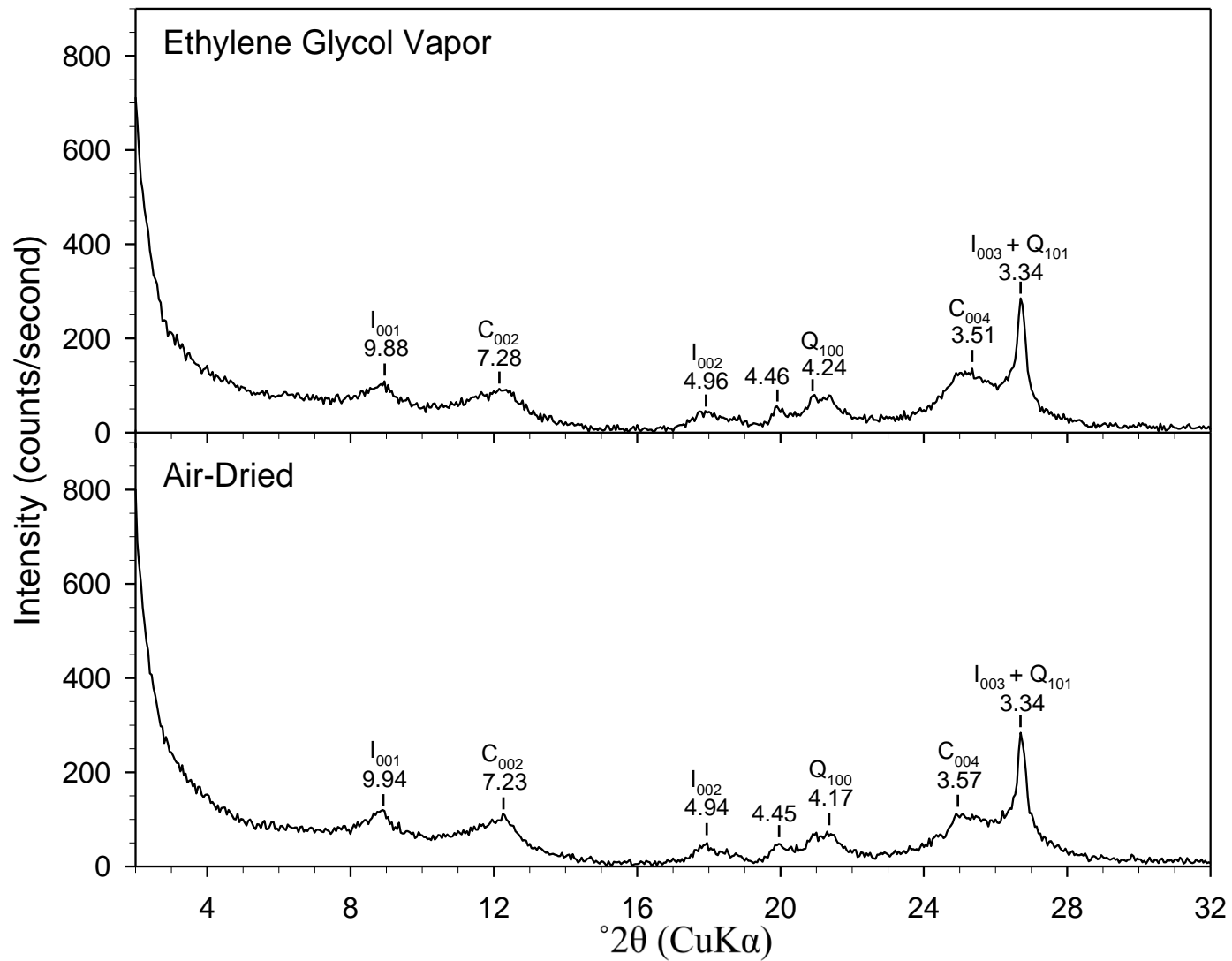
ART-12 Coarse Clay Fraction



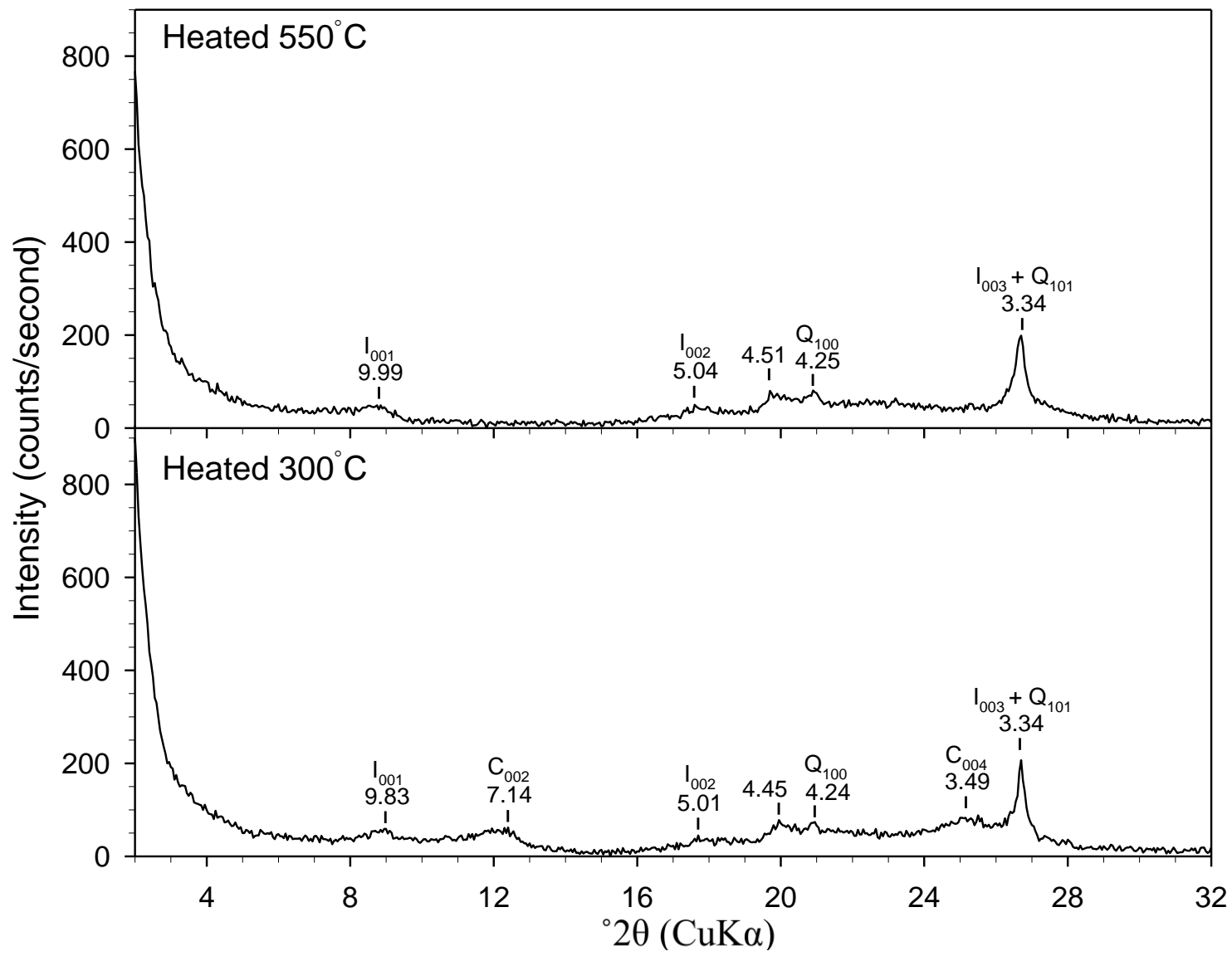
ART-12 Coarse Clay Fraction



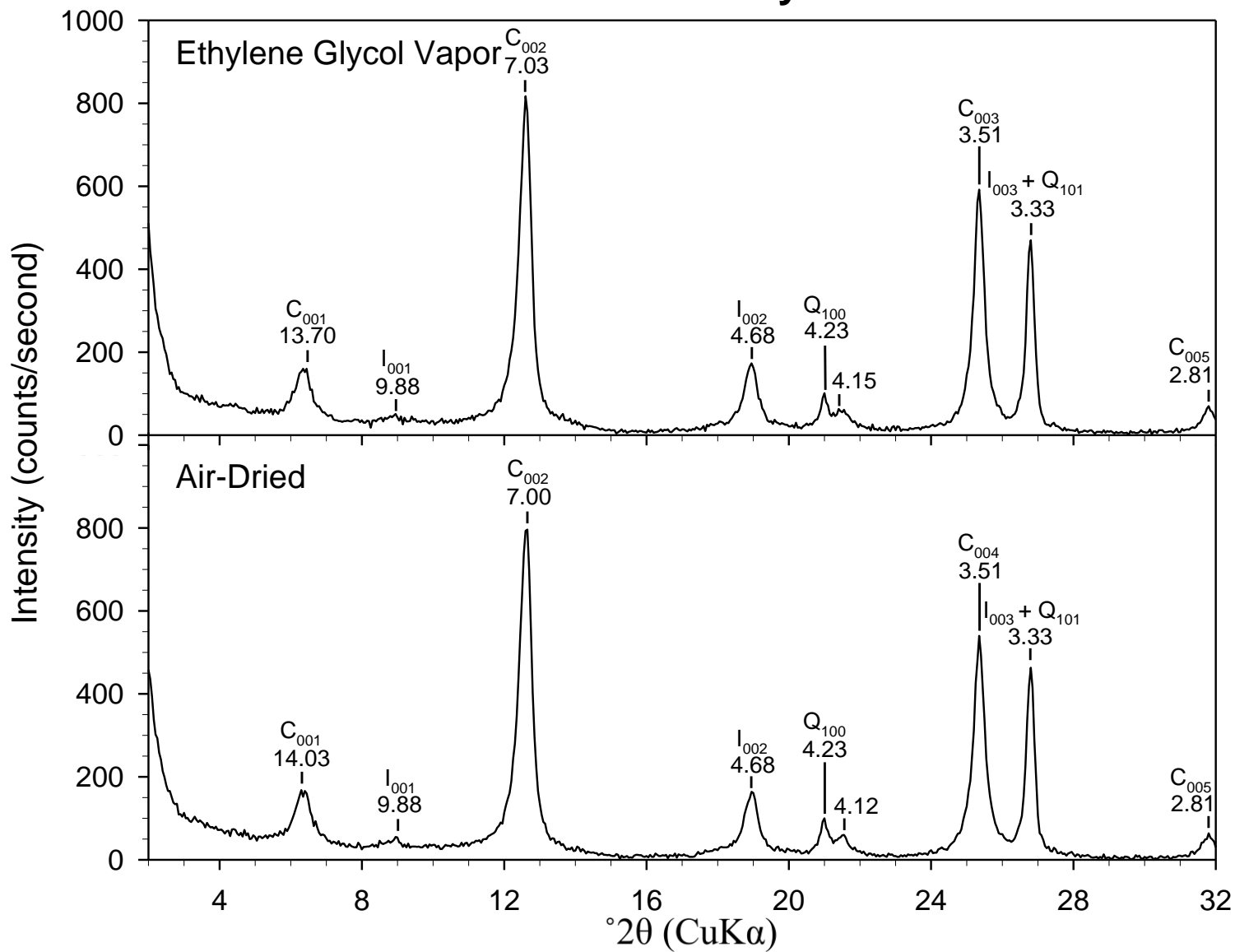
ART-12 Fine Clay Fraction



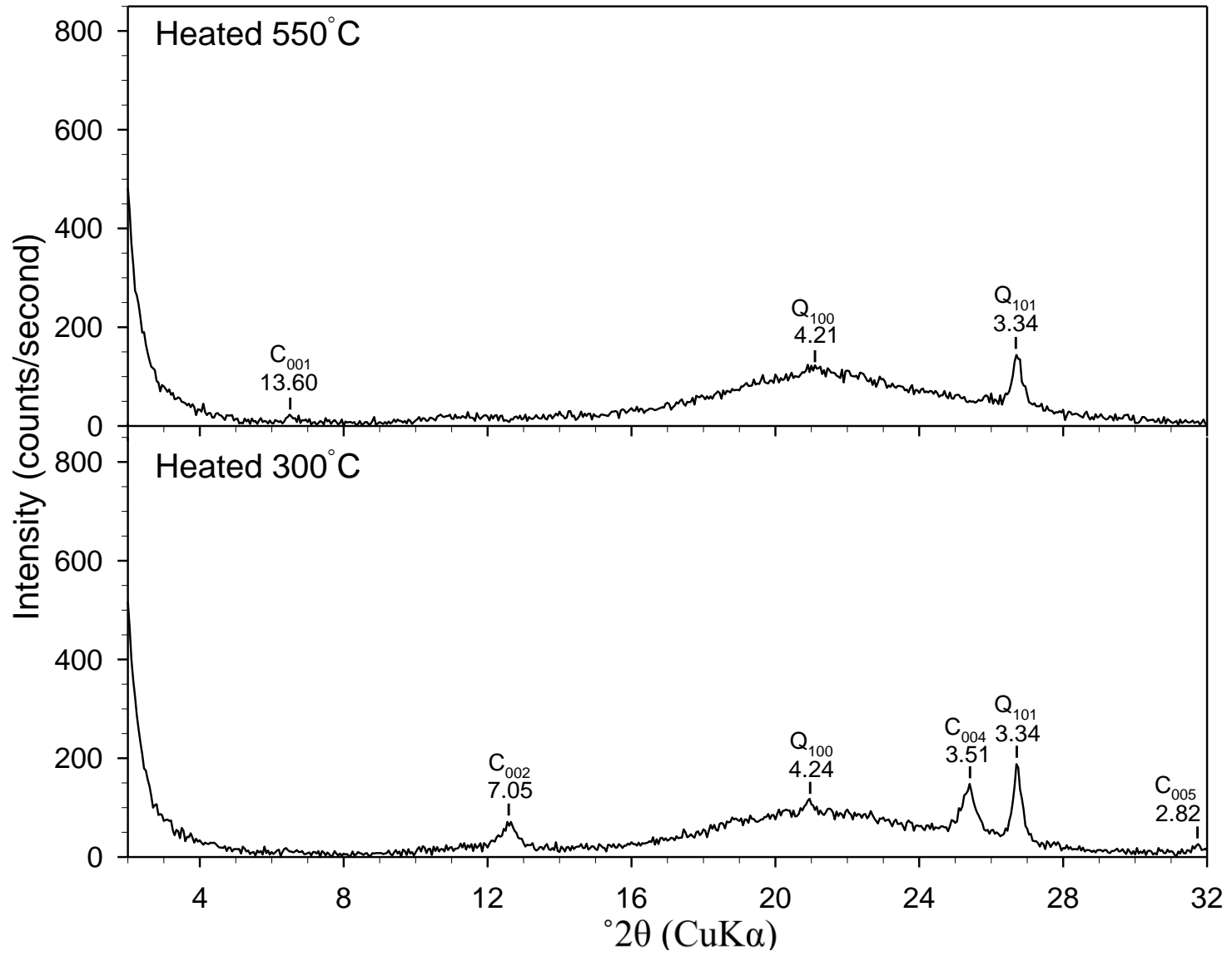
ART-12 Fine Clay Fraction



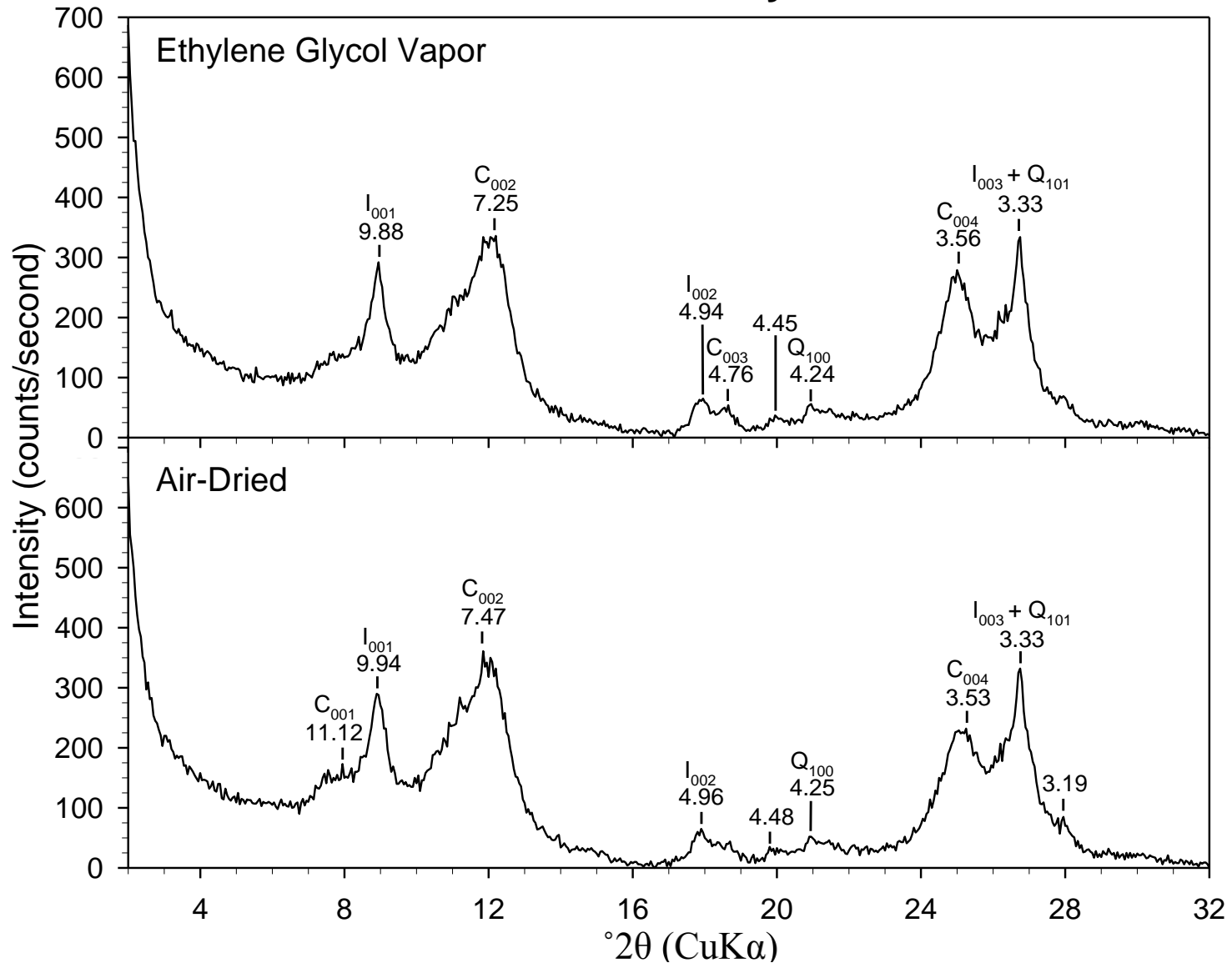
ART-14 Coarse Clay Fraction



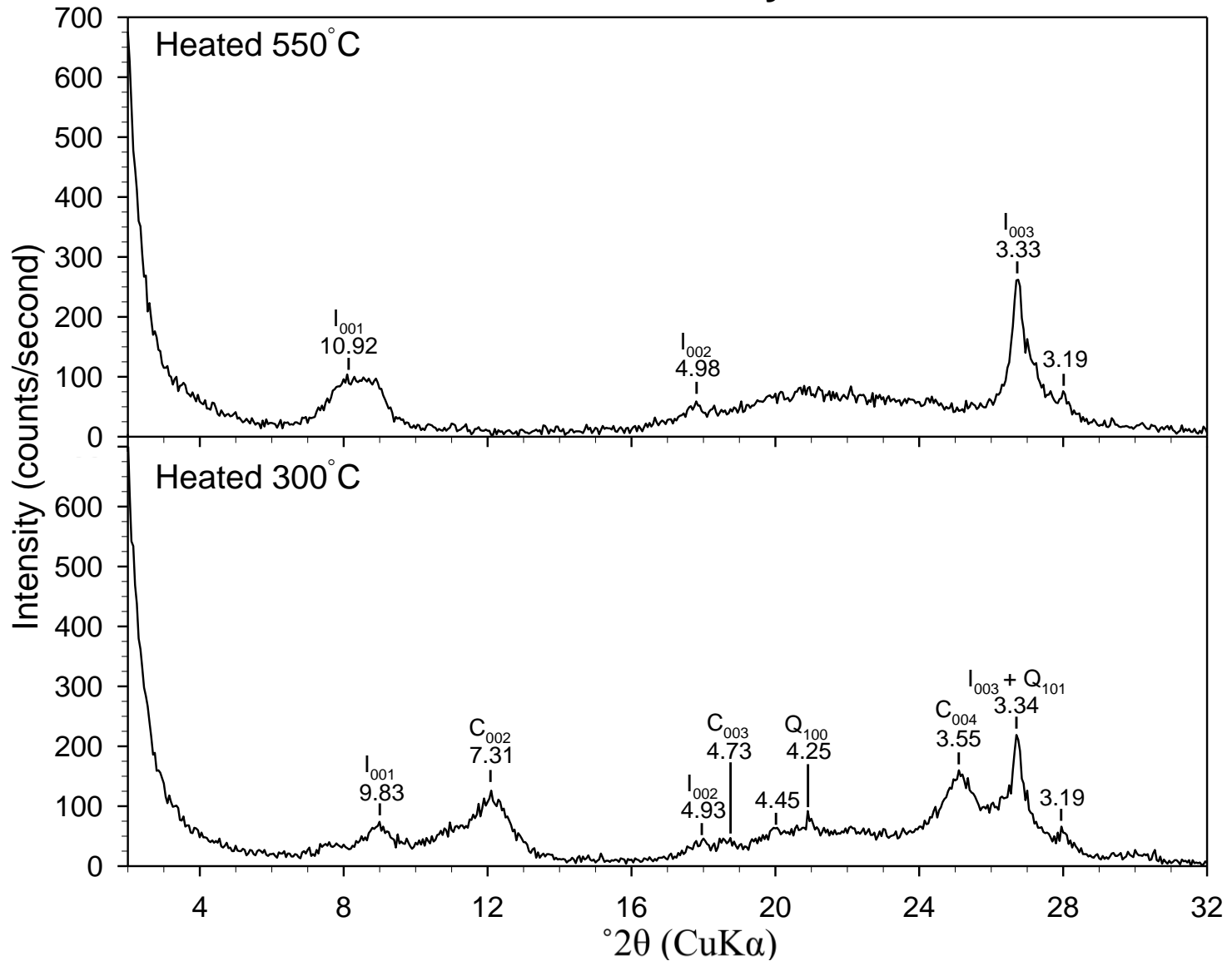
ART-14 Coarse Clay Fraction



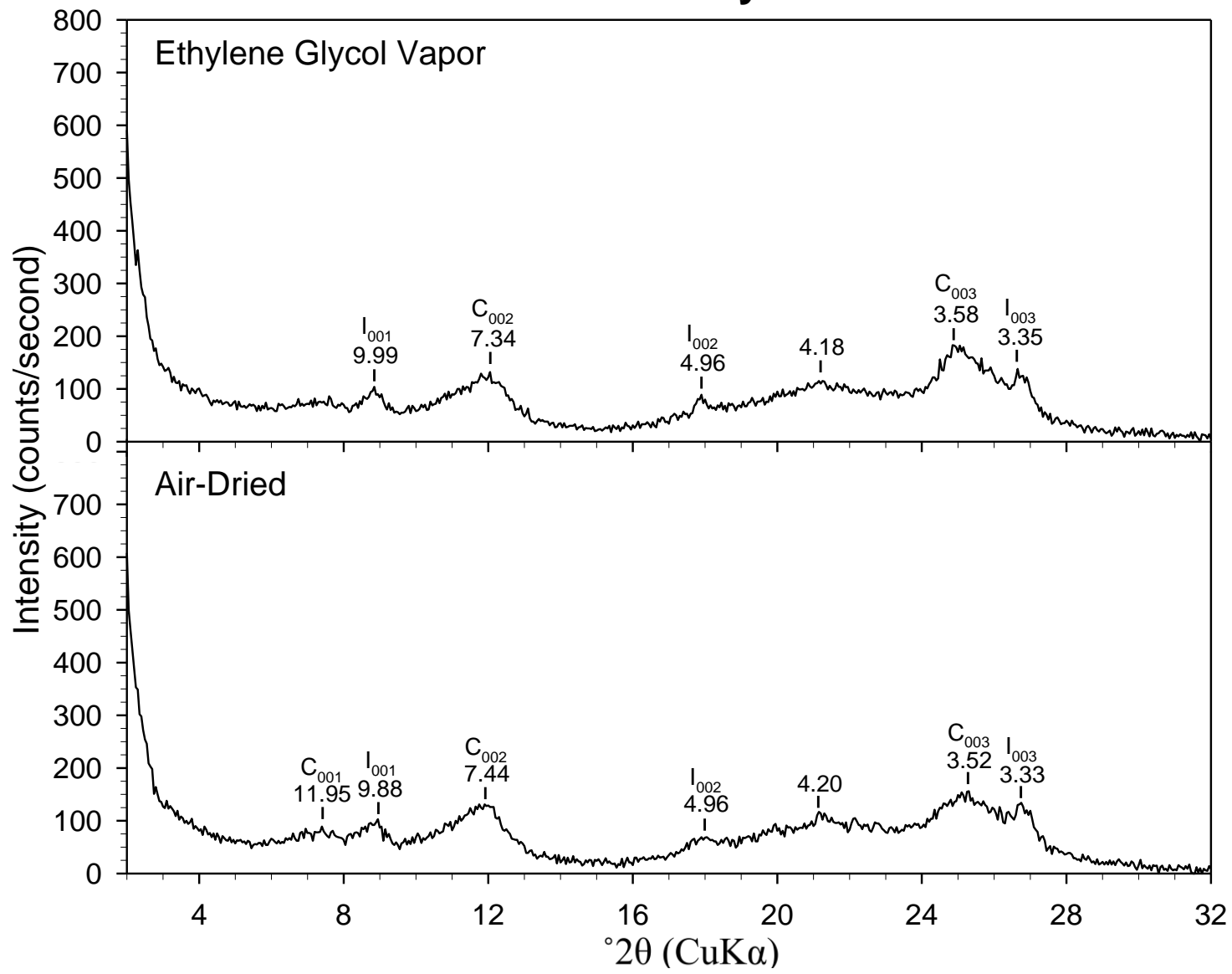
ART-15 Coarse Clay Fraction



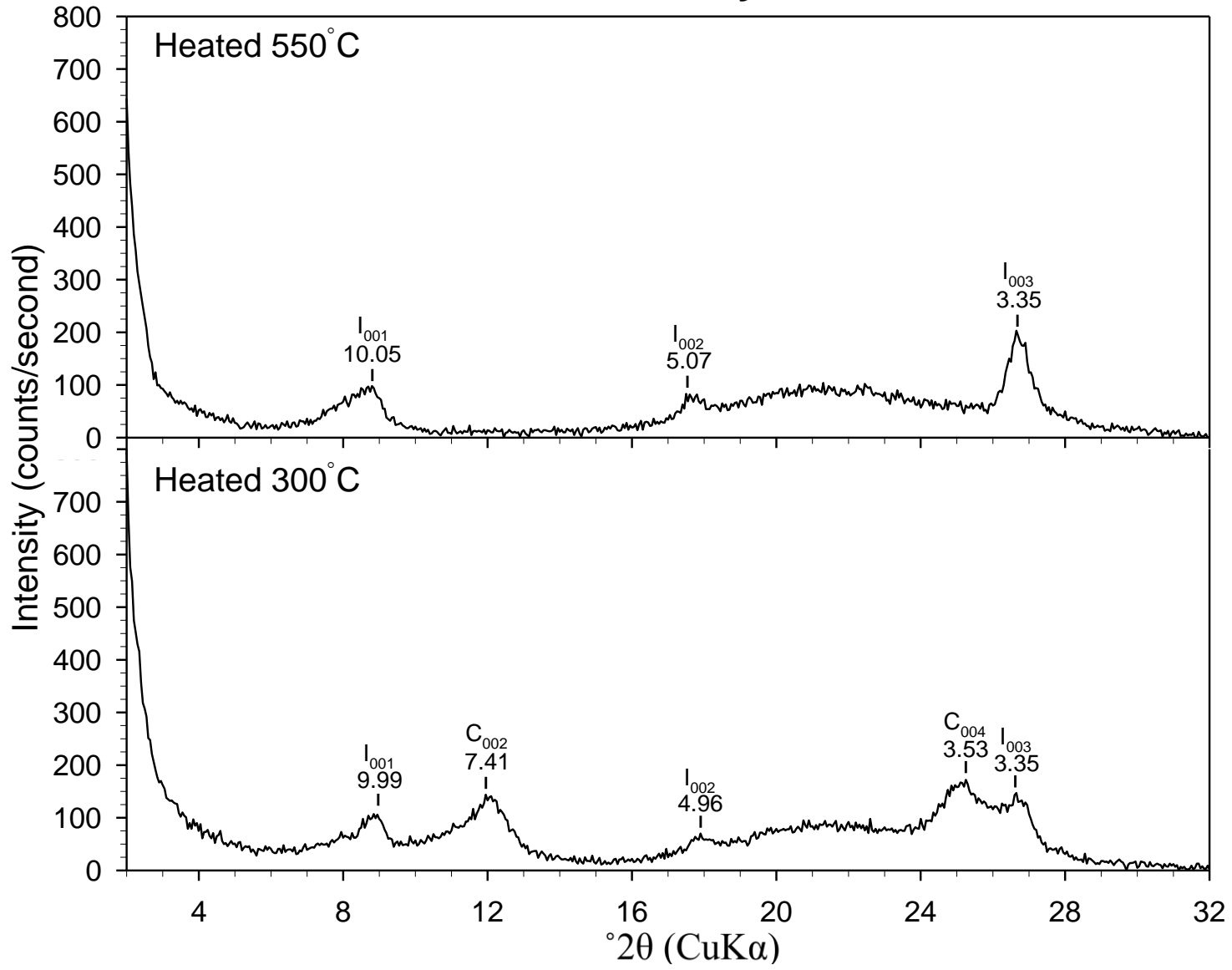
ART-15 Coarse Clay Fraction



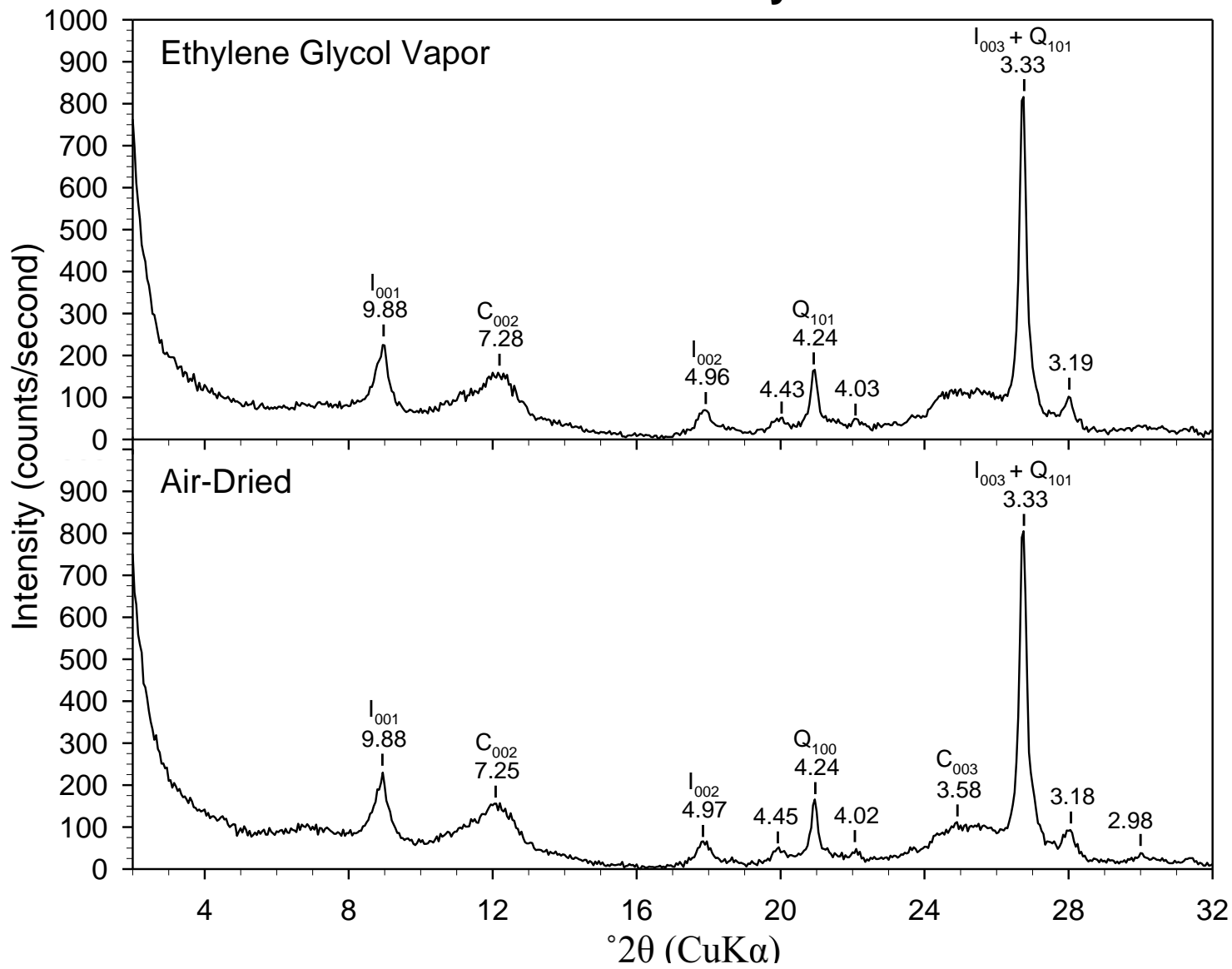
ART-15 Fine Clay Fraction



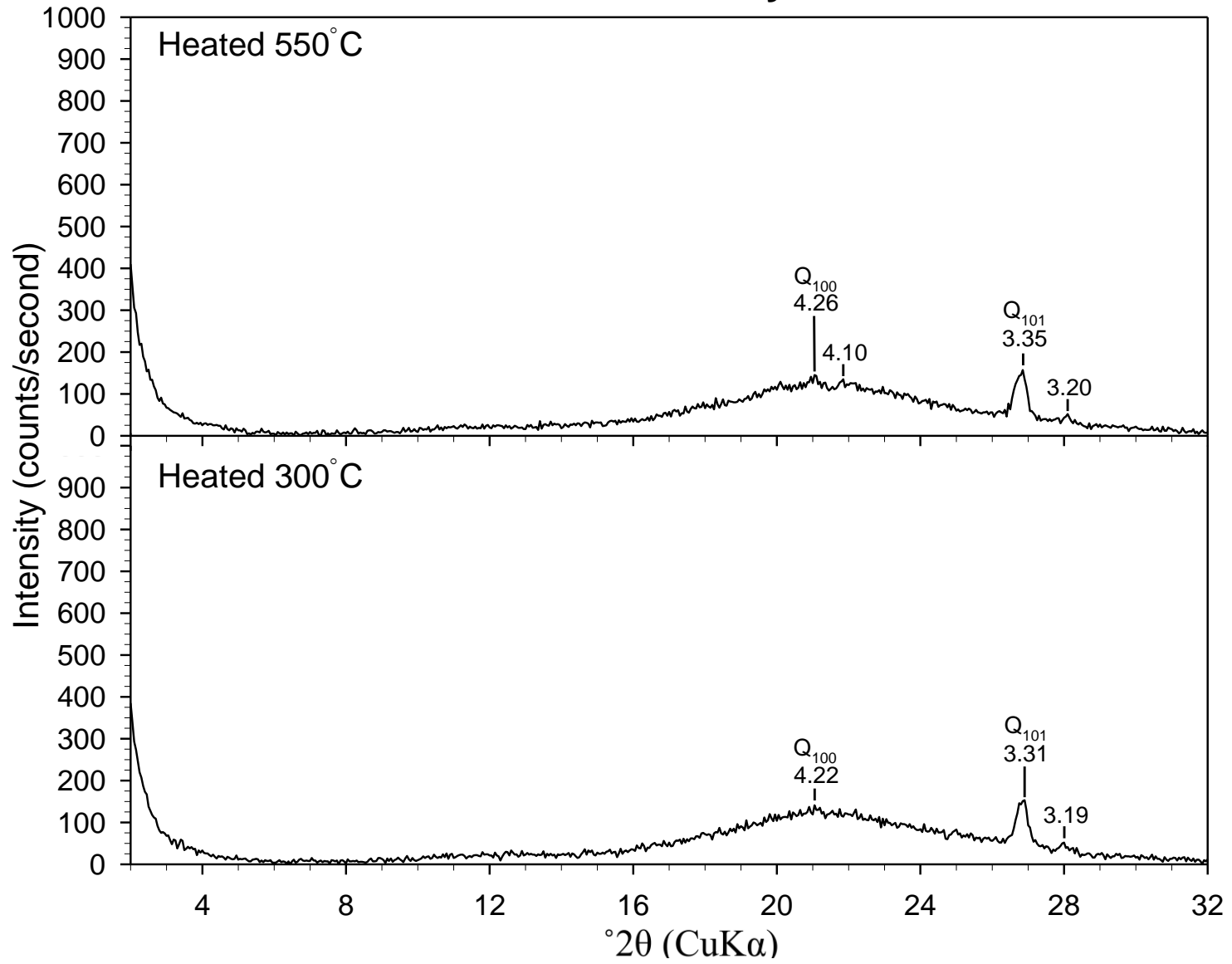
ART-15 Fine Clay Fraction



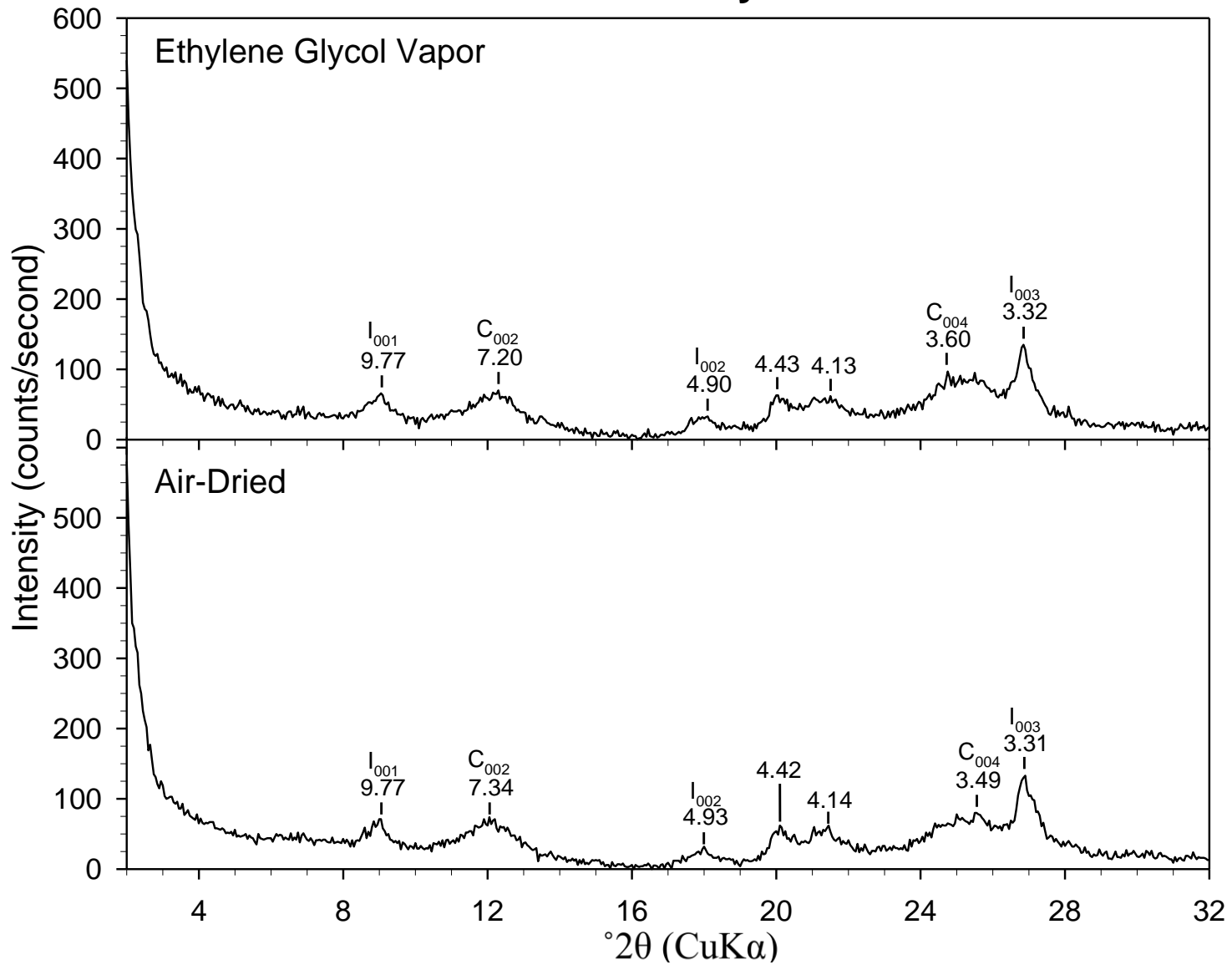
ART-18 Coarse Clay Fraction



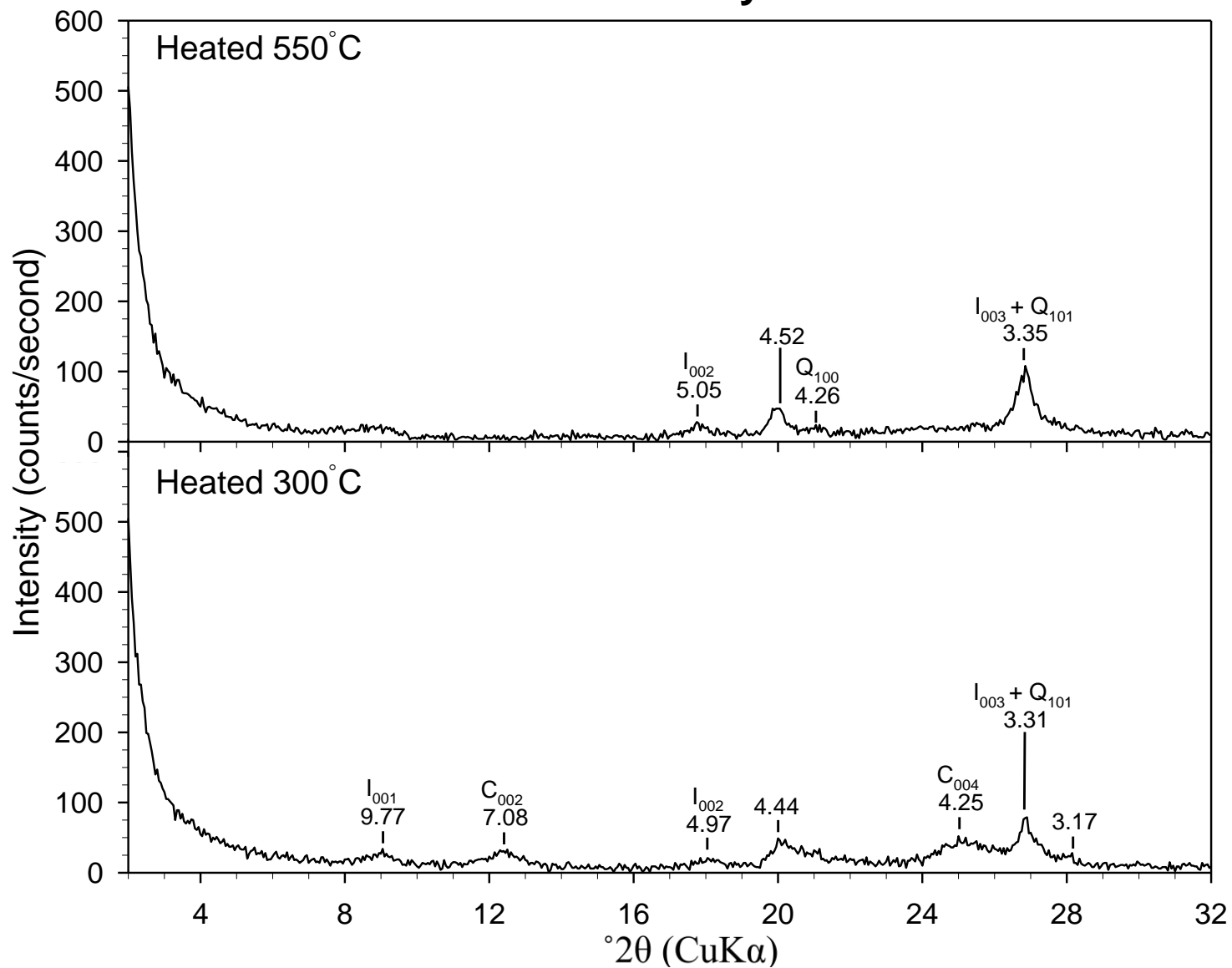
ART-18 Coarse Clay Fraction



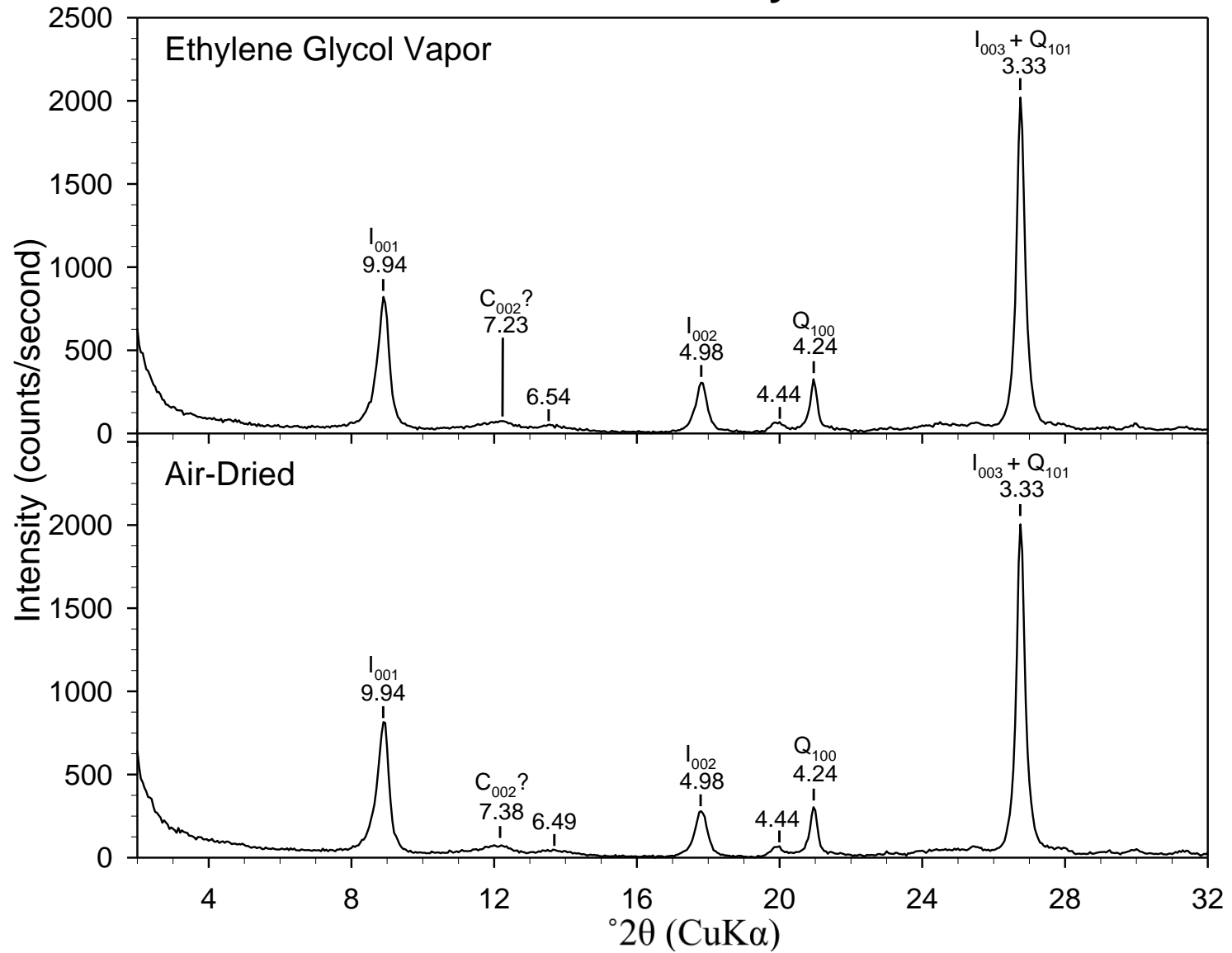
ART-18 Fine Clay Fraction



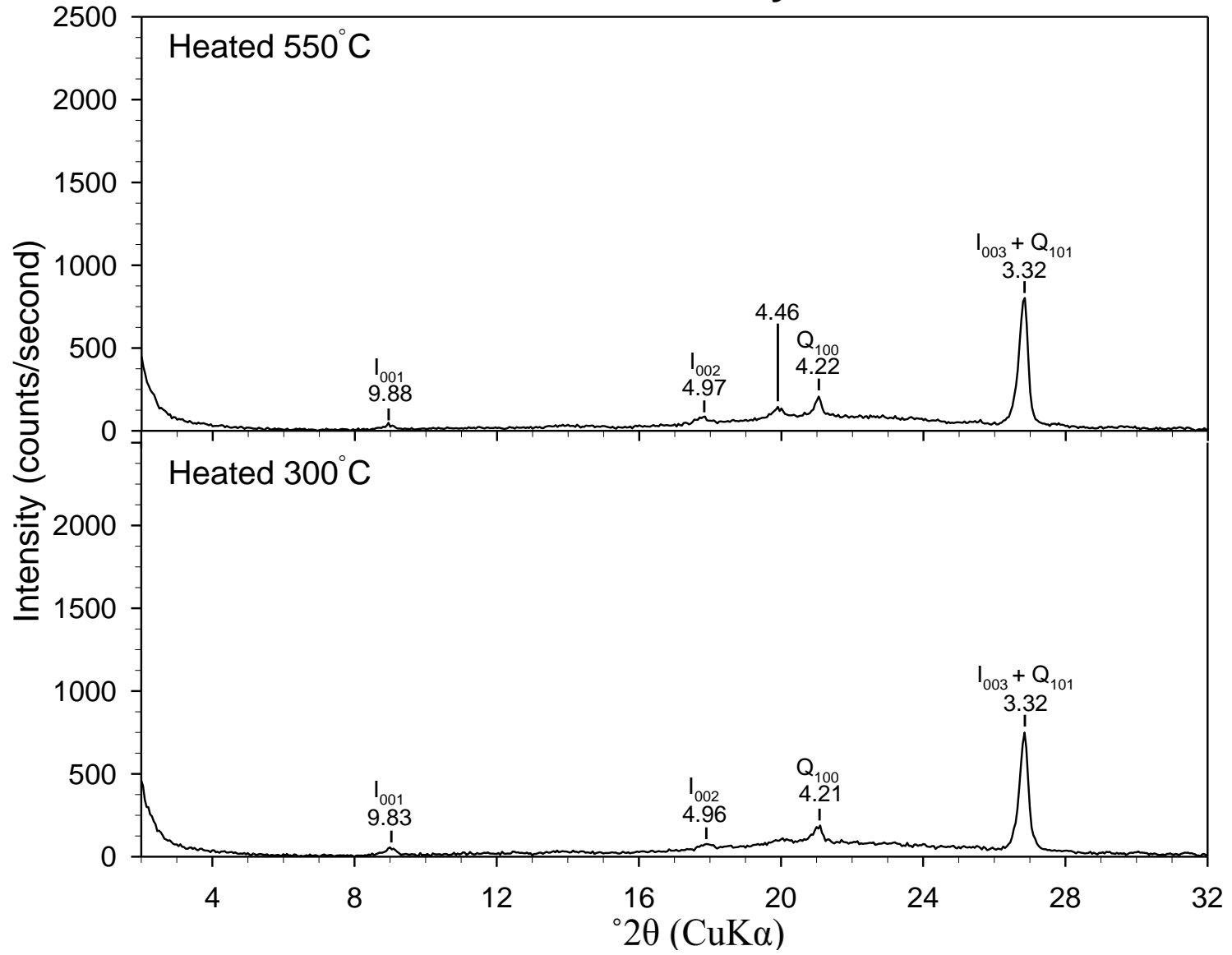
ART-18 Fine Clay Fraction



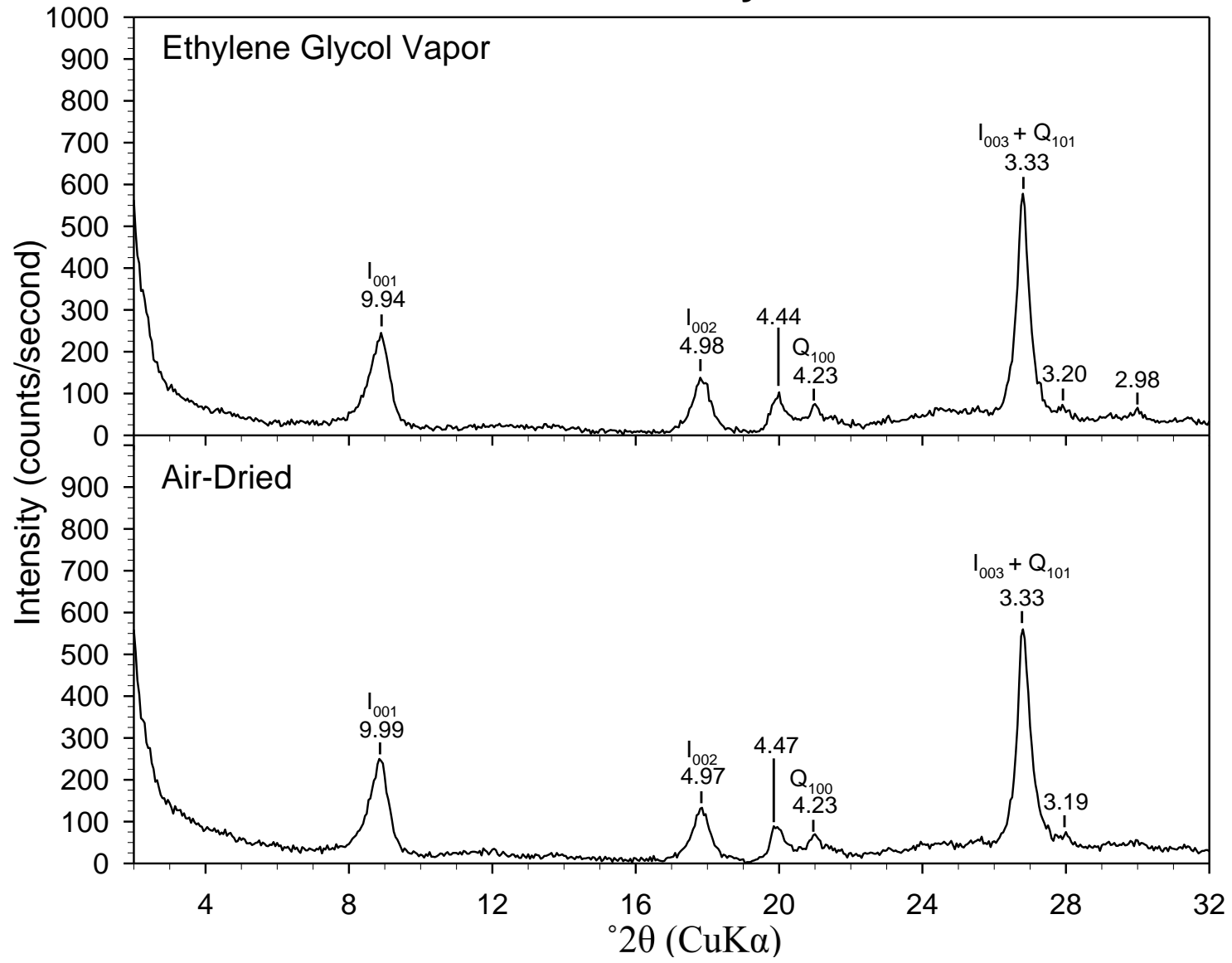
ART-19 Coarse Clay Fraction



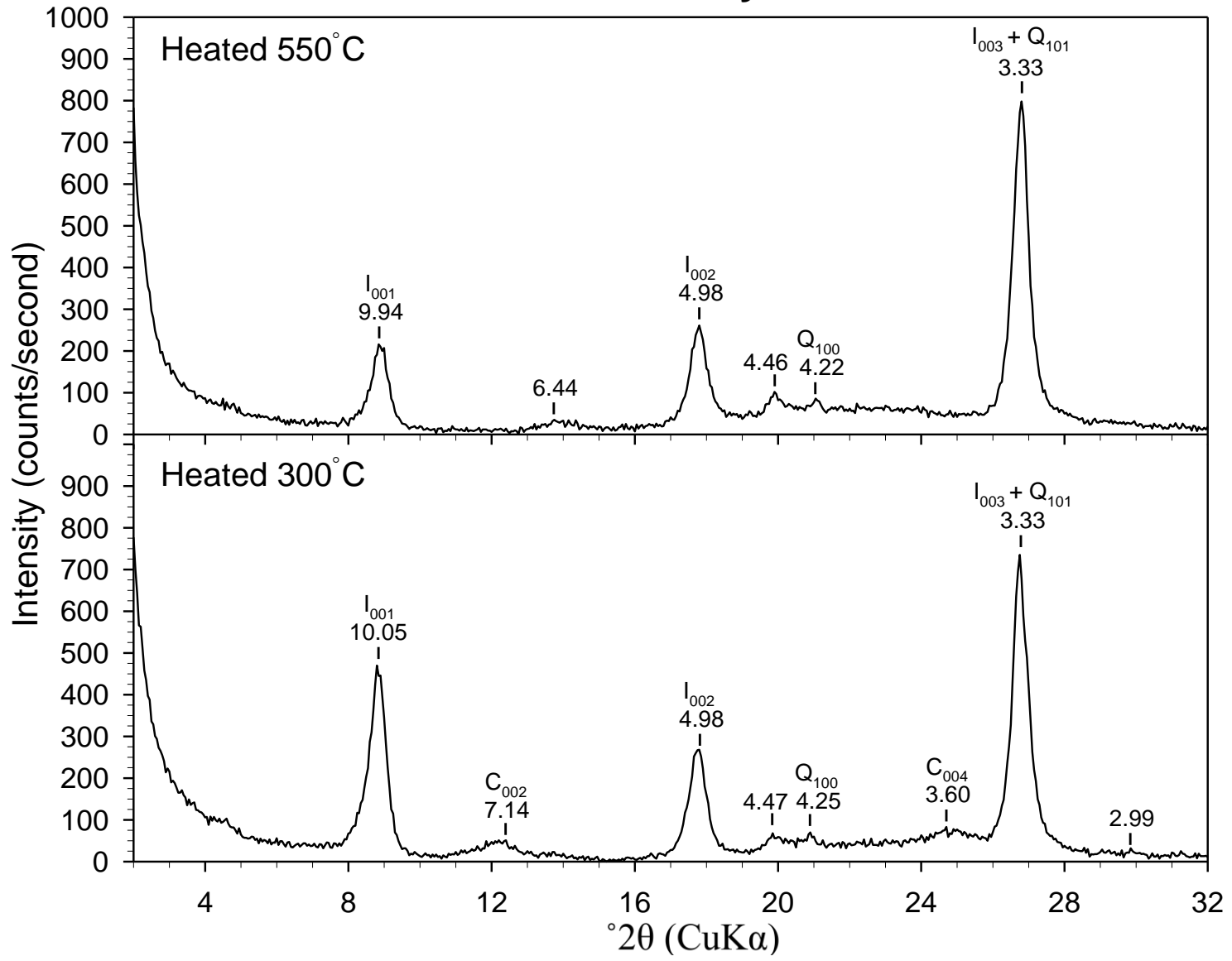
ART-19 Coarse Clay Fraction



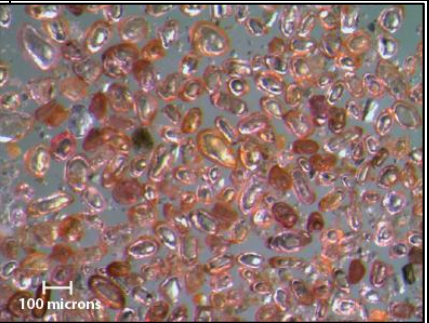
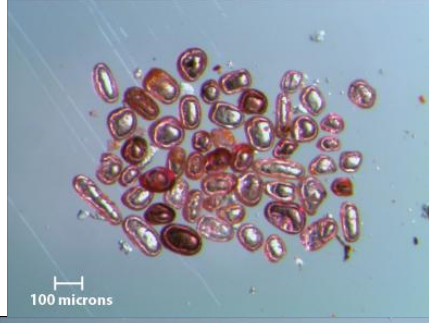
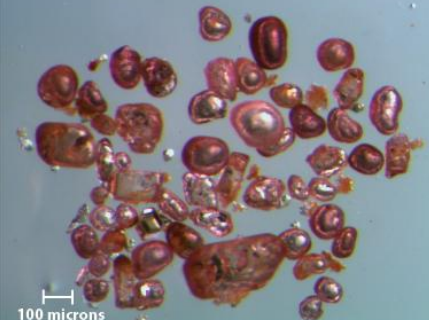
ART-19 Fine Clay Fraction


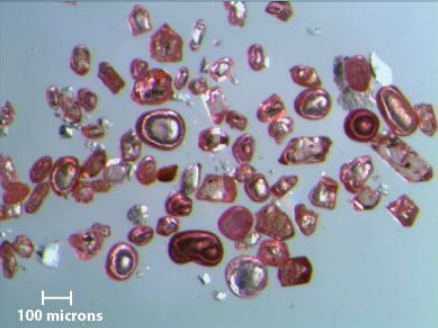
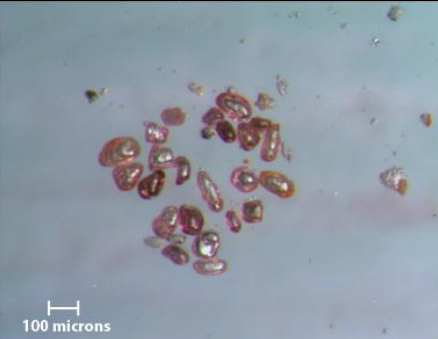


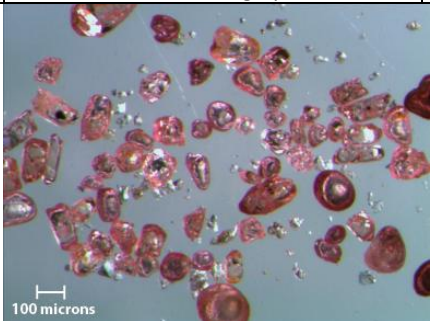
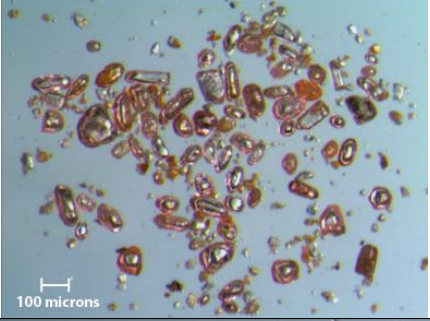
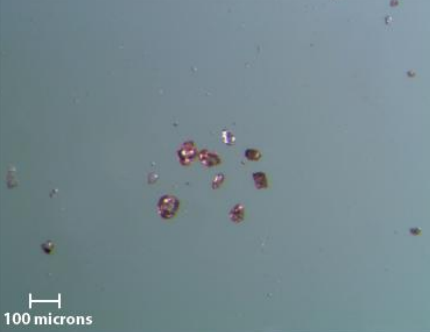
ART-19 Fine Clay Fraction


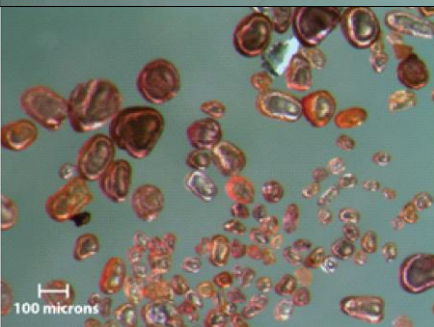
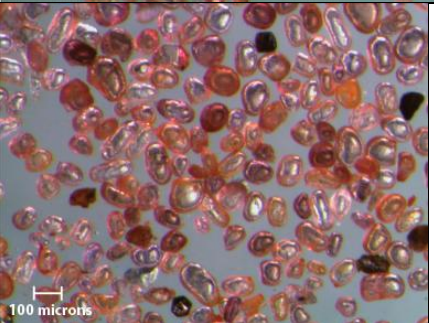


APPENDIX E
ZIRCON DESCRIPTIONS

Sample	Photomicrograph	Shape	Size	Color	Surfaces	Fis?	Other
ART-2		Well-rounded to sub-rounded. Some grains are elongated/equant.	Grains from 35 to 185 microns. Minor fragments present.	Grains are transparent with varying degrees of pink hue. Light purple or tan grains present?	Generally rough surfaces with several grains having smooth surfaces.	Present.	Some grains show internal fractures.
ART-3		Well-rounded to sub-rounded.	Grains from 60 to 235 microns.	Most grains are transparent with varying degrees of a pink hue. Some well-rounded grains are dark purple.	Smooth to irregular "pitted" surfaces.	Present.	Some grains show internal fractures.
ART-4		Well-rounded to sub-angular. Some grains are equant.	Grains from 55 to 365 microns.	Most grains are transparent with varying degrees of a pink hue. Some well-rounded grains are dark purple.	Slightly rough surfaces.	Present and abundant in mostly sub-angular prismatic grains.	None.

Sample	Photomicrograph	Shape	Size	Color	Surfaces	FIs?	Other
ART-8		Well-rounded to sub-rounded	Grains from 55 to 240 microns.	Grains are transparent with varying degrees of pink hue.	Smooth to slightly rough surfaces.	Present.	None.
ART-9		Well-rounded to angular. Some equant.	Grains from 2 to 240 microns. Fragments present.	Most grains are transparent with varying degrees of a pink hue. Some well-rounded grains are dark purple.	Angular prismatic grains have smooth surfaces. Well-rounded grains have slightly rough surfaces.	Present and abundant in mostly angular to sub-angular grains.	Some grains show internal fractures and/or opaque inclusions.
ART-12		Well-rounded to sub-rounded. Some grains are elongated.	Grains from 40 to 140 microns	Most grains are transparent with varying degrees of a pink hue. Some well-rounded grains are dark purple.	Rough surfaces.	Present	Some grains show internal fractures.

Sample	Photomicrograph	Shape	Size	Color	Surfaces	FIs?	Other
ART-16		Sub-angular to well-rounded grains. Some are equant.	Intact grains from 65 to 260 microns. Fragmented grains from 80 to 170 microns.	Most grains are transparent with varying degrees of a pink hue. Several of the well-rounded grains are purple and frosty.	Well-rounded grains show rough surfaces and sub-angular grain surfaces appear smooth.	Present, appear to be mostly in prismatic grains.	Some grains show internal fractures and/or opaque inclusions.
ART-18		Well-rounded to sub-rounded grains. Some grains are elongated.	Intact grains from 20 to 165 microns. Fragmented grains - present from 40 to 110 microns.	Most grains are transparent with varying degrees of a pink hue. Tan grains present?	Most grains have smooth surfaces, except for well-rounded grains that show rough surfaces.	Present, appear to be in prismatic grains.	Some grains show internal fractures.
Chung		Angular to sub-rounded. Some grain(s) are equant.	Grains are from 45 to 75 microns. Fragments present?	Most grains are transparent with pink hue. Tan grains present?	Angular grains show smooth surfaces and sub-rounded grains have rough irregular surfaces.	None.	Specimen description is based on a small number of zircons.

Sample	Photomicrograph	Shape	Size	Color	Surfaces	FIs?	Other
Lake Ouachita 41		Well-rounded to sub-angular.	Grains from 65 to 95 microns. Fragments present?	Most grains are transparent with pink hue. A large (95 micron) well-rounded grain is dark purple.	Grains show smooth surfaces.	None.	Some grains show internal fractures. Specimen description is based on a small number of zircons.
Lake Pineda		Well-rounded.	Grains from 30 to 110 microns.	Most grains are transparent with pink hue. Some larger grains are purple.	Most grains have smooth surfaces. A few grains have a more rough surface.	None.	None
Mount Blakely		Well-rounded to sub-rounded. Some grains are elongated.	Grains from 40 to 165 microns.	Most grains are transparent with varying degrees of a pink hue. Some (well-rounded?) grains are purple	Smooth to slightly rough surfaces on several sub-rounded grains.	Present.	Some grains show internal fractures.

APPENDIX F

ZIRCON FISSION TRACK DATA

Table F1. ART-2 Zircon Fission Track Individual Ages^a

Zircon Number	N s	N i	N g	Rho s	Rho i	Rho s / Rho i	U (ppm)	Age (Ma)	Age error (± 1 S.E.)	50% Age	"+95%"	"-95%"
1	167	16	18	1.450E+07	1.389E+06	10.4375	121.8	346.58	91.43	355.10	252.71	145.63
2	128	14	9	2.222E+07	2.431E+06	9.1429	213.1	304.59	86.34	313.39	248.06	136.59
3	315	32	21	2.344E+07	2.381E+06	9.8438	208.8	327.35	61.71	331.39	149.67	102.45
4	134	12	6	3.490E+07	3.125E+06	11.1667	274.0	370.11	112.20	382.16	332.45	174.53
5	102	13	6	2.656E+07	3.385E+06	7.8462	296.8	262.26	77.73	270.70	229.24	122.67
6	110	12	8	2.148E+07	2.344E+06	9.1667	205.5	305.36	93.39	315.69	279.59	145.95
7	137	14	10	2.141E+07	2.188E+06	9.7857	191.8	325.47	91.97	334.75	263.38	145.26
8	133	18	9	2.309E+07	3.125E+06	7.3889	274.0	247.26	62.64	253.06	171.05	101.37
9	258	25	25	1.613E+07	1.563E+06	10.3200	137.0	342.78	72.71	348.15	183.52	119.12
10	129	15	10	2.016E+07	2.344E+06	8.6000	205.5	286.90	78.85	294.73	223.27	125.55
11	210	20	9	3.646E+07	3.472E+06	10.5000	304.5	348.60	82.40	355.42	216.90	133.20
12	148	17	16	1.445E+07	1.660E+06	8.7059	145.6	290.35	74.98	297.31	206.06	120.44
13	234	23	12	3.047E+07	2.995E+06	10.1739	262.6	338.05	74.73	343.83	191.66	121.91
14	91	11	10	1.422E+07	1.719E+06	8.2727	150.7	276.21	88.65	286.64	273.54	137.86
15	399	42	25	2.494E+07	2.625E+06	9.5000	230.2	316.20	52.37	319.18	122.08	87.93
16	184	18	20	1.438E+07	1.406E+06	10.2222	123.3	339.61	84.63	347.05	228.04	135.97
17	83	12	12	1.081E+07	1.563E+06	6.9167	137.0	231.74	71.99	240.08	218.24	113.20
18	365	38	20	2.852E+07	2.969E+06	9.6053	260.3	319.62	55.51	322.95	131.25	92.87
19	92	10	6	2.396E+07	2.604E+06	9.2000	228.3	306.45	102.55	318.93	324.15	157.79
20	129	16	10	2.016E+07	2.500E+06	8.0625	219.2	269.34	71.95	276.32	201.15	115.27
Totals/Averages	3548	378	262	2.116E+07	2.254E+06	9.3862	197.7	312.50	19.86	312.83	34.60	31.17

^aAnalytical notes: Position # 47, area of graticule square is 6.400E-07, zeta factor±error is 121.1±3.5, Rho d (% relative error) is 5.634E+05 and 1.67, N_d is 3605, glass (U ppm) is 49.4, irradiation is UA-Z2, and analyst was Dr. Stuart N. Thomson.

Table F2. ART-3 Zircon Fission Track Individual Ages^a

Zircon Number	N s	N i	N g	Rho s	Rho i	Rho s / Rho i	U (ppm)	Age (Ma)	Age error (± 1 S.E.)	50% Age	"+95%"	"-95%"
1	144	15	20	1.125E+07	1.172E+06	9.6000	103.0	318.62	87.10	327.12	245.44	138.35
2	77	7	8	1.504E+07	1.367E+06	11.0000	120.2	363.79	144.13	384.49	512.07	213.58
3	66	7	6	1.719E+07	1.823E+06	9.4286	160.3	313.06	124.88	331.41	448.34	185.77
4	157	17	12	2.044E+07	2.214E+06	9.2353	194.6	306.80	79.00	314.06	216.57	126.73
5	120	13	9	2.083E+07	2.257E+06	9.2308	198.4	306.65	90.12	316.19	263.88	141.72
6	80	7	8	1.563E+07	1.367E+06	11.4286	120.2	377.56	149.35	398.89	529.16	221.10
7	121	12	9	2.101E+07	2.083E+06	10.0833	183.2	334.25	101.77	345.34	303.26	158.70
8	120	10	16	1.172E+07	9.766E+05	12.0000	85.9	395.87	130.96	411.21	407.68	200.23
Totals/Averages	885	88	88	1.571E+07	1.563E+06	10.0568	137.4	333.39	38.89	334.87	82.31	65.95

^aAnalytical notes: Position # 49, area of graticule square is 6.400E-07, zeta factor±error is 121.1±3.5, Rho d (% relative error) is 5.604E+05 and 1.67, N_d is 3586, glass (U ppm) is 49.4, irradiation is UA-Z2, and analyst was Dr. Stuart N. Thomson.

Table F3. ART-4 Zircon Fission Track Individual Ages^a

Zircon Number	N _s	N _i	N _g	Rho _s	Rho _i	Rho _s / Rho _i	U (ppm)	Age (Ma)	Age error (± 1 S.E.)	50% Age	"+95%"	"-95%"
1	444	44	40	1.734E+07	1.719E+06	10.0909	151.5	333.62	53.89	336.59	124.55	90.50
2	235	22	21	1.749E+07	1.637E+06	10.6818	144.3	352.63	79.50	358.88	205.23	129.22
3	205	24	20	1.602E+07	1.875E+06	8.5417	165.3	283.51	61.89	288.32	158.61	101.62
4	381	16	30	1.984E+07	8.333E+05	23.8125	73.5	761.24	195.92	777.72	512.26	304.40
5	435	32	25	2.719E+07	2.000E+06	13.5938	176.3	445.51	82.95	450.70	198.37	136.57
6	196	20	12	2.552E+07	2.604E+06	9.8000	229.6	324.24	76.88	330.68	203.02	124.49
7	163	16	20	1.273E+07	1.250E+06	10.1875	110.2	336.73	88.93	345.05	246.14	141.74
8	140	16	12	1.823E+07	2.083E+06	8.7500	183.6	290.27	77.21	297.66	215.17	123.49
9	230	24	15	2.396E+07	2.500E+06	9.5833	220.4	317.25	68.87	322.50	175.71	112.79
10	179	17	12	2.331E+07	2.214E+06	10.5294	195.1	347.74	89.01	355.76	242.60	142.36
11	141	15	12	1.836E+07	1.953E+06	9.4000	172.2	311.32	85.19	319.66	240.32	135.39
Totals/Averages	2749	246	219	1.961E+07	1.755E+06	11.1748	154.7	368.45	27.43	369.03	50.79	44.62

^aAnalytical notes: Position # 49, area of graticule square is 6.400E-07, zeta factor±error is 121.1±3.5, Rho_d (% relative error) is 5.604E+05 and 1.67, N_d is 3586, glass (U ppm) is 49.4, irradiation is UA-Z2, and analyst was Dr. Stuart N. Thomson.

Table F4. ART-8 Zircon Fission Track Individual Ages^a

Zircon Number	N s	N i	N g	Rho s	Rho i	Rho s / Rho i	U (ppm)	Age (Ma)	Age error (\pm 1 S.E.)	50% Age	" +95% "	" -95% "
1	145	15	6	3.776E+07	3.906E+06	9.6667	345.3	319.10	87.20	327.61	245.72	138.51
2	462	43	25	2.888E+07	2.688E+06	10.7442	237.5	353.71	57.62	356.90	133.28	96.54
3	285	32	16	2.783E+07	3.125E+06	8.9063	276.2	294.57	55.79	298.27	135.85	92.85
4	201	21	10	3.141E+07	3.281E+06	9.5714	290.0	316.04	73.24	322.03	191.74	119.03
5	314	33	12	4.089E+07	4.297E+06	9.5152	379.8	314.22	58.45	318.00	141.29	97.26
6	316	32	18	2.743E+07	2.778E+06	9.8750	245.5	325.81	61.41	329.82	148.97	101.96
7	275	26	12	3.581E+07	3.385E+06	10.5769	299.2	348.35	72.41	353.58	181.37	118.84
Totals/Averages	1998	202	99	3.153E+07	3.188E+06	9.8911	281.8	326.33	26.44	326.96	50.55	43.77

^aAnalytical notes: Position # 50, area of graticule square is 6.400E-07, zeta factor \pm error is 121.1 \pm 3.5, Rho d (% relative error) is 5.589E+05 and 1.67, N_d is 3577, glass (U ppm) is 49.4, irradiation is UA-Z2, and analyst was Dr. Stuart N. Thomson.

Table F5. ART-9 Zircon Fission Track Individual Ages^a

Zircon Number	N s	N i	N g	Rho s	Rho i	Rho s / Rho i	U (ppm)	Age (Ma)	Age error (± 1 S.E.)	50% Age	"+95%"	"-95%"
1	140	14	12	1.823E+07	1.823E+06	10.0000	161.6	328.91	92.85	338.25	265.75	146.60
2	81	9	8	1.582E+07	1.758E+06	9.0000	155.8	296.76	104.74	310.30	343.39	159.75
3	242	24	32	1.182E+07	1.172E+06	10.0833	103.9	331.58	71.82	337.02	182.89	117.49
4	192	17	20	1.500E+07	1.328E+06	11.2941	117.7	370.27	94.51	378.71	256.76	150.91
5	62	4	6	1.615E+07	1.042E+06	15.5000	92.3	502.90	259.98	551.57	1174.98	360.14
6	137	12	9	2.378E+07	2.083E+06	11.4167	184.7	374.18	113.34	386.32	335.58	176.23
7	172	15	16	1.680E+07	1.465E+06	11.4667	129.8	375.77	101.94	385.47	284.87	161.27
8	171	19	16	1.670E+07	1.855E+06	9.0000	164.5	296.76	72.45	303.07	194.10	117.16
9	141	12	12	1.836E+07	1.563E+06	11.7500	138.5	384.78	116.42	397.20	344.13	180.89
10	327	7	20	2.555E+07	5.469E+05	46.7143	48.5	1410.21	540.74	1475.33	1606.76	760.05
11	71	7	12	9.245E+06	9.115E+05	10.1429	80.8	333.49	132.58	352.76	473.95	196.89
12	121	11	10	1.891E+07	1.719E+06	11.0000	152.4	360.90	114.29	373.78	347.65	176.58
13	98	10	9	1.701E+07	1.736E+06	9.8000	153.9	322.49	107.60	335.47	339.14	165.33
14	165	16	12	2.148E+07	2.083E+06	10.3125	184.7	338.92	89.46	347.28	247.53	142.55
15	181	8	16	1.768E+07	7.813E+05	22.6250	69.3	721.54	261.79	753.52	830.31	384.96
16	345	8	25	2.156E+07	5.000E+05	43.1250	44.3	1312.15	471.30	1365.52	1363.59	673.69
17	209	20	16	2.041E+07	1.953E+06	10.4500	173.1	343.32	81.17	350.05	213.81	131.25
Totals/Averages	2855	213	251	1.777E+07	1.326E+06	13.4038	117.5	437.14	34.31	437.90	64.35	56.04

^aAnalytical notes: Position # 51, area of graticule square is 6.400E-07, zeta factor±error is 121.1±3.5, Rho d (% relative error) is 5.573E+05 and 1.67, N_d is 3567, glass (U ppm) is 49.4, irradiation is UA-Z2, and analyst was Dr. Stuart N. Thomson.

Table F6. ART-12 Zircon Fission Track Individual Ages^a

Zircon Number	N s	N i	N g	Rho s	Rho i	Rho s / Rho i	U (ppm)	Age (Ma)	Age error (\pm 1 S.E.)	50% Age	"+95%"	"-95%"
1	138	11	6	3.594E+07	2.865E+06	12.5455	254.6	408.95	128.85	423.22	388.91	198.44
2	268	29	12	3.490E+07	3.776E+06	9.2414	335.6	303.74	60.24	307.92	148.89	99.72
3	100	8	6	2.604E+07	2.083E+06	12.5000	185.2	407.51	150.35	427.26	503.38	225.01
4	130	11	9	2.257E+07	1.910E+06	11.8182	169.7	385.94	121.87	399.54	369.20	187.97
5	127	15	8	2.480E+07	2.930E+06	8.4667	260.4	278.82	76.69	286.45	217.42	122.18
6	140	15	6	3.646E+07	3.906E+06	9.3333	347.2	306.69	83.95	314.92	236.98	133.45
Totals/Averages	903	89	47	3.002E+07	2.959E+06	10.1461	263.0	332.72	38.60	334.18	81.58	65.45

^aAnalytical notes: Position # 52, area of graticule square is 6.400E-07, zeta factor \pm error is 121.1 \pm 3.5, Rho d (% relative error) is 5.558E+05 and 1.68, N_d is 3557, glass (U ppm) is 49.4, irradiation is UA-Z2, and analyst was Dr. Stuart N. Thomson.

Table F7. ART-16 Zircon Fission Track Individual Ages^a

Zircon Number	N s	N i	N g	Rho s	Rho i	Rho s / Rho i	U (ppm)	Age (Ma)	Age error (± 1 S.E.)	50% Age	" +95% "	" -95% "
1	171	15	16	1.670E+07	1.465E+06	11.4000	130.5	371.69	100.86	381.30	282.01	159.59
2	214	18	14	2.388E+07	2.009E+06	11.8889	179.0	387.16	95.89	395.41	256.68	153.53
3	145	13	9	2.517E+07	2.257E+06	11.1538	201.1	363.89	106.05	374.81	307.76	166.07
4	75	9	6	1.953E+07	2.344E+06	8.3333	208.9	273.79	97.02	286.49	319.44	148.25
5	158	16	10	2.469E+07	2.500E+06	9.8750	222.8	323.19	85.48	331.23	237.03	136.35
6	337	15	18	2.925E+07	1.302E+06	22.4667	116.0	713.11	189.68	729.73	506.20	294.12
7	203	20	12	2.643E+07	2.604E+06	10.1500	232.1	331.97	78.59	338.51	207.31	127.17
8	202	17	12	2.630E+07	2.214E+06	11.8824	197.3	386.96	98.57	395.70	267.18	157.21
9	416	31	40	1.625E+07	1.211E+06	13.4194	107.9	435.35	82.35	440.60	198.16	135.48
10	139	13	8	2.715E+07	2.539E+06	10.6923	226.3	349.23	101.96	359.80	296.55	159.82
11	325	31	16	3.174E+07	3.027E+06	10.4839	269.8	342.60	65.41	346.91	159.14	108.31
12	190	20	18	1.649E+07	1.736E+06	9.5000	154.7	311.21	73.90	317.43	195.49	119.76
13	181	18	9	3.142E+07	3.125E+06	10.0556	278.5	328.96	82.04	336.18	221.36	131.88
14	188	9	18	1.632E+07	7.813E+05	20.8889	69.6	665.52	228.18	691.94	702.77	340.19
15	341	22	25	2.131E+07	1.375E+06	15.5000	122.5	500.30	111.31	508.63	282.04	179.17
16	138	8	20	1.078E+07	6.250E+05	17.2500	55.7	554.42	202.47	579.95	660.46	300.36
17	216	19	10	3.375E+07	2.969E+06	11.3684	264.6	370.69	89.57	378.23	237.54	144.07
18	243	26	20	1.898E+07	2.031E+06	9.3462	181.0	306.29	64.02	311.00	161.21	105.38
Totals/Averages	3882	320	281	2.159E+07	1.779E+06	12.1313	158.6	394.82	26.48	395.28	46.95	41.94

^aAnalytical notes: Position # 53, area of graticule square is 6.400E-07, zeta factor±error is 121.1±3.5, Rho d (% relative error) is 5.543E+05 and 1.68, N_d is 3548, glass (U ppm) is 49.4, irradiation is UA-Z2, and analyst was Dr. Stuart N. Thomson.

Table F8. ART-18 Zircon Fission Track Individual Ages^a

Zircon Number	N s	N i	N g	Rho s	Rho i	Rho s / Rho i	U (ppm)	Age (Ma)	Age error (± 1 S.E.)	50% Age	" +95% "	" -95% "
1	122	14	15	1.271E+07	1.458E+06	8.7143	130.3	285.28	81.06	293.61	233.58	128.41
2	130	16	16	1.270E+07	1.563E+06	8.1250	139.6	266.38	71.13	273.27	198.93	113.97
3	173	19	10	2.703E+07	2.969E+06	9.1053	265.3	297.79	72.66	304.10	194.63	117.48
4	217	20	16	2.119E+07	1.953E+06	10.8500	174.5	353.31	83.40	360.19	219.38	134.76
5	307	31	24	1.999E+07	2.018E+06	9.9032	180.4	323.24	61.87	327.35	150.88	102.58
6	105	14	10	1.641E+07	2.188E+06	7.5000	195.5	246.28	70.55	253.71	204.57	112.12
7	252	27	20	1.969E+07	2.109E+06	9.3333	188.5	305.07	62.61	309.58	156.63	103.27
8	113	15	16	1.104E+07	1.465E+06	7.5333	130.9	247.35	68.47	254.30	195.08	109.37
9	203	19	20	1.586E+07	1.484E+06	10.6842	132.6	348.05	84.31	355.21	224.28	135.83
10	127	13	12	1.654E+07	1.693E+06	9.7692	151.3	318.97	93.49	328.79	273.21	146.87
11	235	21	18	2.040E+07	1.823E+06	11.1905	162.9	364.09	83.81	370.80	218.01	135.73
12	303	31	28	1.691E+07	1.730E+06	9.7742	154.6	319.13	61.12	323.20	149.12	101.37
13	165	18	15	1.719E+07	1.875E+06	9.1667	167.6	299.75	75.08	306.46	203.41	120.95
14	259	26	30	1.349E+07	1.354E+06	9.9615	121.0	325.10	67.76	330.03	170.20	111.37
15	236	28	25	1.475E+07	1.750E+06	8.4286	156.4	276.12	55.96	280.14	139.63	92.67
16	242	26	24	1.576E+07	1.693E+06	9.3077	151.3	304.25	63.61	308.93	160.21	104.72
17	120	15	12	1.563E+07	1.953E+06	8.0000	174.5	262.36	72.38	269.64	205.73	115.47
18	179	21	20	1.398E+07	1.641E+06	8.5238	146.6	279.18	65.07	284.60	171.19	106.03
19	195	20	24	1.270E+07	1.302E+06	9.7500	116.4	318.36	75.50	324.69	199.54	122.30
20	244	24	24	1.589E+07	1.563E+06	10.1667	139.6	331.62	71.80	337.06	182.84	117.46
Totals/Averages	3927	418	379	1.619E+07	1.723E+06	9.3947	154.0	307.03	18.84	307.32	32.23	29.19

^aAnalytical notes: Position # 54, area of graticule square is 6.400E-07, zeta factor \pm error is 121.1 \pm 3.5, Rho d (% relative error) is 5.528E+05 and 1.68, N_d is 3538, glass (U ppm) is 49.4, irradiation is UA-Z2, and analyst was Dr. Stuart N. Thomson.

Table F9. Chung Zircon Fission Track Individual Ages^a

Zircon Number	N s	N i	N g	Rho s	Rho i	Rho s / Rho i	U (ppm)	Age (Ma)	Age error (± 1 S.E.)	50% Age	"+95%"	"-95%"
1	82	10	6	2.135E+07	2.604E+06	8.2000	227.7	274.55	92.42	286.01	293.81	142.57
2	78	9	8	1.523E+07	1.758E+06	8.6667	153.7	289.83	102.49	303.15	336.46	156.43
3	93	12	6	2.422E+07	3.125E+06	7.7500	273.3	259.78	80.15	268.89	241.81	125.73
4	140	13	12	1.823E+07	1.693E+06	10.7692	148.0	358.22	104.55	369.04	303.69	163.81
5	139	14	8	2.715E+07	2.734E+06	9.9286	239.1	330.96	93.45	340.37	267.42	147.56
6	152	14	9	2.639E+07	2.431E+06	10.8571	212.5	361.06	101.56	371.16	289.30	160.02
Totals/Averages	3927	418	379	1.619E+07	1.723E+06	9.3947	154.0	307.03	18.84	307.32	32.23	29.19

^aAnalytical notes: Position # 46, area of graticule square is 6.400E-07, zeta factor \pm error is 121.1 \pm 3.5, Rho d (% relative error) is 5.649E+05 and 1.66, N_d is 3615, glass (U ppm) is 49.4, irradiation is UA-Z2, and analyst was Dr. Stuart N. Thomson.

Table F10. Mt. Blakely Zircon Fission Track Individual Ages^a

Zircon Number	N _s	N _i	N _g	Rho _s	Rho _i	Rho _s / Rho _i	U (ppm)	Age (Ma)	Age error (± 1 S.E.)	50% Age	"+95%"	"-95%"
1	152	18	20	1.188E+07	1.406E+06	8.4444	122.6	283.29	71.24	289.74	193.51	114.95
2	163	18	12	2.122E+07	2.344E+06	9.0556	204.4	303.32	76.01	310.12	205.86	122.45
3	309	30	20	2.414E+07	2.344E+06	10.3000	204.4	343.91	66.76	348.39	163.29	110.38
4	127	13	15	1.323E+07	1.354E+06	9.7692	118.1	326.62	95.73	336.67	279.45	150.34
5	104	11	10	1.625E+07	1.719E+06	9.4545	149.9	316.36	100.86	327.98	309.08	156.35
6	162	21	12	2.109E+07	2.734E+06	7.7143	238.5	259.28	60.75	264.43	160.31	99.18
7	108	10	10	1.688E+07	1.563E+06	10.8000	136.3	360.14	119.65	374.36	374.71	183.38
8	118	17	8	2.305E+07	3.320E+06	6.9412	289.6	233.76	61.14	239.66	169.46	98.68
9	362	24	16	3.535E+07	2.344E+06	15.0833	204.4	497.58	106.19	505.20	264.89	171.82
10	82	10	12	1.068E+07	1.302E+06	8.2000	113.6	275.26	92.66	286.75	294.54	142.94
11	63	8	6	1.641E+07	2.083E+06	7.8750	181.7	264.57	99.69	278.60	343.15	150.85
12	157	13	8	3.066E+07	2.539E+06	12.0769	221.5	401.42	116.62	413.30	336.56	182.20
13	158	18	8	3.086E+07	3.516E+06	8.7778	306.6	294.22	73.85	300.86	200.26	119.04
14	645	16	50	2.016E+07	5.000E+05	40.3125	43.6	1252.57	319.74	1277.85	786.69	483.98
15	80	9	6	2.083E+07	2.344E+06	8.8889	204.4	297.86	105.19	311.48	344.83	160.46
16	246	26	16	2.402E+07	2.539E+06	9.4615	221.5	316.59	66.13	321.43	166.32	108.79
17	155	16	9	2.691E+07	2.778E+06	9.6875	242.3	323.96	85.75	332.04	237.79	136.81
Totals/Averages	3191	278	238	2.095E+07	1.825E+06	11.4784	159.2	382.11	27.08	382.63	49.18	43.56

^aAnalytical notes: Position # 45, area of graticule square is 6.400E-07, zeta factor±error is 121.1±3.5, Rho_d (% relative error) is 5.664E+05 and 1.66, N_d is 3625, glass (U ppm) is 49.4, irradiation is UA-Z2, and analyst was Dr. Stuart N. Thomson.

Table F11. Lake Pineda Individual Fission Track Ages^a

Zircon number	Natural tracks	Area (cm ²)	U/Ca ratio of the counted area	1 sigma	ZFT age (Ma)	1 sigma (Ma)
1	101	1.02E-05	9.35E-02	1.37E-03	432.54	45.59
2	38	3.84E-06	1.21E-01	1.92E-03	338.04	56.13
3	83	3.84E-06	1.72E-01	2.77E-03	511.56	59.00
4	36	2.56E-06	1.82E-01	3.27E-03	319.69	54.53
5	52	7.68E-06	7.71E-02	1.22E-03	362.07	51.81
6	47	3.84E-06	1.32E-01	2.24E-03	381.51	57.30
7	68	7.68E-06	9.18E-02	1.46E-03	396.71	50.11
8	35	3.84E-06	1.02E-01	1.58E-03	369.75	63.84
9	29	3.84E-06	6.49E-02	1.04E-03	475.18	89.83
10	58	2.56E-06	1.95E-01	3.16E-03	475.53	64.68
11	58	5.12E-06	9.97E-02	1.60E-03	464.86	63.22
12	42	3.84E-06	9.55E-02	1.54E-03	468.24	74.13
13	66	5.12E-06	9.35E-02	1.59E-03	559.45	71.72
14	50	2.56E-06	1.37E-01	2.09E-03	578.02	84.22
15	35	3.84E-06	1.00E-01	1.52E-03	374.99	64.73
16	33	5.76E-06	5.65E-02	8.65E-04	416.22	73.91
17	76	5.76E-06	1.17E-01	1.81E-03	462.80	55.53
18	44	3.84E-06	4.31E-02	6.93E-04	1038.87	160.88
19	48	5.12E-06	1.01E-01	1.67E-03	381.84	56.77
20	61	5.76E-06	1.36E-01	2.32E-03	322.98	42.95

^a Apatite to Zircon, Inc. reference number is 963-1.

Table F11. Lake Ouachita 41 Individual Fission Track Ages^a

Grain Number	Natural Tracks	Area (cm ²)	²³⁸ U/ ²⁹ Si (dmnls)	1 sigma (dmnls)	²⁹ Si back:sig	²³⁸ U back:sig	²³² Th back:sig	¹⁴⁷ Sm back:sig	FT Age (Ma)	1 sigma (Ma)	Uranium (ppm)	Thorium (ppm)	Samarium (ppm)	Pit Depth (microns)
1	94	5.12E-06	9.83E-02	1.97E-03	5.69E-02	4.23E-02	3.97E-02	4.28E-02	640.56	70.26	151.77	139.30	9.05	28.09
2	101	3.84E-06	1.49E-01	2.69E-03	1.17E-01	1.05E-01	8.55E-02	1.21E-01	607.07	64.3	230.03	103.48	9.00	28.56
3	51	2.56E-06	1.30E-01	2.89E-03	1.39E-01	1.48E-01	1.12E-01	1.09E-01	531.00	77.12	200.40	96.41	7.21	29.08
4	82	2.56E-06	1.70E-01	3.75E-03	4.74E-02	3.55E-02	3.03E-02	6.63E-02	645.38	75.46	262.72	137.70	6.28	30.37
5	44	5.12E-06	3.75E-02	8.31E-04	5.09E-02	4.46E-02	7.33E-02	9.80E-02	776.70	120.85	57.96	23.36	3.48	29.59
6	42	2.56E-06	9.68E-02	2.03E-03	4.80E-02	3.26E-02	3.51E-02	5.12E-02	584.09	92.8	149.40	102.66	13.47	28.57
7	59	2.56E-06	1.18E-01	2.71E-03	4.30E-02	2.09E-02	1.73E-02	2.76E-02	669.52	90.99	181.87	200.06	16.38	31.80
8	48	2.56E-06	1.30E-01	2.76E-03	4.95E-02	3.29E-02	3.39E-02	6.66E-02	501.50	74.86	200.17	82.69	7.27	29.53
9	104	2.56E-06	1.87E-01	4.21E-03	4.57E-02	2.32E-02	2.26E-02	3.44E-02	737.76	77.77	289.37	102.35	4.74	30.09
10	29	1.92E-06	9.10E-02	1.30E-03	1.12E-01	1.65E-02	2.63E-02	4.97E-02	572.10	108.06	140.56	112.94	34.70	11.57
11	87	5.76E-06	9.16E-02	1.88E-03	1.03E-01	3.29E-02	3.12E-02	1.69E-01	568.96	64.64	141.37	61.53	2.40	27.57
12	65	3.84E-06	8.42E-02	1.16E-03	1.30E-01	2.73E-02	3.30E-02	4.94E-02	687.16	88.44	129.96	68.90	8.26	10.55
13	126	6.40E-06	7.54E-02	1.10E-03	1.18E-01	3.16E-02	4.64E-02	1.07E-01	878.67	84.01	116.43	79.88	11.88	11.09
14	70	1.02E-05	6.36E-02	8.46E-04	1.22E-01	2.19E-02	2.83E-02	2.11E-01	376.13	46.76	98.26	36.71	2.32	11.38
15	91	3.84E-06	1.31E-01	1.86E-03	1.30E-01	3.78E-02	3.92E-02	1.37E-01	623.51	68.82	201.54	100.60	5.38	11.54
16	66	5.76E-06	9.81E-02	1.38E-03	1.10E-01	1.70E-02	1.62E-02	3.61E-02	408.08	52.17	151.43	135.66	28.90	11.17
17	61	5.76E-06	7.09E-02	9.79E-04	1.10E-01	1.63E-02	2.59E-02	9.43E-02	517.68	68.63	109.38	70.29	9.66	11.44
18	48	3.84E-06	1.07E-01	1.44E-03	1.19E-01	4.60E-02	4.08E-02	5.94E-02	409.94	60.81	164.42	171.19	14.65	11.54
19	78	5.76E-06	7.82E-02	1.09E-03	1.22E-01	2.20E-02	1.85E-02	7.66E-02	595.80	70.51	120.78	90.24	8.91	10.58
20	120	5.76E-06	1.01E-01	1.23E-03	1.63E-01	7.94E-02	5.27E-02	5.56E-02	702.46	68.37	156.29	163.02	7.16	8.20

^a Apatite to Zircon, Inc. reference number is 916-01.

APPENDIX G

BINOMFIT / ISOPLLOT REPORTS

September 22 2011 16:42

BinomFit for Windows ver.1.2

Page 1

Datafile: D:\Users\Working account\Desktop\ART-2.ftz

Title: ART-2, Irradiation US-Z2, Analyst SNT

NEW PARAMETERS - ZETA METHOD

EFFECTIVE TRACK DENSITY FOR FLUENCE MONITOR (tracks/cm²): 5.63E+05
 RELATIVE ERROR (%): 1.67
 EFFECTIVE URANIUM CONTENT OF MONITOR (ppm): 49.40
 ZETA FACTOR AND STANDARD ERROR (yr cm²): 121.10 3.50
 SIZE OF COUNTER SQUARE (cm²): 6.40E-07

GRAIN AGES IN ORIGINAL ORDER

Grain no.	RhoS (cm ⁻²)	(Ns)	RhoI (cm ⁻²)	(Ni)	Squares	U+/-2s	Grain Age (Ma)		
							Age	--95% CI--	
1	1.08E+07	(83)	1.56E+06	(12)	12	137 78	229.1	126.8	458.8
2	1.42E+07	(91)	1.72E+06	(11)	10	151 89	272.8	148.6	560.7
3	2.40E+07	(92)	2.60E+06	(10)	6	228 141	302.2	161.0	643.7
4	2.66E+07	(102)	3.39E+06	(13)	6	297 162	259.5	147.9	500.5
5	2.15E+07	(110)	2.34E+06	(12)	8	206 116	301.8	169.6	595.9
6	2.22E+07	(128)	2.43E+06	(14)	9	213 112	301.5	176.6	562.1
7	2.02E+07	(129)	2.34E+06	(15)	10	206 105	284.2	169.0	518.6
8	2.02E+07	(129)	2.50E+06	(16)	10	219 108	267.0	160.9	478.0
9	2.31E+07	(133)	3.13E+06	(18)	9	274 128	245.4	151.5	424.6
10	3.49E+07	(134)	3.13E+06	(12)	6	274 155	365.7	207.4	715.3
11	2.14E+07	(137)	2.19E+06	(14)	10	192 101	322.2	189.3	598.8
12	1.45E+07	(148)	1.66E+06	(17)	16	146 70	288.0	176.7	504.0
13	1.45E+07	(167)	1.39E+06	(16)	18	122 60	343.5	209.2	608.5
14	1.44E+07	(184)	1.41E+06	(18)	20	123 57	336.9	210.8	575.8
15	3.65E+07	(210)	3.47E+06	(20)	9	304 135	346.1	221.9	573.0
16	3.05E+07	(234)	2.99E+06	(23)	12	263 109	336.0	221.6	536.2
17	1.61E+07	(258)	1.56E+06	(25)	25	137 54	340.8	228.7	532.4
18	2.34E+07	(315)	2.38E+06	(32)	21	209 74	325.9	228.6	481.8
19	2.85E+07	(365)	2.97E+06	(38)	20	260 84	318.5	229.7	455.0
20	2.49E+07	(399)	2.63E+06	(42)	25	230 71	315.2	230.8	442.0
POOLED	2.12E+07	(3548)	2.25E+06	(378)	262	198 21	312.1	276.3	352.4

CHI² PROBABILITY (%):100.0

POOLED AGE W/ 68% CONF. INTERVAL (Ma): 312.1, 293.3 -- 332.1 (-18.8 +20.0)
 95% CONF. INTERVAL (Ma): 276.3 -- 352.4 (-35.8 +40.3)

CENTRAL AGE W/ 68% CONF. INTERVAL (Ma): 312.5, 293.7 -- 332.5 (-18.8 +20.0)
 95% CONF. INTERVAL (Ma): 276.7 -- 352.9 (-35.8 +40.4)
 AGE DISPERSION (%): 0.0

September 22 2011 16:42

BinomFit for Windows ver.1.2

Page 2

Datafile: D:\Users\Working account\Desktop\ART-2.ftz

Title: ART-2, Irradiation US-Z2, Analyst SNT

FIT OPTION: Best-fit peaks using the binomial model of Galbraith and Green

INITIAL GUESS FOR MODEL PARAMETERS (number of peaks to fit = 1)

Peak #.	Peak Age	Theta	Fraction(%)	Count
1.	312.10	0.904	81.1	16.22

Total range for grain ages: 223.9 to 357.0 Ma
 Number of active grains (Num. used for fit): 20
 Number of removed grains: 0
 Degrees of freedom for fit: 19
 Average of the SE(Z)'s for the grains: 0.26
 Estimated width of peaks in PD plot in Z units: 0.3

PARAMETERS FOR BEST-FIT PEAKS

- * Standard error for peak age includes group error
- * Peak width is for PD plot assuming a kernel factor = 0.60

#.	Peak Age(Ma)	68%CI	95%CI	W(Z)	Frac(%)	SE,%	Count
1.	312.5	-18.8 ...+20.0	-35.8 ...+40.4	0.28	100.0	0.0	20.0

Log-likelihood for best fit: -47.912
 Chi-squared value for best fit: 4.262
 Reduced chi-squared value: 0.224
 Probability for F test: 0%
 Condition number for COVAR matrix: 1.00
 Number of iterations: 5

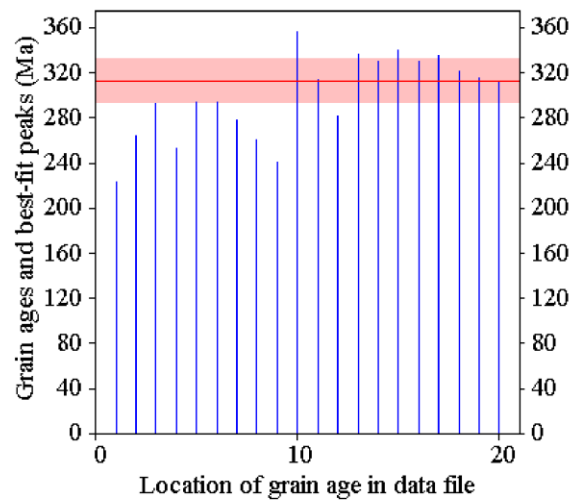
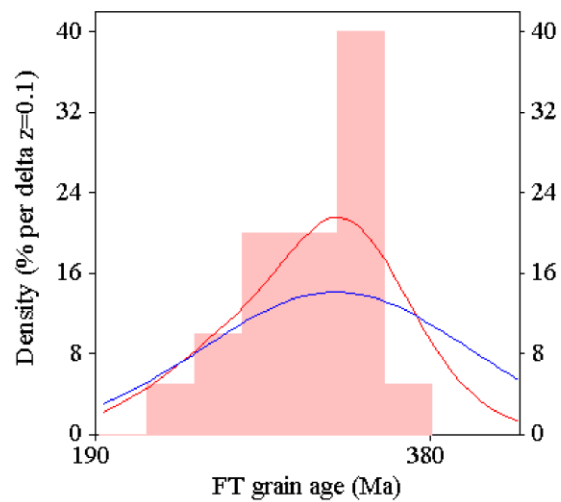
September 22 2011 16:42

BinomFit for Windows ver.1.2

Page 3

Datafile: D:\Users\Working account\Desktop\ART-2.ftz

Title: ART-2, Irradiation US-Z2, Analyst SNT

Plot of Grain Ages (Unsorted)**Probability-Density Plot with Best-Fit Peaks**

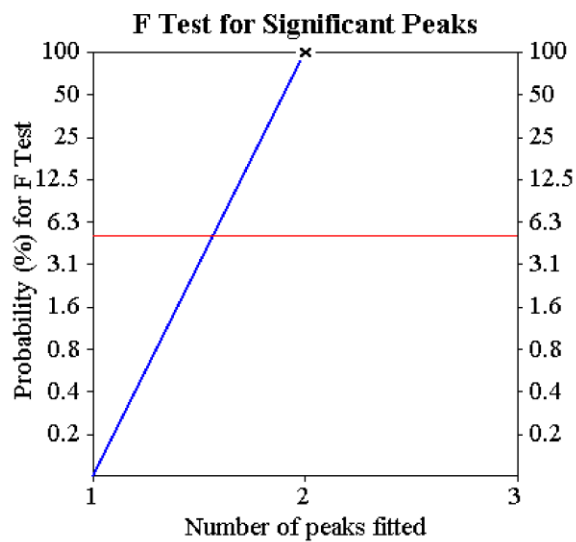
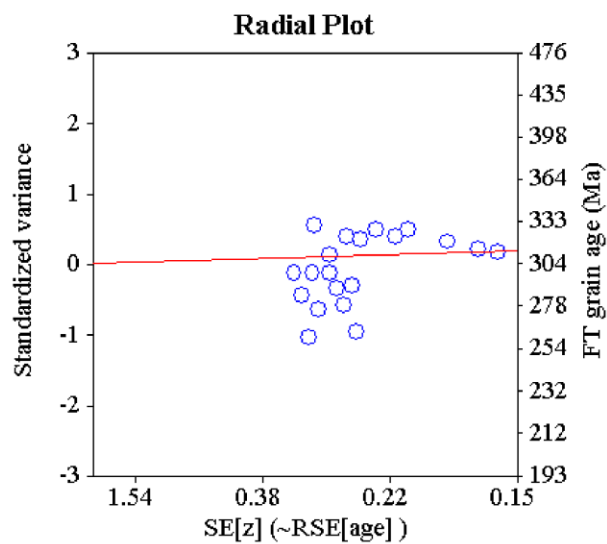
September 22 2011 16:42

BinomFit for Windows ver.1.2

Page 4

Datafile: D:\Users\Working account\Desktop\ART-2.ftz

Title: ART-2, Irradiation US-Z2, Analyst SNT



September 22 2011 18:10

BinomFit for Windows ver.1.2

Page 1

Datafile: F:\Ouachitas\Zircon Fission Track Data\BINOMFIT_results\ART-3_BINOMFIT\ART-3.ftz

Title: ART-3, Irradiation UA-Z2, Analyst SNT

NEW PARAMETERS - ZETA METHOD

EFFECTIVE TRACK DENSITY FOR FLUENCE MONITOR (tracks/cm²): 5.62E+05
 RELATIVE ERROR (%): 1.67
 EFFECTIVE URANIUM CONTENT OF MONITOR (ppm): 49.40
 ZETA FACTOR AND STANDARD ERROR (yr cm²): 121.10 3.50
 SIZE OF COUNTER SQUARE (cm²): 6.40E-07

GRAIN AGES IN ORIGINAL ORDER

Grain no.	RhoS (cm ⁻²)	(Ns)	RhoI (cm ⁻²)	(Ni)	Squares	U+/-2s	Grain Age (Ma)		
							Age	--95% CI--	
1	1.72E+07	(66)	1.82E+06	(7)	6	160 117	306.9	145.5	780.4
2	1.50E+07	(77)	1.37E+06	(7)	8	120 88	356.5	170.8	897.2
3	1.56E+07	(80)	1.37E+06	(7)	8	120 88	370.0	177.6	928.8
4	2.08E+07	(120)	2.26E+06	(13)	9	198 108	303.4	174.3	580.7
5	1.17E+07	(120)	9.77E+05	(10)	16	86 53	390.2	210.8	819.6
6	2.10E+07	(121)	2.08E+06	(12)	9	183 104	330.3	186.5	649.2
7	1.13E+07	(144)	1.17E+06	(15)	20	103 52	315.6	188.6	573.2
8	2.04E+07	(157)	2.21E+06	(17)	12	195 93	304.3	187.1	531.2
POOLED	1.57E+07	(885)	1.56E+06	(88)	88	137 30	331.6	265.3	413.8

CHI² PROBABILITY (%): 99.8

POOLED AGE W/ 68% CONF. INTERVAL(Ma): 331.6, 296.0 -- 371.3 (-35.6 +39.8)
 95% CONF. INTERVAL(Ma): 265.3 -- 413.8 (-66.3 +82.3)

CENTRAL AGE W/ 68% CONF. INTERVAL(Ma): 333.4, 297.5 -- 373.5 (-35.9 +40.1)
 95% CONF. INTERVAL(Ma): 266.6 -- 416.3 (-66.8 +82.9)
 AGE DISPERSION (%): 0.0

September 22 2011 18:10

BinomFit for Windows ver.1.2

Page 2

Datafile: F:\Ouachitas\Zircon Fission Track Data\BINOMFIT_results\ART-3_BINOMFIT\ART-3.ftz

Title: ART-3, Irradiation UA-Z2, Analyst SNT

FIT OPTION: Best-fit peaks using the binomial model of Galbraith and Green

INITIAL GUESS FOR MODEL PARAMETERS (number of peaks to fit = 1)

Peak #.	Peak Age	Theta	Fraction(%)	Count
1.	331.60	0.909	70.0	5.60

Total range for grain ages: 294.8 to 379.1 Ma
 Number of active grains (Num. used for fit): 8
 Number of removed grains: 0
 Degrees of freedom for fit: 7
 Average of the SE(Z)'s for the grains: 0.33
 Estimated width of peaks in PD plot in Z units: 0.38

PARAMETERS FOR BEST-FIT PEAKS

- * Standard error for peak age includes group error
- * Peak width is for PD plot assuming a kernel factor = 0.60

#.	Peak Age(Ma)	68%CI	95%CI	W(Z)	Frac(%)	SE,%	Count
1.	333.4	-35.9 ...+40.1	-66.8 ...+82.9	0.37	100.0	0.0	8.0

Log-likelihood for best fit: -16.716
 Chi-squared value for best fit: 0.699
 Reduced chi-squared value: 0.100
 Probability for F test: 0%
 Condition number for COVAR matrix: 1.00
 Number of iterations: 5

September 22 2011 18:10

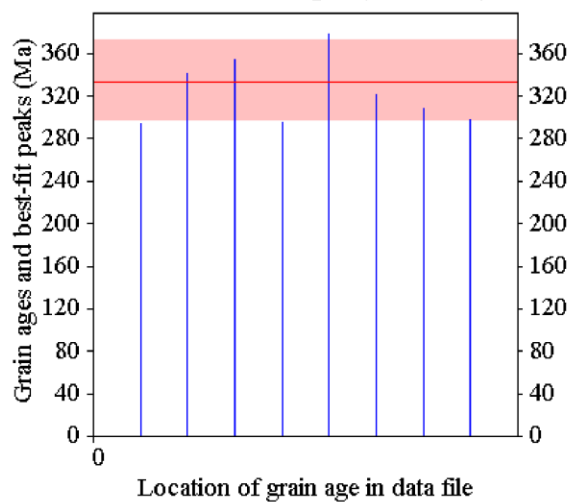
BinomFit for Windows ver.1.2

Page 3

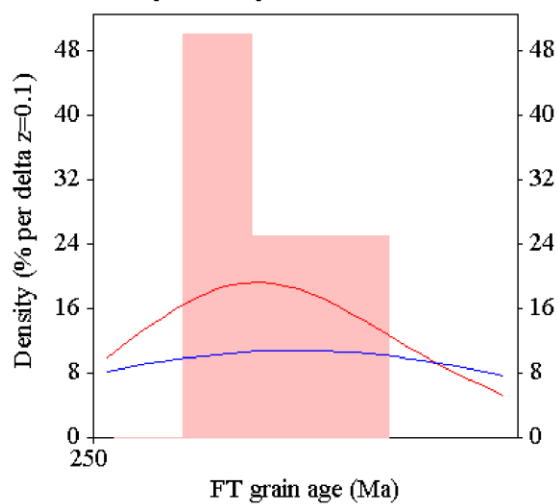
Datafile: F:\Ouachitas\Zircon Fission Track Data\BINOMFIT_results\ART-3_BINOMFIT\ART-3.ftz

Title: ART-3, Irradiation UA-Z2, Analyst SNT

Plot of Grain Ages (Unsorted)



Probability-Density Plot with Best-Fit Peaks



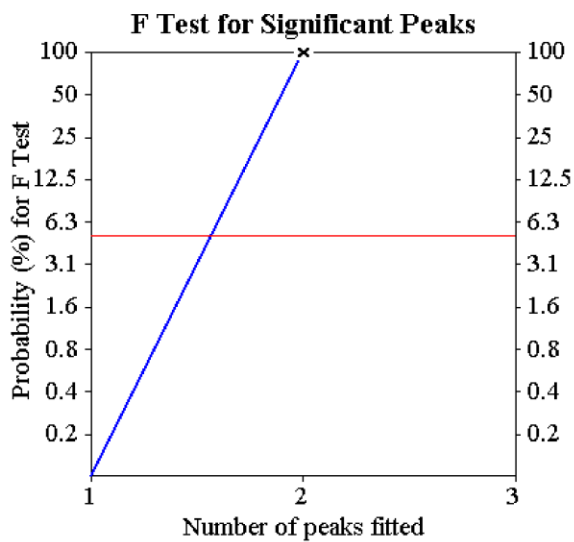
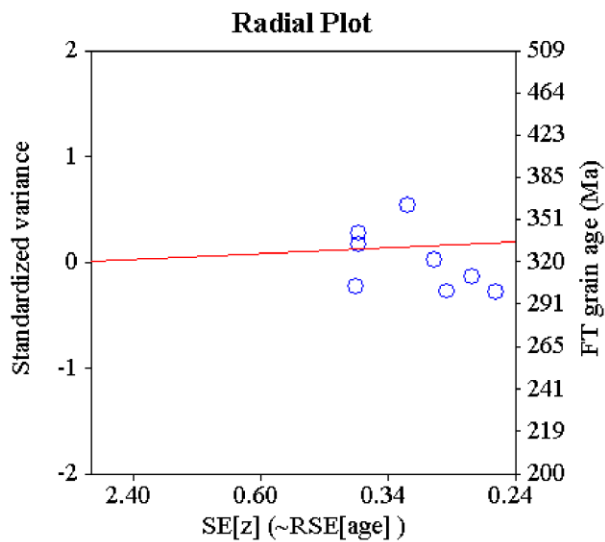
September 22 2011 18:10

BinomFit for Windows ver.1.2

Page 4

Datafile: F:\Ouchitas\Zircon Fission Track Data\BINOMFIT_results\ART-3_BINOMFIT\ART-3.ftz

Title: ART-3, Irradiation UA-Z2, Analyst SNT



September 22 2011 18:37

BinomFit for Windows ver.1.2

Page 1

Datafile: F:\Ouchitas\Zircon Fission Track Data\BINOMFIT_results\ART-4_BINOMFIT\ART-4.ftz

Title: ART-4, Irradiation UA-Z2, Analyst SNT

NEW PARAMETERS - ZETA METHOD

EFFECTIVE TRACK DENSITY FOR FLUENCE MONITOR (tracks/cm²): 5.60E+05
 RELATIVE ERROR (%): 1.67
 EFFECTIVE URANIUM CONTENT OF MONITOR (ppm): 49.40
 ZETA FACTOR AND STANDARD ERROR (yr cm²): 121.10 3.50
 SIZE OF COUNTER SQUARE (cm²): 6.40E-07

GRAIN AGES IN ORIGINAL ORDER

Grain no.	RhoS (cm ⁻²)	(Ns)	RhoI (cm ⁻²)	(Ni)	Squares	U+/-2s	Grain Age (Ma)		
							Age	--95% CI--	
1	1.82E+07	(140)	2.08E+06	(16)	12	184 91	287.7	174.0	513.4
2	1.84E+07	(141)	1.95E+06	(15)	12	172 88	308.4	184.1	560.6
3	1.27E+07	(163)	1.25E+06	(16)	20	110 54	333.8	203.1	591.9
4	2.33E+07	(179)	2.21E+06	(17)	12	195 94	344.8	213.1	599.1
5	2.55E+07	(196)	2.60E+06	(20)	12	230 102	322.0	205.9	534.4
6	1.60E+07	(205)	1.88E+06	(24)	20	165 67	281.9	186.4	447.5
7	2.40E+07	(230)	2.50E+06	(24)	15	220 89	315.4	209.4	498.9
8	1.75E+07	(235)	1.64E+06	(22)	21	144 61	350.4	229.4	564.9
9	1.98E+07	(381)	8.33E+05	(16)	30	73 36	754.3	472.8	1291.4
10	2.72E+07	(435)	2.00E+06	(32)	25	176 62	443.5	313.6	650.1
11	1.73E+07	(444)	1.72E+06	(44)	40	152 46	332.6	245.6	462.0
POOLED	1.96E+07	(2749)	1.76E+06	(246)	219	155 20	367.7	319.1	423.6

CHI² PROBABILITY (%): 14.5

POOLED AGE W/ 68% CONF. INTERVAL(Ma): 367.7, 342.1 -- 395.3 (-25.7 +27.5)
 95% CONF. INTERVAL(Ma): 319.1 -- 423.6 (-48.7 +55.9)

CENTRAL AGE W/ 68% CONF. INTERVAL(Ma): 361.7, 332.0 -- 394.1 (-29.7 +32.3)
 95% CONF. INTERVAL(Ma): 305.7 -- 427.7 (-56.0 +66.0)
 AGE DISPERSION (%): 15.0

September 22 2011 18:37

BinomFit for Windows ver.1.2

Page 2

Datafile: F:\Ouachitas\Zircon Fission Track Data\BINOMFIT_results\ART-4_BINOMFIT\ART-4.ftz

Title: ART-4, Irradiation UA-Z2, Analyst SNT

FIT OPTION: Best-fit peaks using the binomial model of Galbraith and Green

INITIAL GUESS FOR MODEL PARAMETERS (number of peaks to fit = 2)

Peak #.	Peak Age	Theta	Fraction(%)	Count
1.	367.70	0.918	50.5	5.55
2.	739.50	0.958	9.0	0.99

Total range for grain ages: 278.5 to 740.4 Ma
 Number of active grains (Num. used for fit): 11
 Number of removed grains: 0
 Degrees of freedom for fit: 8
 Average of the SE(Z)'s for the grains: 0.23
 Estimated width of peaks in PD plot in Z units: 0.27

PARAMETERS FOR BEST-FIT PEAKS

* Standard error for peak age includes group error

* Peak width is for PD plot assuming a kernel factor = 0.60

#.	Peak Age(Ma)	68%CI	95%CI	W(Z)	Frac(%)	SE, %	Count
1.	340.8	-25.0 ...+26.9	-47.3 ...+54.7	0.25	91.0	8.8	10.0
2.	754.1	-172.8 ...+220.4	-302.6 ...+486.8	0.30	9.0	8.8	1.0

Log-likelihood for best fit: -31.488
 Chi-squared value for best fit: 7.801
 Reduced chi-squared value: 0.975
 Probability for F test: 2%
 Condition number for COVAR matrix: 14.88
 Number of iterations: 6

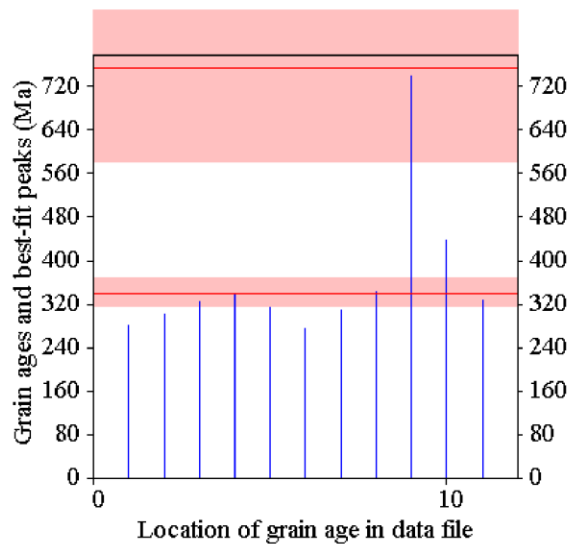
September 22 2011 18:37

BinomFit for Windows ver.1.2

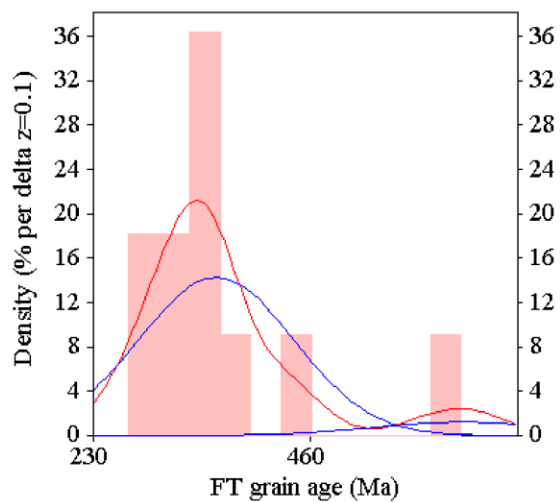
Page 3

Datafile: F:\Ouachitas\Zircon Fission Track Data\BINOMFIT_results\ART-4_BINOMFIT\ART-4.ftz

Title: ART-4, Irradiation UA-Z2, Analyst SNT



Probability-Density Plot with Best-Fit Peaks



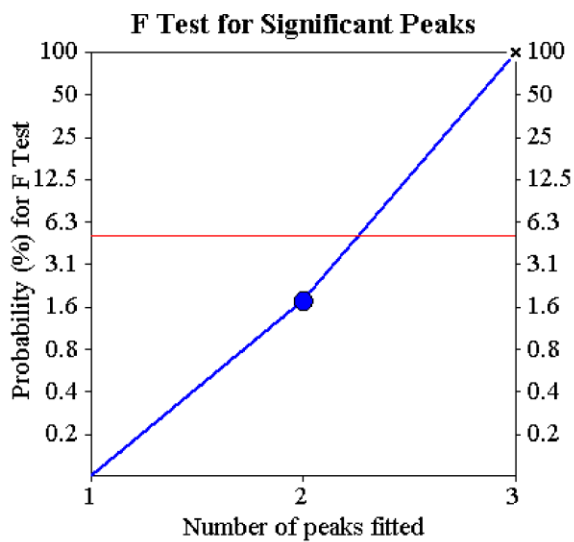
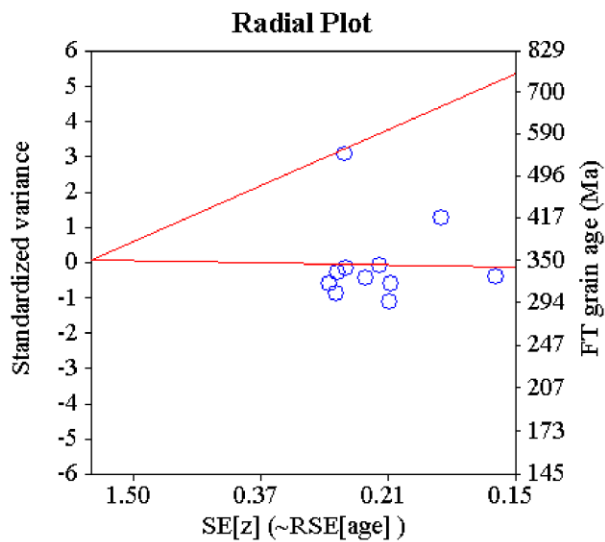
September 22 2011 18:37

BinomFit for Windows ver.1.2

Page 4

Datafile: F:\Ouchitas\Zircon Fission Track Data\BINOMFIT_results\ART-4_BINOMFIT\ART-4.ftz

Title: ART-4, Irradiation UA-Z2, Analyst SNT



September 22 2011 18:47

BinomFit for Windows ver.1.2

Page 1

Datafile: F:\Ouachitas\Zircon Fission Track Data\BINOMFIT_results\ART-8\ART-8.ftz

Title: ART-8, Irradiation UA-Z2, Analyst SNT

NEW PARAMETERS - ZETA METHOD

EFFECTIVE TRACK DENSITY FOR FLUENCE MONITOR (tracks/cm²): 5.59E+05
 RELATIVE ERROR (%): 1.67
 EFFECTIVE URANIUM CONTENT OF MONITOR (ppm): 49.40
 ZETA FACTOR AND STANDARD ERROR (yr cm²): 121.10 3.50
 SIZE OF COUNTER SQUARE (cm²): 6.40E-07

GRAIN AGES IN ORIGINAL ORDER

Grain no.	RhoS (cm ⁻²)	(Ns)	RhoI (cm ⁻²)	(Ni)	Squares	U+/-2s	Grain Age (Ma)		
							Age	--95% CI--	
1	3.78E+07	(145)	3.91E+06	(15)	6	345 176	316.1	188.9	574.0
2	3.14E+07	(201)	3.28E+06	(21)	10	290 125	313.9	202.7	514.4
3	3.58E+07	(275)	3.39E+06	(26)	12	299 117	346.5	234.4	535.7
4	2.78E+07	(285)	3.13E+06	(32)	16	276 97	293.3	205.1	434.8
5	4.09E+07	(314)	4.30E+06	(33)	12	380 132	312.9	220.4	460.0
6	2.74E+07	(316)	2.78E+06	(32)	18	246 87	324.4	227.5	479.5
7	2.89E+07	(462)	2.69E+06	(43)	25	238 72	352.6	259.9	491.1
POOLED	3.15E+07	(1998)	3.19E+06	(202)	99	282 41	325.5	278.8	379.9

CHI² PROBABILITY (%): 99.3

POOLED AGE W/ 68% CONF. INTERVAL (Ma): 325.5, 300.8 -- 352.3 (-24.7 +26.7)
 95% CONF. INTERVAL (Ma): 278.8 -- 379.9 (-46.7 +54.4)

CENTRAL AGE W/ 68% CONF. INTERVAL (Ma): 326.3, 301.5 -- 353.1 (-24.8 +26.8)
 95% CONF. INTERVAL (Ma): 279.4 -- 380.9 (-46.9 +54.5)
 AGE DISPERSION (%): 0.0

September 22 2011 18:47

BinomFit for Windows ver.1.2

Page 2

Datafile: F:\Ouchitas\Zircon Fission Track Data\BINOMFIT_results\ART-8\ART-8.ftz

Title: ART-8, Irradiation UA-Z2, Analyst SNT

FIT OPTION: Best-fit peaks using the binomial model of Galbraith and Green

INITIAL GUESS FOR MODEL PARAMETERS (number of peaks to fit = 1)

Peak #.	Peak Age	Theta	Fraction(%)	Count
1.	325.50	0.908	108.1	7.57

Total range for grain ages: 290.6 to 350.1 Ma
 Number of active grains (Num. used for fit): 7
 Number of removed grains: 0
 Degrees of freedom for fit: 6
 Average of the SE(Z)'s for the grains: 0.2
 Estimated width of peaks in PD plot in Z units: 0.24

PARAMETERS FOR BEST-FIT PEAKS

- * Standard error for peak age includes group error
- * Peak width is for PD plot assuming a kernel factor = 0.60

#.	Peak Age(Ma)	68%CI	95%CI	W(Z)	Frac(%)	SE,%	Count
1.	326.3	-24.8 ...+26.8	-46.9 ...+54.5	0.23	100.0	0.0	7.0

Log-likelihood for best fit: -18.055
 Chi-squared value for best fit: 0.765
 Reduced chi-squared value: 0.128
 Probability for F test: 0%
 Condition number for COVAR matrix: 1.00
 Number of iterations: 5

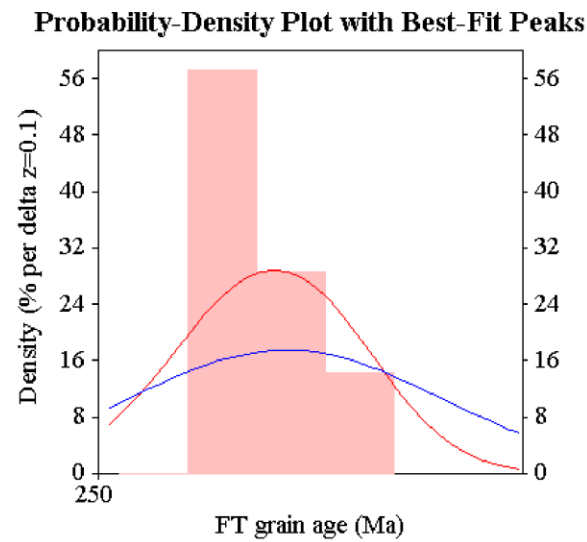
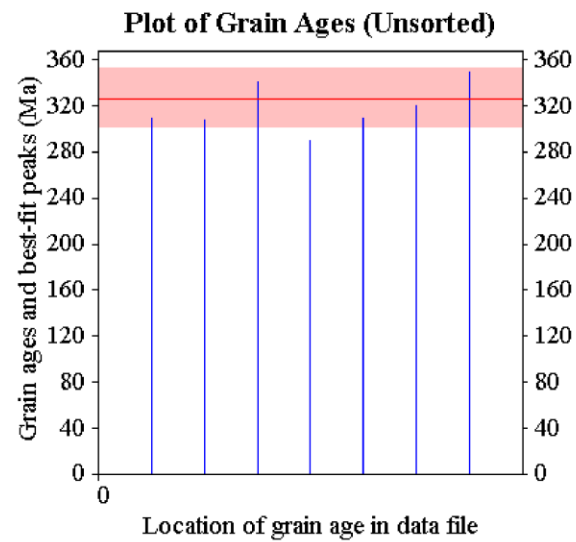
September 22 2011 18:47

BinomFit for Windows ver.1.2

Page 3

Datafile: F:\Ouchitas\Zircon Fission Track Data\BINOMFIT_results\ART-8\ART-8.ftz

Title: ART-8, Irradiation UA-Z2, Analyst SNT

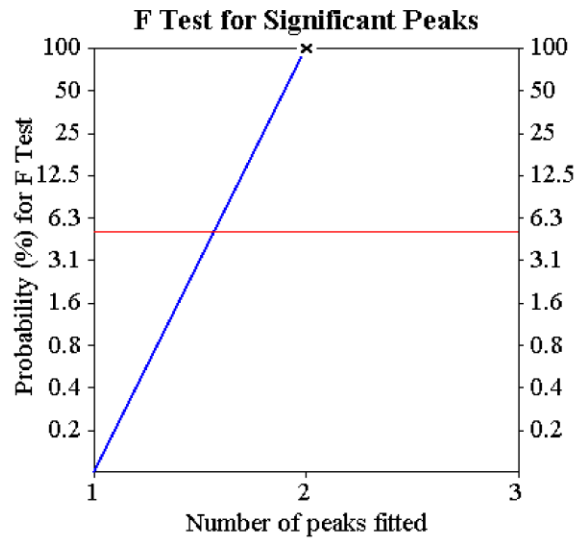
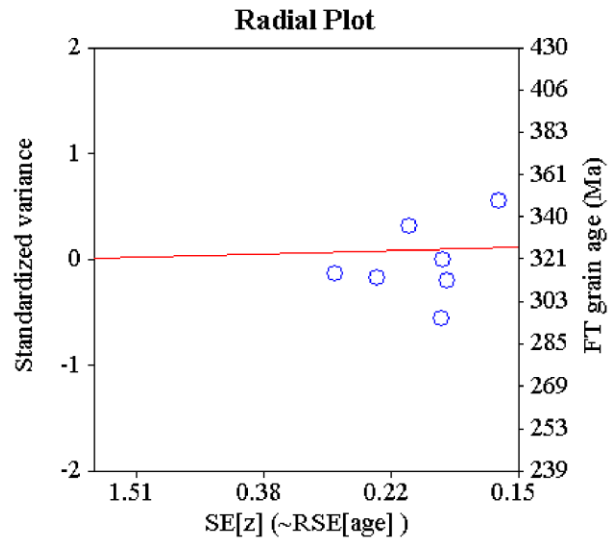


September 22 2011 18:47

BinomFit for Windows ver.1.2

Page 4

Datafile: F:\Ouachitas\Zircon Fission Track Data\BINOMFIT_results\ART-8\ART-8.ftz
 Title: ART-8, Irradiation UA-Z2, Analyst SNT



September 22 2011 13:21

BinomFit for Windows ver.1.2

Page 1

Datafile: D:\Users\Working account\Desktop\ART-9.ftz

Title: ART-9, Irradiation UA-Z2, Analyst SNT

NEW PARAMETERS - ZETA METHOD

EFFECTIVE TRACK DENSITY FOR FLUENCE MONITOR (tracks/cm²): 5.57E+05
 RELATIVE ERROR (%): 1.67
 EFFECTIVE URANIUM CONTENT OF MONITOR (ppm): 49.40
 ZETA FACTOR AND STANDARD ERROR (yr cm²): 121.10 3.50
 SIZE OF COUNTER SQUARE (cm²): 6.40E-07

GRAIN AGES IN ORIGINAL ORDER

Grain no.	RhoS (cm ⁻²)	(Ns)	RhoI (cm ⁻²)	(Ni)	Squares	U+/-2s	Grain Age (Ma)		
							Age	--95% CI--	
1	1.61E+07	(62)	1.04E+06	(4)	6	92 87	485.4	191.3	1727.5
2	9.24E+06	(71)	9.11E+05	(7)	12	81 59	326.9	155.7	827.3
3	1.58E+07	(81)	1.76E+06	(9)	8	156 101	292.2	150.4	654.3
4	1.70E+07	(98)	1.74E+06	(10)	9	154 95	318.0	170.0	675.2
5	1.89E+07	(121)	1.72E+06	(11)	10	152 90	356.2	197.0	722.1
6	2.38E+07	(137)	2.08E+06	(12)	9	185 105	369.7	209.9	722.6
7	1.82E+07	(140)	1.82E+06	(14)	12	162 85	325.6	191.4	604.6
8	1.84E+07	(141)	1.56E+06	(12)	12	139 78	380.2	216.1	742.1
9	2.15E+07	(165)	2.08E+06	(16)	12	185 91	335.9	204.5	595.5
10	1.67E+07	(171)	1.86E+06	(19)	16	164 75	294.6	185.7	497.8
11	1.68E+07	(172)	1.46E+06	(15)	16	130 66	372.2	223.9	671.1
12	1.77E+07	(181)	7.81E+05	(8)	16	69 48	708.5	368.2	1585.0
13	1.50E+07	(192)	1.33E+06	(17)	20	118 56	367.2	227.5	636.2
14	2.04E+07	(209)	1.95E+06	(20)	16	173 77	340.9	218.5	564.6
15	1.18E+07	(242)	1.17E+06	(24)	32	104 42	329.6	219.2	520.6
16	2.55E+07	(327)	5.47E+05	(7)	20	48 35	1382.0	714.7	3084.1
17	2.16E+07	(345)	5.00E+05	(8)	25	44 30	1289.0	691.2	2731.0
POOLED	1.78E+07	(2855)	1.33E+06	(213)	251	118 17	436.2	375.8	505.8

CHI² PROBABILITY (%): 0.1

POOLED AGE W/ 68% CONF. INTERVAL(Ma): 436.2, 404.3 -- 470.5 (-31.9 +34.3)
 95% CONF. INTERVAL(Ma): 375.8 -- 505.8 (-60.4 +69.7)

CENTRAL AGE W/ 68% CONF. INTERVAL(Ma): 412.7, 371.8 -- 458.1 (-41.0 +45.3)
 95% CONF. INTERVAL(Ma): 336.2 -- 506.1 (-76.6 +93.3)
 AGE DISPERSION (%): 29.8

September 22 2011 13:21

BinomFit for Windows ver.1.2

Page 2

Datafile: D:\Users\Working account\Desktop\ART-9.ftz

Title: ART-9, Irradiation UA-Z2, Analyst SNT

FIT OPTION: Best-fit peaks using the binomial model of Galbraith and Green

INITIAL GUESS FOR MODEL PARAMETERS (number of peaks to fit = 2)

Peak #.	Peak Age	Theta	Fraction(%)	Count
1.	436.20	0.930	22.6	3.85
2.	681.30	0.955	5.3	0.90

Total range for grain ages: 283.2 to 1327.0 Ma
 Number of active grains (Num. used for fit): 17
 Number of removed grains: 0
 Degrees of freedom for fit: 14
 Average of the SE(Z)'s for the grains: 0.32
 Estimated width of peaks in PD plot in Z units: 0.37

PARAMETERS FOR BEST-FIT PEAKS

* Standard error for peak age includes group error

* Peak width is for PD plot assuming a kernel factor = 0.60

#.	Peak Age(Ma)	68%CI	95%CI	W(Z)	Frac(%)	SE, %	Count
1.	355.4	-28.8 ...+31.3	-54.4 ...+63.9	0.33	85.5	9.5	14.5
2.	1238.7	-273.6 ...+342.2	-482.6 ...+746.5	0.43	14.5	9.5	2.5

Log-likelihood for best fit: -44.775
 Chi-squared value for best fit: 13.060
 Reduced chi-squared value: 0.933
 Probability for F test: 0%
 Condition number for COVAR matrix: 12.27
 Number of iterations: 9

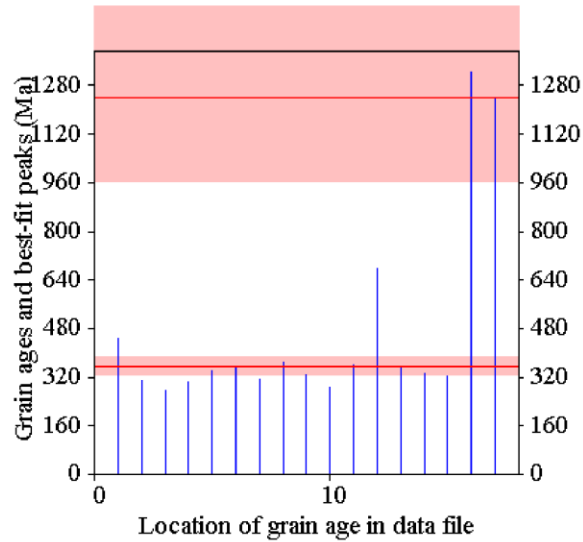
September 22 2011 13:21

BinomFit for Windows ver.1.2

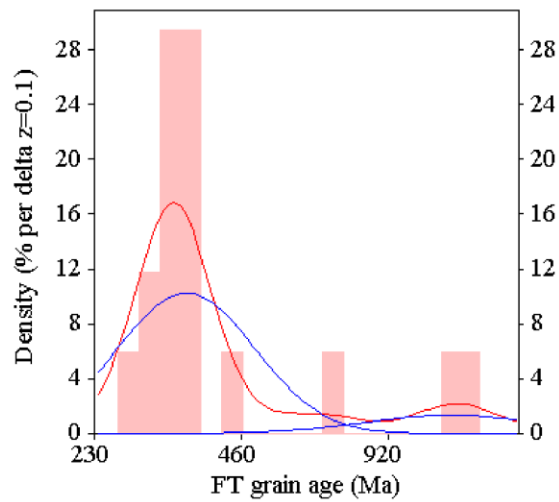
Page 3

Datafile: D:\Users\Working account\Desktop\ART-9.ftz

Title: ART-9, Irradiation UA-Z2, Analyst SNT



Probability-Density Plot with Best-Fit Peaks



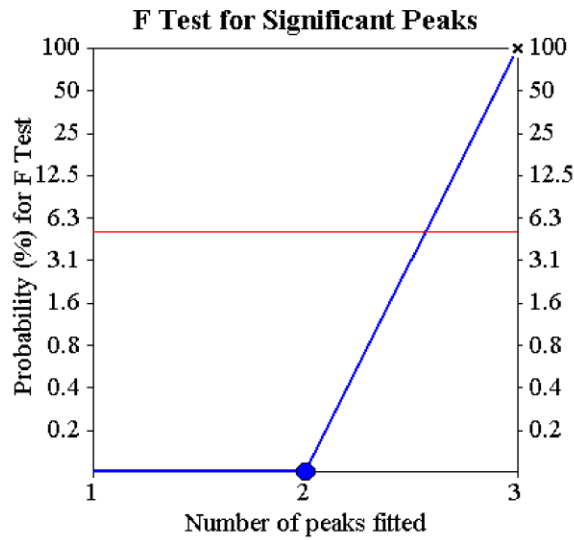
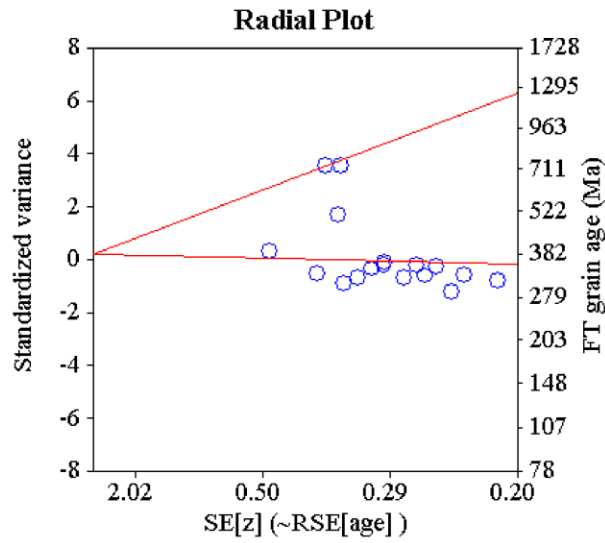
September 22 2011 13:21

BinomFit for Windows ver.1.2

Page 4

Datafile: D:\Users\Working account\Desktop\ART-9.ftz

Title: ART-9, Irradiation UA-Z2, Analyst SNT



September 22 2011 19:05

BinomFit for Windows ver.1.2

Page 1

Datafile: F:\Ouachitas\Zircon Fission Track Data\BINOMFIT_results\ART-12_BINOMFIT\ART-12.ftz

Title: ART-12, Irradiation UA-Z2, Analyst SNT

NEW PARAMETERS - ZETA METHOD

EFFECTIVE TRACK DENSITY FOR FLUENCE MONITOR (tracks/cm²): 5.56E+05
 RELATIVE ERROR (%): 1.68
 EFFECTIVE URANIUM CONTENT OF MONITOR (ppm): 49.40
 ZETA FACTOR AND STANDARD ERROR (yr cm²): 121.10 3.50
 SIZE OF COUNTER SQUARE (cm²): 6.40E-07

GRAIN AGES IN ORIGINAL ORDER

Grain no.	RhoS (cm ⁻²)	(Ns)	RhoI (cm ⁻²)	(Ni)	Squares	U+/-2s	Grain Age (Ma)	
							Age	--95% CI--
1	2.60E+07	(100)	2.08E+06	(8)	6	185 127	400.2	202.0 931.3
2	2.48E+07	(127)	2.93E+06	(15)	8	260 133	276.2	164.1 504.4
3	2.26E+07	(130)	1.91E+06	(11)	9	170 100	380.9	211.3 769.4
4	3.59E+07	(138)	2.86E+06	(11)	6	255 150	403.6	224.5 812.8
5	3.65E+07	(140)	3.91E+06	(15)	6	347 177	303.8	181.2 552.5
6	3.49E+07	(268)	3.78E+06	(29)	12	336 124	302.2	207.9 457.4
POOLED	3.00E+07	(903)	2.96E+06	(89)	47	263 56	330.9	265.1 412.6

CHI² PROBABILITY (%): 87.8

POOLED AGE W/ 68% CONF. INTERVAL (Ma): 330.9, 295.6 -- 370.4 (-35.4 +39.5)
 95% CONF. INTERVAL (Ma): 265.1 -- 412.6 (-65.8 +81.6)

CENTRAL AGE W/ 68% CONF. INTERVAL (Ma): 332.7, 297.1 -- 372.5 (-35.6 +39.8)
 95% CONF. INTERVAL (Ma): 266.4 -- 415.0 (-66.3 +82.3)
 AGE DISPERSION (%): 0.1

September 22 2011 19:05

BinomFit for Windows ver.1.2

Page 2

Datafile: F:\Ouachitas\Zircon Fission Track Data\BINOMFIT_results\ART-12_BINOMFIT\ART-12.ftz

Title: ART-12, Irradiation UA-Z2, Analyst SNT

FIT OPTION: Best-fit peaks using the binomial model of Galbraith and Green

INITIAL GUESS FOR MODEL PARAMETERS (number of peaks to fit = 1)

Peak #.	Peak Age	Theta	Fraction(%)	Count
1.	330.90	0.910	62.4	3.74

Total range for grain ages: 271.0 to 393.1 Ma
 Number of active grains (Num. used for fit): 6
 Number of removed grains: 0
 Degrees of freedom for fit: 5
 Average of the SE(Z)'s for the grains: 0.29
 Estimated width of peaks in PD plot in Z units: 0.34

PARAMETERS FOR BEST-FIT PEAKS

- * Standard error for peak age includes group error
- * Peak width is for PD plot assuming a kernel factor = 0.60

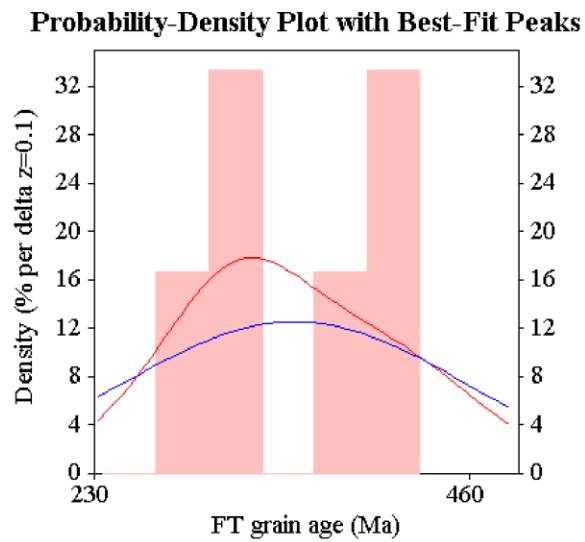
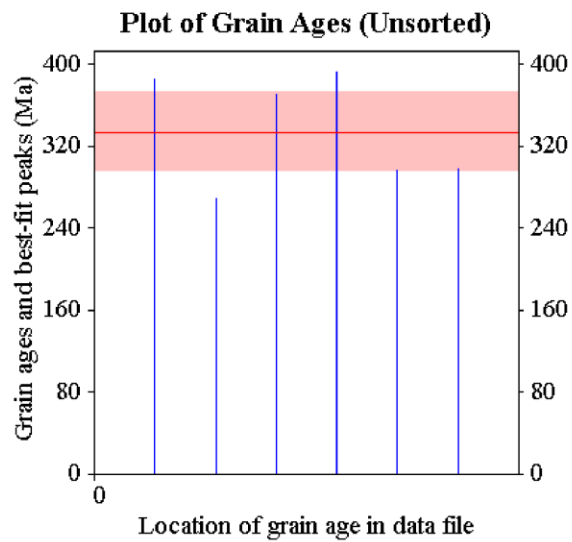
#.	Peak Age(Ma)	68%CI	95%CI	W(Z)	Frac(%)	SE,%	Count
1.	332.7	-35.6 ...+39.8	-66.3 ...+82.3	0.32	100.0	0.0	6.0

Log-likelihood for best fit: -14.054
 Chi-squared value for best fit: 1.784
 Reduced chi-squared value: 0.357
 Probability for F test: 0%
 Condition number for COVAR matrix: 1.00
 Number of iterations: 5

September 22 2011 19:05

BinomFit for Windows ver.1.2

Page 3

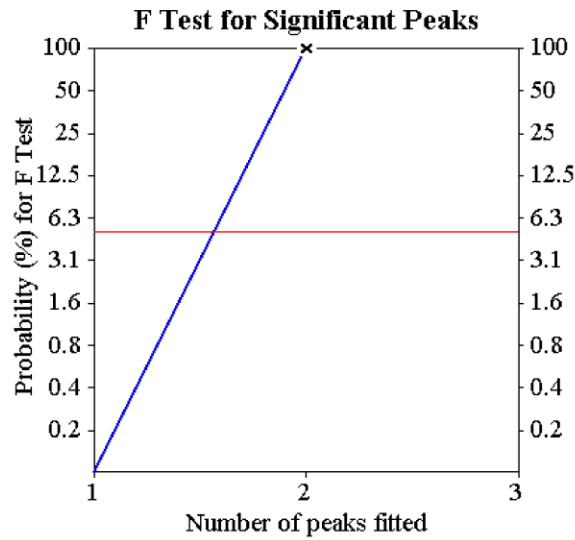
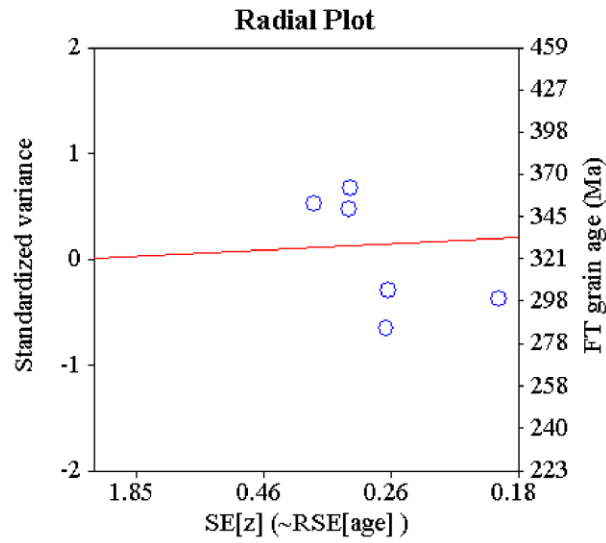
Datafile: F:\Ouchitas\Zircon Fission Track Data\BINOMFIT_results\ART-12_BINOMFIT\ART-12.ftz
Title: ART-12, Irradiation UA-Z2, Analyst SNT

September 22 2011 19:05

BinomFit for Windows ver.1.2

Page 4

Datafile: F:\Ouchitas\Zircon Fission Track Data\BINOMFIT_results\ART-12_BINOMFIT\ART-12.ftz
 Title: ART-12, Irradiation UA-Z2, Analyst SNT



September 22 2011 19:17

BinomFit for Windows ver.1.2

Page 1

Datafile: F:\Ouachitas\Zircon Fission Track Data\BINOMFIT_results\ART-16_BINOMFIT\ART-16.ftz

Title: ART-16, Irradiation UA-Z2, Analyst SNT

NEW PARAMETERS - ZETA METHOD

EFFECTIVE TRACK DENSITY FOR FLUENCE MONITOR (tracks/cm²): 5.54E+05
 RELATIVE ERROR (%): 1.68
 EFFECTIVE URANIUM CONTENT OF MONITOR (ppm): 49.40
 ZETA FACTOR AND STANDARD ERROR (yr cm²): 121.10 3.50
 SIZE OF COUNTER SQUARE (cm²): 6.40E-07

GRAIN AGES IN ORIGINAL ORDER

Grain no.	RhoS (cm ⁻²)	(Ns)	RhoI (cm ⁻²)	(Ni)	Squares	U+/-2s	Grain Age (Ma)	
							Age	--95% CI--
1	1.95E+07 (75)		2.34E+06 (9)		6	209 136	269.6	138.1 606.4
2	1.08E+07 (138)		6.25E+05 (8)		20	56 38	544.4	279.3 1241.3
3	2.71E+07 (139)		2.54E+06 (13)		8	226 123	345.4	199.7 656.9
4	2.52E+07 (145)		2.26E+06 (13)		9	201 110	359.9	208.5 683.2
5	2.47E+07 (158)		2.50E+06 (16)		10	223 110	320.3	194.6 568.8
6	1.67E+07 (171)		1.46E+06 (15)		16	131 66	368.1	221.4 664.0
7	3.14E+07 (181)		3.13E+06 (18)		9	279 130	326.3	204.0 558.2
8	1.63E+07 (188)		7.81E+05 (9)		18	70 45	654.7	351.4 1395.7
9	1.65E+07 (190)		1.74E+06 (20)		18	155 69	309.0	197.4 513.5
10	2.63E+07 (202)		2.21E+06 (17)		12	197 95	383.7	238.2 663.6
11	2.64E+07 (203)		2.60E+06 (20)		12	232 103	329.6	211.0 546.4
12	2.39E+07 (214)		2.01E+06 (18)		14	179 83	384.0	241.6 652.8
13	3.38E+07 (216)		2.97E+06 (19)		10	265 120	367.9	233.8 616.5
14	1.90E+07 (243)		2.03E+06 (26)		20	181 71	304.6	205.3 472.8
15	3.17E+07 (325)		3.03E+06 (31)		16	270 97	341.0	238.2 506.8
16	2.93E+07 (337)		1.30E+06 (15)		18	116 59	706.1	435.1 1237.1
17	2.13E+07 (341)		1.38E+06 (22)		25	123 52	496.9	329.0 791.6
18	1.63E+07 (416)		1.21E+06 (31)		40	108 39	433.3	304.6 639.7
POOLED	2.16E+07(3882)		1.78E+06(320)		281	159 19	394.2	347.0 447.7

CHI² PROBABILITY (%): 43.1

POOLED AGE W/ 68% CONF. INTERVAL (Ma): 394.2, 369.4 -- 420.7 (-24.8 +26.5)
 95% CONF. INTERVAL (Ma): 347.0 -- 447.7 (-47.3 +53.5)

CENTRAL AGE W/ 68% CONF. INTERVAL (Ma): 393.6, 367.9 -- 421.1 (-25.7 +27.5)
 95% CONF. INTERVAL (Ma): 344.8 -- 449.2 (-48.9 +55.6)
 AGE DISPERSION (%): 7.4

September 22 2011 19:17

BinomFit for Windows ver.1.2

Page 2

Datafile: F:\Ouachitas\Zircon Fission Track Data\BINOMFIT_results\ART-16_BINOMFIT\ART-16.ftz

Title: ART-16, Irradiation UA-Z2, Analyst SNT

FIT OPTION: Best-fit peaks using the binomial model of Galbraith and Green

INITIAL GUESS FOR MODEL PARAMETERS (number of peaks to fit = 2)

Peak #.	Peak Age	Theta	Fraction(%)	Count
1.	394.20	0.924	46.4	8.36
2.	692.10	0.956	10.8	1.94

Total range for grain ages: 261.4 to 692.3 Ma
 Number of active grains (Num. used for fit): 18
 Number of removed grains: 0
 Degrees of freedom for fit: 15
 Average of the SE(Z)'s for the grains: 0.26
 Estimated width of peaks in PD plot in Z units: 0.3

PARAMETERS FOR BEST-FIT PEAKS

* Standard error for peak age includes group error

* Peak width is for PD plot assuming a kernel factor = 0.60

#.	Peak Age(Ma)	68%CI	95%CI	W(Z)	Frac(%)	SE,%	Count
1.	378.5	-29.4 ...+31.9	-55.6 ...+64.9	0.29	91.7	12.8	16.5
2.	629.9	-186.1 ...+258.9	-314.0 ...+597.9	0.32	8.3	12.8	1.5

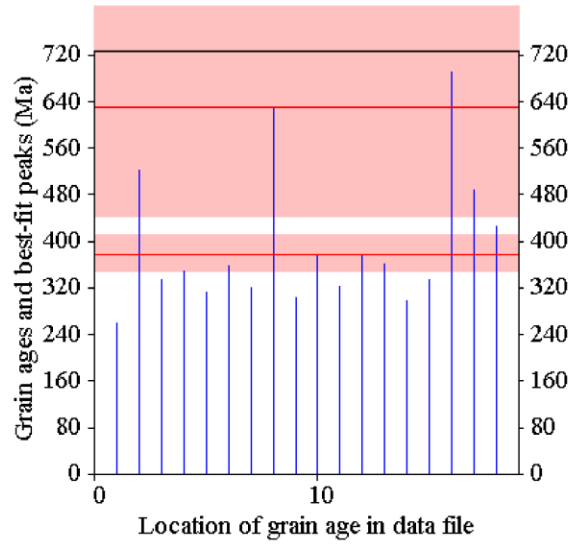
Log-likelihood for best fit: -49.549
 Chi-squared value for best fit: 13.612
 Reduced chi-squared value: 0.907
 Probability for F test: 4%
 Condition number for COVAR matrix: 34.86
 Number of iterations: 10

September 22 2011 19:17

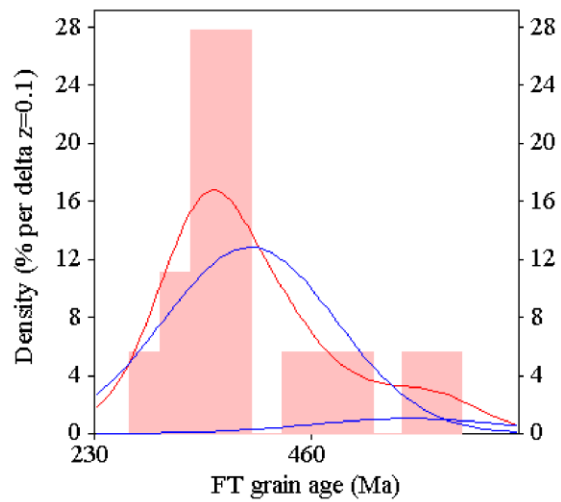
BinomFit for Windows ver.1.2

Page 3

Datafile: F:\Ouchitas\Zircon Fission Track Data\BINOMFIT_results\ART-16_BINOMFIT\ART-16.ftz
 Title: ART-16, Irradiation UA-Z2, Analyst SNT



Probability-Density Plot with Best-Fit Peaks

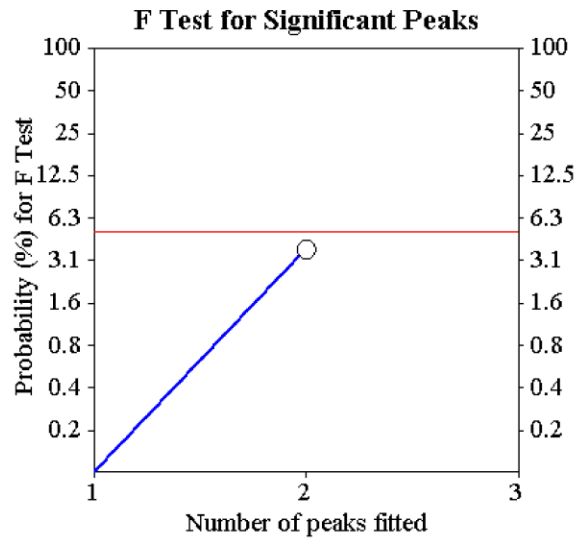
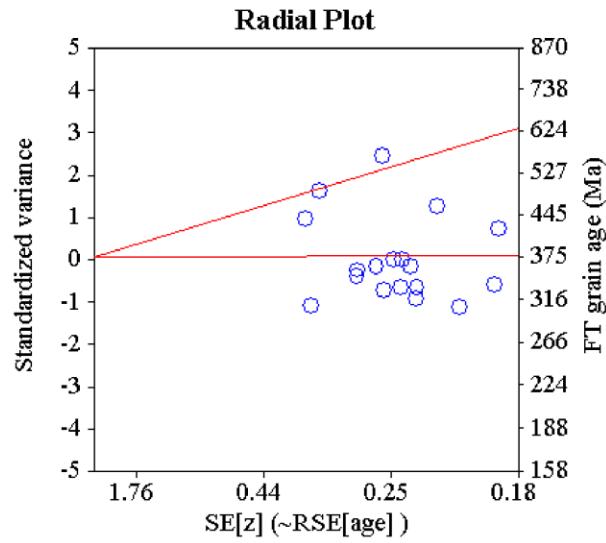


September 22 2011 19:17

BinomFit for Windows ver.1.2

Page 4

Datafile: F:\Ouchitas\Zircon Fission Track Data\BINOMFIT_results\ART-16_BINOMFIT\ART-16.ftz
 Title: ART-16, Irradiation UA-Z2, Analyst SNT



September 22 2011 19:31

BinomFit for Windows ver.1.2

Page 1

Datafile: F:\Ouachitas\Zircon Fission Track Data\BINOMFIT_results\ART-18_BINOMFIT\ART-18.ftz

Title: ART-18, Irradiation UA-Z2, Analyst SNT

NEW PARAMETERS - ZETA METHOD

EFFECTIVE TRACK DENSITY FOR FLUENCE MONITOR (tracks/cm²): 5.53E+05
 RELATIVE ERROR (%): 1.68
 EFFECTIVE URANIUM CONTENT OF MONITOR (ppm): 49.40
 ZETA FACTOR AND STANDARD ERROR (yr cm²): 121.10 3.50
 SIZE OF COUNTER SQUARE (cm²): 6.40E-07

GRAIN AGES IN ORIGINAL ORDER

Grain no.	RhoS (cm ⁻²)	(Ns)	RhoI (cm ⁻²)	(Ni)	Squares	U+/-2s	Grain Age (Ma)		
							Age	--95% CI--	
1	1.64E+07 (105)		2.19E+06 (14)		10	195 103	243.8	141.4	458.7
2	1.10E+07 (113)		1.46E+06 (15)		16	131 67	245.1	144.8	449.8
3	1.56E+07 (120)		1.95E+06 (15)		12	175 89	259.9	154.0	475.8
4	1.27E+07 (122)		1.46E+06 (14)		15	130 69	282.4	165.0	527.7
5	1.65E+07 (127)		1.69E+06 (13)		12	151 82	315.5	181.7	602.6
6	1.27E+07 (130)		1.56E+06 (16)		16	140 69	264.1	159.1	472.7
7	1.72E+07 (165)		1.88E+06 (18)		15	168 78	297.4	185.3	510.4
8	2.70E+07 (173)		2.97E+06 (19)		10	265 120	295.6	186.4	499.3
9	1.40E+07 (179)		1.64E+06 (21)		20	147 63	277.3	178.3	456.3
10	1.27E+07 (195)		1.30E+06 (20)		24	116 52	316.1	202.1	524.8
11	1.59E+07 (203)		1.48E+06 (19)		20	133 60	345.4	219.1	580.1
12	2.12E+07 (217)		1.95E+06 (20)		16	175 77	350.8	225.1	580.2
13	2.04E+07 (235)		1.82E+06 (21)		18	163 70	361.6	234.7	589.5
14	1.48E+07 (236)		1.75E+06 (28)		25	156 59	274.7	187.2	420.3
15	1.58E+07 (242)		1.69E+06 (26)		24	151 59	302.6	203.9	469.8
16	1.59E+07 (244)		1.56E+06 (24)		24	140 57	329.6	219.3	520.5
17	1.97E+07 (252)		2.11E+06 (27)		20	189 72	303.5	206.0	466.8
18	1.35E+07 (259)		1.35E+06 (26)		30	121 47	323.3	218.3	500.9
19	1.69E+07 (303)		1.73E+06 (31)		28	155 55	317.7	221.5	473.0
20	2.00E+07 (307)		2.02E+06 (31)		24	180 65	321.7	224.4	478.9
POOLED	1.62E+07 (3927)		1.72E+06 (418)		379	154 16	306.7	272.7	344.8

CHI² PROBABILITY (%):100.0

POOLED AGE W/ 68% CONF. INTERVAL (Ma): 306.7, 288.8 -- 325.6 (-17.8 +18.9)
 95% CONF. INTERVAL (Ma): 272.7 -- 344.8 (-34.0 +38.1)

CENTRAL AGE W/ 68% CONF. INTERVAL (Ma): 307.0, 289.2 -- 326.0 (-17.9 +18.9)
 95% CONF. INTERVAL (Ma): 273.0 -- 345.2 (-34.1 +38.2)
 AGE DISPERSION (%): 0.0

September 22 2011 19:31

BinomFit for Windows ver.1.2

Page 2

Datafile: F:\Ouachitas\Zircon Fission Track Data\BINOMFIT_results\ART-18_BINOMFIT\ART-18.ftz

Title: ART-18, Irradiation UA-Z2, Analyst SNT

FIT OPTION: Best-fit peaks using the binomial model of Galbraith and Green

INITIAL GUESS FOR MODEL PARAMETERS (number of peaks to fit = 1)

Peak #.	Peak Age	Theta	Fraction(%)	Count
1.	306.70	0.904	84.9	16.98

Total range for grain ages: 239.1 to 356.6 Ma
 Number of active grains (Num. used for fit): 20
 Number of removed grains: 0
 Degrees of freedom for fit: 19
 Average of the SE(Z)'s for the grains: 0.24
 Estimated width of peaks in PD plot in Z units: 0.28

PARAMETERS FOR BEST-FIT PEAKS

- * Standard error for peak age includes group error
- * Peak width is for PD plot assuming a kernel factor = 0.60

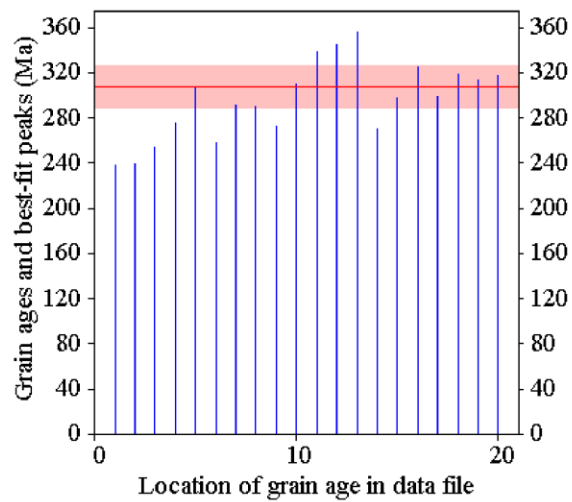
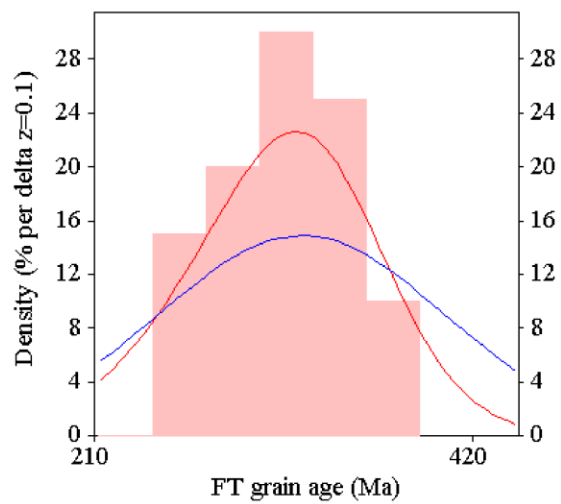
#.	Peak Age(Ma)	68%CI	95%CI	W(Z)	Frac(%)	SE,%	Count
1.	307.0	-17.9 ...+18.9	-34.1 ...+38.2	0.27	100.0	0.0	20.0

Log-likelihood for best fit: -49.325
 Chi-squared value for best fit: 4.140
 Reduced chi-squared value: 0.218
 Probability for F test: 0%
 Condition number for COVAR matrix: 1.00
 Number of iterations: 5

September 22 2011 19:31

BinomFit for Windows ver.1.2

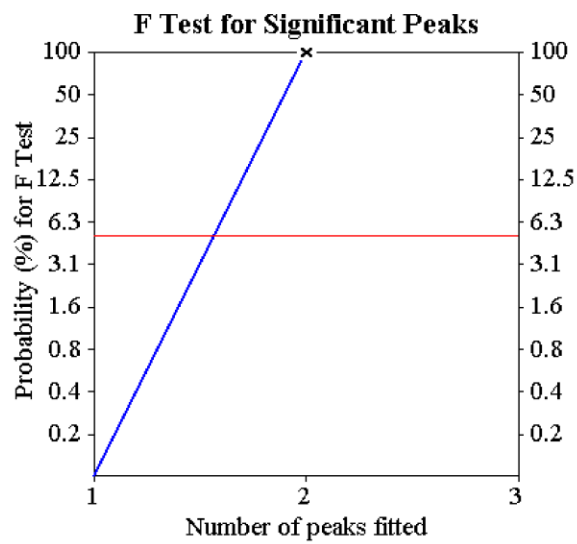
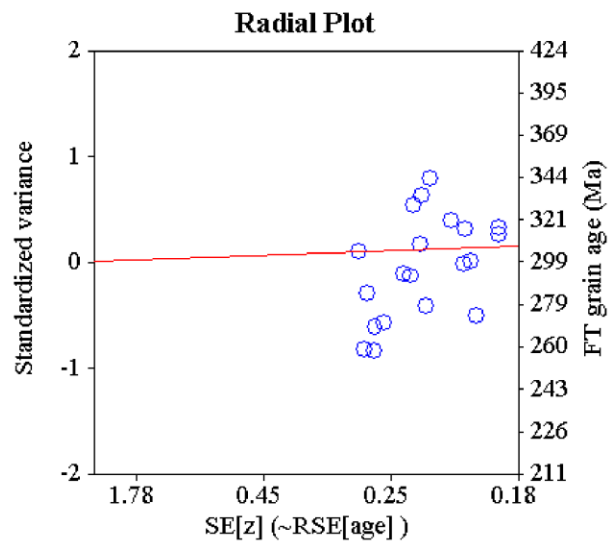
Page 3

Datafile: F:\Ouchitas\Zircon Fission Track Data\BINOMFIT_results\ART-18_BINOMFIT\ART-18.ftz
Title: ART-18, Irradiation UA-Z2, Analyst SNT**Plot of Grain Ages (Unsorted)****Probability-Density Plot with Best-Fit Peaks**

September 22 2011 19:31

BinomFit for Windows ver.1.2

Page 4

Datafile: F:\Ouchitas\Zircon Fission Track Data\BINOMFIT_results\ART-18_BINOMFIT\ART-18.ftz
Title: ART-18, Irradiation UA-Z2, Analyst SNT

September 22 2011 19:34

BinomFit for Windows ver.1.2

Page 1

Datafile: F:\Ouachitas\Zircon Fission Track Data\BINOMFIT_results\Chung_BINOMFIT\Chung.ftz

Title: Chung, Irradiation UA-Z2, Analyst SNT

NEW PARAMETERS - ZETA METHOD

EFFECTIVE TRACK DENSITY FOR FLUENCE MONITOR (tracks/cm²): 5.65E+05
 RELATIVE ERROR (%): 1.68
 EFFECTIVE URANIUM CONTENT OF MONITOR (ppm): 49.40
 ZETA FACTOR AND STANDARD ERROR (yr cm²): 121.10 3.50
 SIZE OF COUNTER SQUARE (cm²): 6.40E-07

GRAIN AGES IN ORIGINAL ORDER

Grain no.	RhoS (cm ⁻²)	(Ns)	RhoI (cm ⁻²)	(Ni)	Squares	U+/-2s	Grain Age (Ma)		
							Age	--95% CI--	
1	1.52E+07	(78)	1.76E+06	(9)	8	154 100	285.3	146.6	640.1
2	2.14E+07	(82)	2.60E+06	(10)	6	228 141	270.7	143.3	580.3
3	2.42E+07	(93)	3.13E+06	(12)	6	273 155	256.8	143.0	511.1
4	2.71E+07	(139)	2.73E+06	(14)	8	239 126	327.6	192.6	608.4
5	1.82E+07	(140)	1.69E+06	(13)	12	148 81	354.3	205.0	673.3
6	2.64E+07	(152)	2.43E+06	(14)	9	213 112	357.4	210.9	661.1
POOLED	2.18E+07	(684)	2.30E+06	(72)	49	201 48	314.9	246.4	401.9

CHI² PROBABILITY (%): 95.0

POOLED AGE W/ 68% CONF. INTERVAL(Ma): 314.9, 277.9 -- 356.7 (-37.0 +41.8)
 95% CONF. INTERVAL(Ma): 246.4 -- 401.9 (-68.5 +87.0)

CENTRAL AGE W/ 68% CONF. INTERVAL(Ma): 317.0, 279.7 -- 359.2 (-37.4 +42.2)
 95% CONF. INTERVAL(Ma): 247.9 -- 404.9 (-69.2 +87.9)
 AGE DISPERSION (%): 0.1

September 22 2011 19:34

BinomFit for Windows ver.1.2

Page 2

Datafile: F:\Ouachitas\Zircon Fission Track Data\BINOMFIT_results\Chung_BINOMFIT\Chung.ftz

Title: Chung, Irradiation UA-Z2, Analyst SNT

FIT OPTION: Best-fit peaks using the binomial model of Galbraith and Green

INITIAL GUESS FOR MODEL PARAMETERS (number of peaks to fit = 1)

Peak #.	Peak Age	Theta	Fraction(%)	Count
1.	314.90	0.904	63.8	3.83

Total range for grain ages: 250.9 to 350.1 Ma
 Number of active grains (Num. used for fit): 6
 Number of removed grains: 0
 Degrees of freedom for fit: 5
 Average of the SE(Z)'s for the grains: 0.3
 Estimated width of peaks in PD plot in Z units: 0.35

PARAMETERS FOR BEST-FIT PEAKS

- * Standard error for peak age includes group error
- * Peak width is for PD plot assuming a kernel factor = 0.60

#.	Peak Age(Ma)	68%CI	95%CI	W(Z)	Frac(%)	SE,%	Count
1.	317.0	-37.4 ...+42.2	-69.2 ...+87.9	0.35	100.0	0.0	6.0

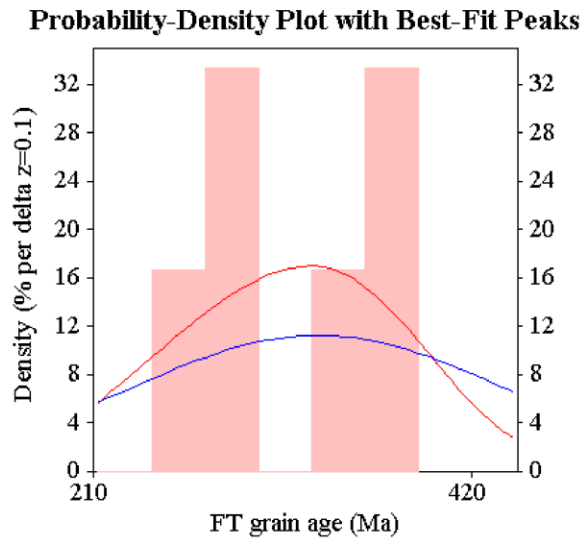
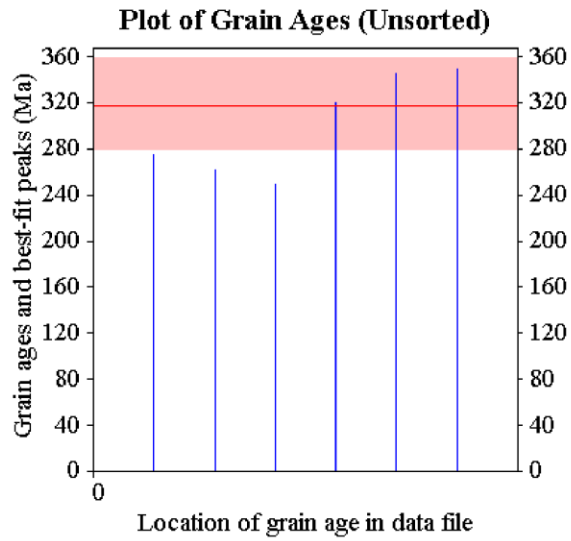
Log-likelihood for best fit: -13.247
 Chi-squared value for best fit: 1.145
 Reduced chi-squared value: 0.229
 Probability for F test: 0%
 Condition number for COVAR matrix: 1.00
 Number of iterations: 5

September 22 2011 19:34

BinomFit for Windows ver.1.2

Page 3

Datafile: F:\Ouachitas\Zircon Fission Track Data\BINOMFIT_results\Chung_BINOMFIT\Chung.ftz
 Title: Chung, Irradiation UA-Z2, Analyst SNT

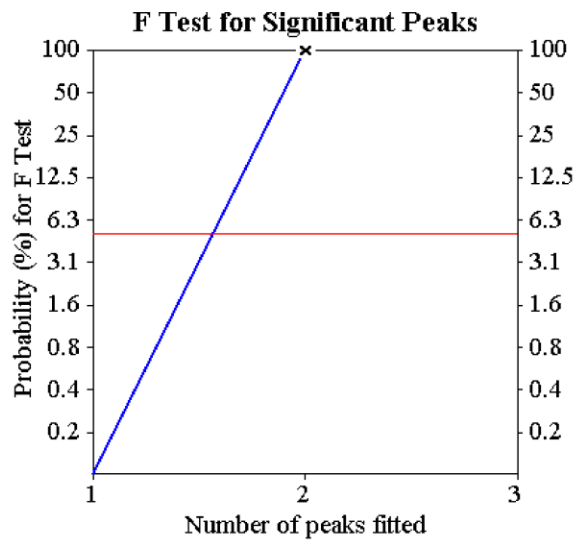
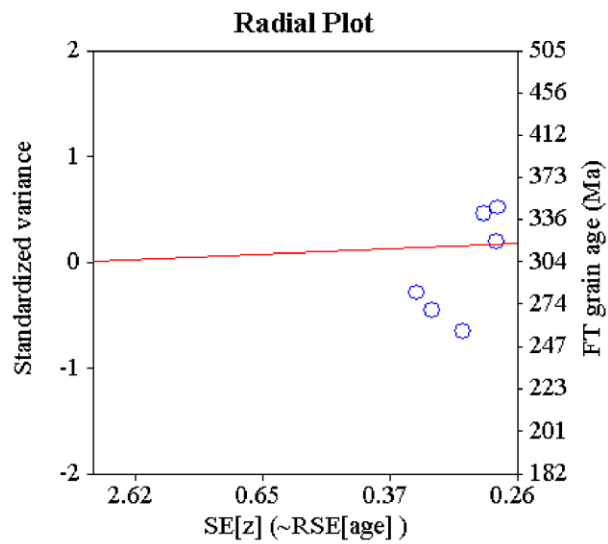


September 22 2011 19:34

BinomFit for Windows ver.1.2

Page 4

Datafile: F:\Ouachitas\Zircon Fission Track Data\BINOMFIT_results\Chung_BINOMFIT\Chung.ftz
 Title: Chung, Irradiation UA-Z2, Analyst SNT



September 22 2011 19:43

BinomFit for Windows ver.1.2

Page 1

Datafile: F:\Ouchitas\Zircon Fission Track Data\BINOMFIT_results\Mt_Blakely_BINOMFIT\Mt_Blakely.ftz

Title: Mt. Blakely, Irradiation UA-Z2, Analyst SNT

NEW PARAMETERS - ZETA METHOD

EFFECTIVE TRACK DENSITY FOR FLUENCE MONITOR (tracks/cm²): 5.66E+05
 RELATIVE ERROR (%): 1.66
 EFFECTIVE URANIUM CONTENT OF MONITOR (ppm): 49.40
 ZETA FACTOR AND STANDARD ERROR (yr cm²): 121.10 3.50
 SIZE OF COUNTER SQUARE (cm²): 6.40E-07

GRAIN AGES IN ORIGINAL ORDER

Grain no.	RhoS (cm ⁻²)	(Ns)	RhoI (cm ⁻²)	(Ni)	Squares	U+/-2s	Grain Age (Ma)		
							Age	--95% CI--	
1	1.64E+07 (63)		2.08E+06 (8)		6	182 125	260.1	127.6	622.2
2	2.08E+07 (80)		2.34E+06 (9)		6	204 133	293.3	150.9	656.8
3	1.07E+07 (82)		1.30E+06 (10)		12	114 70	271.5	143.7	581.8
4	1.63E+07 (104)		1.72E+06 (11)		10	150 89	312.3	171.4	637.6
5	1.69E+07 (108)		1.56E+06 (10)		10	136 84	355.0	190.8	749.7
6	2.30E+07 (118)		3.32E+06 (17)		8	290 139	231.9	140.8	409.6
7	1.32E+07 (127)		1.35E+06 (13)		15	118 64	323.1	186.1	616.7
8	1.19E+07 (152)		1.41E+06 (18)		20	123 57	281.1	174.6	483.8
9	2.69E+07 (155)		2.78E+06 (16)		9	242 120	321.1	195.0	570.4
10	3.07E+07 (157)		2.54E+06 (13)		8	221 121	397.0	230.8	750.5
11	3.09E+07 (158)		3.52E+06 (18)		8	307 143	291.9	181.6	501.7
12	2.11E+07 (162)		2.73E+06 (21)		12	238 103	257.6	165.0	425.2
13	2.12E+07 (163)		2.34E+06 (18)		12	204 95	300.9	187.4	516.5
14	2.40E+07 (246)		2.54E+06 (26)		16	221 86	314.9	212.3	488.4
15	2.41E+07 (309)		2.34E+06 (30)		20	204 74	342.3	237.6	512.4
16	3.54E+07 (362)		2.34E+06 (24)		16	204 83	494.5	332.9	771.0
17	2.02E+07 (645)		5.00E+05 (16)		50	44 22	1241.3	792.9	2066.5
POOLED	2.09E+07(3191)		1.83E+06(278)		238	159 20	381.4	333.3	436.4

CHI² PROBABILITY (%): 0.0

POOLED AGE W/ 68% CONF. INTERVAL(Ma): 381.4, 356.1 -- 408.6 (-25.4 +27.1)
 95% CONF. INTERVAL(Ma): 333.3 -- 436.4 (-48.2 +54.9)

CENTRAL AGE W/ 68% CONF. INTERVAL(Ma): 342.3, 311.6 -- 376.0 (-30.7 +33.6)
 95% CONF. INTERVAL(Ma): 284.7 -- 411.3 (-57.6 +68.9)
 AGE DISPERSION (%): 25.9

September 22 2011 19:43

BinomFit for Windows ver.1.2

Page 2

Datafile: F:\Ouachitas\Zircon Fission Track Data\BINOMFIT_results\Mt_Blakely_BINOMFIT\Mt_Blakely.ftz

Title: Mt. Blakely, Irradiation UA-Z2, Analyst SNT

FIT OPTION: Best-fit peaks using the binomial model of Galbraith and Green

INITIAL GUESS FOR MODEL PARAMETERS (number of peaks to fit = 2)

Peak #.	Peak Age	Theta	Fraction(%)	Count
1.	381.40	0.920	29.0	4.94
2.	496.40	0.938	9.9	1.68

Total range for grain ages: 228.1 to 1218.8 Ma
 Number of active grains (Num. used for fit): 17
 Number of removed grains: 0
 Degrees of freedom for fit: 14
 Average of the SE(Z)'s for the grains: 0.27
 Estimated width of peaks in PD plot in Z units: 0.32

PARAMETERS FOR BEST-FIT PEAKS

* Standard error for peak age includes group error

* Peak width is for PD plot assuming a kernel factor = 0.60

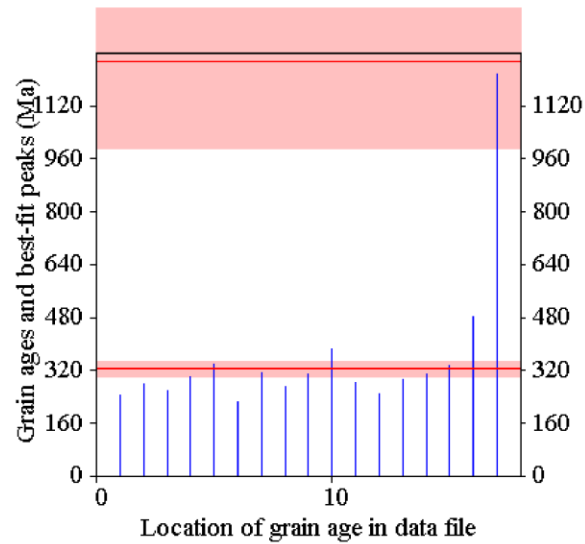
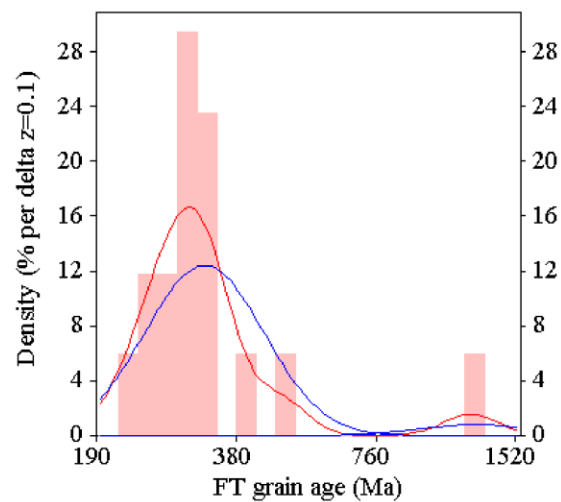
#.	Peak Age(Ma)	68%CI	95%CI	W(Z)	Frac(%)	SE, %	Count
1.	324.9	-22.3 ...+23.9	-42.4 ...+48.5	0.30	94.1	5.7	16.0
2.	1252.0	-262.1 ...+323.5	-465.1 ...+701.3	0.30	5.9	5.7	1.0

Log-likelihood for best fit: -46.306
 Chi-squared value for best fit: 16.943
 Reduced chi-squared value: 1.210
 Probability for F test: 0%
 Condition number for COVAR matrix: 19.72
 Number of iterations: 8

September 22 2011 19:43

BinomFit for Windows ver.1.2

Page 3

Datafile: F:\Ouachitas\Zircon Fission Track Data\BINOMFIT_results\Mt_Blakely_BINOMFIT\Mt_Blakely.ftz
Title: Mt. Blakely, Irradiation UA-Z2, Analyst SNT**Probability-Density Plot with Best-Fit Peaks**

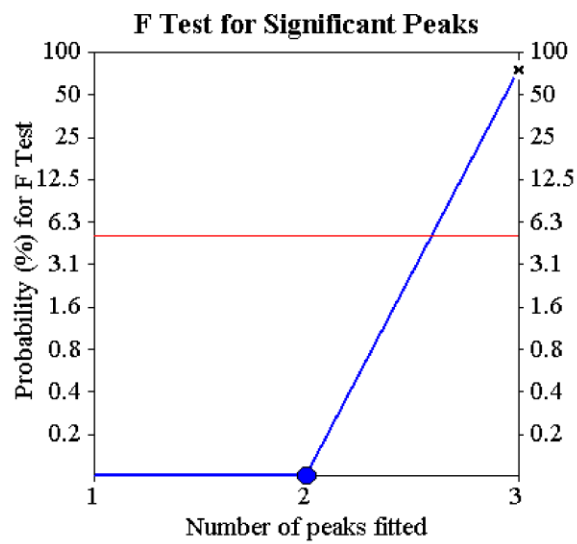
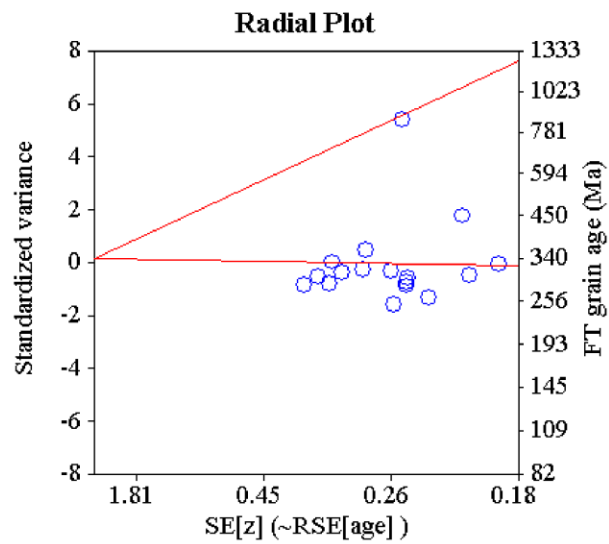
September 22 2011 19:43

BinomFit for Windows ver.1.2

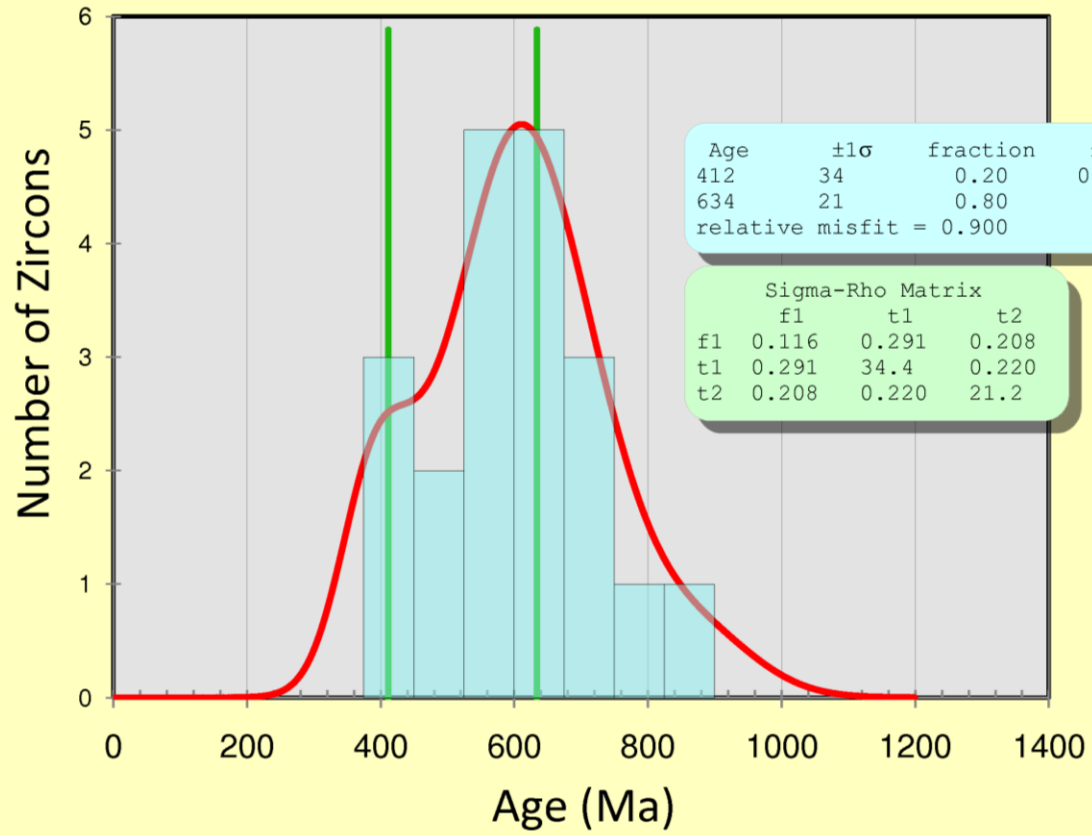
Page 4

Datafile: F:\Ouchitas\Zircon Fission Track Data\BINOMFIT_results\Mt_Blakely_BINOMFIT\Mt_Blakely.ftz

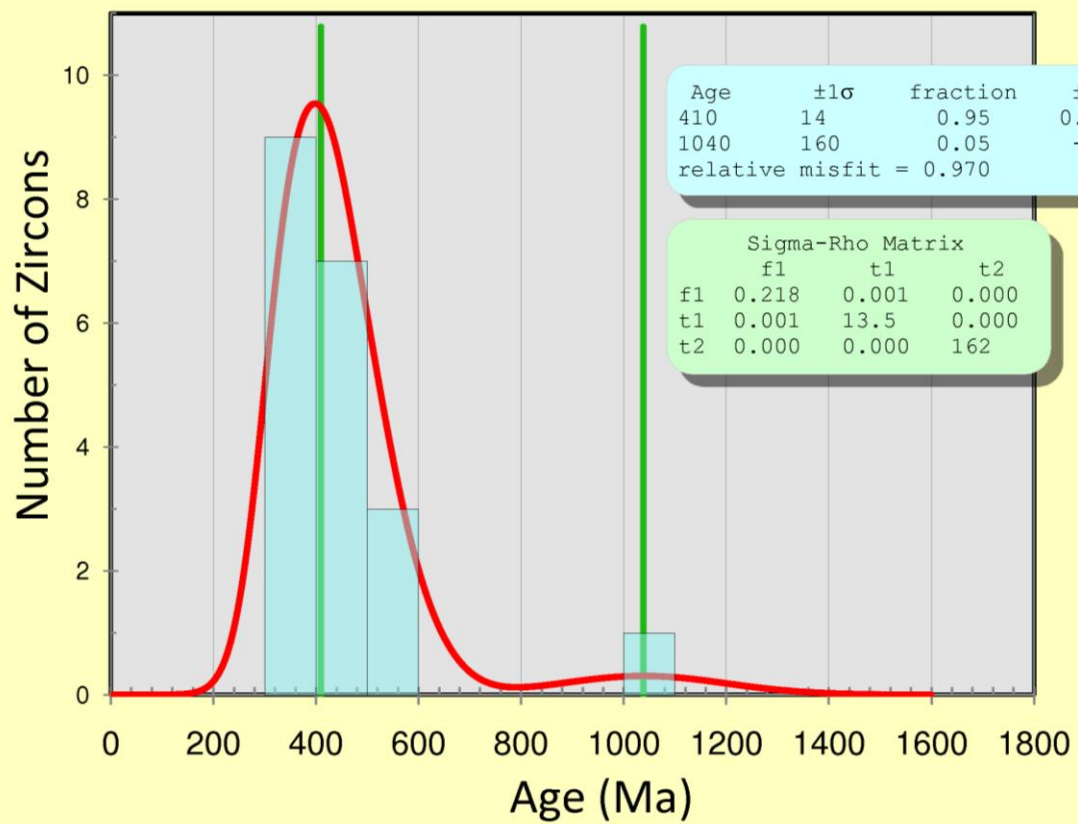
Title: Mt. Blakely, Irradiation UA-Z2, Analyst SNT



Lake Ouachita 41



Lake Pineda



VITA

Name: Harold Everett Johnson II

Address: Dept. of Geology and Geophysics, 3115 TAMU, College Station,
Texas 77843-3115

Email Addresses: hjohnson@geo.tamu.edu; johnsonwelldrilling@gmail.com

Education: B.S., Geology, The Ohio State University, 2005
M.S., Geology, Texas A&M University, 2011